Division of space by Voronoi graphs, percolation within percolation and application to the models of porous membranes

A thesis submitted to the

University of Manchester Institute of Science and Technology

for the degree of Doctor of Philosophy

Kittisak Nui Tiyapan

BEng, BSc, BEng, MSc

15^{th} October, 2003

No portion of the work referred to in this thesis has been submitted in support of an application for another degree or qualification of this or any other university, or other institute of learning.

K N Tiyapan

To my father and my mother Niwat and Somjit Tiyapan (*Nivat, Somcitṭa Tiyabandḥa)*,
my chemistry and sword teacher Siddhiponr Songsataya (*Sidhibaur Drongsatya*), and
my dad and mum Allister and Patricia Johnstone.
To Emeritus Professor David John Bell and
Emeritus Professor Graham Arthur Davies,
both of whom had started this project,
one of whom had powered it.
To these people, then, is my dedication of this thesis,
but the thesis may dedicate itself to whomever it wishes.

Abstract

Statistics for Voronoi Tessellations are obtained from numerical simulation. These are, for example, the number of edges, faces, and vertices per cell, and the cell's surface area and volume. Statistics are obtained for the 2-d section of 3-d Voronoi networks and for compressed VT. For networks of from two to ten dimensions are given the number of vertices per cell and the ratio between the volume and the hypercubic volume. The similarity between a percolation curve and an s-curve is discussed. Percolation is applied to the study of traffic congestion. In filtration problems sometimes tiny particles come together to form clusters which block the pores. This is due to the Van der Waals force which acts to pull them together and bind them. It is proposed here that such phenomena may be represented as a percolation within percolation, or more precisely a *continuum* percolation within a *network* percolation. Here channelling occurred in filters causes the concentration of the suspension to fluctuate. Pores whose internal concentration exceeds the continuum percolation threshold become blocked. This blockage may not be wholly random but depend on the quantum-mechanical wavefunction of the particles when their wave-particle duality are taken into account, as described by the de Broglie formula $\lambda = h/p$. These blocked pores then act to percolate the filter as a network percolation problem. Algorithms and programs for doing the simulation and compiling the thesis are given, and so are translation of three seminal papers by Voronoi (1908 and 1909) and another one by Dirichlet (1850).

Table of contents

a. List of figures vii
b. List of tables ix
c. List of theorems x
d. List of algorithms x
e. List of definitions xi
f. List of assumptions xi
g. Acknowledgements 12
h. Notation 14
1. Preface and introductions 1
1.1. Mathematics 5
1.2. Geometry 6
1.3. Physics 15
1.4. Cosmological structure 18
1.5. Filtration 19
1.6. Statistics 22
1.7. Poisson process 23
1.8. Phase transition 23
1.9. Random processes 24
1.10. Structures in nature 29
1.11. Computational geometry 31
1.12. Geometric algorithms 37
1.13. TEXnicalities 38
2. Division of space 41
2.1. Stereographic projection 42
2.2. Covering lattices 45
2.3. Viscous fingers 47
2.4. Crystals, quasicrystals, and polycrystals 48
2.5. Random lines and percolation 51
2.6. Convex hull 52
2.7. From convex hull to the Voronoi tessellation 53
2.8. Tilings and patterns 60
3. Voronoi tessellation 65
3.1. Quadratic equations 68
3.2. Quadratic forms 68
3.3. Voronoi algorithms 68
3.4. Voronoi statistics in literature 69
3.5. Voronoi statistics 71
3.6. Voronoi section 74
3.7. Number of vertices and edges 74
3.8. Faces in different dimensions 86
3.9. Beam intersection study 92
3.10. Voronoi of a Voronoi 96
3.11. Transformations of a Voronoi 97
3.12. Compressed Voronoi 98
3.13. Voronoi tessellation in higher dimensions 108
4. Percolation 111
4.1. S-curves and the percolative phenomena 116
4.2. Voronoi percolation in two dimensions 117
4.3. Voronoi percolation in three dimensions 118
4.4. Percolation of 2-dimensional Voronoi sections 120
4.5. Network percolation 122
4.6. Percolation statistics in literature 122
4.7. Percolation of n-gons in continuum 124
4.8. Polygon percolation threshold 127

4.9. 2-homohedral tilings 132
4.10. Cosmology 145
4.11. CCTV, forest fire, the navy and porcupines 146
4.12. Fractals 149
5. Porous media 151
5.1. Zeolites 151
5.2. Crystalisation 152
5.3. Fluid flow within networks 153
5.4. Material science 153
5.5. Forces between particles 155
5.6. Arbitrarily shaped particles 156
5.7. Non Poisson number distributions of particles 158
6. Filtering membranes 161
6.1. Separation processes 170
6.2. Dead-end filtration 170
6.3. The centre of gravity 171
6.4. Molecular dynamics 174
6.5. Problem definition and algorithms 176
6.6. Simplified algorithm for filtration 177
6.7. Filtering problem when physical blockage is prominent 178
6.8. Percolative filtering with very small particles 179
6.9. Percolation within percolation 182
6.10. The first part, suspended particles 183
6.11. The second part, flow through the cells 188
7. Percolation in traffic modelling 193
7.1. Percolation of road networks 196
7.2. Graphs theory and its applications 201
8. Conclusion 203
8.1. Suggestions for future work 203
9. Bibliography 205
9.1. Publication and writings, Kittisak Nui Tiyapan 211
A. Programs 213
A.1. Object location 213
A.2. Network percolation, two dimensions 214
A.3. Network percolation, three dimensions 217
A.4. Network percolation, 2–d section 222
A.5. Continuum percolation of n-gons 225
A.6. Tilings 227
A.7. Covering lattices 238
A.8. Covering contour 239
A.9. Number of vertices 240
A.10. Vertices per cell and cell ratio 240
A.11. TEX's macros 241
A.12. Language macros for TEX 249
A.13. Program for the dissertation 255
A.14. Program for the thesis 257
A.15. Degeneracy test and other programs 259
A.16. Face statistics in n dimensions 260
A.17. Beam intersection program 262
A.18. Number of vertices in high dimensions 263
A.19. Example batch program, simulation and data extraction 263
A.20. Voronoi operator of various order 263
A.21. Voronoi data structure for filtering membrane study 264
A.22. Centroid process on 2-d VT 266
A.23. Centroid process on 3-d VT 267
A.24. Defining irregular objects 271
A.25. Investigating the distribution observed from within the network 273
A.26. Miscellaneous functions 274

A.27. Percolated traffic networks 277
A.28. Volume, surface area, cell- and face perimeters 283
A.29. Volume in higher dimensions 288
A.30. Regular lattices in three dimensions 289
A.31. Effects of channelling 293
A.32. Stereographic projection 298
A.33. Percolation of regular polygons in two dimensions 300
B. Terminology and other resources 304
B.1. Abbreviation 308
B.2. Biographies 308
B.3. Computation and softwares 311
B.4. Internet resources 313
9.5. TEXnicalities 313
9.6. Voronoi statistics of earlier simulations 314
C. Publications and submissions of papers 319
C.1. Critical probability of 2-d tessellation 319
C.2. Abstracts of books I wrote 321
D. Translation 326
D.1. G. L. Dirichlet, 1848 326
D.2. G. F. Voronoi, 1908 (I) 333
D.3. G. F. Voronoi, 1908 (II) 373
D.4. G. F. Voronoi, 1909 413
E. Index 463

List of figures

1.1. Kissing number versus dimension 6
1.2. Icosidodecahedron and small ditriagonal icosidodecahedron 10
1.3. Great ditrigonal icosidodecahedron and great dodecahedron 11
1.4. Truncated tetrahedron and octahemioctahedron 11
1.5. Tetrahemihexahedron and truncated octahedron 11
1.6. Truncated cube and rhombicuboctahedron 12
1.7. Pentagrammic polyhedra 12
1.8. Temperature of the universe 17
1.9. Voronoi graph with bridge-shaped beta distribution 24
1.10. Voronoi graph with J-shaped beta distribution 24
1.11. Voronoi graph with U-shaped Beta distribution 25
1.12. Voronoi graphs of various random p.d.f.'s 25
1.13. Point process $r(\theta)$, where both r and θ are independent random generators 27
1.14. Point process x, y in a circular domain, where x and y are independent random generators 28
1.15. Point process x, y in a square domain, where x and y are independent random generators . 28
1.16. Additional generators for the incremental method 37
2.1. Stereographic projection of a cube 42
2.2. Rotated cube 43
2.3. Developmental stages of programs for the stereographic projection 44
2.4. Covering lattice, stone pavement, or galaxies in the forming 46
2.5. The area of multiply covered cells 47
2.6. Face number of non isometric crystal forms 49
2.7. The 71 Voronoi cells in an aggregation 53
2.8. Four groups of tiles 60
2.9. Percolation of networks related to the square lattice 61
2.10. Percolation of networks related to the honeycomb lattice 62
2.11. Percolation of networks related to the basket pattern, kagome lattice 62
3.1. Rooms with doors puzzle 65
3.2. Departure and arrival rooms 65
3.3. Voronoi from degenerative data 66
3.4. Shifted hexagonal lattices 66
3.5. Hexagonal, Kagome, and the covering of the latter 66
3.6. The next covering lattice 67
3.7. Voronoi graphs of covering lattices 67

3.8. The minimum of the average normalised edge length 71
3.9. The maximum of the average normalised edge length 71
3.10. The mean of the average normalised edge length 72
3.11. Mean, maximum, and mean of the cell-average normalised edge length. 72
3.12. The variance of the expected values of the normalised length of edges of a cell 73
3.13. Number of vertices per cell 73
3.14. Ratio of cells in the original domain 73
3.15. Sectioning by a plane 74
3.16. Abundance of elements 75
3.17. The electrical resistivity and conductivity of elements 75
3.18. Space covered by Voronoi 76
3.19. Number of vertices versus number of cells 77
3.20. The CPU time in seconds 77
3.21. Characteristic length versus the number of cells 77
3.22. Characteristic area versus the number of cells 78
3.23. Distribution of the number of edges per face 78
3.24. Statistics of a 231 cells Voronoi structure 81
3.25. The distributions of the number of faces and edges per cell 81
3.26. v_n/c_n in Voronoi networks of various dimensions 83
3.27. CPU time in creating the Voronoi networks 83
3.28. Distribution of vertices in high dimensions 83
3.29. Distribution of vertices in a 6-d Voronoi structure 84
3.30. Number of cells having a particular number of vertices 85
3.31. Counting the valences 86
3.32. Distribution of v_c in two dimensions 87
3.33. Distribution of vertices in 3-d Voronoi. 88
3.34. Distribution of vertices in 4-d Voronoi, 100 nuclei 89
3.35. Distribution of vertices in 4-d Voronoi, 300 nuclei points 91
3.36. Distribution of vertices in 5-d Voronoi, 200 nuclei points 91
3.37. Intersection by a line 92
3.38. Line intersection in a Voronoi with Rayleigh distribution 95
3.39. Two Voronoi operators applied in succession 96
3.40. The Voronoi operator applied six times 96
3.41. The number of cells and vertices when recursively applying the Voronoi operator 97
3.42. The effects of axis compression 98
3.43. Mean and standard deviation of surface area of cells under compression 98
3.44. Some hidden characteristics revealed 99
3.45. Volume of compressed Voronoi cells 99
3.46. Cell perimeter 100
3.47. Face perimeter 101
3.48. The cell perimeter and the face perimeter 102
3.49. Area, volume and perimeter; past results 105
3.50. Statistics of face areas under compression 106
3.51. Number of generators required for ten inner cells 109
3.52. Mean and standard deviation of the ratio Voronoi per defining cube 109
3.53. The ratio V_p/V_h, dimension from 1 to 6 110
4.1. predicted value of the heat capacity of monoatomic solids according to Debye 117
4.2. Section by the plane (0.01, 0.5, 0.5, -0.5) 121
4.3. Section by the plane (0.5, -0.5, 0.5, 0.01) 122
4.4. Section by the plane (-0.7, -0.3, 1, 0.01) 122
4.5. Regular polygon 124
4.6. Star 124
4.7. Tilting 125
4.8. When two n-gons practise the Ayudhya sword together 126
4.9. n-gons 127
4.10. Finding the threshold area ratio of pantagons 128
4.11. Percolation of n-gons 129
4.12. Thirty-nine 2-homohedral tilings 132

4.13. Sample trend of the biggest, the second biggest, and the smallest cluster 137
4.14. Basic units of the thirty-nine 2-homohedral tilings 138
4.15. Range of observatory towers 147
4.16. Tortuous boundaries 148
4.17. Porcupine diagram superimposed on a map 148
5.1. Schematic diagram of a separator 154
5.2. Coulomb force *vs* distance in log-log scale 156
5.3. *Kit* the existential object 157
5.4. Distributions by weight and by number 158
5.5. Spherical object on a sieve 160
6.1. Centroid of the Voronoi tessellation 171
6.2. Evolution of nuclei towards centroids 172
6.3. Evolution of nuclei towards centroids in three dimensions 173
6.4. Change in size distribution as a result of a nuclei adjustment process 174
6.5. Lennard-Jones potential 175
6.6. Force corresponding to the Lennard-Jones potential 176
6.7. Force balance with one particle fixed 180
6.8. The packing density calculation of the closest-packed densities 181
6.9. Quantum-mechanical effect in filtration 182
6.10. Percolation within percolation 183
6.11. Percolation of the cubic close-packed lattice 185
6.12. The eight areas defined by the eight types of unit blocks 188
6.13. Intersection of convex hull faces and the horizontal plane 189
6.14. Correcting the effect of rounding or discretisation 190
6.15. After increasing the precision 190
6.16. `Spying` the neighbours 191
6.17. Sections of bonds and cells 192
7.1. Traffic status, $p_c > 0.5$ 193
7.2. Traffic status, $p_c < 0.5$ 194
7.3. Traffic control algorithm 194
7.4. Proposed traffic control in real time 194
7.5. Manchester road networks 196
7.6. Plots of the largest clusters, Manchester 197
7.7. Road networks of Amsterdam 197
7.8. Plots of the largest clusters, Amsterdam 198
7.9. Road networks of Brussel 199
7.10. Plots of the largest clusters, Brussel 199
7.11. Road networks of Freiburg 200
7.12. Plots of the largest clusters, Freiburg 200

List of tables

1.1. Three types of function 5
1.2. Perimeter per unit area of n-gons 8
1.3. Some important properties of regular solids 8
1.4. Surface area per volume of regular solids 8
1.5. The number of vertices, edges and faces of some polyhedra 10
1.6. Archimedean solids 14
1.7. Origin of membrane processes 17
1.8. Methods of preparation of membranes 18
1.9. Probability density functions 25
2.1. Symmetries of crystals 48
3.1. Moments of 3-d Poisson-Voronoi tessellation, *cf* van de Weygaert (1994) 69
3.2. Moments of 2-d section of 3-d Voronoi, *cf* van de Weygaert (1994) 69
3.3. Statistics of 3-d VT, van de Weygaert (1994) 70
3.4. Statistics of the planar section of the 3-d Voronoi tessellation, van de Weygaert (1994) 70
3.5. Statistics for the line section of the 3-d Voronoi tessellation, van de Weygaert (1994) 70
3.6. Statistics of a 3-d Voronoi network 74
3.7. Neighbour statistics 76

3.8. Three dimensions, statistics 78
3.9. Results from 527 Voronoi cells 82
3.10. Statistics of the number of vertices in high dimensions 83
3.11. Two-dimensional Voronoi, 100 nuclei 86
3.12. Three-dimensional Voronoi, 50 nuclei 87
3.13. Four-dimensional Voronoi, 100 nuclei 89
3.14. Four-dimensional Voronoi, 300 nuclei 91
3.15. Five-dimensional Voronoi, 200 nuclei 91
3.16. Intersection by a line, statistics 93
3.17. Rayleigh distribution, line intersection statistics 95
3.18. Mean of the cell surface area of compressed Voronoi 98
3.19. Standard deviation of the cell surface area of compressed Voronoi 98
3.20. Numerical values of the mean of the compressed cell volume 100
3.21. Numerical values of the standard deviation of compressed cell volume 100
3.22. Mean cell perimeter, numerical values 101
3.23. Mean face perimeter, numerical values 102
3.24. Standard deviation of the face perimeter, numerical values 102
3.25. Cell and face perimeters, numerical values 103
3.26. Numerical statistics of the area and perimeter of face 105
3.27. The numerical values of face area 107
3.28. Volume of d-hypercubes whose dimension is ℓ 108
3.29. Voronoi volume in higher dimensions 109
4.1. Percolation thresholds, Stauffer and Aharony (1998) 114
4.2. Percolation probabilities, *cf* Sahimi (1994) 115
4.3. Critical exponents and fractal dimensions, *cf* Sahimi (1994) 115
4.4. Critical probabilities from Frisch *et al* (1961) 123
4.5. Critical probabilities from Dean (1963) 123
4.6. Critical probabilities and connective constants, Shante and Kirkpatrick (1971) 124
4.7. Percolation statistics of the 2-homohedral tilings 140
5.1. Particle size definitions 153
6.1. Statistics of the modified Voronoi cells, Jafferali (1995) 167
6.2. Comparative Voronoi statistics, Jafferali (1995) 167
6.3. More comparative Voronoi statistics, Jafferali (1995) 167

List of theorems

1.1. Relationship between α and r 9
1.1[1]. Relationship between A, V and r_f 10
1.2. Average number of edge per polygon 30
3.1. Starting and ending nodes 65
3.1[1]. Path along two dimensional Voronoi network 65
3.1[2]. Path along three dimensional Voronoi network 66
3.1[3]. Path along a two dimensional face of a three dimensional Voronoi network 66
3.2. Vertices and edges, Euler 74
3.3. Vertices in three dimensions, Tiyapan 74
3.4. Edges in three dimensions, Tiyapan 74
4.1. Setments always intersect 125
4.2. Aggressive party 125
4.3. Finding overlap 126
6.1. The centre of gravity 173

List of algorithms

1.1. Perimeter per unit area of regular polygons 8
1.2. Area per volume of regular polyhedra 9
1.3. Thinning algorithm 27
1.4. Triangulation edge length distribution 29
1.5. Intersection between three planes 32
1.6. Point inside a polygon 32

1.7. Euclidean minimum spanning tree 33
1.8. Rotation in three dimensions 33
1.9. Ray and triangle intersection 34
1.10. Convex hull in three dimensions 35
1.11. Convex hull in two dimensions 35
1.12. Quick hull algorithm 36
1.13. Quaternary incremental method 36
2.1. Generalised Johnson-Mehl model, Miles (1972) 41
2.2. Drawing stereograms from crystal models 44
2.3. Graham's scan 52
2.4. Quickhull in two dimensions 52
2.5. Convex hull of convex hulls 52
2.6. Tilings in two dimensions 60
3.1. Voronoi 2-d algorithm, Green and Sibson (1978) 69
3.2. Valence relations 86
3.3. Volume, area and perimeter algorithms 104
4.1. Ant in a labyrinth 114
4.2. Network percolation in 2-d 117
4.3. Managing the Voronoi data in three dimensions 119
4.4. Voronoi percolation in three dimensions 120
4.5. Plane section of Voronoi in three dimensions 121
4.6. Continuum percolation of regular polygons 126
4.7. Threshold area ratio 129
5.1. Fracture by attrition, Lim *et al* (1999) 152
5.2. Arbitrarily shaped particles 157
6.1. Voronoi construction in three dimensions, *cf* Tanemura *et al* (1983) 161
6.2. Find the largest inscribed circle 162
6.3. Interaction between particles and surface pores 162
6.4. Interaction between each internal particle and the pores 163
6.5. Particle cake formation, *cf* Jackson (1994) 163
6.6. Flux decline across the membrane model 164
6.7. The random walk of particles during removal by backflushing 164
6.8. Non-woven fibre simulation, *cf* Wilkinson *et al*, 1986 165
6.9. Voronoi construction in 3-d 165
6.10. Find faces of a polyhedron 166
6.11. Nuclei points of the modified point process, *cf* Jafferali (1995) 166
6.12. Asymmetric Voronoi tessellation, *cf* Jafferali (1995) 167
6.13. Pore property evaluation, *cf* Jafferali (1995) 168
6.14. Inscribed circle of faces 168
6.15. Inscribed sphere of a polyhedron 169
6.16. Verlet algorithm 174
6.17. Filtration in Voronoi tessellation 176
6.18. Voronoi data structure for the study of membrane filters 177
6.19. Percolation by tiny particles due to attrition in membranes, preparing the structure 184
6.20. Percolation by tiny particles due to attrition in membranes, percolation simulation 184
9.1. Beneath-Beyond algorithm 311

List of definitions

3.4. Volume of a d-simplex 108
4.3. Threshold area ratio 127

List of assumptions

3.4. Volume of a unit cube 108
3.4. Volume of d-simplices 108

Acknowledgements

There are no less than two Emeritus Professor's to whom this present work is indebted. They are David John Bell and Graham Arthur Davies, both of whom I thank for the supervision and also the latter for the maintenance fund throughout the course of the project. I thank Simon Hood and Zaiem Bakker for the help in computing matters, and Stuart Holmes *et al* for suggesting zeolites. I thank Walter Korchinsky for the lab demonstrating jobs, Ted Roberts for the extended computer access and for giving me a visitor's status for a few weeks in September 2003 to conclude my thesis for submission, and Ian Rosindale for extending the computer access for me. These people mentioned, unless stated otherwise, are all titled Dr. I thank the graduate school administrator Muriel Shingler, Rodney Holt at the helpdesk of UMIST's ISD and also Steven Coppersthwaite-Lewis who looks after the computers at the Chemical Engineering Department. I thank Peter Senior who is an excellent teacher, and Professor Ian Metcalfe, both for letting me help with the demonstrations.

For the help with my everyday's work I thank all the staffs at the John Rylands Library at Deansgate, the John Rylands University Library and the Joule Library, especially but not only those at the issuing desks whom I see regularly. For encouragement I thank Carlos Cervantes, Dirk Engelberg, Clara Entwistle and Yann Frouin. For inspiration I thank mathematicians like Descartes, Dirichlet, Euler, and Voronoi.

Many of the ideas and solutions described herein came to me while I was on an excursion away from Manchester. I thank those people who had taken me to those far corners, away from the madding crowd, places as unique and distant from one another as Penzance, Portree, Llandudno, Nagazaki and Nice. These people are in particular the drivers of National Express's coaches, train operators in Europe and Japan, pilots, and also Aoife O'Higgins who organised several trips for us.

I thank Sister Eileen and all the staffs at the St. Gabriel Hall of Residence who have made my stay there during the summer of 2002 a memorable experience. Special thank to Yann Frouin my flatmate at St. Gabriel for his encouraging words in times of turmoils, 'Believe in your ideas moreover they are beautifull'. [sic] I thank Carlos Manuel Cervantes Lara, Daniel Scamman, Ewan of the Spitalfields Market's poi-swinging and blaung-spinning workshops, Carlos Harrison for encouragement and accommodation.

I also would like to thank PCA 4819, one of the two policemen who helped me once in time of trouble. My interest is rather eclectic. But it may be true what Debussy says, perhaps *nothing that has happened is ever useless.* How could I possibly forget to thank our security staffs, in particular Richard and Graham. Because of them UMIST is made safe for all.

Above all I thank God for letting me be and for everything.

No writings can be too long
nor tunes futile in any song
where to someone thanks we say
and in our heart for them we pray.

Yet at times we forget
and amidst our busy tasks let
all the pains in and here reside.
We could have let God us abide.

O, gentle reader, never judge!
We last no longer while we grudge!
Search again, and you shall find so much
there is nothing meaningless as such.

Kit Tiyapan
Manchester, 2003

The above poem was written on 24^{th} September 2003 . By the end of the month I have already given a copy of it to many people, and many more in the form of emails to friends in the UK, the US, Japan and Thailand. This is how I come to realise that I have missed out quite a few of the names of those people who have helped. If I had to rid my writing of all the stuffs it is made of, I would never have even dreamt about ridding it of each and every one of all the thanks I have put therein. I thank Peter Fawcett for having had decided to supervise my projects on languages though in the end I had to do them all by myself and on my own. I thank Graham Davies again for the full two years of financial support, the inspiration, compassion and encouragement received. I thank Mona Baker for having given me an office and access to a unix machine at the translation group. Though I had to return them all to her for my works for Graham, it had been a wonderful experience for me to have done some work for her translational corpus.

I thank Louis Papworth, Lesley McDonagh, Pauline Howarth, Stewart Grace, Helen Cooke for getting office-procedural things done. For chemical engineering helpdesk I thank Jacqie Kitson, Simon Perry and Fran Stanley. I thank Dr's Michael Anthony Allen, Stuart Holmes, Aṃṇac Gịtábarrṇạ, Bronislav Librovich, Leo Lue, Andrew Nowakowski, Jinávudh and Kriangsakdżi Śirisambandha for the encouragement. For the same I thank Zoë Speakman.

Last but not least I thank Ted Roberts again and also Ian Bradley, both for having read the previous versions of this thesis and given some comments all of which are valuable. It is remarkable not only that their names are of exactly the same length but also that both are very kind. As a result of this, the thesis owes much of its good points to them whereas all of its shortcomings are because of Me who is itself imperfect being merely a tiny subset of the Whole.

Notation

$0(n)$. a zero vector of n dimensions.

$0(n,n)$. an $n \times n$ zero-matrix.

$1(n)$. a one vector of n dimensions.

$1(n,n)$. an $n \times n$ one-matrix.

a. surface area of a cell.

a^{ij}. cofactor of a_{ij}, $a^{ij} = (-1)^{i+j} \det(a_i, b_i)$.

$\aleph$. neighbour.

α. surface area per unit volume.

β. area of face.

c. cell; concentration.

d. length.

D. diffusion coefficient.

δ. thicness of the boundary layer.

ϵ. porosity.

ϵ_0. permittivity of free space, $\epsilon_0 = 8.854 \times 10^{-12}$ Fm^{-1}.

η. viscosity of liquid.

e. edge; the charge of an electron, $e = -q$. See q.

$E(x)$. expected number of x

f. form factor, f_c, of a cell, f_f, of a face; face, nf, n-face.

h. Planck's constant, 6.626×10^{-34} J $\cdot$ s.

he. he; he or she.

$\mathrm{I}(n)$. an $n \times n$ identity matrix.

I_r. integers in the interval r *eg*, $I_{[0,\infty)}$.

J. flux.

κ. Kurtosis.

$\mathcal{K}$. Kurtosis.

λ. wavelength. m.

μ. weight of particles in the cake per unit of filter surface; fluid viscosity; magnetic moment.

$\mu(\cdot)$. mean; also μ_g the geometrical mean, μ_h the harmonic mean.

$m^n(\cdot)$. the n^{th}-moment of.

$\mathrm{mad}(\cdot)$. mean absolute deviation.

$\mathrm{med}(\cdot)$. median.

$\mathcal{M}^n(\cdot)$. the n^{th}-moment of.

N. original total number, for example N_c is the total number of cells, and N_v of vertices, created which may include those that are out of bound.

n_x. number of x. n_c, number of cells. n_e, number of edges. n_v, number of vertices.

n_y^x. number of x of a y. n_c^e, number of edges of a cell. n_c^f, number of faces of a cell. n_c^v, number of vertices of a cell.

$n_{y,z}^x$. number of x per y of z. $n_{f,c}^e$, number of edges per face of a cell.

ω. angular velocity.

p. probability; (with subscript) percolation probability. p_c, p_b, p_v, p_e, percolation probability of cells, bonds, vertices, and edges respectively. alternatively, p_c^c, p_c^b, p_c^v, p_c^e,.

$p(\cdot)$. probability density function, probability distribution.

P. pressure.

q. the charge of a proton, 1.6×10^{-19} C; feed rate.

Q. flow rate, $Q = \mathrm{d}V/\mathrm{d}t$.

r. radius. r_v, r_e, r_f, radius to a vertex, edge, or face, respectively.

ρ. density; number density.

r. specific resistance.

§. (s) section or chapter.

s. perimeter, for example s_c the perimeter of cell; cell perimeter.

σ. spin variable.

θ. time.

v. velocity.

vertice. any vertex.

V. volume.

W. fluid velocity.

x. coordinates; coordination number.

$\bar{x}$. mean value of x, *cf* $E(x)$.

z. face perimeter.

§ 1. Preface and introductions

This work began in 1995 under the co-supervision of now Emiritus Professor David John Bell and Emiritus Professor Graham Arthur Davies. The main theme of it is the percolation on porous media and Voronoi tessellation. The objectives are to study the characteristics and nature of Voronoi tessellation and percolation, and then look at their application on porous media, which includes such things as membranes.

As a brief background to this project, the dissertation for my master degree in Control and Information Technology, dated September 1995, was on the percolation on a two-dimensional Voronoi tessellation. From 1996 to 1998 I had been doing a PhD in Japan on topics related to Control System. Parts of my work there are recorded in the few *technical reports* that I wrote during that time and presented to my supervisor, now Emeritus Professor Katsuhisa Furuta. In September 2000 I came back to UMIST to do a PhD in Translation but a few months later changed my mind to resume this research on Tessellation with Graham Davies.

Throughout my research I kept hand written notes which I called *work books*. All results exist in two places, either in the thesis or in the form of the TEX documents which I call *work notes*. Materials sometimes move from the work notes to the thesis. Apart from simulation results, these work notes also contains ideas for future works. All these worknotes were written during 2001. Their importance is that they represent the essential momentum or the underlying potential at work behind every percolative process. But most of the breakthroughs in this project came during 2002. I solved numerically a problem on the two-dimensional continuum percolation of squares on the plane. My algorithm can also give solutions for the continuum percolations of n-polygons, for $n \geq 3$ and $n \in I^+$.

The idea of writing these worknotes came from a book I had read about the work notes written by Michael Ventriswhile he was deciphering the Mycenean Linear B script. I wrote no worknotes during 2002. During the first half of 2003, however, I resumed my writing again and this time produced not worknotes but books which I published under the trademark name of ≻Kittix.

I started to use Latex in 1994 to write a design exercise report for Dr. Martin Zarrop of the Control System Centre at UMIST. Back then, most people I know liked the program better than its progenitor TEX, which most thought was difficult. I used Latex for writing my master degree dissertation in 1995, and continued using while in Japan and until early 2001 when I first turned to TEX then held fast to it. In the past when I still used LaTEX I could hardly adjust, but has to accept the existing formats. One awkward example is seen in my technical report number 6 where one reference (Fitzgerald *et al*, 1971) appears everywhere as "[FCKK71]", which looks very awkward.

Topics are divided into Voronoi structure and geometry, percolation, and membrane science. Voronoi tessellation has been used to model the array of the somata and cone cells in retina of mammals. (Ammermuller et al 1993; Ahnelt et al, 2000; Zhan et al, 2000) Curcio et al (1992) found anisotropy in cone spacing. For readers who are interested in the theoretical works on stochastic geometry may look at Møller (1989).

None of the papers and articles in § C has appeared in print elsewhere. It may be true that nothing worthwhile is ever without trouble. This project has had its share of problems. But 'What happened is history!', as Graham once said to me, or 'It is over!' as I to students in a lab I demonstrated with whom at times I had sympathised regarding problems beyond their power which affected them, and to whom I had passed down all the essentials of a programmer, there is no point keep on complaining about the past. Being a subset of the Superset I shall not judge. Being a me then the Me in Christ in God, how could I judge other subsets myself being merely another subset. It is not for a part to judge a fellow part, but let the Whole be the only One who judges, and let that alone suffice! Having done my tasks I am now only a writer who believes in the one Creator from whom all things come and to whom the same return. As Percolation may compass percolations my works is in Science in Him.

I completed a two-dimensional percolation program and used it to compute the critical probability of a Voronoi graph in time for my M.Sc. dissertation. I used the C program developed by Nicholas Jackson and maintained by Riaz Jafferali to generate the Voronoi network, and wrote my own program on Matlab to find the percolation probability. Before I went to Tokyo in September of the same year, we agreed that I would carry on doing some more work along the same line while I was in Japan. Graham suggested that I looked at the viscous fingering, a phenomenon which occurs

when a low viscosity fluid penetrates a high viscosity one in the form of thin branches, which is of great importance in the replacement of oil in a reservoir by water.

I telneted across half the globe from Tokyo to log on to the workstations at the Chemical Engineering Department in Manchester, but instead of writing another program to do viscous fingering I only managed to find the percolation probability of the road network in Bangkok using the program I from my M.Sc. I also carried further the work I had previously done with Martin Zarrop on object location using self-tuning control; and had an idea that if we could construct a network of people with an internal flow of money, we would be able to explain economic crises such as hyperinflation by using the percolation theory. On the topic of percolation and Voronoi tessellation I presented one paper at a conference in St. Louis (1996); on object location at two conferences, one in Atagawa (1996) and another one in Singapore (1997); and on economic modelling one at a conference in Tokyo (1997).

The original objectives of the present project are the following. Firstly, to study the statistics of the three-dimensional Voronoi tessellation, namely the number of vertices, coordination probabilities of nodes, number of faces, volumes, area of each face, number of sides and edges of faces, and perimeter. Next, to 'formulate a simulation of Voronoi tessellation,' that is to say, polygons in two dimensions and polyhedra in three dimensions; then analyse the lattices for the number of cells, sides, and edges. In two dimensions find the fractional expected area per cell, and expected number of vertices and edges. In three dimensions find the expected number of vertices, edges, faces, the fractional expected volume per cell, area of faces and fractional area per cell. Then section the Voronoi tessellation in two dimensions using a straight line and repeat the same thing in three dimensions using a random plane. In two-dimensional section of three-dimensional lattices using orthogonal planes, find the number of cells, edges, and the area. And then compress the lattice in one plane, with compression ratios $0 \leq c \leq 0.8$, and find the volume and surface area of cells for $c = 0$, 0.4, and 0.6; plot a section structure for $(\text{x–y})_{c_z=0}$, $0 < z < 1.0$, $c_y = 0$, 0.4, 0.6; $(\text{x–z})_{c_y=0}$, $0 < y < 1.0$, $c_z = 0$, 0.4, 0.6; compare the number of vertices, edges, and the area with those obtained from the case when $c_z = 0$, $c_y = 0$, and $z = 1$. Study transformations of Voronoi structures, for example the effect on the statistics when Voronoi graphs have a thickness. For each of the expected values mentioned above, find the first, second, and third moments. And finally, from the observation I have made that a three-dimensional tessellation have a bias towards an even number of vertices, find an explanation. To conclude the study of Voronoi tessellation, find affine transformations on two- and three-dimensional lattices and use the AVS program to print out sections of 3-d lattices †. Then for affine transformations, for example stretching, write algorithms to reposition the structure. For 2-d lattices, find the critical percolation probability (CPP), compare these with previous data and carry on to find the CPP on higher dimension lattices. To look at the application to the technical problems of membranes, foams, plant cells, *etc*, and if possible to compare my results with models to describe other physical and natural phenomena. Relevant to the application in foams is perhaps the population balance equations. Care should be taken to ensure that any application mentioned is described in details how it can fit in with real problems. Of no less importance is to study methods of adjusting structures to fit the applications. These methods include modifications to Poisson point processes and, again, affine transformations of the cellular structure.

Filters used in aluminium smeltering must withstand a temperature higher than 700°Csince aluminium alloy melts at 650–680°C. These filters are used in order to separate the oxide froth which otherwise would form pits when the aluminium is casted. The process of manufacturing filters often introduces asymmetry elements to their structure, for instance there may be elongation in one dimension because of gravity, or in cases where material is drawn out to make the filter the structure may become distorted from the shear force of drawing. The texture of bread is anisotropic because the internal pressure from gas produced by the yeast press es the dough against its own surface tension. The elongated cells inside bamboos appear in various sizes, which explain why bamboos are at the same time strong and flexible. Certainly one sees the Voronoi tessellation wherever one looks. I feel that I have learnt so much from Graham.

The following summarises our original outline of the project. The objective is to study a *foam like* porous medium. Describe the statistics of structures in three-dimensional space, state the reason why we need the statistics and the roles they play in application. For the Voronoi tessellation, created from the Delaunay triangulation of Poisson points, give algorithms which generate the structure from

---

† This has been done using Matlab instead.

one- up to n-space ‡, and give examples of these [structures found in nature]. Give the analyses of the static geometrical data, namely the length scale $l < L$ in one dimension; the area $a < A$, n_1, n_2, L in two dimensions; and the volume $v < V$, n_1, n_2, n_3 in three dimensions, where n_{d+1} is the number of the d-dimensional entities, $L = V^{\frac{1}{3}}$, $A = V^{\frac{2}{3}}$, and $V = \sum_i v_i$. Include the translation that I have made of the seminal papers by Voronoi and Dirichlet, a section on the transformations made on the structures, possible future developments of the project, and the applications.

Over the course of doing the project its title has changed from the original *Voronoi tessellation and porous media*, to *Division of space by Voronoi graphs, application to the models of porous membranes*, then to *A twentieth-century definition of the ancient theme, Voronoi network and percolation in porous media*, and to *On suspension blockages of filtering membranes as continuum percolation under van der Waals influences in centroidal Voronoi networks*, and finally into the present name.

I have observed that a Voronoi cell in three dimensions always have vertices and edges in an integral multiple of two and three respectively. I found the reason for this and have given one proof for the first observation, and two for the second one (§ 3.7).

Related to the present study is the stress-strain analysis in the bonds of a Voronoi structure in three dimensions as well as the study of randomly placed rods. Also interesting is the problem of percolation of randomly placed squares, which he thought would be useful in the growth process of synthetic zeolites. The zeolite problem mentioned above I have found to be identical to the so-called *continuum percolation* of squares. I have developed an algorithm to solve this not only for squares but also for the general case of n-gons. The program uses some of the ideas behind the basic movements in the Ayudhàyạ sword fighting. The algorithm has been intuitively arrived at from my own experience of several years holding a square, hind shield in one hand while in another brandishing a Thai sword for a troupe when our sword school demonstrated for that matter. It was only afterwards that I found the rigorous proofs for all its parts. However, I have not carried the work further to three dimensions because, for one thing, I personally do not believe the crystal growing to be random. Crystals grown within the same solution should have some kind of quantum coordination which allows them to align themselves with one another when they meet. The random appearance seems to be only their various habits.

The nature of discoveries and progresses in science is according to Bacon (Francis Bacon, 1620) *a birth of Time rather than a birth of Wit.* This is the same idea of percolation and the description he gave is the very picture of the theory. According to him major scientific progresses come in revolutions which are sparsely distributed in both time and regions. There have only been three periods of major progress out of the *five and twenty centuries over which the memory and learning of men extends*, namely the Greeks, the Romans and the nations of Western Europe. These are narrow limits of time, the periods in between of which are unfavourable to development. A discovery or an invention, then, comes as a chance accident in the scale of an individual, and as a certainty when looking from a distance.

When the time is right and all the hidden momentum built up, theories will come on by itself as a rule. This does not negate the excellence of an individual, but in a society where there are enough multitude of individuals the show will always go on, with or without a particular genius. This idea can very well explain cases of multiple discoveries. According to Kekulé in his *Benzolfest* speech in 1890, when he ascribed his conception of the cyclic nature of Benzene in dreams, *certain ideas at certain times are in the air* and *if one man does not enunciate them, other will do so soon afterwards.*

To see the relationship of this with percolation it is possible to look at two different things in turn, first at the discoveries and then at the discoverers. With a unit being that of a *discovery* the connection to percolation is that big discoveries come as connections of other smaller and less obvious ones. A theory often has more than one perspective, and which one of them comes to the fore first depends much on which combination happens to percolate through first. The discoveries of Schrödinger and Heisenberg in Quantum Physics can bear witness to this both in the *combination* and the *multiple discoveries* parts of this argument.

Let us turn our attention now to the scientist and look at the one who does the discovering instead. The theory of percolation tells us that at the point of discovery he is by no mean the sole integral ingredient. If he does not do it, then someone else will certainly do. In order to see this, I did four simulations for the cell, bond, vertice, and edge percolations on a two-dimensional Voronoi network and then another four with the same respective blockage of each case but considering the

‡ In one variation, $n \leq 5$.

inverse phase instead. The number of units considered for the four cases are $n_c = 200$, $n_b = 416$, $n_v = 298$, and $n_e = 426$. With the order of simulations as described above, at just one step before percolation occurs there are respectively 10.6, 13.4, 11.5, 1.1, 11.24, 10.0, 19.4, and 7.9 percents among the remaining units which will readily trigger the onset of percolation. In other words, these are atoms which are able to link up existing clusters and form a percolating cluster.

The formation of mobs is an interesting phenomenon comparable with phase change in physics. What happens is that an agglomerate of individuals becomes one and a single creature, the underlying mechanism of which still baffles any effort towards understanding it. Likely enough it has got something to do with psychology and the mind. But to me at least, the phenomenon is percolative. Having gained some acceptance from my previous writings (Tiyapan, 1995–1996, KNT3(iv), KNT4(i) and [kbukt]; respectively §'s E.5, E.6 and E.7 of Tiyapan, 2003, KNT8(iii)) I gave my new work which briefly discusses the mechanism underlying the formation of mobs to an editor of the Sakkayaphab journal whom I know. At that time a political turmoil unequal in its degree and extent has been going on for five years. Whether by fate or by design there has been a successful but tragic use of mob in Bangkok. The word *mob* has joined the list of those synonym to *distrust*, namely *communist* or, in western community now for that matter, *Islam* and *evil*. Whether because of this or something else, the article (Tiyapan, 1996, KNT4(vii); or § E.15 of Tiyapan, KNT8(iii)) simply and mysteriously got lost; no one would admit having seen it, and the translation of another subsequent article of mine (1996, KNT4(viii); or § E.16 of Tiyapan, KNT8(iii)) has not been without a noticeable negligence. Thus to me distrust is also percolative. The list of things one finds over-distrusted without reasonable explanation goes on indefinitely, homosexuality, communism, *etc.* The same seems to be the case with bad habits. My father used to teach me using the following poem,

> Bad habit gathers by unseen degree
> like brook makes river, river runs to sea.

Looking back, it could have been the title of that article, *on pragmatists and idealists*, which has somehow convinced the editors into believing that it was political which to me is nonsensical. I only meant literary, even if at times philosophical. I include it here because it contains a curve showing a critical emotional transition.

The formation of the United States, the European Union, or the Commonwealth comes from the trust which acts to join countries together like glue boxes in TEX. Like all binding forces, trust is mutual and spreads in the same way as a growing cluster does. The cluster grows bigger as one or more members are added, and it becomes stronger as the level of the mutual trust increases. In a similar way, distrust is also mutual and also spreads. If I distrust you and you distrust me, I will make sure that I remain as far away from you as possible while you will certainly avoid me by all means in return.

Only these two are possible, so there are only two phases to consider, that of trust and distrust. The relationship where one trusts while the other distrusts would not be stable, since the former will soon learn to join the latter. Trust forms clusters of one phase, distrust another. The size of these clusters vary in a way similar to those in percolation of geometrical networks. The strength of the glue is analogous to the probability either of becoming or remaining a member of a cluster.

The rise of dictators, the proliferation of weapons of mass destruction, *etc*, these things I believe are the products of changes of something hidden within the underlying structure. Unless we find out what is happing in the background, these things will unavoidably occur. I believe that this unseen thing behind the scene is governed by some phenomena similar to that of percolation. I think that the key towards understanding many unexplainable phenomena is to investigate, in the light of the percolation theory, the working of agglomeration of countries or states like those of the United States and the European Union.

The believe that scientific discoveries are a birth of time, rather than of wit (*cf* Larsen, 1993), is the same as the idea of percolation. We know because we remember. And all the various discoveries of our time together with the knowledge we possess of the past bring us closer to another discovery. Scientific discoveries, then, is the collective product of humanity rather than property of a single person (*cf* Merton, 1965).

And because all species are also the product of percolation in time, our knowledge and consciousness, too, are the product of the universe. One may say that it is a personification when we refer to a collective noun, for instance a mob, as an individual. But the truth is that, under the percolation theory, it is in fact a separate individual without any need for the use of a simile. The renormalisation group theory tells us that there exists a structure in a bigger scale that behaves like the individual components that comprise it. It seems, therefore, that for humans these collective

beings of ours are still primitive compared with each of us as an individual. This is the reason why, whenever we come together, we alway make wars. In our case, then, we seem to be conscientiously percolated only individually not collectively. In the case of bees, on the other hand, it is the other way round. This is why a colony of bees does things which make far better sense than a bee does. But one can not say that even a *colony* of bees has consciousness, because there seems to be no morals in what it does. I do not know whether there are other beings in the universe both the collective and individual beings of whom have percolated conscientiously. But I believe they exist, in which case they should be more intelligent than us, though this is by no means necessarily the case.

§ 1.1 Mathematics

A map, denoted by $f : \mathrm{X} \mapsto \mathrm{Y}$, is an assignment of an image y in the target Y to a preimage x in the source X, where f is called a function and $f(x) = y$. A composition of $f : \mathrm{X} \mapsto \mathrm{Y}$ and $g : \mathrm{Y} \mapsto \mathrm{Z}$ is the map $h : \mathrm{X} \mapsto \mathrm{Z}$ such that $h(x) = g(f(x))$ for every x in X. There are three types of function, each one having at least three names. Table 1.1 lists these three types together with the sources of their various names. The prefix *epi-* in Greek means *on* and *isos-* means *equal*.

Anglo-Saxon		*Greek*		*Latin*	
an to an	one to one	monomorphos	monomorphism	injectus	injective
on to	onto	epimorphos	epimorphism	superjectus	surjective
an to an and on to	1–1 and onto	isomorphos	isomorphism	bijectus	bijective

Table 1.1 *Three types of function and the source of their names.*

A concrete category is a set of function that is closed under composition and contains the identity map for every source and target. The maps in C are the morphisms of a category $\mathcal{C}$, and both its sources and targets are objects. The topological category $\mathcal{T}$ is a category of topological spaces and continuous maps.

Furthermore, a functor is a map of categories which preserves composition and takes identities to identities. A covariant functor has $F(f \circ g) = F(f) \circ F(g)$, whereas a contravariant functor has $F(f \circ g) = F(g) \circ F(f)$. Homology is a covariant functor from $\mathcal{T}$ to the category of abelian groups and homomorphisms, while cohomology is a contravariant functor from $\mathcal{T}$ to the category of rings and ring homomorphisms.

A relation is an equivalent relation, denoted by $\sim$, if and only if three axioms, namely that of reflexivity, symmetry and transitivity are satisfied. A set of all x in A such that $x \sim a \in A$ is the equivalence class of a. A partition of A is formed by the set of equivalence classes of equivalence relations, and is a family of disjoint subsets of A covering A. Then A is the union of the equivalence classes, and each equivalence class has an empty intersection with any other. That is, every a in A is also in an equivalence class $E(a)$, and $E(a) \cap E(b) \neq \emptyset$ implies that $E(a) = E(b)$. Conversely, every partition of A gives an equivalence relation on A, and a is equivalent to b if and only if a and b are in the same subset of the partition.

With the discovery of the equation $f_0 - f_1 + f_2$ by Euler in 1752 a new era of mathematic began, and that is the era of topology. The Euler's equation in its equivalent forms are written as $\sum_{i=0}^{d}(-1)^i f_i(P) = 1$ or $\sum_{i=-1}^{d}(-1)^i f_i(P) = 0$ (*cf* Grünbaum, 1967).

Partitions of numbers in the theory of numbers (*cf* Hardy and Wright, 1979) has a similar idea to what we shall do in § 6.11 for finding the Voronoi sections and their grids. Moreover, the random nature of these two problems, that is percolation and the number theory, as well as their omnipotence seem to point out that there could be some closer relationship between the two than mathematicians and physicists believe at present.

Also there is another similarity between these two fields, that is both are easy to state but very difficult to solve.

Sphere packing studies the density of packings of hard spheres. Here the kissing number problem studies the number of spheres that can be arranged such that all of them touch one central sphere of the same size. In other words it is the maximum number of neighbours that a sphere can have. It is also called the ligancy or Newton-, contact or coordination numbers.

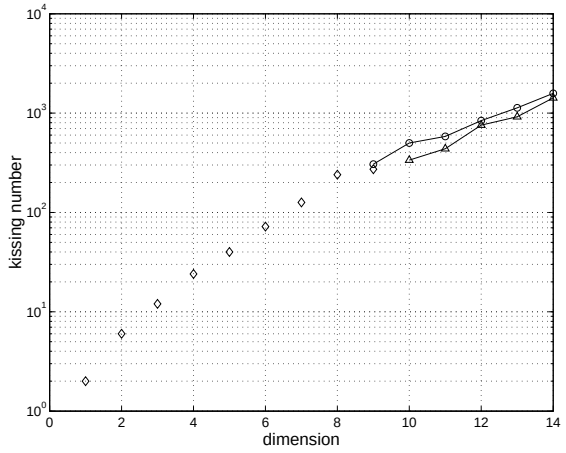

For n dimensions the lower bound for the kissing number is $\eta = \zeta(n)/2^{n-1}$, where

$$\zeta(n) = \frac{1}{\Gamma(n)} \int_0^\infty \frac{x^{n-1}}{e^x - 1} \mathrm{d}x$$

is the Riemann zeta function. In Figure 1.1 the a diamond symbol represents an exact value for a lattice, a triangle the lower bound for a lattice, while a circle the lower bound for a nonlattice. The lines linking these symbols are for the ease of look only.

Figure 1.1 Kissing number versus dimension.

On the other hand, the covering problem is a problem that tries to find the least dense way to cover a space in n dimensions with overlapping spheres of the same size while the quantising problem studies how to place points in such a way that minimise the average second moment of their Voronoi cell, which finds application in the conversion from analogue to digital (Conway, 1988). In two dimensions the hexagonal lattice solves the packing, kissing, covering and quantising problems. But the packing problem of hard spheres is still unsolved. Everybody knows that the solution is approximately 0.7405 or exactly $\pi/3\sqrt{2}$ but no one has been able to prove it.

For any lattice the fundamental polytope, *i.e.* a polytope consisting of points $\sum_i^n \theta_i \nu_i$ where $0 \leq \theta_i < 1$, is its fundamental region. The proportion of space occupied by the spheres is the volume of one sphere divided by the volume of fundamental region, while the latter quantity is equal to $(\det \Lambda)^{1/2} = \det M$. Here $M = [\nu_{i,j}]$, $1 \leq \nu_{ij} \leq m$, is the generator matrix for lattice Λ and each ν_i is a basis vector having ν_{ij} coordinates.

§ 1.2 Geometry

If the equation of a plane be $ax + by + cz + d = 0$, then $(a, b, c)^T$ is a vector normal to it and the parametric equations of this line is $x = at + p$, $y = bt + q$ and $z = ct + r$, $t \in R$, and (p, q, r) is a point on the line.

The simplest geometrical figure is a circle while the simplest of all polygons is a triangle. The degree of freedom of triangles increases from the equilateral to the isosceles and the right triangles to the scalene triangles. While spending the summer of 1990 in a traineeship through AIESEC the author was introduced to a geometrical puzzle which, as he later knew, is called the *flexatube*. It could have come from ancient China. This puzzle is made up of sixteen right isosceles triangles tiled into four squares, each comprising of four triangles, which are in turn joined together to form a loop. It can be easily made up using some hard papers, a pair of scissors and cello tape. There are in total twenty hinges, four of which are as long as the hypothenuse while the other sixteen have their length equal to the shorter side of the triangle. By turning these rigid triangles upon their hinges the inside surface of the strip can become the outside and vice versa. Tiyapan found one solution and later on the same year learnt about another. It has not yet been proved whether these two are the only possible solutions. Geometry plays not a small part in our everyday's life, for instance the symbol for the men's toilets in Budapest is an equilateral triangle, while that for women's toilets is a circle. Thus the geometrical information, having passed through the eyes, goes directly to the brain and we understand with no words being needed.

The median of a triangle is the line joining its vertex with the mid point of the opposite side. All the medians of a triangle intersect one another at its centroid. The lines connecting all mid points of a triangle divide it into four equal triangles. Let the length of the median from the corner A to its opposite side a of a triangle be m_a, then $m_a = (2b^2 + 2c^2 - a^2)^{1/2}/2$, and similarly for m_b and m_c. We have the relations $\mathrm{A}(\triangle m_a m_b m_c) = 3\mathrm{A}(\triangle abc)/4$, where $\mathrm{A}(\triangle \cdot)$ is the area of a triangle, and $m_a^2 + m_b^2 + m_c^2 = 3(a^2 + b^2 + c^2)/4$.

One end of a median is at a vertex, the other one at the mid point of a side. The lines which bound the first ones is the triangle itself, those which join the second ones create the medial triangle. A bisector of a medial triangle divides the perimeter of the original triangle into two equal parts.

The incentre of the medial triangle, the Spieke point, is the c.g. of the wire-framed triangle $\triangle ABC$. The incentre, the geocentre and the Spieke point, all lie on a single straight line. The geocentre on the Euler line is one third away from the circumcentre to the orthocentre, that point where the altitudes of the triangle intersect.

In general dimension we talk about spheres. A sphere in d dimensions has its volume, V, proportional to r^d and its surface, A, to r^{d-1}, so that $V \propto A^{d/(d-1)}$.

The area of sphere in three dimensions is $A = 4\pi r^2$ and the volume $V = \frac{4}{3}\pi r^3$. When $V = 1$, $r = -(-3/\pi)^{1/3}/2^{2/3}$, $(3/\pi)^{1/3}/2^{2/3}$, or $(-1)^{2/3}(3/\pi)^{1/3}/2^{2/3}$ which are numerically $-0.310175 - 0.537239\imath$, 0.62035, -0.310175, $-0.310175 + 0.537239\imath$ in that order. Therefore $\alpha = A|_{V=1} = 6^{2/3}\sqrt[3]{\pi} = 4.83598$

When $V = 8$, $r = (6/\pi)^{1/3}$ and therefore $A = 46^{2/3}\pi^{1/3} = 19.3439$. In order to find α, the surface area per unit volume, one divide the area by $V^{2/3}$, in other words $\alpha = V^{1/3} \cdot A/V = A/V^{2/3}$.

The same is true for other polyhedra. For example in a tetrahedron where x is the length of the side, the vertices can be $(0,0,0)$, $(x,0,0)$, $\left(\frac{x}{2}, \frac{\sqrt{3}}{2}x, 0\right)$, $\left(\frac{x}{2}, \frac{\sqrt{3}}{6}x, \frac{1}{2}\sqrt{\frac{93}{35}}x\right)$. When $V = 1$, one can obtain x by solving the equation

$$1 = \frac{1}{6}\,\mathrm{abs}\begin{pmatrix}\begin{vmatrix} 0 & 0 & 0 & 1 \\ x & 0 & 0 & 1 \\ \frac{x}{2} & \frac{\sqrt{3}}{2}x & 0 & 1 \\ \frac{x}{2} & \frac{\sqrt{3}}{6}x & \frac{1}{2}\sqrt{\frac{93}{35}}x & 1 \end{vmatrix}\end{pmatrix}.$$

This gives $x = 2\left(\frac{35}{31}\right)^{\frac{1}{6}} = 2.0409$ as the only real positive answer. When x is doubled, V increases from 1 to 8, which means that one would be dividing A by $V^{\frac{2}{3}}$ to obtain α.

The perimeter of a triangle is $s = 3d_e$ and the area $A = (\sqrt{3}/4)l^2$. When $A = 1$, $d_e = \pm 2/3^{1/4} = \pm 1.51967$. Therefore $s = 4.55901$.

Vertices shared by two cells make up a common face between them. Two way have been tried for finding the edges. The first one was by looking at all neighbouring cells of every cell in turn three at a time. The edges are then made up of those vertices that are common among these three cells. Only those edges which have exactly two vertices are considered. They are called *good edges* as contrasted with edges on the boundary. This is a much longer way than the second one, which is to consider vertices common to any two faces of a cell. Similar to the first case, such vertices forms a good edge if and only if there are only two of them. The two methods above give exactly the same list of edges, so they confirm each other. It has been tested that all edges having more than two vertices are boundary ones, that is they have at least one vertex outside the boundary of the unit cube considered.

By drawing some of the cells as a solid using *fill* command it has been tested that the result from `convhull` covers the entire cell surface. This confirms the step where areas are calculated.

The hexagon or honeycomb is perhaps the pattern which is most frequently found in nature. Even though the world we live in is three-dimensional, cells normally divide and spread in two dimensions in the form of layers. Moreover, they are packed in these layers in patterns which most often resemble the honeycomb (*cf* Williams and Bjerknes, 1972).

An octagon is an eight-sided polygon. It is the shape of the cross section of every chimney in the mills built in Manchester during its industrial era of the nineteenth century, as well as that of the terrets in the Main Building of UMIST. Perhaps one of the reasons for its popularity is that it looks strong while having the style of a good taste. May be the reason why it looks strong is that it possesses eight axes of symmetry, on top of another symmetry around the origin.

There are nine regular polyhedra. Among these are five regular convex solids known to the ancient Greek called Platonic polyhedra. They are tetrahedron, cube, dodecahedron, octahedron, and icosahedron. They have regular congruent faces and regular polyhedral angle vertices. Their face angles and their dihedral angles at every vertex are equal. The other four regular polyhedra have only been discovered much later and are not convex. They are called the Kepler-Poinsot polyhedra and are nonconvex. The small stellated dodecahedron and the great stellated dodecahedron were found by Kepler (1571–1630). The great icosahedron and the great dodecahedron were found by Poinsot (1777–1859). The small stellated dodecahedron and the great dodecahedron do not satisfy Euler's equation. The process of creating it by extending nonadjacent faces until they meet is called *stellating*. There are also polyhedra called quasi-regular.

The semi-regular polyhedra are called the Archimedean polyhedra. Here all faces are regular polygons but not all are of the same kind. Every vertex is congruent to all others. They comprise of an infinite group of prisms, an infinite group of antiprisms or prismoid, and another thirteen polyhedra. Each prism or prismoid is made up of two regular polygons on parallel planes where the vertices are aligned in the former case or shifted half way to the next neighbouring vertices in the latter case. Each vertex in prisms is joined to a corresponding vertex of the opposite polygon, while in prismoid it is joined to two corresponding vertices. All faces of an Archimedean solid are regular and all its polyhedral angle vertices congruent.

On the other hand the Archimedean duals have the property that all their faces are congruent to one another and all their polyhedral angles regular. These solids are important in crystallography. They are vertically regular and include an infinite group of dipyramids, an infinite group of trapezohedra, and additionally thirteen other polyhedra.

The surface area per unit volume α of a solid can be computed from the actual volume V and the actual surface area A as $\alpha = V^{1/3}A/V = AV^{-2/3}$. Another way of finding the perimeter per unit area of an n-gon follows the steps listed in Algorithm 1.1. Here θ is the angle made by the lines from the centre of gravity of an n-gon to its two consecutive vertices, α half the angle between two edges, h the distance from the c.g. to each edge, that is the height of one of the n identical triangles all of which have a vertex at the c.g., a the area of each of such triangles, $A(d)$ the area of the n-gon in terms of the edge length, s the perimeter and d the edge length d_e. Algorithm 1.1, however, may be reduced to two steps, namely solving for $(nd^2/4)\tan[(n-2)\pi/(2n)]$ and then $s = nd$. Of course, if n increases towards infinity then s approaches $2\sqrt{\pi} \approx 3.5449$.

Algorithm 1.1 *Perimeter per unit area of regular polygons.*

$\theta \leftarrow 2\pi/n$;
$\alpha \leftarrow (\pi - 2\pi/n)/2$;
$h \leftarrow (d/2)\tan\alpha$;
$a \leftarrow (1/2)dh$;
$A(d) \leftarrow na$;
solve $A(d) = 1$ **for** d
$s \leftarrow nd$; □

Polygon	n_e	A	s *(numerical)*
Triangle	3	$(\sqrt{3}/4)d^2$	4.55901
Square	4	d^2	4
Pentagon	5	$5(1+\sqrt{5})d^2/\left[4(10-2\sqrt{5})^{1/2}\right]$	3.8119
Hexagon	6	$3\sqrt{3}d^2/2$	3.7224
Heptagon	7	$(7/4)d^2\tan(5\pi/14)$	3.6721
Octagon	8	$2d^2\tan(3\pi/8)$	3.6407
Nonagon	9	$(9/4)d^2\tan(7\pi/18)$	3.6198
Decagon	10	$5\left[(5+\sqrt{5})/2\right]^{1/2}d^2/(-1+\sqrt{5})$	0.3605
Undecagon	11	$(11/4)d^2\tan(9\pi/22)$	3.5944
Dodecagon	12	$3(2+\sqrt{3})d^2$	3.5863

Table 1.2 *Perimeter per unit area of n-gons.*

In a similar fashion the surface area and volume of regular solids can be found, but first we need to know more about these solids. Table 1.3 lists some of the important properties of regular solids. Here cyc$(\cdot)$ is the cyclical permutations and $\tau = (1+\sqrt{5})/2$, *i.e.* the golden ratio. Regular polyhedra can also be represented by Schlafi's symbol as $\{p, q\}$ where p and q are respectively the face- and vertex figures.

solid	*aka*	n_v	n_e	n_f	x_v	d_e	r_v	r_e	r_f	*dual*
tetrahedron	3|2 3	4	6	4	$(\pm1,\pm1,\pm1)$ even or odd -1's	$2\sqrt{2}$	$\sqrt{3}$	1	$1/\sqrt{3}$	itself
cube	3|2 4	8	12	6	$(\pm1,\pm1,\pm1)$	2	$\sqrt{3}$	$\sqrt{2}$	1	octahedron
octahedron	4|2 3	6	12	8	cyc$(\pm1,0,0)$	$\sqrt{2}$	1	$1/\sqrt{2}$	$1/\sqrt{3}$	cube
dodecahedron	3|2 5	20	30	12	cyc$(0,\pm\tau,\pm1/\tau)$, $(\pm1,\pm1,\pm1)$	$2/\tau$	$\sqrt{3}$	τ	$\tau[(\tau+2)/5]^{1/2}$	icosahedron
icosahedron	5|2 3	12	30	20	cyc$(\pm1,0,\pm\tau)$	2τ	$\sqrt{2+\tau}$	1	$(6+5\tau)^{1/2}/3$	dodecahedron

Table 1.3 *Some important properties of regular solids.*

The ratio between the edge length and distance to face, the surface area, the volume and the ratio between surface area and volume of some solids are shown in Table 1.4.

solid	d_e/r_f	A	V	α
Tetrahedron (3^3)	$2\sqrt{6}$	$24\sqrt{3}r^2$	$8\sqrt{3}r^3$	7.2056
Cube, (4^3)	2	$24r^2$	$8d^3$	6
Octahedron, (3^4)	$\sqrt{6}$	$12\sqrt{3}r^2$	$4\sqrt{3}r^3$	5.7191
Dodecahedron,(5^3)	$\frac{4\sqrt{10}}{(3+\sqrt{5})(5+\sqrt{5})}$	$300\frac{2}{5-\sqrt{5}}^{\frac{1}{2}}\frac{(1+\sqrt{5})r^2}{25+11\sqrt{5}}$	$100\left(\frac{2}{5-\sqrt{5}}\right)^{\frac{1}{2}}\frac{(1+\sqrt{5})r^3}{25+11\sqrt{5}}$	5.3116
Icosahedron, (3^5)	$3(1+\sqrt{5})\left[6+\frac{5}{2}(1+\sqrt{5})\right]^{\frac{1}{2}}$	$180\sqrt{3}\frac{(3+\sqrt{5})r^2}{17+5\sqrt{5}}$	$60\sqrt{3}\frac{(3+\sqrt{5})r^3}{17+5\sqrt{5}}$	8.0484
Sphere	∞	$4\pi r^2$	$(4/3)\pi r^3$	4.8360

Table 1.4 *Surface area per volume of regular solids.*

Algorithm 1.2 finds the values given in Table 1.4. Here p is the face figure, $n = n_f$ the number of faces, $r = r_f$ the distance from the centre of the polyhedron to each face, $d = d_e$ the edge length, $s = A/V$ and $\tau = \left[1+\sqrt{5}\right]^{1/2}/2$ the golden mean. Furthermore, a and v are respectively the area of each face and the volume of the pyramid whose base is the face and the apex of which is the centre of the polyhedron.

Algorithm 1.2 *Area per volume of regular polyhedra.*

$\theta \leftarrow 2\pi$;
$\alpha \leftarrow (\pi - 2\pi/p)/2$;
$h \leftarrow d\tan\alpha/2$;
$a \leftarrow pdh/2$;
$v \leftarrow ar/3$;
$A(r) \leftarrow na$;
$V(r) \leftarrow nv$;
solve $V = 1$ for r;
$s(r) \leftarrow A(r)/V(r)$; □

Since Algorithm 1.2 will be used to proof Theorem 1.1, we shall give it a formal proof.

Proof. Each face of a regular polyhedron is a regular polygon by definition. The lines connecting the centre and c.g. of a face with all its vertices divide 2π radian into p equal portions, where p is the face figure. Each portion then represents the angle in radian made by two consecutive vertices of the face as seen from its centre. Let this angle be θ, then it follows that $\theta = 2\pi/p$. From the symmetry around the c.g., all these angles together with the sides of the face form p identical isosceles triangles whose two equal triangles are at the vertices of the face. Moreover, this angle, α, is half the internal angle of a face vertex. Then, because we know that all the internal angles of a regular polygon sum up to $2\pi(n-1)/n$ radian, it follows that $\alpha = (\pi - 2\pi/p)/2$. The area of each face is therefore $a = p(d_e h/2)$, where $h = (d_e/2)\tan\alpha$ is the distance from the centre of the face to its edges. The volume of the pyramid which have the face as its base and the c.g. of the polyhedron as its apex is thus $v = ar_f/3$, and the polyhedral surface area and volume are respectively $A = n_f a$ and $n_f v$. Comparing the above with Algorithm 1.2 completes the proof. □

From the results in Table 1.4 we can see that the sphere has the ratio α less than every regular polyhedron; in fact one could conjecture that it has the smallest s of all solids. Icosahedron, on the other hand, is a regular polyhedron which has maximised α. So now we know, for instance, that a virus wants to maximise its surface area.

The ratio α here is not simply obtained by dividing the surface area by the volume of a solid, as Algorithm 1.4 also tells. We take the volume of a solid to be the unity first, then proceed to find its correspondent surface area. As an example to show that these two values are not the same, consider an icosahedron whose $d_e = 2\sqrt{2}$ and $r_f = 1/\sqrt{3}$. From the values of d_e and r_f the surface area and volume are respectively 362.765 and 37.8252, which result in A/V being 9.5906 which is not the same as our α.

The numerical ratios given in both Tables 1.4 and 1.4 are rounded approximates, to make them easier to read. The exact values can easily be obtained by following the steps of calculation in Algorithms 1.2 and 1.2.

After having worked with Algorithm 1.4 it turns out that α depends on r_f. A little investigation confirms this, and Theorem 1.1 arises as a result. A platonic solid is a regular solid and vice versa.

Theorem 1.1. *Let α be the surface area of a Platonic solid and r_f the distance from its centre to each face. Then $\alpha r_f = 3$.*

Proof. There are five and only five such solids, therefore we find α of every one of them. Assuming that Algorithm 1.2 together with the resulting A's and V's shown in Table 1.4 are correct. Then

simply divide each $A(r)$ by the corresponding $V(r)$ for the regular solids from the table to get $\alpha = A(r)/V(r) = 3/r$. □

Collorary 1.1[1] follows immediately from Theorem 1.1 and the definition of α, but such interesting consequence as it is deserves being called a collorary.

Corollary 1.1[1]. *In a regular polyhedron,* $Ar_f = 3V$.

The duality among regular polyhedra is shown in Table 1.4. In particular, the tetrahedron is dual to itself, the octahedron and the cube are dual to each other and likewise the dodecahedron and the icosahedron. The icosahedron is a popular shape among viruses. As regarding duality, it is worth noting that all pyramid are self-dual.

Deltahedra are polyhedra which have all faces equilateral triangles. They have $2n$ faces, $3n$ edges and $n + 2$ vertices. There are eight deltahedra, namely regular tetrahedron (4 faces), triangular dipyramid (6), regular octahedron (8), pentagonal dipyramid (10), snub disphenoid (12), triaugmented triangular prism (14), gyroelongated square dipyramid (16) and icosahedron (20).

A cube is sometimes called a hexahedron because it has six faces. But there are other polyhedra which also have six faces, for instance the triangular dipyramid (5 vertices, 9 edges), the pentagonal pyramid and the tetragonal antiwedge (6, 10), the hemiobelisk and hemicube (7, 11) and the pentagonal wedge (8, 12).

polyhedron	n_v	n_e	n_f
antiprism	$2n$	$4n$	$2n+2$
antiwedge	$2n-2$	$4n-6$	$2n-2$
cupola	$3n$	$5n$	$2n+2$
cupola pyramid	$3n+1$	$7n$	$4n+1$
cupolarotunda (ortho-, gyro-)	$5n$	$10n$	$5n+2$
deltohedron	$2n+2$	$4n$	$2n$
dipyramid	$n+2$	$3n$	$2n$
hemiprism	$2n-1$	$3n-1$	$n+2$
ortho(,gyro-)bicupola	$4n$	$8n$	$4n+2$
ortho(,gyro-)birotunda	$6n$	$12n$	$6n+2$
prism	$2n$	$3n$	$n+2$
pyramid	$n+1$	$2n$	$n+1$
rotunda	$4n$	$7n$	$3n+2$
rotundapyramid	$4n+1$	$9n$	$5n+1$
wedge	$2n-2$	$3n-3$	$n+1$

Table 1.5 *The number of vertices, edges and faces of some polyhedra*

The nearest neighbour and minimum spanning tree have been applied to the problem of taxonomy in botany. Clayton (1972), working on the characters of plants to manually classify them (*eg* Clayton, 1970) with the use of only the binary dendrogram and trial and error, adopted a numerical method which finds the minimum spanning tree in a multi-dimensional character space. Since taxonomy can be considered as a kind of dictionary, it is possible to apply a similar approach to machine translation and the compilation of dictionaries.

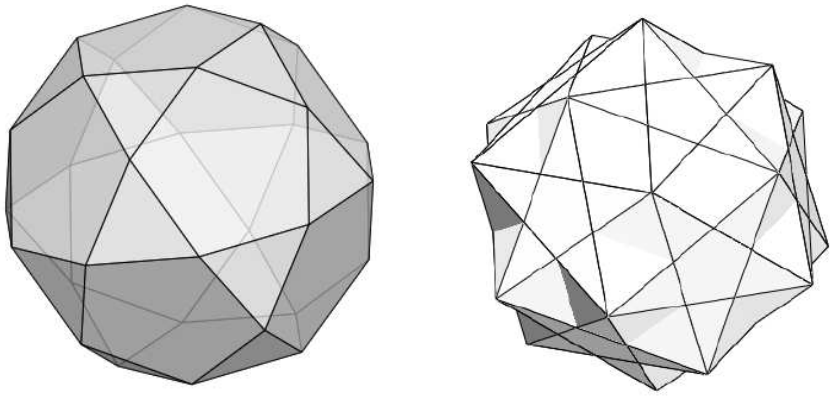

(a) (b)

Figure 1.2 (a) *Icosidodecahedron, rhombic triacontahedron,* 2|3 5. (b) *Small ditriagonal icosidodecahedron, small triambic icosahedron,* 3|5/2 3

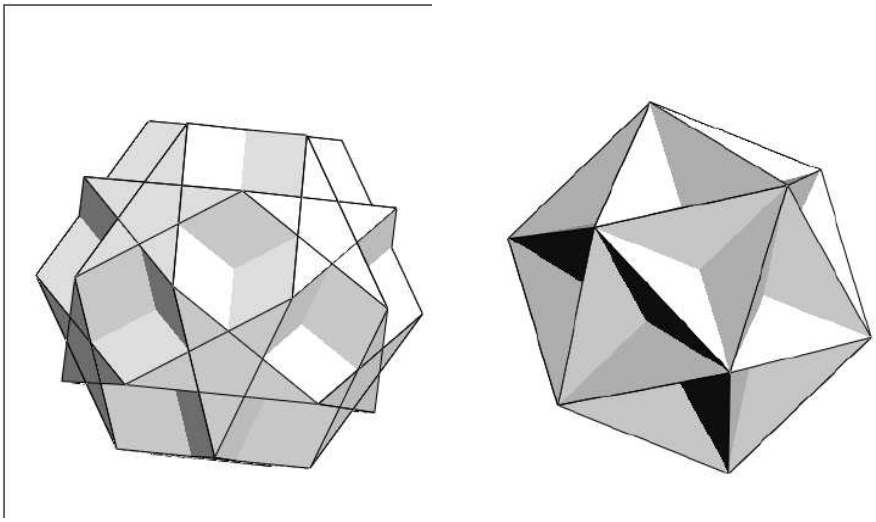

(a) (b)

Figure 1.3 (a) *Great dodecadodecahedron, medial rhombic triacontrahedron,* 2|5/2 5. (b) *Great dodecahedron, small stellated dodecahedron,* 5/2|2 5

The polyhedra from Figure 1.4 to 1.6 are semi-regular.

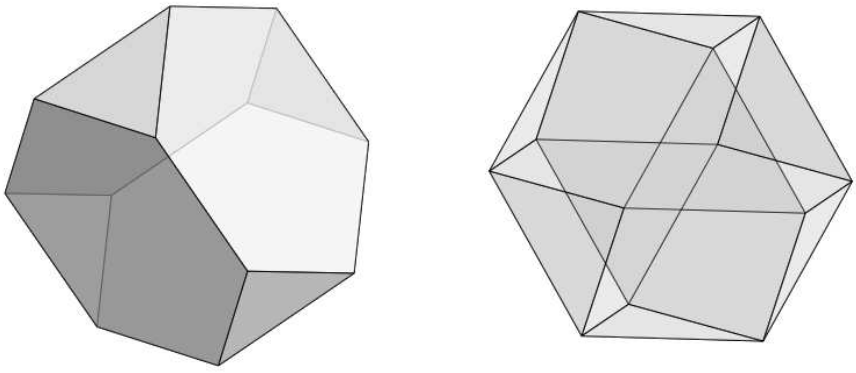

(a) (b)

Figure 1.4 (a) *Truncated tetrahedron, triakistetrahedron,* 2 3|3. (b) *Octahemioctahedron, octahemioctacron,* 3/2 3|3

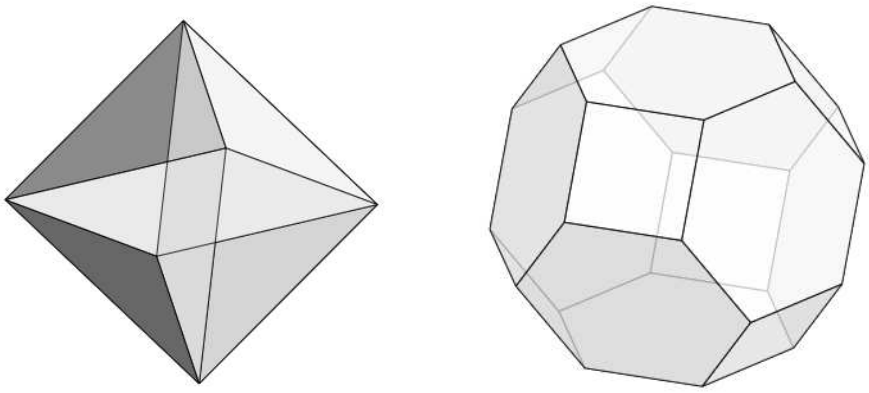

(a) (b)

Figure 1.5 (a) *Tetrahemihexahedron, tetrahemihexacron,* 3/2 3|2. (b) *Truncated octahedron, tetrakishexahedron,* 2 4|3

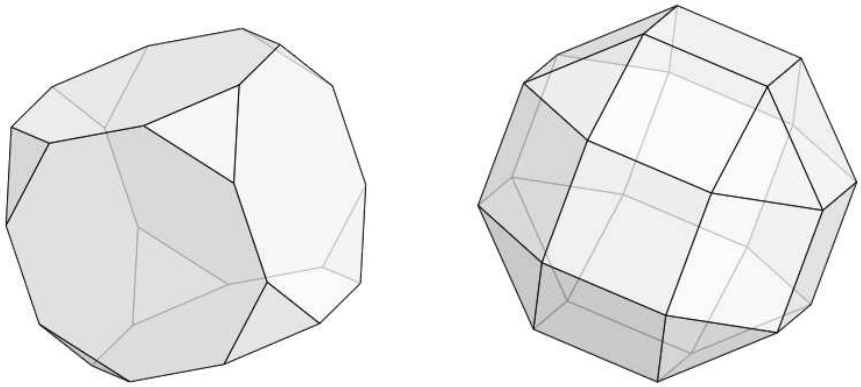

(a) (b)

Figure 1.6 (a) *Truncated cube, triakisoctrahedron,* 2 3|4. (b) *Rhombicuboctahedron, deltoidal icositetrahedron,* 3 4|2

Polyhedra in Figure 1.7 are snub polyhedra.

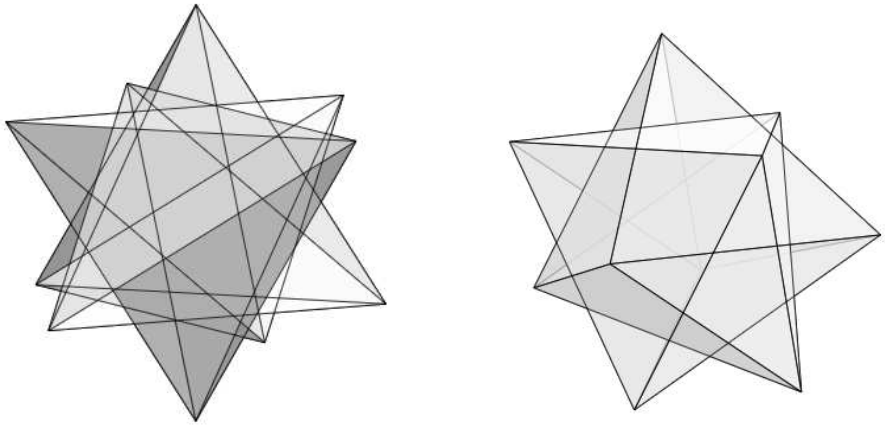

(a) (b)

Figure 1.7 (a) *Pentagrammic crossed antiprism, pentagrammic concave deltohedron,* |2 2 5/3. (b) *Pentagrammic antiprism, pentagrammic deltohedron,* |2 2 5/2

The surface of Fullerene is made up of pentagons six-sided figures. Its shape represents that of the geodesic domes developed by Buckminster Fuller, and hence the name *Fullerene*. The latter may either be hexagons or figures all the six sides in each one of which form two sets of three sides having an equal length. The simplest Fullerene, the carbon-60 molecule, has the same shape as that of a football and a handball. With some thought the reason for this is not difficult to see. With its thirty-two faces it closely resemble the sphere. Also the two different shapes of all its components are symmetrically distributed and therefore enable colouring with only two different colours, namely one for each of the two shapes. To see how this helps, suppose one made a football in the shape of a bloated dodecahedron. Then it would be impossible to colour it using more than one colour at the same time of giving it a symmetrical appearance when viewed from more than a few directions. With the fullerene shape and the colouring scheme mentioned, however, the football looks symmetrical when viewed from 54 different directions symmetrically distributed around it. These directions corresponds to those when one looks at it in the direction perpendicular to the centre of each of its faces and when in the direction through the middle of each of the 22 edges lying between two hexagonal faces.

Making polyhedron models is an educating experience. Contrary to the general believe that you need to make an accurate drawing for the required parts (Wenninger, 1971), this needs not be so. Examples of this are the origami models of polyhedra where complex polyhedron structures are

made from interlocking pieces each of which is made by folding a piece of paper of a rectangular or square shape.

A set of elements with the sum and the product of any two elements defined is a commutative ring if under these two operations it satisfies the following postulates: closure, uniqueness, commutative, associative, and distributive laws, identity (zero and unity), and additive inverse. An integral domain is an ordered domain if its positive elements satisfy the laws of addition, multiplication, and trichotomy. A subset of an ordered domain is well-ordered if every nonempty subset of it contains a smallest member. $a|b$ means that $.b$ is divisible by a. The Euclidean algorithm or division algorithm states that $a = bq + r, 0 \leq r < b$. Two integers are relatively prime if their only common divisors are ± 1. $a \equiv b (\mathrm{mod}\, m)$ if and only if $m|(a - b)$. The commutative ring Z_2 is the properties of multiplication and addition of even (0) and odd (1) numbers.

$+$	*0*	*1*
0	0	1
1	1	0

$\cdot$	*0*	*1*
0	0	0
1	0	1

The following is Z_5.

$+$	*0*	*1*	*2*	*3*	*4*
0	0	1	2	3	4
1	1	2	3	4	0
2	2	3	4	0	1
3	3	4	0	1	2
4	4	0	1	2	3

$\cdot$	*0*	*1*	*2*	*3*	*4*
0	0	0	0	0	0
1	0	1	2	3	4
2	0	2	4	1	3
3	0	3	1	4	2
4	0	4	3	2	1

There is a close link between geometry and algebra. Geometrical surfaces can be described as algebraical equations. For example, for circles and polygons the equations are binary quadratic, while for spheres and polyhedra they are ternary quadratic. Even one-sided surfaces can be described algebraically. The equation of Klein bottle, when deformed into a sphere with two circles removed and replaced by two cross-caps, is a quartic equation

$$a^2(x^2 + y^2)(b^2 - x^2 - y^2) = z^2(a^2x^2 + b^2y^2),$$

while the Steiner surface is also a quartic one

$$y^2z^2 + z^2x^2 + x^2y^2 + xyz = 0.$$

Two surfaces is homomorphic to each other if it is possible to continuously transform one into the other. All convex polyhedra are homomorphic to a sphere. The Steiner surface is homomorphic to the heptahedron, which is an Archimedean polyhedron with diametral plane.

In the plane, a second-degree equation gives either two straight lines, a circle, an ellipse, a parabola, or a hyperbola. In space, it can give two planes, cylinders and cones (circular, elleptic, parabolic, or hyperbolic), aphere, spheroid, ellipsoid, two hyperboloids, and (elliptic or hyperbolic) paraboloid.

Partition, *tessellation* and *division of space* are the same thing. In the context of set theory, a partition of set X is a family of sets A_1, A_2, ..., A_k which are subsets of X, such that $A_i \neq \emptyset$; $A_i \cap A_j = \emptyset$; $\bigcup_i A_i = X$, where i, $j = 1, 2, \ldots, k$ and $i \neq j$. (*cf* Berge, 1958) A further condition that makes any tessellation a Voronoi one is that, for all i there exists a unique point a_i within A_i such that every point in A_i is closer to a_i than to any other a_j, $j \neq i$.

Voronoi tessellation in three dimensions can be constructed by imagining each region as a spherical cell growing outwards to meet neighbouring cells and continue growing to fill the gaps. The centre of each sphere is a unique nucleus point of the region such that it is closest to any point belonging to that region than any nuclei points. If the rate of growth is the same from every cell, the resulting partitions will be planes which can be described by ternary quadratic equations. However, if this rate differs from one cell to another, the partitions will be curved surfaces and the result is a non-Voronoi tessellation. It is possible to impose a constraint of minimum distance between neighbouring nuclei. Such cases can be looked at as spheres of an equal nonzero radius expanding away from nucleus centre points. If the radii differ from one sphere to another, or if some nonspherical solids are used instead of spheres, the tessellation obtained will be non-Voronoi.

Consider the case where all spheres are of equal size. If these spheres already touch their neighbours before the expanding starts, the case is that of packed spheres expanded to form a Voronoi tessellation. There are two types of close-packing: cubic (face-centred) and hexagonal. In both cases each sphere has twelve neighbours. Both cases have the same density, which is $\frac{\pi}{3\sqrt{2}}$. The Voronoi regions produced from the cubic case are rhombic dodecahedra and the faces are rhombuses.

In the case of hexagonal close-packing, the corresponding regions are trapezo-rhombic dodecahedra and the faces are either rhombics or trapezia. Where the spheres meet with their three neighbours in the layer above and their three neighbours in the layer below, the faces are rhombics. Where they meet with the six neighbours on the same layer they are trapezia.

For geometrical calculation, an example of a definitive book is that written by Salmon (1912).

The gamma function,

$$\Gamma(z) = \int_0^\infty e^{-t} t^{z-1} \mathrm{d}t, \quad \mathrm{Re}(z) > 0, \qquad (\mathbf{1})_\mathrm{i}$$

got its name from Legendre and is known as the Euler gamma function or simply the second Euler function. The formula $\Gamma(z+1) = z\Gamma(z) = z!$ recursively calculates the gamma function from, for instance, $\Gamma(1/5) \approx 4.5908$, $\Gamma(1/4) \approx 3.6256$, $\Gamma(1/3) \approx 2.6789$, $\Gamma(2/5) \approx 2.2182$, $\Gamma(1/2) = \sqrt{\pi} \approx 1.7725$, $\Gamma(3/5) \approx 1.4892$, $\Gamma(2/3) \approx 1.3541$, $\Gamma(3/4) \approx 1.2254$, and $\Gamma(4/5) \approx 1.1642$. The Stirling's formula was found by de Moivre which approximates the gamma function. The gamma function expansions is

$$\Gamma(x+1) = \lim_{k\to\infty} \frac{k^x 1 \cdot 2 \cdot 3 \cdots k}{(x+1)(x+2)\cdots(x+k)}, \qquad (\mathbf{2})_\mathrm{i}$$

and the gamma function of negative numbers can be obtained from

$$\Gamma(-z) = \frac{-\pi}{z\Gamma(z)\sin \pi z}. \qquad (\mathbf{3})_\mathrm{i}$$

The incomplete gamma function is

$$\Gamma(z,x) = \int_0^x e^{-t} t^{z-1} \mathrm{d}t = \int_x^\infty e^{-t} t^{z-1} \mathrm{d}t, \qquad (\mathbf{4})_\mathrm{i}$$

and the normalised or regularised incomplete gamma function is $\Gamma(z,x)/\Gamma(z)$

Archimedean solids are dual to Catalan solids. The fullerene C_{60} is the truncated icosahedron, an Archimedean solid. Table 1.6 shows some statistics of the Archimedean solids.

Archimedean solid	n_v	n_e	n_f	*dual, Catalan solid*
truncated tetrahedron	12	18	8	triakis tetrahedron
cuboctahedron	12	24	14	rhombic dodecahedron
truncated cube	24	36	14	triakis octahedron
truncated octahedron	24	36	14	tetrakis cube
rhombicuboctahedron	24	48	26	deltoidal icositetrahedron
snub cube	24	60	38	pentagonal icositetrahedron
icosidodecahedron	30	60	32	rhombic triacontahedron
great rhombicuboctahedron	48	72	26	disdyakis dodecahedron
truncated icosahedron	60	90	32	pentakis dodecahedron
truncated dodecahedron	60	90	32	triakis icosahedron
rhombicosidodecahedron	60	120	62	deltoidal hexacontahedron
snub dodecahedron	60	150	92	pentagonal hexacontahedron
great rhombicosidodecahedron	120	180	62	disdyakis triacontahedron

Table 1.6 *Archimedean solids*

The analogue of polyhedra in four dimensions is sometimes called polychora, with the 4-d equivalent of the Euler-Descartes formula being $n_v - n_e + n_f - n_c = 0$ where n_c is the number of its 3-d facets called cells. For dimensions higher than four the analogies are polytopes. An n-dimensional polytope is bound by hyperfaces of polytopes of $(n-1)$ dimension which join at hyperedges of $(n-2)$ dimensions.

The Euler characteristic χ is 1 for a point, invariant in a topological homeomorphism and additive for disjoint sets. For Euclidean space in n dimensions, $\chi = (-1)^n$ as that of ordinary open polytopes. The χ of all ordinary closed polytopes is the χ of a closed n-dimensional ball, and $\chi = 1$ for any n dimensions. If the hypercell itself, *i.e.* the interior of the polytope, is not counted then the right hand side of the formula becomes 2 when n is odd and 0 otherwise, for example $n_v - n_e + n_f - n_c + n_t - n_p + n_h = 2$ in 7 dimensions, where t, p and h are respectively the tetrafaces (sometimes called hyperpoints), pentafaces (hyperedges) and hexafaces (hyperfaces).

As a revision of the sixth form mathematics, selections are *combination* if the order is irrelevant, and are *permutation* otherwise. The formula is for the former ${}^nC_k = n!/[n!(n-k)!]$, and ${}^nP_k = n!/(n-k)!$ for the latter.

Definitions which are useful when describing the time- and storage complexities of an algorithm are $O(f(n)) = \{g(n) : \exists c, n_0 \in R^+, g(n) \leq cf(n) \forall n \geq n_0\}$, $\Omega(f(n)) = \{g(n) : \exists c, n_0 \in R^+, cf(n) \leq g(n) \forall n \geq n_0\}$, $\theta(f(n)) = \{g(n) : \exists c_1, c_2, n_0 \in R^+, c_1 f(n) \leq g(n) \leq c_2 f(n) \forall n \geq n_0\}$ and $o(f(n)) = \{g(n) : \forall c \in R^+ \exists n_0 \in R^+, g(n) \leq cf(n) \forall n \geq n_0\}$, the most commonly used for the purpose being the $O(\cdot)$.

A geometry, in Klein's view, is a set S and a subgroup G of the group $B_{ij}(S)$ of all bijections from S to itself. The elements of S are points, and G acts on S by mapping points to points. Two subsets of S are equivalent if there is an element of G which takes one set into the other. In general, S has an extra structure which $B_{ij}(S)$ preserves. A map $f : \mathrm{R}^m \mapsto \mathrm{R}^n$ is linear if it maps a linear combination of vectors to the same linear combination of the images. A matrix (a_{ij}), $1 \leq i \leq m$ and $1 \leq j \leq n$, transforms each basis element b_i to a combination of the basis elements b_j. The map is a bijection if f^{-1} exists or equivalently if the determinant of its matrix is non-zero. The general linear group, $GL(n, \mathrm{R})$, is the set of all invertible linear transformations from the vector space R^n to itself. The special linear group $SL(n, \mathrm{R})$, a subgroup of $GL(n, \mathrm{R})$, is the set of all invertible transformations with determinant 1. The orthogonal group, $O(n)$, the set of all orthogonal transformations T. The special orthogonal group $SO(n)$, a subgroup of $O(n)$, is the set of all orthogonal transformations whose matrix has determinant 1.

The group $l(\mathrm{R}^n)$ of all isometries of R^n consists of composites $T_a \circ L$, where $T_a : x \mapsto x + a$ is a translation and L an orthogonal map. The set of all translations forms a normal subgroup of $l(\mathrm{R}^n)$ which is isomorphic to the group R^n under addition.

A summetry group of the subset X of $S = \mathrm{R}^2$ is the subgroup of $l(\mathrm{R}^2)$ whose all elements map to themselves. Rotation by π/n generates a subgroup which is isomorphic to C_n, the cyclic group of order n. The dihedral group D_n, whose order is $2n$, is the group of symmetries of a regular n-gon. For $n \geq 3$, D_n is a non-abelian group.

The affine group, $A(\mathrm{R}^n)$, is the group of all affine transformations or affinities of R^n, that is to say, the transformation of the form $T_a \circ L$ where T_a is a translation and $L \in GL(n, \mathrm{R})$. Affine transformations preserve no distance, angle, area or volume. But they preserve collinearity, parallelism and ratios. A similarity transformation or similitude, $T_a \circ \lambda L$ with $L \in O(n)$ and $\lambda > 0$, is an affine map which preserves angles.

Affine theorems are theorems which can be proved by only those concepts which are preserved by affine transformations. In other words, they are theorems which can be proved by vector methods without using norms, dot- or vector products. Examples of such theorems are the coincidence of the medians of a triangle, Ceva's theorem and Menelaus's theorem.

The homogeneous coordinates of a point x on the affine line are (α, β), where $x = \alpha/bta$. Here a line OA through the origin and a point A on the line $y = 1$ is described by a vector (α, β) in it. The point at infinity has homogeneous coordinates $(1, 0)$. The projective line is denoted by RP^1.

The projective group, $PGL(n, F) = GL(n, F)/\{\lambda I | \lambda \in F - \{0\}\}$ where F is any field, is the set of all projective transformations or projectivities. The standard reference points on RP^1 are ∞, 0 and 1. There is a unique projective transformation which takes any three distinct points to any other three distinct points. Let a, b, c and d be points in RP^1, and θ the map which takes a, b and c respectively to ∞, 0 and 1. Then the cross-ratio is $\theta(d) = (a, b; c, d) = (d-b)/(d-a) \cdot (c-a)/(c-b)$. This cross-ratio is preserved by projective transformations.

The general form of an algebraic surface is $f(x, y, z) = 0$l, where $f(x, y, z)$ is a polynomial in x, y and z. A surface of order one is a plane, of order two a quadratic surface, for example ellipsoids and hyperboloids, and of order three a cubic surface.

§ 1.3 Physics

Percolation has been introduced and developed in the 1950s. (Hammersley et. al., 1954; Broadbent et. al., 1957) A typical physical problem which gives rise to problems in percolation is that of finding the probability that the centre of a sufficiently large porous stone gets wet when immersed in water. The internal structure of such a stone can be viewed as comprised of pores and solids. Water can seep through clusters of pores but is blocked when solids are encountered. Therefore the water can only reach the centre of the stone if there exists an open path, in other words a single cluster of pores, which leads it there. When the size of the rock is sufficiently large, this cluster is called an infinite cluster.

If on the other hand we consider the solids instead of the voids, we can reason that since the stone is rigid there have to exist at least one infinite cluster of solids. Then, because there must be rocks of various degrees of porosity which allow water to pass through, there must be a range

of porosity which at one end is a nonpermeable stone where there exists an infinite cluster of solids but not an infinite cluster of pores, while at the other end it is the other way round, that is there exists an infinite cluster of pores but not one of solids. In other words, the latter case is the case where the rock has disintegrated into pieces. If one considers the pores and the solids as being two phases opposite to each other, then one can reason that the total volume of the two stays the same, whereas the ratio between them could vary.

The study of blockages in porous media can be translated into the study of percolation on the media when pores randomly turn into solids. In other words, it is the study of the formation of an infinite cluster of one phase within the infinite mass of the other. More often the latter infinite mass is taken for granted as always exists and remains the same. The domain of consideration is thus reduced to only the original pore spaces. Then, the study becomes that of inversion between two phases, namely the infinite cluster of free pores and the finite clusters of free pores. While the existence of an infinite cluster or finite clusters of blockages is of no consequences when one is only interested in the percolation point, it is considerably important when one wants to contemplate on the behaviours on either side of that critical point. It is important also when one studies changes in the rate of flow through the media.

One example is the study of traffic networks. Traffic congestion can be described as three degrees of flowability: free-flowing, congested, and stand-still. In a free-flowing traffic there are infinite clusters of roads and finite clusters of blocked roads. In a congested traffic there are both infinite clusters of roads and infinite clusters of blocked roads. In a stand-still traffic there are no infinite clusters of roads, while there are infinite clusters of blocked roads.

Applications of the percolation theory includes the study of forest fires and epidemics, the study of defects in semiconductors, the study of the effective resistance of a disordered mixture of two materials, the study of the Curie point of spontaneous magnetisation in ferromagnets and the Ising model, and the study of the rigidity of networks.

Phenomena which contain phase transitions are normally related to percolation theory. Examples of physical phase transition includes the boiling point and the point of evaporation, the transition of materials into superconductivity state, the triggering of a chain reaction in nuclear fission, and the triggering of nuclear fusion of hydrogen burning in a new-born star. Apart from these, there are philosophical phase transitions which include the nature of understanding, the nature of scientific discoveries and technological progress, the making of mobs, revolutions and wars, enlightenment, and, of course, love. Nature is essentially made up of numerous local linear or gradual relationships bound together in a larger scale by abrupt transitions.

The word *percolation* is derived from the word *percolator*, a coffee making machine. The connotation is therefore that of fluid flowing through a porous medium. In dynamic and everyday applications the emphasis is usually on the fluid part, and one studies the point of transition when the flow becomes blocked. There is another side of the same system where one studies the structure of underlying network. In that case the emphasis is on the solid part, and one is interested to find the point where particles percolate to form a solid structure.

Thus the study of percolation falls broadly into two branches, the continuum percolation and the network percolation. The former finds applications in crystallisation where one would like to know the number density of crystals that will make, for example, a synthetic zeolite membrane; in etching of metallic surface where one would like to find the estimates of the shapes and sizes of the etch pits which overlap and form clusters according to etching time and concentration of the acid; or in telecommunication networks where one would like to determine the number of mobile phone cells which percolates a city. The latter finds applications in filtration where one would like to discard filters just before they become blocked or in traffic networks where one could compare the robustness to standstill between two traffic network configurations.

Phase transition occurs in various areas. Wherever it is seen, it has the same characteristic of an intensely exponential change in a short period within a long stretch of a much more gradual one. The rate of change at the point of transition is generally astronomical. The sudden switch from one phase to another found in the study of percolation is a phase transition. The assumption of the existence and occurrence of infinite clusters as an explanation for these transitions can be justified by considering the promptness and the scale of theoretical transitions in a cosmological setting, namely the turning on of the general relativity at Planck time 10^{-43} seconds after the bigbang, the Grand Unified phase transition at 10^{-35} seconds and the start of nucleosynthesis at 1 second (cf. Croswell, 1995).

Temperature of the universe according to the Big Bang theory. The temperature of the universe decreases exponentially and its trend against time has to be plotted on a log-log scale to be comprehensible for otherwise it would lie almost on top of the coordinate axes. Such a plot as shown in Figure 1.8, produced from the data taken from Vaas (2002), roughly approximates a straight line with a negative slope. The percolation at the big bang could possibly be a phase change between matter and antimatter.

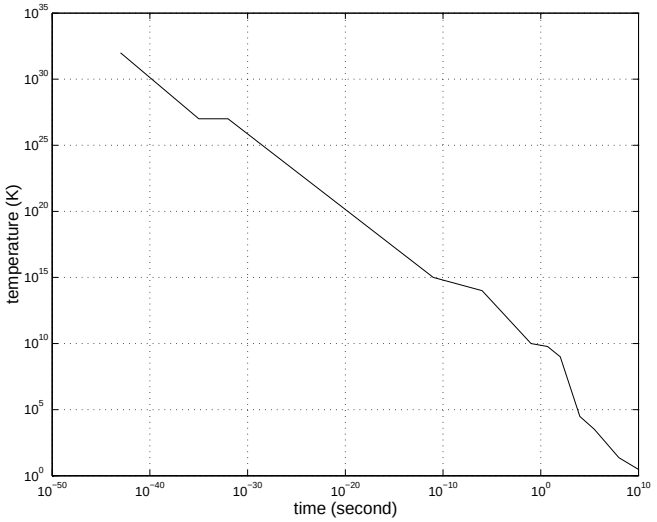

Figure 1.8 Temperature of the universe.

There is an idea in cosmology which could easily be as old as the oldest known religion, that describes the universe as alternating in cycles of destruction and creation. One current theory holding that idea tries to explain the big bang as the collision between two universes in five dimensional space-time. I believe that the universe undergoes phase changes periodically and percolates at the point the same one of which is differently called the big bang, the big crunch, or the big bounce depending how one looks at it. What we see now is only one side of the coin. We can not calculate pass the singularity at the big bang using our present theories because it is another phase complementary to us. That is why that creative singularity baffles us. I believe a theory must exist which can explain both or, if there are more than two, all phases as well as the transition point. And when we finally discover it we will understand the cosmic history and, hopefully, percolation.

In an asymmetric membrane the top dense layer determines the transport rate while the porous sublayer acts as a support. Because the permeation rate is inversely proportional to the thickness of the transport barrier, asymmetric membranes show a much higher permeation rate than homogeneous symmetric membranes of the same thickness.

Soap is solution of a sodium salt of a fatty acid, for example sodium stearate ($C_{17}H_{35}COO^{-}Na^{+}$). The films of soap bubbles are made up of a monomolecular layer of amphipathic ions, which have a hydrophilic and a hydrophobic parts. The former forms a hydrophilic polar carboxyl head, which in the case of sodium stearate is the COO^{-}. The latter forms a tail of hydrocarbon chain, in this case $C_{17}H_{35}$.

	Laboratorical scale		**Industrial scale**	
Process	*Origin*	*Application*	*Origin*	*Application*
microfiltration	Germany, 1920	bacteria filter		
ultrafiltration	Germany, 1930	laboratory use	America, 1960	concentration of macromolecules
hemodialysis	Netherland, 1950	artificial kidney		
electrodialysis			America, 1955	desalination
hyperfiltration			America, 1960	sea water desalination
gas separation	1860	gas treatment	America, 1979	hydrogen recovery
membrane distil -lation			Germany, 1981	concentration of aqueous solutions
pervaporation			Germany and Netherlands, 1982	dehydration of organic solvents

Table 1.7 *Origin of membrane processes.*

J K Mitchell observed gas separation in 1831. In 1860 Thomas Graham made a systematic study of it (*cf* Ismail *et al*, 2002).

There are three categories of synthetic membranes: porous, nonporous, and carrier. Micro- and ultrafiltration use porous membranes while nonporous membranes are used for dialysis, vapour permeation, gas separation and pervaporation. All membranes are required to be mechanically, thermally, and chemically stable. The means of separation, however, varies. For porous membranes

it is the pore dimension, for nonporous membranes the difference in diffusivity or solubility, and for carrier membranes the properties of carrier molecules.

Methods	*pore size (μm)*	*porosity*
coating		
phase inversion		
sintering	0.1–10	10–20%
stretching	0.1–3	90% max
leaching	0.005 min	
etching	0.02–10	10% max

Table 1.8 *Methods of preparation of membranes.*

In cosmology, the structure of the Abell Clusters shows a nonrandom distribution which suggests the existence of a second-order grouping, the clusters of clusters of galaxies (Abell, 1958). Apart from the Milky Way and the Andromeda galaxies (M31 or NGC224) there are at least 44 other galaxies in our Local Cluster. The Local Cluster is on the edge of the Local Supercluster which is flattened in shape and the approximate centre of which is at the Virgo Cluster. The Local Supercluster is separated by a nonspherical void of low galaxy density from the Pisces-Perseus supercluster. The latter lies nearly perpendicular to our line of sight, has the shape of a linear filament, and spans over 90° across the sky. The study of superclusters of galaxies often requires the use of superclusters of computers.

Abell (1958) plotted the distribution of the clusters in what he called, the 'Aitoff equal area projection'. By this he probably means the Hammer, aka Hammer-Aitoff, projection because that is what is normally used for astronomical maps in galactic coordinates as well as for maps of the whole world. Inspired by the Aitoff projection, it was created by H. H. Ernst von Hammer as a modification of the Lambert Azimuthal Equal Area projection. The Hammer projection is equal area while the Aitoff projection is not. Both are similar to each other in that both are modified azimuthal projections where the central meridian is a straight line half the length of the equator, the only point free from distortion is the centre point, and there is a moderate distortion throughout. From investigations I conclude that it is a normal practice in Astronomy and Cosmology to call the Hammer projection as the Aitoff projection.

Powles and Quirke (1984) analyse the numerical trajectory of a molecule in liquid circles by using an empirical fractal parameter called the Richardson coefficient, α. In their simulation they used the Lennard-Jones (12,6) intermolecular potential together with a reduced density and pressure. For the length of molecular trajectories in an argonlike liquid they found $\alpha = 0.65$, in comparison with a similar analysis done on a randomised Koch curve of order 6 which gives $\alpha = 0.25$ and the exact $\alpha = 0.2618\ldots$ for K_∞, the Koch curve of an infinite order. The length of a fractal curve is $L(\epsilon) \propto \epsilon^{-\alpha}$, where ϵ is the step distance or scale. The graph between $\log(L(\epsilon)/\sigma)$ and $-\log(\epsilon/2)$ is a straight line with a positive slope represented by the equation $\log(L(\epsilon)/\sigma) = -\alpha \log(\epsilon/\sigma) + K$ where $K = \log k - (1+\alpha)\log 2$, k being a constant. The Leonard-Jones (n,6) potential is the Van der Waals potential between two atoms which is described in the form $V(r) = C_n/r^n - C^6/r^6$ where C_n and C_6 are constants, and r is the distance between the centres of the two atoms. Similarly, the Leonard-Jones (12,6) potential is $V(r) = 4\epsilon\left((\sigma/r)^{12} - (\sigma/r)^6\right)$. It is sometimes written as $V(r) = \epsilon\left((R/r)^{12} - 2(R/r)^6\right)$, where $R = R_i + R_j$, $\epsilon = \sqrt{\epsilon_i \epsilon_j}$, R_i and ϵ_i being the radius and respactively the interaction energy of each atom. In other words, in the last formula ϵ is the geometrical mean of the interaction energy of each atom while R is the atomic cross-section which is a property of a pair of atoms.

§ 1.4 Cosmological structure

The Lorentz transformation was first written down by Voigt in 1887 as $x' = x - vt$, $y' = y/g$, $z' = z/g$, and $t' = t - vx/c^2$, then by Larmor in 1898, and finally by Lorentz in 1899. Poincaré stated in 1898 on the measure of time that there is no absolute equality of two time intervals. He named the Lorentz transformation after Lorentz and showed that together with the rotations they form a group. Working on the transformations, Einstein announced the special relativity in 1905 as a theory merited by its simplicity and beauty rather than being an explanation of experimental results. For the special relativity and the Lorentz transformations Minkowski founded a four dimensional non-Euclidean space to represent space-time which Einstein adopted used as a basis for his general relativity which appeared in 1915.

Whether the universe is homogeneous or isotropic depends on the scale in which one consider. If the scale is large enough then they can be considered both so but not otherwise. Similarly, an infinite Voronoi network originated from Poisson generators may be considered as being both isotropic and homogeneous because all the irregularities averages out.

Cosmology is related to the study of membranes and filters. Molecules of liquids in a membrane experience forces due to induced dipoles and fixed dipoles. The induced dipoles results in the Lennard–Jones potential whereas the fixed dipoles give rise to a permanent dipole moment between fluid molecules or between molecules of very fine particles.

Inter molecular interactions are approximated by considering the charged parts of the molecule as point charges. The force between charged parts of each molecule and those of its neighbours can be estimated by the Coulomb potential, $V = q_1 q_2/(4\pi\varepsilon_0 r)$, and the Coulomb force between each pair of molecules is $F = q_1 q_2/(4\pi\varepsilon_0 r^2)$.

Analogous to the $1/r$, Coulomb potential in electrostatics is the $1/r$ potential in Swarzshield's expansion for the ten metric or gravitational potential of Einstein for the effect of an elementary concentration of mass in a space-time continuum that is asymptotically flat, that is

$$\mathrm{d}s^2 = \sum_{\alpha\beta} g_{\alpha\beta}\mathrm{d}x^\alpha \mathrm{d}x^\beta = \left(1 - \frac{2Gm}{(c^2 r)}\right)\mathrm{d}r^2 + r^2[\mathrm{d}\theta^2 + \sin^2\theta \mathrm{d}\psi^2] - \left(1 - \frac{2Gm}{(c^2 r)}\right)\mathrm{d}T^2. \qquad (\mathbf{5})_{\mathrm{i}}$$

However, this is not as applicable as the Coulomb potential since the equations in the gravitation theory are nonlinear and therefore the superposition principle does not apply.

The Big Bang can be nothing but a change of phase of the universe. What the other phase may be we can not know, because there is a singularity which divides us from the Yonder Side. But one thing is indisputable, that is if we want to understand the universe, or in plainer words to make any sense out of it, we need to understand the singularity. And since we have to include the percolation theory in our final calculations, we might as well make it the beginning of our quest for a grand unified theory. Whether it is the percolation theory that we already know or another one not yet found is of no consequence. A percolation theory will still be a percolation theory no matter what form it may take, or indeed whatever name you may call it by. Our percolation theory is no percolation theory in a sense that it leaves out half of the picture, that is to say, the singularity that it still does not know how to explain. A true percolation theory is a theory which can includes singularities in its calculation while leaving out nothing that we know already. Give it some other name if you like, but *that* is the real percolation theory.

We now know many things in details, for example how stellar equations must account for mechanical, energy and thermal equilibria and that nuclear reactions imply conservation of charge, nuclear number and lepton number (*cf* Cooper *et al*, 1985). But at the Big Bang every one of these is supposed to break down. Because of this, our picture of the universe will always be incomplete until we can come to terms with that singularity which is our theoretical creator, the Big Bang.

§ 1.5 Filtration

Filtrationis the operation of separating a heterogeneous mixture of a fluid and particles of solids by means of a filtering medium which lets the fluid pass through but not the particles. The name filtration comes from the art of wine making. There are two processes involved, namely the flow of the fluid through the cake and the medium, and the filtration where particles are deposited on or in the medium. The objective is to understand how the rate of flow depends on the properties of both the suspension and the medium, and on the operational conditions.

Both the cake and the medium are porous. As is the case with the cosmological structure (*cf* § ℵ), a filtering medium can be considered as being homogeneous on the large scale, whereas on the small scale it nearly never is (*cf* Heertjes, 1964). In other words, on the scale of the particles and the pores everything concerned is inhomogeneous to a high degree, that is to say, the slurry, the flow, and the cake. The micro-inhomogeneity in the cake can lead to a macro-inhomogeneity. Furthermore, the interaction among the particles, cake, medium and fluid makes the study of filtration ideal ground for numerical studies.

Heertjes (1964) describes the flow through a filter by the Fanning equation, $v = \mathrm{d}V/\mathrm{d}t = (1/\eta\gamma)\mathrm{d}(\Delta P)^\delta/\mathrm{d}R$, where η is viscosity and R the resistance. For viscous flow $\gamma = \delta = 1$, whereas for turbulent flow $\gamma = 0.11$ and $\delta = 0.55$. Both the cake (c) and the medium (m) have the say, so $R_c + R_m = R$, $\Delta P_c + \Delta P_m = P$, and $\Delta P_c/R_c = \Delta P_m/R_m$. The specific resistance of the cake is $r = \mathrm{d}R_c/\mathrm{d}w$, and therefore $R_c = \int_0^w r\mathrm{d}w = w(r)w$, where $w(\cdot)$ represents the mean value in contrast with w which is the weight of particles in the cake per unit surface of filter. From slurry (s) the

filtrate passes through the slurry-cake (sc-) and the cake-medium (cm) interfaces. A volume $V_{sc} = (1 + c/\rho_s)$ of slurry is needed to produce V_{sc}. Here c is the concentration- and ρ_s the density of particles. Assuming the amount of particles contained in the filter to be negligible, then $w = cV_{sc}$. Then from $V_c = V_m$, $V_{sc} = V_m + V_R$, $V_R = w \cdot \bar{\epsilon}/[\rho_s(1 - \bar{\epsilon})]$ and $\epsilon_s = \rho_s/(\rho_s + c)$ we have

$$w = \frac{cV_m}{1 - \frac{(1-\epsilon_s)}{\epsilon_s}\frac{\bar{\epsilon}}{(1-\bar{\epsilon})}} \qquad (6)_{\mathrm{i}}$$

The filtration coefficient λ in $-\mathrm{d}c/\mathrm{d}l = \lambda c$ is not a constant but change with time because of particles adsorbed by the bed. If one assumes that particles are bound to the wall by London-van der Waals force only, then $\lambda = K(\epsilon_0 - \sigma)$ where σ is the specific deposit of solids in filter bed described as volume of solid per unit filter volume, ϵ_0 the initial porosity of the bed and K a function of London-van der Waals constant, d, ϵ, η and W. The equation of continuity is $W_0(\mathrm{d}c/\mathrm{d}l) = \mathrm{d}(\sigma)/\mathrm{d}\theta$. Cake is stabilised by the flow force and consolidates when it has reached a critical thickness and the velocity dropped below a critical value. The cake pressure is highest at the interface with the filter, so it is here that it starts to consolidate. Vibration is normally used to loosen it.

In the Diffusion Limited Aggregation model (*cf* Houi and Lenormand, 1986) particles a_i are placed on the lattice while particles b_i move towards them from a distance. These travelling particles stick to the first thing they meet, thus forming clusters, but they disappear whenever they stray too far away from the clusters. The density $\rho \sim nd^2/(hl) = na/(\tilde{x}l)$, $\tilde{x} = x/a$, approaches a fractal power law $\rho \sim \tilde{x}^{D-2}$ with the fractal dimension D such that the deposit is homogeneous when $D = 2$ and heterogeneous when $D < 2$; l is the length of the filter, x the thickness of the deposit and d the particle diameter. They consider two models, one to study the effects of random motion while the other that of ballistic trajectory. In the first model particles move in a square network, jumping from one site to one of its nearest neighbours with a probability q towards the filter and p in the other three directions. The diffusive- and the ballistic probabilities are respectively $4p$ and $1 - 4p$. The ratio between convective and diffusive displacement, a Péclet number, is defined as $P_e = (1 - 4p)/4p$. For the ballistic motion $P_e \to \infty$ while for the Brownian motion $P_e = 0$. In their second model particles move through space and $P_e = |u|/|r|$, where u is a constant displacement vector in the flow direction while r is in random direction. Particle A sticks to B when $\alpha < \beta$ or rolls on it if $\beta < \alpha < \gamma$. In this latter situation, A will stick to B if it is prevented from reaching the angle γ comparative to A, but if at last $\alpha > \gamma$ A and B will separate.

The hydro dynamic forces act to transport particles through the medium. When the solid parts come close together, there is a viscous resistance which increases with the inverse of the separation between them. The van der Waals force acts at a close range, is always attractive and is theoretically infinite when particles touch a solid. Brownian motion affects particles smaller than 1μm and results in a heterogeneous deposit, whereas the ballistic trajectory occurred in sedimentation or filtration of big particles yield a deposit that is homogeneous.

Prefilters used to protect fibre bed coalescers from the damage caused by suspended solid can become a bottle neck from being ladened with the solids itself. Chan (1990) was interested in such problem as the processing of hydrocarbon liquids on offshore platforms. In this process the four phase system, that of hydrocarbon gas, condensate, glycol and solids, is treated. The gas is separated and distillated to fractionate off butane and propane for uses in petrochemical manufacture. The other fluids contain hydrocarbon condensate and glycol which is added to prevent gas hydrates, a solid phase, from forming. But ethylene glycol has to be separated before it enters the purification system, for otherwise it would foul heat exchangers and the trays of distillation column. This can be conveniently done using a fibre bed coalescer. But solids suspended in one of the constituents, gas condensate glycol, will deposit and block these beds unless removed first by using a prefilter, which would then in turn become blocked and causes the bottle neck to the whole process.

Dead end filtration is simpler to simulate on the computer, but crossflow filtration is used more often in industry. Hydrophobic polymers in general have the advantage of good chemical and thermal stability, but hydrophilic polymers are becoming more and more attractive as membrane materials because they tend to have less adsorption. Adsorbed layer means more resistance to flow and a decline in flux. Moreover, these layers are difficult to remove by normal cleaning methods. Cellulose and its derivatives are among the best known hydrophilic polymers used as membrane materials. Examples of these are cellulose acetate, cellulose triacetate, cellulose tripropionate, cellulose nitrate, cellulose acetate-butyrate and ethyl cellulose. They are used in micro-, ultra- and hyperfiltration as well as in dyalysis and gas separation. Cellulose is hydrophilic but not soluble in water. It has a regular chain structure and is quite crystalline. Cellulose nitrate and cellulose acetate are used in

micro- and ultrafiltration. Cellulose esters have excellent membrane properties except with regard to their sensitivity to biological-, chemical- and thermal degradations. They are made by air-casting or dry phase inversion. In phase inversion, a polymer is transformed from a liquid- to a solid state. Solidification is often started by liquid demixing, the transition of one liquid into two liquids. Phase inversion techniques include evaporation and precipitation the widely used for membrane of which is immersion precipitation (*cf* Schumacher, 1996). The top layer of an asymmetric membrane is dense and therefore responsible for most of the filtration. The sublayer is porous and provides the support to the top layer. Macrovoids are often found in the sublayer which lead to weak spots in the membrane and must be avoided, especially in high pressure applications which use dead end filtration. Tetrahydrofunate and acetone give membranes with a dense top layer as the result of delayed demixing. Dimethylsulfoxid and Dimethylformiade give membranes with a more porous structure from instantaneous demixing. Analogous to this is how pumice is very porous from the instantaneous solidification when it forms.

During the separation the flux through the membranes declines or decreases with time from adsorption, concentration polarisation, fouling, gel layer formation and pore pluggings. This is especially severe in micro- and ultrafiltration, with the decline in the flux often exceeding ninety per cent.

Darcy's law gives the volumetric flux of a pure liquid through a membrane, $J = \Delta P/(\eta R)$ where R is the overall resistance of the membrane which includes the resistances from adsorbed particles, cake, concentration polarisation, gel, pore blocking and membrane. Adsorption decreases the pore radius according to the Hagen-Poiseuille equation, $\Delta r/r = 1 - (J/J_m)^{1/4}$. At steady state the convective transport balances the permeate flow past the membrane and the diffusive back flow which results from the accumulation of solute at the membrane surface, $Jc + D\partial c/\partial x = Jc_p$ where D is the diffusion coefficient. Then from the boundary conditions $c = c_m$ at $x = 0$ and $c = c_b$ at $x = 1$, $(c_m - c_p)/(c_b - c_p) = \exp(J\delta/D)$. In other words, $c_m/c_b = \exp(J/k)/[R_n + (1 - R_n)\exp(J/k)]$ where the mass transfer coefficient $k = D/\delta$ and the intrinsic retention $R_n = 1 - c_p/c_m$. When the solute is completely retained by the membrane, $R_n = 1$ and $c_p = 0$, and therefore $c_m/c_b = \exp(J/k)$.

Across the filtering medium there is a driving force, in other words the pressure drop. There are four driving forces, centrifugal, gravity, pressure and vacuum. Filters in use in practice are either surface- or depth filters. In the former the solids are deposited on the surface in the form of a cake, thus the name *cake filtration*, while in the latter they are deposited inside the medium, thus *deep bed filtration.*

In filtration, Darcy's law is often written $Q = A\Delta p/(\mu R)$, where $R = L/K$ is the medium resistance, L the thickness- and K the permeability of the bed. If there is a cake, $R = R + R_c$ where R_c, the cake resistance, is $R_c = \alpha w$, α being the specific cake resistance in mkg^{-1} and w is the mass of cake deposited per unit area. Cakes are normally compressible, so α changes with Δp_c and is approximated as α_a, where $1/\alpha_a = (1/\Delta p_c)\int_0^{\Delta p_c} \mathrm{d}(\Delta p_c)/\alpha$. There is an experimental empirical relation $\alpha = \alpha_0/(\Delta p_c)^n$, where n is the compressibility index, and $\alpha_a = (1 - n)\alpha_0(\Delta p_c)^n$.

The mass of cake deposited is $wA = cV$, where c is the concentration of solids in the suspension. For incompressible cake, $Q = \Delta pA/[\alpha\mu c(V/A) + \mu R]$ or equivalently $\mathrm{d}t/\mathrm{d}V = \alpha\mu cV/(A^2\Delta p) + \mu R/(A\Delta p)$. If Δp is constant, $t = a_1V^2/(2A^2\Delta p) + b_1V/(A\Delta p)$, where $a_1 = \alpha\mu c$ and $b_1 = \mu R$. The experimental determination of α and R works with this equation in the form $t/V = aV + b$, where $a = a_1/(2A^2\Delta p)$ and $b = b_1/(A\Delta p)$; or rather in a more detailed form $(t - t_s)/(V - Vs) = \alpha\mu c(V + V_s)/(2A^2\Delta p) + \mu R/(A\Delta p)$, where t_s is the starting time at the beginning of the truly constant pressure period.

In constant rate filtration, Q is kept constant,

$$Q = \frac{\Delta p(t)A}{\frac{\alpha\mu cV(t)}{A+\mu R}}.$$

In other words, $\Delta p = \alpha\mu cQ^2t/A^2 + \mu RQ/A$, or $\Delta p = a_1v^2t + b_1v$, where $v = Q/A$ is the approach velocity of the filtrate.

In many cases, operation demands constant rate followed by constant pressure, in which case $\Delta p = a_1v^2t + b_1v$ for $t < t_s$ and $\Delta p = \Delta p_s$ a constant for $t \geq t_s$. This amounts to $V = Q_1t$ for $V \leq V_s$ and $(t - t_s)/(V - V_s) = a(V + V_s) + b$ for $V > V_s$.

If a centrifugal pump is used, it is the case of variable pressure and variable rate. Here the equation is $V = A(\Delta pA/Q - \mu R)/(\alpha\mu c)$, and the filtration time necessary is $t = \int_0^V \mathrm{d}V/Q$.

For compressible cakes, $\Delta p = \Delta p_c + \Delta p_m$, where $\Delta p_m = \mu RQ/A$ and $\Delta p_c = \alpha_a\mu cVQ/A^2$.

And $\Delta p_c = (1-n)\alpha_0 \Delta p_c^n \mu c V Q / A^2$, that is to say,

$$\frac{\mu c V Q}{A^2} = \frac{(\Delta p_c)^{1-n}}{(1-n)\alpha_0}.$$

Then, for the constant rate filtration, $(\Delta p_c)^{1-n} = \alpha_0(1-n)\mu c Q^2 t / A^2$. And for the variable pressure and variable rate operation,

$$V = \frac{A^2}{((1-n)\alpha_0 \mu c)} \cdot \frac{(\Delta p - \Delta p_m)^{1-n}}{Q}, \qquad (7)_{\mathrm{i}}$$

where Δp_c, Δp_m, V, Q and t are all variable.

The relationship between the specific cake resistance, porosity and specific surface is the Kozeny-Carman equation, $\alpha = K_0 S_0^2 (1-\varepsilon)/(\rho_s \varepsilon^3)$, where K_0 is the Kozeny constant which is approximately 5 for the lower porosity ranges, S_0 is the specific surface of the particles making up the bed, that is the ratio between the surface area and the volume of solids, ρ_s the solid density and ε the porosity, that is the ratio between the volume of voids and the volume of cake.

Fluid within porous media is essentially stagnant and the flow is laminar. Perhaps second only to the Hubble's constant in Cosmology in the matter of elusiveness is the k-factor which accounts for the tortuosity in porous filters, which, according to Kozeny and Carman, is $k = k_0(L_e/L)^2$, where k_0 is the shape factor, L_e/L the tortuosity factor, L_e being the interstitial length followed by the streamline and L is the thickness of the bed. There are many other formulae (*cf* Piekaar and Clarenburg, 1967), for instance $k = k_0/\rho$ suggested by Sullivan where $\rho = \overline{(\sin^2 \phi)}$ is the orientation factor.

Transport mechanism in filters is due to diffusion, gravity and hydrodynamic force. The efficiency is minimum at about the particle size of 1 μm. Filter normally runs about 24 hours between washes, with a rate between 5 and 15 $\mathrm{m \cdot h^{-1}}$. Wash rates are approximately 0.5 $\mathrm{m \cdot min^{-1}}$. (*cf* Ives, 1977).

§ 1.6 Statistics

Poisson distribution, defined by $p(x,\lambda) = \left[\lambda^x e^{-\lambda}/x!\right] \mathrm{I}_{[0,\infty)}$, is the binomial distribution, $p(x,n,p) = {}^n\mathrm{C}_x \theta^x (1-\theta)^{n-x} \mathrm{I}_{[0,n]}$, when n goes to infinity, θ goes to zero, while $n\theta = \lambda$. Here θ is the probability of success of each trial. It is used when counting the number of occurences of a random event. Analogously Poisson point process, which has $p(x = n(v)) = \left[\lambda |v| e^{-\lambda |v| x}/x!\right] \mathrm{I}_{[0,\infty)}$, is the binomial point process, $p(x = n(v)) = {}^n\mathrm{C}_x \theta^x (1-\theta)^{n-x} \mathrm{I}_{[0,n]}$, when the volume V goes to infinity, while $n/|V| = \lambda$. Here $\theta = |v|/|V|$ is the probability of points within V being placed in $v \subset V \subset R^d$, and λ the density or intensity of points. Therefore the density of point of a Poisson point process is constant by definition. A point process is a procedure which generates points on a domain within a space of d dimensions.

The Poisson point process thus derived has the properties that $0 < p_{n(v)=0} < 1$ for $0 < |v| < \infty$, $\lim_{|v|\to 0} p(n(v) \geq 1) = 0$, $n(v_i)$ mutually independent and $n(\bigcup_n v_i) = \sum_n n(v_i)$ when A_i are disjoint, and $\lim_{|v|\to 0} [p(n(v) \geq 1)/p(n(v) = 1)] = 1$.

The weighted mean of a group of data is $\mathbf{x} = \sum_i f_i x_i / n$ and the weighted variance is $\sigma^2 = \sum_i f_i (x_i - \mathbf{x})^2 / n$, where f_i is the occurrence frequency of x_i and $\sum_i f_i = n$. Likewise the r^{th}-moment around the average is $m_r = \sum_i f_i (x - \mathbf{x})^r / n$, while the r^{th}-moment around the origin is $m'_r = \sum_i f_i x^r / n$ (*cf* Spiegel, 1975). Some relations among these various moments are $m_1 = 0$, $m_2 = m'_2 - {m'_1}^2$, $m_3 = m'_3 - 3m'_1 m'_2 + 2{m'_1}^2$, and $m_4 = m'_4 - 4m'_1 m'_3 + 6{m'_1}^2 m'_2 - 3{m'_1}^4$.

The variance when normalised by $n-1$ gives the best unbiased estimated variance if the sample has a normal distribution. On the other hand the variance which is normalised by n is identical with the second moment of the sample about its mean.

The log-normal distribution is closely related to the normal distribution. If $\ln x$ has a normal distribution with μ and σ^2, then x has a log-normal distribution with μ and σ^2. In other words, a log-normal distribution curve will appear as a normal curve when plotted with a log scale in the x axis. Its probability distribution function is

$$f(x|\mu,\sigma) = \frac{1}{x\sigma\sqrt{2\pi}} e^{-\frac{(\ln x - \mu)^2}{(2\sigma^2)}}. \qquad (8)_{\mathrm{i}}$$

It is positive definite, and therefore attractive in some areas of application where this is required, for example the amount of rain fall or particle size distribution. Both the log-normal and the normal distributions require only two parameters to describe, that is its mean and variance.

The most common drop size distribution in agitated heterogeneous liquid-liquid systems are the normal and the log-normal distributions (Giles *et al*, 1971). A straight line is obtained when the diameter of drops, d,with normal size distribution is plotted against cumulative percentage frequency, or in the case where they have log-normal size distribution, when $\log d$ is plotted against cumulative percentage frequency.

Monte Carlo methods (*cf* Hammersley and Morton, 1954) use random numbers. They have found applications in a wide variety of fields, ranging from numerical analysis to recreation. Random numbers sometime come from nature, for instance the generator which creates random numbers from a resistance noise suggested by A. M. Turing, in which case they are truly random in nature. In 1927 L. H. C. Tippett compiled a table of random numbers, and in 1955 RAND Corporation (*cf* Knuth, 1998). For the premium bonds lottery ERNIE is used in the UK since 2^{nd} June 1957 to generate a 9-digit sequence of random numbers by exploiting the random frequency instability in a free-running oscillator. ERNIE was upgraded in 1973 and the present version, introduced in 1988, is Mark 3.

Normal distribution is a family of curves which have two parameters, namely the mean μ and the standard deviation σ. The standard normal distribution, $\Phi(x)$, has $\mu = 0$ and $\sigma = 1$. It is related to the error function by the relation $\mathrm{erf}(x) = 2\Phi(x\sqrt{2}) - 1$. The central limit theoram states that, as the sample size increases to infinity, the sum of independent samples from some distribution of finite mean and variance converges to the normal distribution.

§ 1.7 Poisson process

The Poisson process is the probability model with one parameter, which represents all processes in which points occur randomly in time. The gamma experiment is to run the process to find the time t_k of the k^{th} arrival, whereas the Poisson experiment is to run it to find the number of arrivals n_t in the interval $(0, t]$, $t \geq 0$. These two experiments give rise to two sets of random variables dual to one another, and $n_t \geq k$ if and only if $t_k \leq t$. The regeneration property says that the process after any time t is independent of the process before t and is probabilistically the same as the original process. The interarrival time is $x_1 = t_1$, $x_k = t_k - t_{k-1}$ for $k = 2, 3, \cdots$.

In a Poisson process the number of changes in each of the non-overlapping intervals is independent from that in the others. Let ν be the number of one change, $h = 1/n$ a sufficiently small interval and n the number of trials. Then the probability of exactly one change in h is $p = \nu h = \nu/n$. The probability of two or more changes in h is zero. The number of k changes occurring in n trials is the continuous limit of the discrete binomial distribution

$$p(k) = \frac{n!}{k!(n-k)!}\left(\frac{\nu}{n}\right)^k \left(1 - \frac{\nu}{n}\right)^{n-k} \qquad (\mathbf{9})_{\mathrm{i}}$$

§ 1.8 Phase transition

In the Ising model each spin has two possible states, that is up and down, and the hamiltonian is $H = J_0 \sum_{<i,j>} \sigma_i \sigma_j$ where the summation is over the nearest neighbours. Since it has been exactly solved, the Ising model provides a good model for the understanding of phase transition. This model can represent the transition from ferro- to paramagnetic at the critical temperature where the correlation length becomes infinite. Characteristic to the Ising model is the peak in the specific heat at the critical temperature.

The two-dimensional xy model is a model of spins confined to a plane, the hamiltonian of which is $H = J_0 \sum_{<i,j>} \cos(\theta_i - \theta_j)$. This model can represent the superconducting and the superfluid films. For this model there is no phase transition showing long-range ordering. One example is the two-dimensional Coulomb gas model where the vortex-antivortex pairs, which are bound to each other at low temperature, increases in number as the temperature increases and become separated at the KT temperature that marks the phase transition.

It had been generally believed that no phase transition can exist for the xy model when Kosterlitz *et al* (1973) showed that there is another kind of phase transition, arisen from the topological excitation of vortex-antivortex pairs instead of from the long-range ordering found in a spontaneous magnetisation. They consider the two-dimensional model of gas with charges $\pm q$ where the interaction potential is

$$U(|\mathbf{r}_i - \mathbf{r}_j|) = -2q_i q_j \ln \left| \frac{(\mathbf{r}_i - \mathbf{r}_j)}{\mathbf{r}_0} \right| + 2\mu \qquad (\mathbf{10})_{\mathrm{i}}$$

when $r > r_0$, and 0 when $r < r_0$. The problem is reduced to that of solving an equation of the form $(\mathrm{d}y/\mathrm{d}x) = -e^{-xy}$. The application mentioned there is in the xy model of magnetism, the solid-liquid transition, and the neutral superfluid, but not in a superconductor and a Heisenberg ferromagnet.

The frustrated xy model, the hamiltonian of which is $H = J_0 \sum_{<i,j>} \cos(\theta_i - \theta_j - A_{ij})$, occurs when a magnetic field is applied perpendicular to the two-dimensional plane of the xy model. The frustration parameter, $f = \Phi/Phi_0$, is a measure of the average external magnetic flux. When $f = 1/2$ the model is called the fully frustrated xy model. The local chirallity, $m(r_i) = \frac{1}{2\pi}\sum(\theta_i - \theta_j - A_{ij})$, which describes the property of the ground state, where it can either be $+\frac{1}{2}$ or $-\frac{1}{2}$. The network configuration at $\mathrm{T} < \mathrm{T}_c$ is that of a draught board, and has Z_2 symmetry. This regularity is broken by the formation of domain walls in an Ising phase transition at T_c.

Renormalisation group method has shown that there exist larger structures that behave like a smaller one. This means that the same structure can recur infinitely many times in infinitely many different scales, and that is the same idea that makes fractal geometry. This is why the study of cluster structure and the use of fractal dimension to characterise clusters becomes important (*cf* Stauffer and Aharony, 1985).

Percolation in Physics means Statistical Mechanics. Much of the contemporary vocabularies in the former has come from the lexicons of the latter from Ising Models to Renormalisation group and then to finite size scaling (*cf* Pathria, 1996).

§ 1.9 Random processes

A synonym to *random* is *stochastic* (*cf* Miles, 1972). Any algorithm which employs a random element is called Monte Carlo. Random processes can have various types of distribution. The beta distribution has a probability density function $f_{X_{\alpha,\beta}}(x) = x^{\alpha-1}(1-x)^{\beta-1}/B(\alpha,\beta)$, $0 \le x \le 1$, where $\alpha > 0$ and $\beta > 0$ are shape parameters, and $B(\alpha,\beta)$ is the beta function. There are three types of shape; the bridge shape has $\alpha > 1$ and $\beta > 1$, the J-shape $\alpha \le 1$ and $\beta \ge 1$, or $\alpha \ge 1$ and $\beta \le 1$, and the U-shape $\alpha < 1$ and $\beta < 1$.

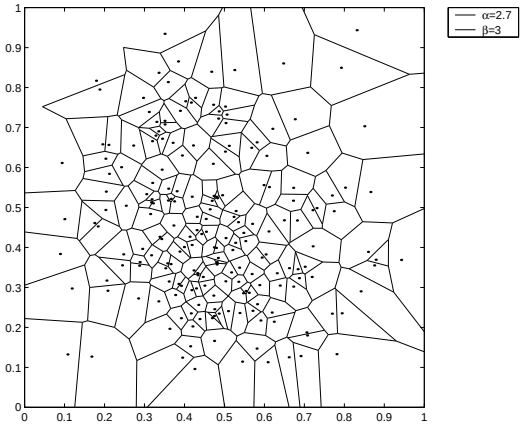

The 200 generators used in Figure 1.9 are randomly chosen with beta distribution with the shape parameters $\alpha = 2.7$ and $\beta = 3$, that is bridge shape. Both x and y in Figure 1.10 have J-shaped distribution with the shape parameters $\alpha = 2$ and $\beta = 0.8$. The density is unbounded at $x = 1$ and at $y = 1$ because $\beta < 0$ for both. The shape parameters in Figure 1.11 are $\alpha = 0.5$ and $\beta = 0.3$, that is U shape. The density is unbounded at $x = 0$, 1 and at $y = 0$, 1 because α is also less than zero.

Figure 1.9 Voronoi graph with bridge-shaped beta distribution..

The random variable of the F-distribution is $F_{n_1,n_2} = n_2 X/(n_1(1-X))$, where X is a beta variate with $\alpha = n_1/2$ and $\beta = n_2/2$.

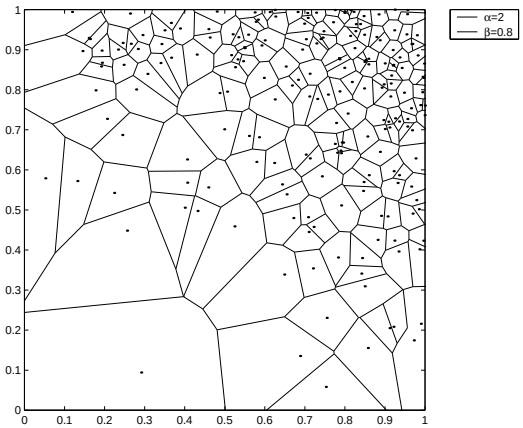

The probability density function of some of the distributions of random numbers found in practice are shown in Table 1.9. For the negative binomial distribution, p is a probability of success and is constant and r the number of successes required before stopping. With rq/p as the mean, $q = 1 - p$, and the variance rq/p^2,it is used to model consecutive trials. For the noncentral$f$ distribution, S_{n_1,μ_1} and S_{n_2,μ_2} are chi-squared random variables which are independent and noncentral, $S_{n,\mu} = \chi^2_{n-1} + (Z_n - \mu^{1/2})^2$.

Figure 1.10 Voronoi graph with J-shaped beta distribution..

It has the mean $\nu_2(\delta+\nu_1)/\nu(\nu_2-2)$, where $\nu > 2$, and the variance

$$2\left(\frac{\nu_2}{\nu_1}\right)^2 \left[\frac{(\delta+\nu_1)^2+(2\delta+\nu_1)(\nu_2-2)}{(\nu_2-2)^2(\nu_2-4)}\right],$$

where $\nu_2 > 4$. This means that it is the general case of the f-distribution, which is the case where $\delta = 0$. The parameters ν_1 and ν_2 are degrees of freedom.

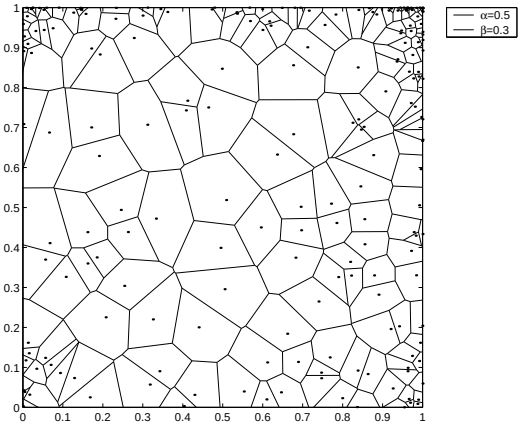

Figure 1.11 Voronoi graph with U-shaped Beta distribution..

The noncentral t distribution has $F(x|a,b)$ as the incomplete beta function with parameters a and b, and ν the degrees of freedom. It is the generalisation of the student's t-distribution. It's mean is

$$\delta\left(\frac{\nu}{2}\right)^{\frac{1}{2}} \frac{\Gamma\left(\frac{(\nu-1)}{2}\right)}{\Gamma\left(\frac{\nu}{2}\right)}, \qquad (\mathbf{11})_{\mathrm{i}}$$

where $\nu > 1$, and it's variance $\nu/(\nu-2)(1+\delta^2) - \nu/2\delta^2\left[\Gamma((\nu-1)/2)/\Gamma(\nu/2)\right]^2$. The noncentrality parameter for all noncentral distributions, *viz.* the noncentral f-, t- and chi-square distributions is represented by δ.

The mean of the normal distribution is μ and the variance σ^2. The standard normal distribution has $\mu = 0$ and $\sigma = 1$. The probability mass function of the Poisson distribution is sometimes written $y = f(x|\lambda) = \lambda^x/x!e^{-\lambda}\mathrm{I}_{0,1,\ldots}(x)$. It has a value when x is a nonnegative integer. Otherwise the density function is zero.

The Rayleigh distribution has a parameter b. Its mean is $b\sqrt{x/2}$ and its variance $(4-x)b^2/2$. The uniform distribution has the mean $(a+b)/2$ and the variance $(b-a)^2/12$. For the standard uniform distribution $a = 0$ and $b = 1$. The discrete uniform has the mean $(N+1)/2$ and the variance $(N^2-1)/12$.

The Weibull distribution is sometimes written $y = f(x|a,b) = abx^{b-1}e^{-ax^b}\mathrm{I}_{0,\infty}(x)$. The Weibull distribution with a single parameter has $a = 1$. The three-parameter Weibull distribution has a p.d.f. $f_X(x) = c(x-a)^{c-1}e^{-((x-a)/b)^c}b^{-c}$ when $x \geq a$, otherwise $f_X(x) = 0$.. The mean is $a^{-(1/b)\Gamma(1+b^{-1})}$ and the variance is $a^{-2/b}\left[\Gamma(1+2b^{-1}) - \Gamma^2(1+b^{-1})\right]$.

Beta	$f_{X_{\alpha,\beta}}(x) = x^{\alpha-1}(1-x)^{\beta-1}/B(\alpha,\beta),\ 0 \leq x \leq 1$
Binomial	$f_{X_{n,p}}(x) = {}^n\mathrm{C}_x p^x q^{n-x},\ x = 0,1,\ldots,n,\ 0 \leq p \leq 1$ and $q = 1-p$
Chi-square	$f_{\chi^2_n}(x) = e^{-x/2}x^{(n/2)-1}/2^{n/2}\Gamma(n/2),\ 0 \leq x \leq 1$
Exponential	$y = f_{x|\mu} = e^{-x/\mu}/\mu$
F	$f_{F_{n_1,n_2}}(x) = n_1^{n_1/2}n_2^{n_2/2}x^{(n_1/2)-1}/B(n_1/2,n_2/2)(n_2+n_1x)^{(n_1+n_2)/2}$
Lognormal	$y = f_{x|\mu,\sigma} = e^{-(\ln(x)-\mu)^2/2\sigma^2}/x\sigma\sqrt{2x}$
Negative Binomial	$y = f_{x|r,p} = {}^{r+x-1}\mathrm{C}_x p^r q^x \mathrm{I}_{0,1,\ldots}(x),$
Noncentral f	$F_{n_1,n_2} = \sqrt{S_{n_1,\mu_1}/n_1}/\sqrt{S_{n_2,\mu_2}/n_2}$
Noncentral t	$\mathrm{P}(-t < x < t|(\nu,\delta)) = \sum_{j=0}^{\infty}\left[(\delta^2/2)^j e^{\delta^2/2}/j!\right]\mathrm{I}\left(x^2/(\nu+x^2)|1/2+j,\nu/2\right)$
Noncentral Chi-square	$F(x|\nu,\delta) = \sum_{j=0}^{\infty}\left[(\delta/2)^j e^{\delta/2}/j!\right]\mathrm{P}(\chi^2_{\nu+2j} \leq x)$
Normal	$y = f(x|\mu,\sigma) = e^{-(x-\mu)^2/2\sigma^2}/(\sigma\sqrt{2\pi}),\ \mu > 0$
Poisson	$f_X(x) = \mu^x e^{-\mu}/x!,\ x \geq 0$
Rayleigh	$y = f(x|b) = (x/b^2)e^{(-x^2/2b^2)}$
T	$y = f(x|\nu) = \Gamma((\nu+1)/2)/\Gamma(\nu/2)\cdot 1/\sqrt{\nu x}\cdot 1/(1+x^2/\nu)^{\nu+1/2}$
Uniform	$y = f(x|a,b) = (1/(b-a))\mathrm{I}_{[a,b]}(x),\ b > a$
Discrete Uniform	$y = f(x|N) = (1/N)\mathrm{I}(1,\ldots,N)(x)$
Weibull	$f_X(x) = ax^{a-1}e^{-(x/b)^a}/b^a,\ x \geq 0$ and $a,b > 0$

Table 1.9 *Probability density functions.*

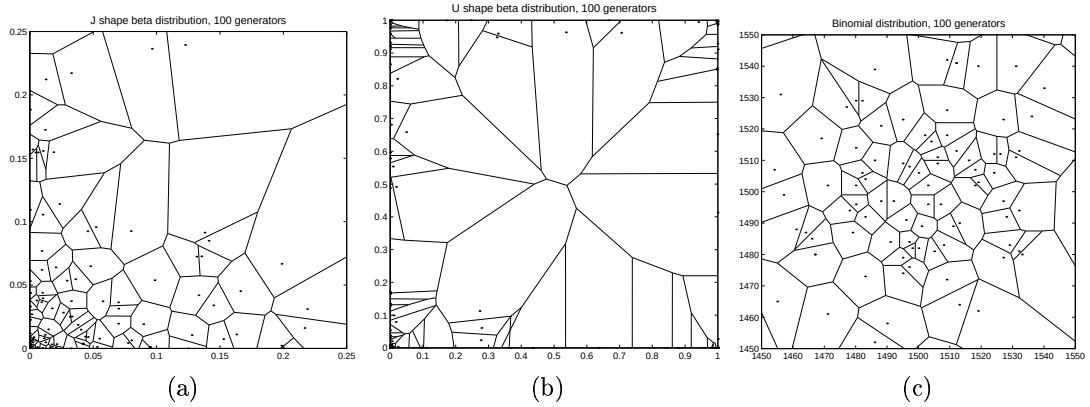
J shape beta distribution, 100 generators
U shape beta distribution, 100 generators
Binomial distribution, 100 generators

(a) (b) (c)

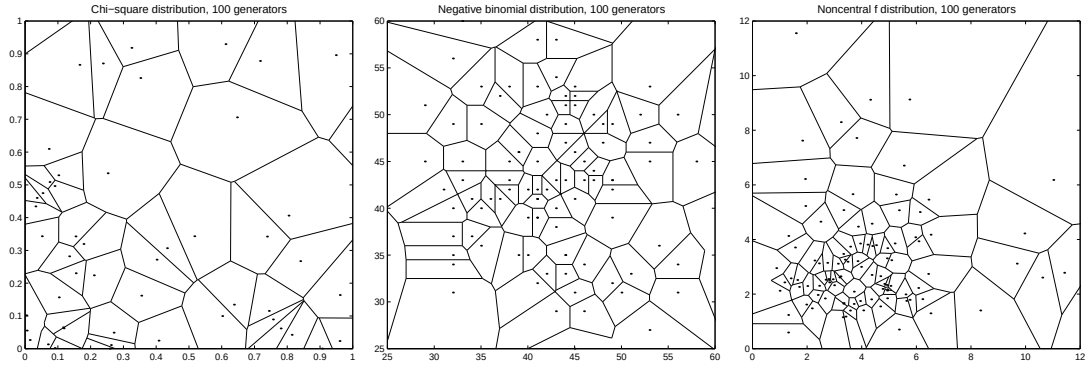
Chi−square distribution, 100 generators
Negative binomial distribution, 100 generators
Noncentral f distribution, 100 generators

(d) (e) (f)

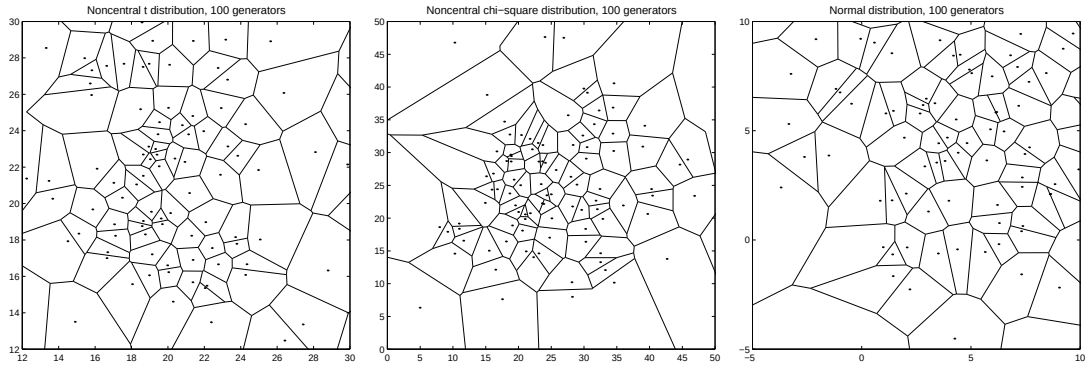
Noncentral t distribution, 100 generators
Noncentral chi−square distribution, 100 generators
Normal distribution, 100 generators

(g) (h) (i)

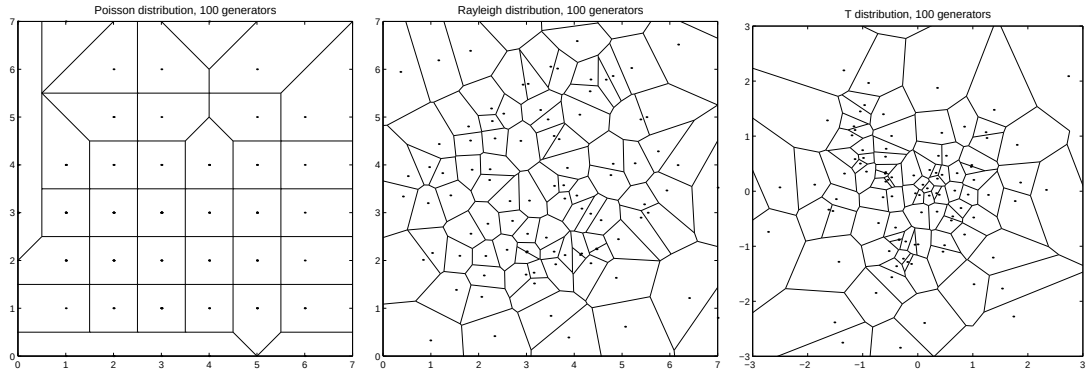

(j) (k) (l)

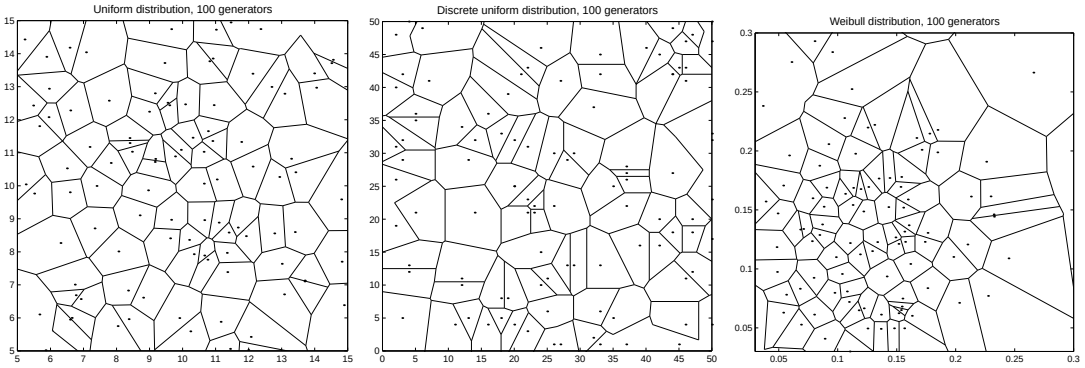
Uniform distribution, 100 generators
Discrete uniform distribution, 100 generators
Weibull distribution, 100 generators

(m) (n) (o)

Figure 1.12 *Voronoi graphs of various random p.d.f.'s, whose distributions are* (a) *J-shaped Beta,* $\alpha = 0.5$ *and* $\beta = 10$*, in both* x *and* y*,* (b) *U-shaped Beta,* $\alpha = 0.1$ *and* $\beta = 0.2$*,* (c) *Binomial,* $n = 3{,}000$ *and* $p = 0.5$*,* (d) *Chi-squared,* $n = 1$*,* (e) *negative binomial,* $p = 0.7$ *and* $r = 100$*,* (f) *noncentral* f*,* $\nu_1 = 7$ *and* $\nu_1 = 12$*,* $\delta = 20$*,* (g) *noncentral* t*,* $\nu = 10$ *and* $\delta = 20$*,* (h) *noncentral chi-square,* $\nu = 7$ *and* $\delta = 20$*,* (i) *normal,* $\mu = 5$ *and* $\sigma = 4$*,* (j) *Poisson, 100 generators* (x, y)*,* $\lambda = 3$*,* (k) *Rayleigh,* $b = 3$*,* (l) t*,*$\nu = 7$*,* (m) *uniform,* $a = 15$ *and* $b = 5$*,* (n) *discrete uniform, from 100 points,* $N = 50$ *and* (o) *Weibull,* $a = 50$ *and* $b = 2$*.*

There are five methods for generation of Poisson processes, two of which are the time-scale transformation and the thinning algorithm. The first one changes a heterogeneous process $T_{(i)}$ in $[0, t_0]$ into a homogeneous process $\tau_{(i)}$ by a new time scale $\tau = \in t_0^T \lambda(u)du$, where λ is the rate function. We have $\tau_{(i)} = \Delta(T_{(i)})$ and $T_{(i)} = \Delta^{-1}(\tau_{(i)})$, for $\tau_{(i)} \leq \Delta(t_0)$. If $\lambda(t) = e^{\alpha+\beta t}$, then $\Delta(T) = e^{\alpha}(e^{\beta T} - 1)/\beta$ and $T_{(i)} = (1/\beta)\ln(\beta\tau/e^{\alpha} + 1)$. The second one follows Algorithm 1.3 with the input $\lambda^*, \lambda(\cdot), t_0$.

Algorithm 1.3 *Thinning algorithm.*

$T \leftarrow 0$;
while $T \geq t_0$ **do**
  generate U, $V \sim U(0,1)$;
  while $V > \lambda(T)/\lambda^*$ **do**
    $T \leftarrow T - \ln U/\lambda^*$;
  endwhile
endwhile

□

Figure 1.13 shows that the result from the point process in two dimensions involving two random variables, *i.e.* $r(\theta) = r\angle\theta$, is not homogeneous even though it may be on average isotropic with respect to the centre for a very large network. In Figure 1.14 where the domain is also circular but each point is simply a 2-d Poisson point process, the average distance is constant for a large system. Figure 1.15 is also 2-d Poisson point process, but the space here is square. In all of the figures, *i.e.* Figure 1.13–1.15, (a) and (b) start from 200-, whereas (c) and (d) from 1,000 point generators. Boundary effects are reduced by excluding those vertices and edges along the border.

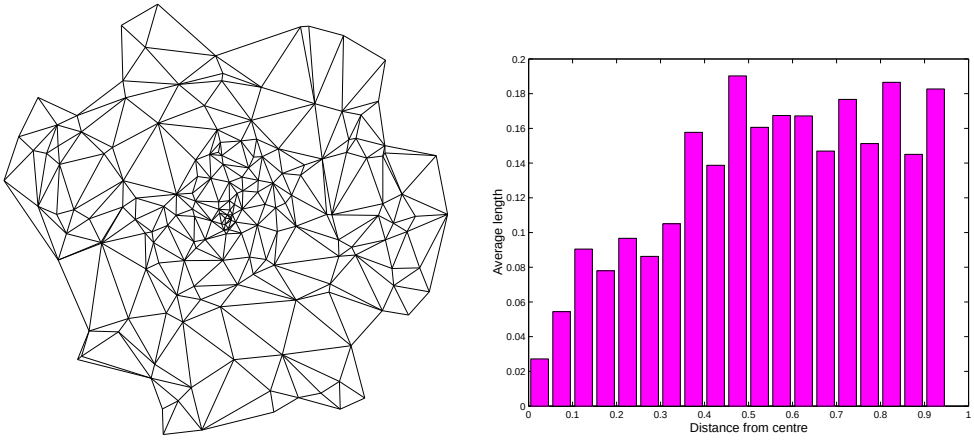

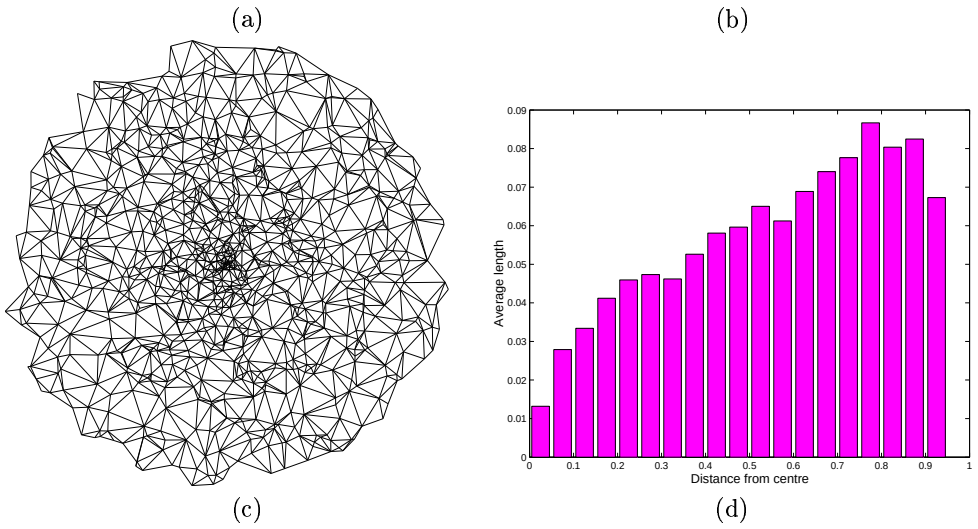

Figure 1.13 *Point process $r\angle\theta$, where both r and θ are independent random generators; (a) the Delaunay triangulation, 182 vertices shown, (b) average distance between neighbours vs distance from centre of the network, (c) another similar network, 947 vertices shown in total, (d) average edge length of the Delaunay triangulation.*

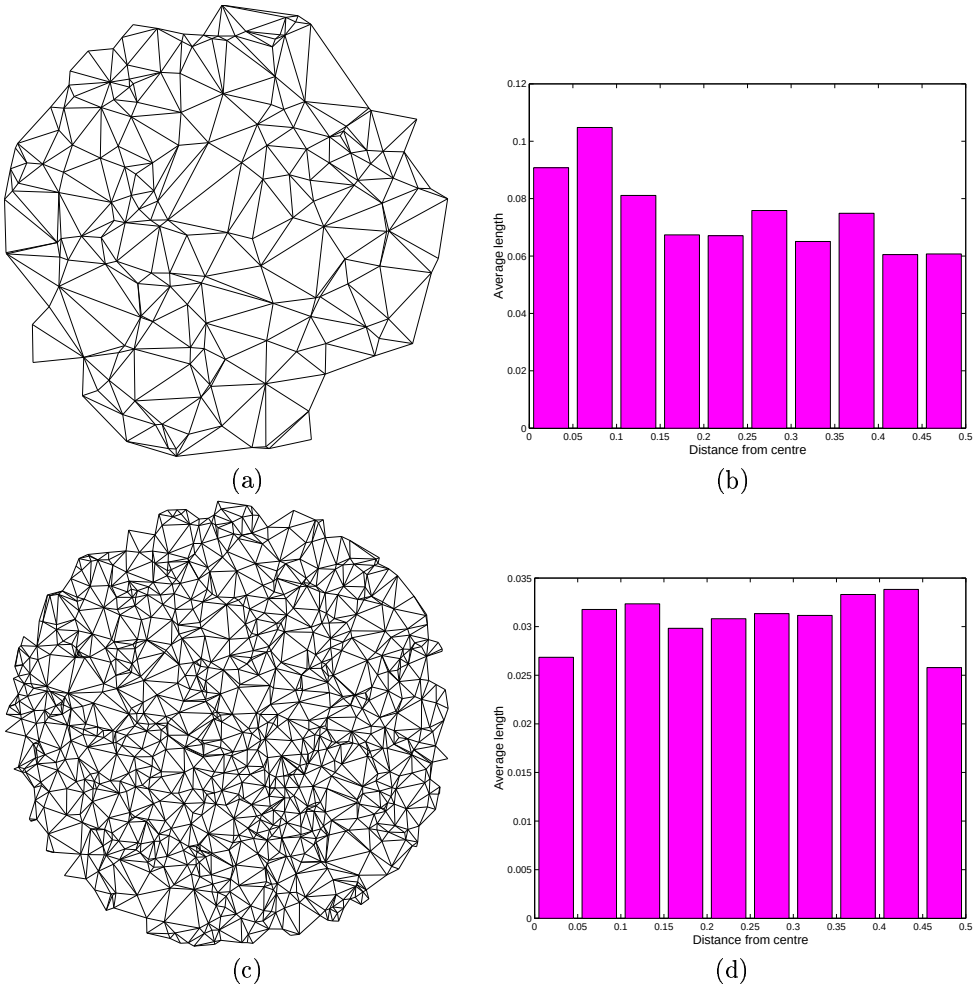

Figure 1.14 *Point process x, y, where x and y are independent random generators in a circular domain; (a) the Delaunay triangulation with 184 vertices, (b) average edge length vs distance from centre of the network, (c) another similar network, 909 vertices shown in total, (d) average edge length of the Delaunay triangulation.*

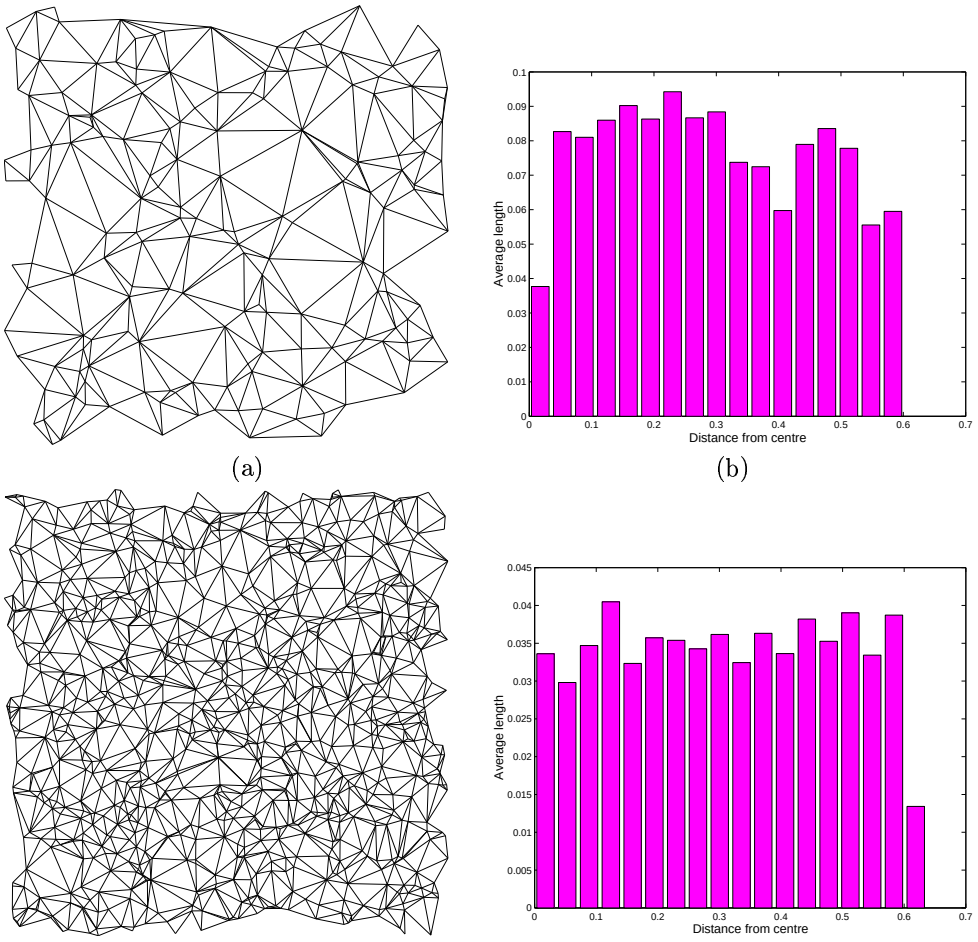

Figure 1.15 *Point process x, y, where x and y are independent random generators within a square domain; (a) the Delaunay triangulation with 168 vertices, (b) average edge length vs distance from centre of the network, (c) another similar network, 816 vertices shown in total, (d) average edge length of the Delaunay triangulation vs the distance from centre.*

The codes used in carrying out these investigations are listed in § A.25. Figure 1.15 effectively tells us that the random point process $r\angle\theta$ gives particle distribution shaped like a bell with density decreasing away from the centre. One might almost say that this is similar to what a spiral galaxy looks like. There is still much room to explore what particle distribution the different topologies of random process give rise to, for example, 'What would the distribution in 2-d be of points that are generated from random points on a line swept in circle at a constant speed?' The algorithm is as simple as Algorithm 1.4, but the room for imagination and the scope of exploration are unlimited. There are only two variables, that is the nuclei positions x and the triangulation edges e.

Algorithm 1.4 *Triangulation edge length distribution.*

$x \leftarrow$ random process**;**
$e \leftarrow$ **find** triangulation of x**;**
$(x, e) \leftarrow (x - \partial x, e - \partial e)$**;**
compare $|e|$**;**

□

§ 1.10 Structures in nature

Prusinkiewicz and Lindenmayer (1990) model the structures in plants after having briefly discussed about the difference between the Chomsky grammars and the L-system, both of which being a mean for doing string rewriting, but the latter is based on the Turtle geometry which makes it convenient for the geometric rewriting of fractals. The states of a turtle consists of its position coordinates and the direction in which it is facing. Meinhardt (1995) models the patterns on sea shells by using mathematical based on the partial differential equations governing the system of activator, inhibitor,

and substrate. Starting from a homogeneous initial condition, small deviations therein undergo a positive feedback and therefore increase. Activator catalyses both the production of itself and that of its inhibitor. The latter acts as a negative feedback which limits and makes the reaction local.

Random tissue in three dimensions has four edges, six faces and four cells meeting at each vertex. It is thus surrounded by four cell nuclei, as well as by six bonds forming a tetrahedral cage. The four edges meeting at a vertex resemble a caltrop, and similarly the lines from it to the four nuclei. If a vertex had more than four edges it would have been structurally unstable, because then it can be split into two normal vertices by an infinitesimal deformation. Continuous random networks, for example models of covalent glasses like vitreous silica, are excluded from this restricted class since theirs may be more than three non-planar faces to an edge even if they still have four edges to a vertex (Revier, 1982).

Unlike crystallography, the ideal random structure is by no means unique because it is the solution of a statistical problem. There are, however, certain geometrical and topological invariances, the most famous of which is possibly the Euler's theorem. In two dimensions this theorem states that $f - e + v = \chi$, where χ is an Euler-Poincaré characteristic and integer of order one, χ being for instance 1 and 2 respectively for plane and sphere; in three dimensions it is $f - e + v = 2$. The valence relations, $\sum nf_n = 2e = 3v$, hold for 2-d and 3-d alike.

Stumbling upon some observations, Theorem's 3.3 and 3.4 resulted. These two theorems help explain together with Algorithm 3.2 on page 86, the valence relations. Theorem 1.2 is also another product obtainable from applying both the Euler's theorem and the valence relations (*cf* Prause, 2000).

Theorem 1.2. *The average number of edges per polygon in a large pattern is six.:*

Proof. From Euler's theorem, $f - e + v = 1$, and the valence relations, $\sum_n f_n = 2e = 3v$, it follows by applying the latter to the former that $f - \sum nf/2 + \sum nf/3 = 1$. Since $\bar{n}$ is the average number of edges per face, it follows that $f - \bar{n}f/2 + \bar{n}f/3 = 1$. Then $f(1 - n/6) = 1$, and consequently $1 - 1/f = n/6$. As the network becomes large, f becomes infinite and as a result $\bar{n} = 6$. □

It is interesting to note that Theorem 1.2 posts no restrictions on whether the network is random or regular. The only assumption made is that three and only three edges meet at each vertex. One is almost tempted to say that, as the size of a network becomes infinite, nature somehow follows this theorem and make sure that each of the polygons has six edges on average.

When I translated the three papers by Voronoi (Tiyapan, 2001) I used the term *vertex* to mean a vertex of a specific polygon or polyhedron. For any vertex, I used the term *vertice*, and for more than one vertex vertices. It turns out that I am not the only one who concerns himself with the word. Moore and Angell (1993), for instance, use *apex* for a single corner, *vertex* to mean any point in a tessellation in two or three dimensions where its apices meet.

Rivulets flowing inside a pack bed have been studied by several authors (*cf* Porter, 1968). They are said to flow independently of each other, with no mixing among one another. Diffusion theory has been used to treat a random walk process.

The van der Waals force in combination with double layer repulsion play an important part in the study of filter and particle movements in porous media. Both are electrical forces and can be used to explain the particle capturing mechanism.

Percolation is related to chemical engineering contexts (*cf* Mohanty *et al*, 1982). But the necessary background in stochastic processes for the purpose of simulation has already been described earlier, for example the modelling of colmatage, the retaining of particles suspended in a fluid flowing through a porous medium (Litwiniszyn, 1963 and 1967). In general, however, few authors in all engineering fields relate their works directly to the percolation theory. The majority of studies in this area are based on dynamics and fluid dynamics theories (*cf* Mulder and Gimbel, 1990; Kock and Judd, 1965).

The reason for the lack of percolation material in engineering literature may be because the percolation process generally works behind the scene and only shows itself as critical phenomena. Most engineering studies are concerned with things under some operational condition, within the range of which percolation seems to be absent. By contrast, in Physics where extreme conditions are considered, there is an enormous and increasing amount of publications which are directly under the topic of percolation. But this by no means means that within a pacific range there is no place for percolation. In fact it is precisely this lack of mentioning in the literature that induces one to this kind of research. Because our idea of criticality is by tradition closely linked to the idea of time, percolation seems to be present only when there are instantaneous changes. But if in a steep s-curve

we only rotate the axis clockwise by $\pi/2$ radian, such that to make the time axis vertical instead of horizontal, then we will see that in place of one critical point in the middle of the graph connecting two different levels, there are now two critical phenomena on both sides, one on each side, and in the middle a flat region where time hardly changes. Looking at it this way percolation seems to be a symmetry between time and space. In physical systems spaces percolates, but in the dual world where criticality is continuity it is the time instead which percolates.

Having said that, without rotating the time-space axes backwards and forwards too often one should still find ways to investigate what a pacified percolation does. In this regard, the study of economics seems to be an ideal place to start, if simply because one knows there exists such thing as hyperinflation but one never wants to study that when it happens. This automatically forces the researcher to find ways of doing researches which would not ruin his pocket or put his life in jeopardy. Another ground with a good prospect is in traffic congestion, even though its worst effect is not yet devastating, apart from what it sometimes does to the economy.

With these digressions in mind, if we now turn our thought at this point to our chemical engineering studies, we will not fail to see how ideal filtration fits the no-ruins requirement. For here we have a process which percolates routinely, often needs to be backflushed, but where the effect it produce is probably that of giving engineers a headache and, at its worst, putting a decent company out of business. But even with this advantage, I still believe that the study of filtration should not concentrate only on the fouling of filters, but should try to understand both the percolated and nonpercolated situations, preferably the latter for the lack of it in literature, and to connect what happens in a working filter to what happens, or does not happen, in a fouled one.

The revolutionising discovery made by F. August Kekulé (Kekulé, 1865, cited in Wotiz, 1993) that benzene has cyclic nature gave rise to the structural theory of organic chemistry.

§ 1.11 Computational geometry

The altitude lines of a triangle are concurrent. The bisectors of the angles of a triangle are concurrent. Ceva's theorem says that, all the three lines in a triangle which contain a vertex and a point on its opposite side are concurrent if and only if no two among them are parallel and the product of the three ratios of division of the sides made in one direction around the circumference of the triangle is one. In Gergonne's theorem, the three lines of a triangle which are made by the vertices and the points of tangency of the incircle on the side opposite to them are concurrent. The intersection between the three lines tangent to the circumcircle of a triangle and the sidelines opposite to them are collinear.

A point is an extreme point of a plane convex set s unless it lies in a triangle which has vertices in s but is no vertex of the triangle. A ray from inside a bounded convex figure intersects the boundary of the latter at exactly one point. Consecutive vertices of a convex polygon exist in sorted angular order about any interior point. A subfacet of a simple polytope is shared by two and only two facets. Two facets share a subfacet if and only if the latter is determined by $d-1$ vertices in their set; these two facets and the subfacet are called adjacent. A line segment defined by two points is an edge of the convex hull if and only if all other points of the set lie on, or to one side of it.

The diameter of a convex figure is the largest distance between parallel lines of support. The diameter of its convex hull determines the diameter of a set. Every vertex of the Voronoi graph is the intersection of three of its edges. Every nearest neighbour of a Voronoi polygon defines an edge.

VT and the triangulation of its nuclei are dual to each other. A Voronoi graph on n points has at most $2n-5$ vertices and $3n-6$ edges. The convex hull of a Voronoi graph on n can be found in linear time.

Modern programming philosophy puts much emphasise on modularity of a program and on information hiding of modules. Though undoubtedly information hiding can be good for the finished products, during the course of development it sometimes works against yourself when you try to pin-point an error in order to debug. Some modularisations are more about hierarchies than simplicity. Whenever this is the case, it is necessary to unconventionally seek a simpler path.

The explicit equation in 2-d is $y = mx + c$ or $ax + by + c = 0$. Imposing the constraint $a^2 + b^2 = 1$, that is multiplying all the terms by $(a^2 + b^2)^{-1/2}$, puts the equation into the canonical or normalised form. This makes $a = \cos\alpha$, $b\cos\beta$ and $c = -r$, where a and b are directional cosines, *i.e.* the cosines of the angles that the normal line makes with the x and y axes respectively. Examples of possible conventions are to have a normal line point towards outside of the region, to have the line direction always to the right of the normal vector, or to keep c positive always.

A parametric form of line equation in 2-d is by introducing a third variable t and write the equations as $x = x_0 + ft$ and $y = y_0 + gt$, where (x_0, y_0) is the point on the line corresponding to $t = 0$. A line through a point p which makes angles α and β with the x and the y axes respectively has the parametric equations $x = x_p + t\cos\alpha$ and $y = y_p t\cos\beta$. One convention is to vary t from 0 to 1 over a line segment, another is to normalise it by multiplying its coefficient by $(f^2 + g^2)^{-1/2}$.

An implicit line equation $ax + by + c = 0$ can be turned into a parametric form as $x = -ac/(a^2 + b^2)^{1/2} + bt$ and $y = -bc/(a^2 + b^2)^{1/2} - at$. And a parametric line described by $x = x_0 + ft$ and $y = y_0 + gt$ is converted into the implicit form as $-gx + fy + (x_0 g - y_0 f) = 0$

The implicit plane equation in three dimensions is $ax + by + cz + d = 0$. The parameters can be found by using Cramer's rule, $a = \det(1, y_i, z_i)$, $b = \det(x_i, 1, z_i)$, $c = \det(x_i, y_i, 1)$ and $d = \det(x_i, y_i, z_i)$, which gives $a = y_1 z_{32} + y_2 z_{13} + y_3 z_{21}$, $b = z_1 x_{32} + z_2 x_{13} + z_3 x_{21}$, $c = x_1 y_{32} + x_2 y_{13} + x_3 y_{21}$ and $d = x_1(y_2 z_3 - y_3 z_2) + x_2(y_3 z_1 - y_1 z_3) + x_3(y_1 z_2 - y_2 z_1)$.

A normalised form has a constraint $a^2 + b^2 + c^2 = 1$. This amounts to multiplying its implicit equation by $(a^2 + b^2 + c^2)^{-1/2}$ to get $\alpha x + \beta y + \gamma z + \delta = 0$. Here α, β and γ are cosines of the angles which the normal to the plane makes with the coordinate axes. The distance between two parallel normalised planes is $\delta_2 - \delta_1$. A normalised implicit plane equation can be used to represent a planar half-space by multiplying every tems by -1 and then assign a convention that the vector formed by the direction cosines always points towards the outside or the inside of the region.

The distance from a point to a plane, if the plane is $ax + by + cz + d = 0$ and the point is (x_p, y_p, z_p), is $r = \left[(ax_p + by_p + cz_p + d)^2/(a^2 + b^2 + c^2)\right]^{1/2}$. The intersection of two planes, from the planes $a_1 x + b_1 y + c_1 z + d_1 = 0$ and $a_2 x + b_2 y + c_2 z + d_2 = 0$, is $x = x_0 + ft$, $y = y_0 + gt$ and $z = z_0 + ht$ where $f = \det(b_i, c_i)$, $g = \det(c_i, a_i)$ and $h = \det(a_i, b_i)$, $i = 1$ and 2.

The intersection of three planes is found by Algorithm 1.5, Here the minor matrices a^{ij} is δ_{23}^{ab}, δ_{23}^{ac}, or δ_{23}^{bc} as the case may be.

Algorithm 1.5 *Intersection among three planes.*

$\Delta \leftarrow \sum_{(a,b,c)}(-1)^{i+j} a_{ij} a^{ij}$;
if $|\Delta| < \epsilon$ **then**
  at least two of the planes are parallel;
else
  $x \leftarrow (b_1\delta_{23}^{dc} - d_1\delta_{23}^{bc} - c_1\delta_{23}^{db})/\Delta$;
  $y \leftarrow (d_1\delta_{23}^{ac} - a_1\delta_{23}^{dc} - c_1\delta_{23}^{ad})/\Delta$;
  $z \leftarrow (b_1\delta_{23}^{ad} + a_1\delta_{23}^{db} - d_1\delta_{23}^{ab})/\Delta$;
endif □

The intersection between a line and the plane $ax + by + cz + d = 0$ is $(x_1 + x_{12}a, y_1 + y_{12}a, z_1 + z_{12}a)$, where $a = -(ax_1 + by_1 + cz_1 + d)/(ax_{12} + by_{12} + cz_{12})$, $x_{12} = x_2 - x_1$ and similarly for y_{12} and z_{12}.

The area of a circle is πr^2 and that of its segment is $\theta r^2/2$. A segment is its pie cut reaching its centre while a sector is a plane slice through the sphere. The area of a sector is this area subtracted by that of a triangle, or $r^2(\theta - \sin\theta)/2$. The centre of gravity or the centroid lies on the bisector of the central angle with the distance of $4r\sin(\theta/2)/3\theta$ for a sector and $4r\sin^3(\theta/2)/3(\theta - \sin\theta)$ for a segment.

The volume of a pyramid is $Ah/3$, where A is the area of base and h is the height of the pyramid. The volume of a sphere is $4\pi r^3/3$, and the distance from its centroid to the sphere centre is $(3r/4)\left[\sin^4(\theta/2)/(2 - 3\cos(\theta/2) + \cos^3(\theta/2))\right]$ That of a sector of a sphere is $(\pi r^3/3)(2 - 3\cos(\theta/2) + \cos^3(\theta/2))$ The volume of a tetrahedron is $V = (1/6)\det(x_{12}, x_{13}, x_{14}; y_{12}, y_{13}, y_{14}; z_{12}, z_{13}, z_{14})$, where $x_{ij} = x_j - x_i$,or $V = (1/6)\det(x_i, y_i, z_i, 1)$. The former is limited to the case of three dimensions, and is in fact $V = (1/6)(a \times b) \cdot c$, where a, b and c are respectively the lines from O to A, B and C in a tetrahedron OABC.

Generalising the latter to higher dimensions, we have the volume of a d-dimensional simplex $V = (1/d!)\det(x_{ij}, 1)$, where x_{ij} is now $(x_j)_i$, $1 \le i \le (d + 1)$ and $1 \le j \le d$. Here the information found in existing literature seems to be wrong, some lists the multiplying factor as $1/d$, some simply uses $1/6$ throughout all $(d \ge 3)!$ § 3.13 mentions in more detail how I arrived at the value used here.

Some of of the algorithms found in literature are the following. The algorithm to find whether a point is inside a polygon, Algorithm 1.6. The arbitrary line l here, which is taken for simplicity to be horizontal, passes through z.

Algorithm 1.6 *Point inside a polygon.*

$r \leftarrow 0$;
for $i = 1$ to n **do**
  if edge i and l not parallel **then**
    if i intersects l to the left of z at any point except its lower extreme **then**
      $r \leftarrow r + 1$;
    endif
  endif
  if r odd **then**
    z is internal to p;
  else
    z is external;
  endif
endfor □

To find the inclusion in a convex polygon, $q \in p$ being a known fixed point within the polygon, find the wedge in which z lies by doing a binary search and test whether $\angle(zqp_{i+1})$ is a right turn-while $\angle(zqp_i)$ a left turn angle. If $\angle(p_ip_{i+1}z)$ is a left turn angle, then z is inside p.

The Euclidean minimum spanning tree may be obtained by Algorithm 1.7.

Algorithm 1.7 *Euclidean minimum spanning tree.*

$f \leftarrow 0$;
for i from 1 to n **do**
  $s(p_i) \leftarrow 0$;
  $f \leftarrow p_i$;
endfor
while f contains more than one number **do**
  $t \leftarrow f$;
  if (s(t)=j) **then**
    clean up;
    $j \leftarrow j + 1$;
  endif
$(u, v) \leftarrow$ shortest unselected edge incident on t, $u \in t$;
$t' \leftarrow$ tree in f containing v;
$t'' \leftarrow$ **merge** (t, t')];
delete (t') from f;
$s(t'') \leftarrow \min(s(t), s(t')) + 1$;
$f \leftarrow t''$
endwhile □

To rotate $v = (v_1, v_2)^{\mathrm{T}}$ to $v' = (v_1', v_2')^{\mathrm{T}}$, use $v^{\mathrm{T}} = Av$ where $A = [\cos\theta, -\sin\theta; \sin\theta, \cos\theta]$ is the transformation matrix and θ is the anti-clockwise angle of the rotation.

To rotate a general line in three dimensions by θ around an arbitrary axis, the transformation matrix becomes $A = T^{-1}RT$, where

$$R(\theta) = R_x^{-1}(\alpha)R_y^{-1}(\beta)R_z(\theta)R_y(\beta)R_x(\alpha)T = R_x(-\alpha)R_y(-\beta)R_z(\theta)R_y(\beta)R_x(\alpha).$$

The translation T translates one point of the line to the origin and R_x rotates around the x-axis by α which puts u on to the xz axis, R_y around y-axis by β and puts u' on to the z axis, and R_z around z-axis. Since the vector v is (x_{12}, y_{12}, z_{12}), we have the a, b, c and the unit vector $u = (a, b, c)/|v| = (x_{12}, y_{12}, z_{12})/|v|$. Then it follows that $\cos\alpha = c/d$, $\sin\alpha = b/d$, $\cos\beta = d$ and $\sin\beta = -a$. All of these can perhaps be summarised as a linear procedure in Algorithm 1.8.

Algorithm 1.8 *Rotation in three dimensions*

$v \leftarrow (x_{12}, y_{12}, z_{12})$;
$m \leftarrow |v|$; $a \leftarrow x_{12}/m$;
$b \leftarrow y_{12}/m$;
$c \leftarrow z_{12}/m$;
$d \leftarrow (b^2 + c^2)^{1/2}$;
$r_{xx} \leftarrow c/d$;
$r_{xy} \leftarrow b/d$;
$r_{yx} \leftarrow d$;

$r_{yy} \leftarrow -a$;
$T \leftarrow [\mathrm{I}(3), -(x_1, y_1, z_1)^{\mathrm{T}}; 0(3)^{\mathrm{T}}, 1]$;
$R_x \leftarrow [1, 0(3)^{\mathrm{T}}; 0, r_{xx}, -r_{xy}, 0; 0, r_{xy}, r_{xx}, 0; 0(3)^{\mathrm{T}}, 1]$;
$R_y \leftarrow [r_{yx}, 0, -r_{yy}, 0; 0, 1, 0, 0; -r_{yy}, 0, r_{yx}, 0; 0(3)^{\mathrm{T}}, 1]$;
$R_z \leftarrow [[\cos\theta, -\sin\theta; \sin\theta, \cos\theta], 0(2,2); 0(2,2), \mathrm{I}(2)]$;
$R \leftarrow T^{-1} R_y^{-1} R_z R_y R_x$; $v' = Rv$. □

Also in three dimensions, the rotation around the x-axis is

$$R_x = [\{r_{11} = 1, m_{23} = [\cos\theta, -\sin\theta; \sin\theta, \cos\theta]\}],$$

around y-axis is

$$R_y = [\{r_{22} = 1, m_{13} = [\cos\theta, \sin\theta; -\sin\theta, \cos\theta]\}]$$

and around z-axis is

$$R_z = [\{r_{33} = 1, m_{12} = [\cos\theta, -\sin\theta; \sin\theta, \cos\theta]\}].$$

The minor containing parts of the i^{th} and j^{th} rows and columns is m_{ij}.

The right hand coordinate system is where a 90° rotation around the x-, y- and z-axis bring respectively the y- to z-, z- to x- and x- to y-axis. Scaling and translating a vector v in three dimensions amounts to calculating $[v'; w] = A[v; w]$, where A is respectively $[\mathrm{I}(3)s, 0(3); 0(3)^{\mathrm{T}}, 1]$ and $[\mathrm{I}(3), \Delta v; 0(3)^{\mathrm{T}}, 1]$, $\Delta v = (\Delta x, \Delta y, \Delta z)^{\mathrm{T}}$.

A quaternion can be described as a pair (s, v) of a scalar s and a vector $v = (a, b, c)$. The rotation by θ around an axis in the direction of a unit vector u is then the quaternion $(\cos\theta/2, u\sin\theta/2)$. Let $q = (s, v)$. Then $q^{-1} = (s, -v)$. The multiplication of quaternions is $q_1 q_2 = (s_1, v_1) \cdot (s_2, v_2) = (s_1 s_2 - v_1 \cdot v_2, s_1 v_2 + s_2 v_1 + v_1 \times v_2)$, where the cross product is described in minors as $v_1 \times v_2 = [\delta^{yz}; -\delta^{xz}; \delta^{xy}]$.

Let q represent a rotation. Then a vector p is rotated to p' by $P' = qPq^{-1}$, where P and P' are respectively $(0, p)$ and $(0, p')$. In simplified words, this means $p' = s^2 p + (p \cdot v)v + 2s(v \times p) + v \times (v \times p)$. Then we have the transformation matrix for the general rotation around u in three dimensions,

$$R_u(\theta) = \begin{bmatrix} (1 - 2b^2 - 2c^2) & (2ab - 2sc) & (2ac + 2sb) \\ (2ab + 2sc) & (1 - 2a^2 - 2c^2) & (2bc - 2sa) \\ (2ac - 2sb) & (2bc + 2sa) & (1 - 2a^2 - 2b^2) \end{bmatrix}$$

where $s = \cos\theta/2$ and $v = (a, b, c) = u\sin\theta/2$. Furthermore, if q_1 is a rotation by θ_1 around v_1 and likewise q_2 by θ_2 around v_2, then $q_3 = q_2 q_1$ is a rotation by $\theta_3 = 2\cos^{-1} s_3$ around v_3 such that $\sin\theta_3 \geq 0$.

Quaternion is an extension of complex number to higher dimensions where there are three imaginary parts instead of one. It is defined as $q = s + ia + jb + kc$, where a, b, c and s are real numbers, $i^2 = j^2 = k^2 = -1$ and $ij = -ji = k$.

Let a plane be described by $(v - p) \cdot n = 0$, where p is a point on-, and n a perpendicular to the plane. This means that, for all points v lying in the plane (p, n), $(v - p) \cdot n = 0$. If the plane (p, n) is transformed into (Ap, m), then Av lies in (Ap, m) and consequently $A^{\mathrm{T}} m = n$ or $m = (A^{\mathrm{T}})^{-1} n$.

A vector normal to the surface remains normal if it is transformed by $(A^{\mathrm{T}})^{-1}$. When a transformation matrix A has the property $A = (A^{\mathrm{T}})^{-1}$, for example rotation, all surface normals remain normal. But in general this equality does not hold, so we have for instance the non-uniform scaling where these normals cease to be normal.

To test for the intersection between a ray and a triangle using Plücker's coordinates is described in Algorithm 1.9.

Algorithm 1.9 *Ray and triangle intersection.*

find Plücker's coordinates for vertices and the ray;
test ray against each of the edges;
if ray hits an edge, passes all of them clockwisely or all of them counter-clockwisely **then**
  ray intersects the triangle;
else
  ray and triangle intersect not;
endif □

If these vertices are v_1, v_2 and v_3, and the ray is $r = r_{12} = r_2 - r_1$, where r_1 and r_2 are any two points on the ray, then Plücker's coordinates for the vector v_{12} are $(u, v) = (v_2 - v_1, v_2 \times v_1)$, and similarly for v_{23}, v_{31} and r_{12}. For the test between the ray and each edge, find $c = u_r \cdot v_i + v_r \cdot u_i$.

Then the ray r counter-clockwisely passes the edge i, hits it or clockwisely passes it respectively as $c < 0$, $c = 0$ or $c > 0$.

A 3-d line can be represented by the six numbers that come with coordinates of two distinct points, or by the eight numbers that come with the coordinates of two distinct planes. Plücker's coordinates, however, provides a mean which suits geometrical computation better than both of these. It redefines the coordinates as $u = p - q$ and $v = p \times q$, where p and q are two points on a line, neither quantity of which depends on p or q.

Let a tetrahedron has its vertices at a_i, $i = 1$ to 4. Then the centre of its circumsphere is at $a_1 + \delta$ and its corresponding radius $r = |\delta|$, where

$$\delta = \left[|a_{12}|^2(a_{13} \times a_{14}) + |a_{13}|^2(a_{14} \times a_{12}) + |a_{14}|^2(a_{12} \times a_{13})\right] /2|a_{12}^{\mathrm{T}}; a_{13}^{\mathrm{T}}; a_{14}^{\mathrm{T}}|.$$

A triangle $\triangle p_1p_2p_3$, where $p_i = (x_i, y_i)$ and $i = 1$ to 3, has an area $A = |x, y, 1(3)|$, which is positive if and only if $\triangle p_1p_2p_3$ forms a counter clockwise cycle or $\angle p_1p_2p_3$ is left-turned. Or equivalently the area is $A = \det(x_{12}, x_{13}; y_{12}, y_{13})$, which is positive if the points are in anti-clockwise order of the indices and negative otherwise. Or the area is $A = [s(s - d_1)(s - d_2)(s - d_3)]^{1/2}$, where the the semi perimetre s is $s = \sum_i d_i/2$, where d_i, $i = 1$ to 3, are the lengths of the three sides of the triangle.

For a convex polygon, the area can be found by adding together the n triangles formed by any two adjacent vertices and one fixed point within the polygon. Here n is the number of vertices it contains. Or it can be found by adding the $(n - 2)$ triangles formed by one fixed vertex and any two adjacent vertices of those remaining. Another way of finding the area is $A = (1/2)\sum_{i=0}^{n-1}(x_iy_{i+1} - y_ix_{i+1})$, where (x_i, y_i) are vertices. Rearranging to make it faster and more accurate, $A = (1/2)\sum_{i=0}^{n-1}((x_i + x_{i+1})(y_{i+1} - y_i))$. If the dimension of the polygon is higher than two, $A = (1/2)\left|N \cdot \sum_{i=0}^{n-1}(v_i \times v_{i+1})\right|$, where N is a unit vector normal to the plane. The area of a polygon can also be computed, without loosing generality, by subtracting the area under its lower edges by that of its upper edges.

A vector normal to a plane is simply $n = v_{12} \times v_{13}$.

The ordering of vertices on a face of a polygon is done for the purpose of drawing it or for finding vertice pairs which form edges. This can be done in two ways. One is to get inside the polygon and look at all the vertices around comparing their angles relative to one another. Another one is to look at the polygon from a distance and compare their angles as before, as well as their distance from the viewing point. The angle is $\theta = \arccos[(v_1 \cdot v_2)/(|v_1||v_2|)]$, where v_1 and v_2 are vectors to vertices from the distant point, and θ the angle between them.

To find the convex hull in three dimensions, one may use Algorithm 1.10.

Algorithm 1.10 *Convex hull in three dimensions.*

sort s by x_1 such that $x_i(p_i) < x_i(p_j)$ if and only if $i < j$;
if $|s \leq k|$ **then**
  construct $c(s)$;
else
  $s_1 \leftarrow \{p_1, \ldots, p_{\lfloor n/2 \rfloor}\}$;
  $s_2 \leftarrow \{p_{\lfloor n/2 \rfloor}, \ldots, p_n\}$;
  $p_1 \leftarrow c(s_1)$;
  $p_2 \leftarrow c(s_2)$;
  $p \leftarrow$ **merge** p_1 and p_2;
endif □

Here $c(s)$ is the convex hull of s. Two convex hulls are merged with each other by first constructing a cylindrical triangulation T which supports p_1 and p_2 along two circuits e_1 and e_2 respectively, then remove from both p_1 and p_2 the portions which have been obscured by T.

The following Jarvis's march algorithm, Algorithm 1.11, finds a convex hull in two dimensions.

Algorithm 1.11 *Convex hull in two dimensions*

$p_1 \leftarrow$ the lowest point in s;
$q_1 \leftarrow$ the highest point in s;
while next point $\neq q_1$ **do**
  find $p_i \in s$, $i = 2, 3, \ldots$, with an increasing order of the polar angles
    with respect to p_1;
endwhile

while next point $\neq p_1$ **do**
  find $q_i \in s$, $i = 2, 3, \ldots$, with an increasing order of the polar angles
    with respect to q_1 and the negative x axis;
endwhile □

The polar angle is an angle with respect to the positive x-axis. The lowest and the highest points are on the convex hull.

Algorithm 1.12 is the quick hull algorithm.

Algorithm 1.12 *Quick hull algorithm.*

$l \leftarrow (x_0, y_0)$;
$r \leftarrow (x_0, y_0 + \epsilon)$;
if $s = \{l, r\}$ **then**
  return (l, r);
else
  find $k \in s$ that gives $\max A_{\triangle klr}$ or ($\max A_{\triangle klr}$ and $\max \angle klr$);
  $s^1 \leftarrow p \in s$, such that p is on the left of $\overrightarrow{lh}$;
  $s^2 \leftarrow q \in s$, such that q is on the left of $\overrightarrow{hr}$;
  $\{h\} \leftarrow (s^1; l, h)$;
  $\{h\} \leftarrow (s^2; h, r) - h$;
endif □

The convex hull is $\{h\}$. The points l and r are with respectively the smallest and the largest abscissa. In other words they are the left-most and the right-most points. And k is the furthest point with respect to l and r.

Let $p = \{p_1, p_2, \ldots, p_n\}$ be a set of n generators in ν-dimensional space, the coordinates of which are (x_{ij}), $i = 1$ to d and $j = 1$ to n. Then the Delaunay tessellation in d dimensions which spans p is generated by,

for $j = 1$ to n **do**
  $\{q\} \leftarrow q_j = (x_{ij}, \sum_j x_{ij}^2)$;
endfor
$h \leftarrow c(q)$;
project all the lower n-faces of $c(q)$ parallel to the d^{th} axis on to the original n-d space;
□

Okabe *et al* (1992) give a good review of algorithms for generating VT's. Given the set of generator points $\{p_i\}$, $i = 1$ to n, a brute force albeit simple method generates for all i and j from 1 to n the $(n-1)$ half planes $h(p_i, p_j)$, $1 \leq j \leq n$, $i \neq j$, and then proceeds to construct all $\mathcal{V}(p_i)$ of the VT from their common intersections.

On the other hand, the following Algorithm 1.13 is the quaternary incremental method whose inputs comprise the $(n-3)$ generators p_i, $i = 4$ to n, where all the p_i are in $s = \{(x, y) | 0 \leq x, y \leq 1\}$, and three additional generators $p_1 = (0.5, 0.5(1 + 3\sqrt{2}))$, $p_3 = (0.25(2 - 3\sqrt{6}), 0.25(2 - 3\sqrt{2}))$ and $p_3 = (0.25(2 + 3\sqrt{6}), 0.25(2 - 3\sqrt{2}))$.

Algorithm 1.13 *Quaternary incremental method.*

$k \leftarrow \min(k_i)$ such that $k_i \in \mathrm{I}^+$ and $n < 4^{k_i}$;
$s_{ij} \leftarrow (i - 1, i/2^k, j - 1, j/2^k)$;
construct a quaternary tree;
scan leave buckets from left to right, top to bottom, **put** generators in buckets;
$\{p_i\}$ **do** quaternary reordering on the generators;
$\mathcal{V} \leftarrow$ **construct** Voronoi for p_1, p_2 and p_3;
for $i =$ **4 to** n **do**
  repeat $\leftarrow 1$;
  while repeat **do**
    find p_α such that $\mathrm{d}(p_\alpha, p_\ell) = \min_j \mathrm{d}(p_j, p_\ell)$;
    if $\mathrm{d}(p_m, p_\ell) < \mathrm{d}(p_\alpha, p_\ell)$ **then**
      repeat $\leftarrow \neg$**repeat**;
    elseif $p_m \leftarrow p_\alpha$ **do** nothing;
    else
      repeat $\leftarrow \neg$**repeat**;
    endif

endwhile
$\{w_{i1}, w_{i2}\} \leftarrow$ the intersections between the perpendicular
bisector of $p_i p_l$ and $\Omega(\mathcal{V}(p_i))$, $1 \leq i \leq \ell - 1$;
$\Omega \leftarrow$ **construct** the boundary of $\mathcal{V}(p_i)$ formed by these $\overline{w_{i1} w_{i2}}$;
$\{\mathcal{V}_\ell\} \leftarrow (\{\mathcal{V}_{\ell-1}\} \bigcup \Omega) - \{\mathcal{V} | \mathcal{V} \in \{\mathcal{V}_{\ell-1}\}, \mathcal{V}$ is within $\Omega\}$;
endfor
$\{\mathcal{V}\} \leftarrow \{\mathcal{V}_n\}$;

□

The construction of s_{ij} is such that $s_{ij} = (i-1, i/2^k] \times (j-1, j/2^k]$, where $i, j \in \mathrm{I}^+$, i and j are 1, 2, ... up to 2^k. The nearest neighbour search finds from ℓ generators, $p_1, \ldots, p_\ell$, and $\{\mathcal{V}_{\ell-1}\}$, the generator point p_m such that $\mathrm{d}(p_m, p_\ell) < \mathrm{d}(p_m, p_i)$ for all $i = 1$ to ℓ, $i \neq m$ and $i \neq \ell$; p_j are all generators adjacent to $\mathcal{V}(p_i)$. The boundary growing procedure gives the sequence of boundaries $\{\Omega\}$. The additional generators mentioned in the procedure is graphically shown in Figure 1.16.

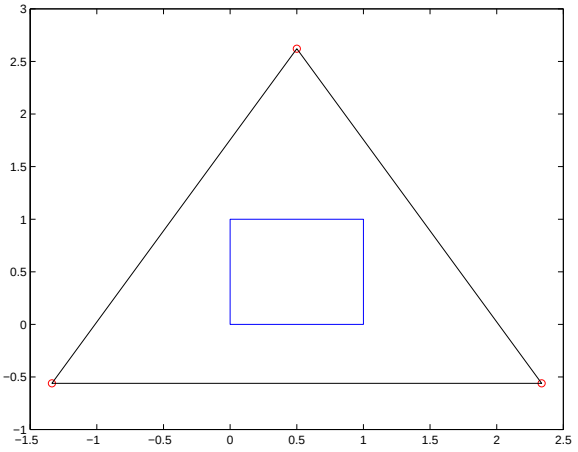

Figure 1.16 Additional generators for the incremental method.

If we draw a horizontal line through each point in two dimensions, or a horizontal plane each point in three dimensions, we divide the space into slabs the line segments within which do not intersect one another. In three dimensions, and for a polygonal model of porous media, we can for instance divide the model into such slabs, then find the effective cross sectional area of each slab, and then determine where the bottle neck to the flow occurs within the media. Whether this would produce the correct determination of the pressure of flow across the material is another matter because flows through porous media may be governed by the combination of the various tortuous paths through the pores, the interrelationship of which can be complicated.

These slabs provide another method in finding the area, or in three dimensions the volume, of each cell of the tessellation. Here the cell is divided into slabs, and then the area or volume of each section calculated.

In three dimensions, rotation around the x-axis is done by $\begin{bmatrix} 1 & 0 & 0 \\ 0 & \cos\theta & -\sin\theta \\ 0 & \sin\theta & \cos\theta \end{bmatrix}$, around y-axis by $\begin{bmatrix} \cos\theta & 0 & \sin\theta \\ 0 & 1 & 0 \\ -\sin\theta & 0 & \cos\theta \end{bmatrix}$ and around z-axis by $\begin{bmatrix} \cos\theta & -\sin\theta & 0 \\ \sin\theta & \cos\theta & 0 \\ 0 & 0 & 1 \end{bmatrix}$.

§ 1.12 Geometric algorithms

The program `findfarea.m` in § A.26 finds the area and plane parameters of a face from a matrix containing the list of the coordinates of the ordered vertices. Its synopsis is `(a,p)=findfarea(v)`, where `a` is the face area, `p` the list of the plane parameters and `v` the coordinate matrix.

Real problems are algebraical or analytical whereas computer simulations are arithmetical and numerical (*cf* Knuth, 1997). In between these two lie computer programs. Therefore the latter are mapping from the analytical to the arithmetical world. There are different ways to solve a problem analytically, and there are different ways numerically. Therefore numerical study by simulation is an endless pursuit. Several programs listed in § A do the same job, but each one does it differently.

Hamiltonian's are essentially a function that maps N bodies pairwisely to account for all pairs of their mutual interactions. They occur in most fields where there are particles interacting with each other. In quantum mechanics, for example, the time independent Schrödinger equation for a system of N particles interacting via the Coulomb interaction is $H\Psi = E\Psi$, where the Hamiltonian is

$$H = \sum_{i=1}^{N} \left(-\frac{\hbar}{2m_i} \nabla_i^2 \right) + \frac{1}{2} \sum_{i=1}^{N} \sum_{j \neq i}^{N} \frac{z_i z_j}{4\pi\epsilon_0 |r_i - r_j|}, \qquad (12)_{\mathrm{i}}$$

where Ψ is the N-body wavefunction, z the charges of the individual particles and E the energy of either the ground or an excited state of the system. Similarly from Rushbrooke and Morgan (1961), using their notations, the Hamiltonian of the Ising problem is

$$\mathcal{H} = -2J \sum_{\langle i,j \rangle} s_3^{(i)} s_3^{(j)} - g\beta H \sum_{(i)} s_3^{(i)}, \qquad (\mathbf{13})_{\mathrm{i}}$$

where β is the Bohr magneton, g the gyromagnetic ratio and J the magnitude of the exchange interaction.

When simulating such systems, the number of pairwise summation terms can be reduced by half because they represents a symmetric matrix. The total number of terms is thus reduced from $N(N-1)$ to $N(N-1)/2$ (*cf* Wray *et al*, 1983). Because $i \neq j$, all the diagonal components of the matrix are excluded, which makes the number of pairs $n^2 - n = n(n-1)$. In a program, this is equivalent to two if statements, one embedded within the other in the form $i(j(\cdot))$, where the index i runs from 1 to $(n-1)$ and j from $(i+1)$ to n; this has been discovered from experience, as can be seen by comparing the present work with the earlier one (Tiyapan, 1995, KNT3(iii)).

§ 1.13 TEXnicalities

LaTEX is a macro which runs on TEX. It gives one convenience but not without a tradeoff in understanding. Also one may not have much freedom in writing macros on LaTEX. Tiyapan used TEX for his Work Notes dated 12^{th} February 2001 .

LaTEX(Lamport, 1985) is written by Leslie Lamport. Newer versions of it has come up at a regular interval. Unlike most other macros which run on TEX, her source code is free for none but herself. Moreover, having used TEX to do what it wants, LaTEX thereby castrates her progenitor in such a way that it is impossible for her users to define new macros efficiently by using the `\def` command. With `\def` disabled, the lion has lost its fangs and users become as docile and dependent as a lobotomised patient. There can be no doubt that with the TEX users having such idea as this, sooner or later LaTEX will have to change in these respects. But this is the way things are at present.

One of the first macros written is the code to change the date format. The algorithm first sets $x = date$, then it assigns the ordinate endings *st, nd, rd* or *th* depending on the value of *ordinate*, which is calculated from

if $x > 30$ then $ordinate = 1$ else
  if $x > 20$ then $ordinate = x - 20$ else
    $ordinate = date$
  endif
endif

The macros which are either newly written or adapted from elsewhere, mainly from the *manmac* macroby Knuth, are listed in § 1.13. Apart from these, this thesis uses the *plain* and the *manmac* macros. Another set of macros developed here is that which deals with languages. The definition of language here is quite wide. It contains many languages among which are those which are used here, for example the languages for Chemistry, Chinese, Czech, German, French, grammatical jargons, Japanese, Lanna, Latin, latin grammar, Mathematics, Pali, Physics, Russian, Sanskrit, and Thai (Daiy), *etc.* Only parts of this set of macros are useful for the writing of this thesis, not least so those which are used for writing the dedication page.

In the original account of his, Tiyapan (2003, KNT8(iii)) wrote,

> When I first started using TEX instead of LaTEX, I only used the macro `plain.tex`. Then in my first book typeset with TEX (Tiyapan, 2001, KNT8(ii)), I used in addition to the plain TEX `manmac.tex` and `epsf.tex`. Now to my amazement, I have discovered many other excellent macros, for instance `rotate.tex`, and found that I could understand how they work when I read them. This is one of the benefits that comes with talking in TEX instead of, for instance, LaTEX. I also know now the difference between the primitive TEX and plain TEX, and that the latter is only one of the infinitely many possible implementations of TEX. However, since all TEX gurus I know use plain TEX as a basis, there is no reason why I should be too proud to follow the practice. Having said that, my next plan is to improvise on the primitive TEX without any direct reference to the plain TEX macro.

The citation program BibTEX was intended to be used with LaTEX. Karl Berry and Oren Patashnik have written `btxmac.tex` which makes BibTEX usable from plain TEX. But for the present

purpose I merely use my own macros, which are much simpler, and do not need BibTEX. Ultimately such database program as BibTEX would have been extremely useful. But I wish to develop something similar to it on my own.

There are still some unsolved problems in the TEX macros, for example the page references which are embedded within groups are sometimes slightly wrong, that is they may appear to be one more or one less than their actual position. Since publishing macros play but a minor part here compared with mathematics and physics, this problem has been systematically minimised and then tolerated. The solution and explanation of it will be dealt with and published elsewhere.

When lines of text appear beside a picture there are macros which make the latter always stay next to the outer rim of the page. These work satisfactorily well, and those cases in the results which appear to say otherwise are in fact the result of some other more primitive macros earlier written.

§ 2. Division of space

A stochastic system which is stochastically invariant under arbitrary translation, that is under the transformation $x \to a + x$, is homogeneous. Homogeneity lets us use the ergodic theory, namely $\dot{F}_{Z,q}(z) \to \dot{F}_Z(z)$ with probability one as q approaches infinity for all z in Z, in other words the empiric- implies the ergodic distribution function of the characteristic Z for the cell C in $Q(q)$. Empirical moments, $\dot{E}_q(z) = \int z \mathrm{d}\dot{F}_{Z,q}$, almost surely converge to the corresponding ergodic moments, $E(z) = \int z \mathrm{d}F_Z(z)$. The study of random division of space aims at defining classes of parameter dependent random divisions and determining their important ergodic distribution. The most important ergodic distribution is the volume (Miles, 1972). But $E(V)$ itself is not particularly informative because it only shows the scale of the model. The best representative of the nature of a random division is then the *coefficient of variation*, $\mathrm{cv}(V)$, which is the ratio of the standard deviation to the mean. The mean 1-projection or mean caliper diameter, M_1, of a domain is the mean length of its orthogonal projection onto an isotropic random line, whereas the mean 2-projection is the mean area of its orthogonal projection onto the same. For a polyhedron, $M_1(4\pi)^{-1} \sum d_e^i(\pi - \theta_i)$ where θ_i is the dihedral angles in radians. The i-facets of a polyhedron, $i = 0, 1, 2$, are its vertices, edges and faces respectively. The seven values of the basic integral geometric polyhedral quantities are V, A, M_1, d_e, n_c^f, n_c^e and n_c^v. If a polyhedron is simple, *i.e.* each vertex is in three and only three faces, then $3n_c^v = 2n_c^e$ and from Euler's formula, $n_c^v - n_c^e + n_c^f = 2$, then it follows that the value of any one of n_c^v, n_c^e and n_c^f determines the value of the other two. The mean value of n_c^f give a good idea of the overall interface structure, and so is only next in importance to the $\mathrm{cv}(V)$. The homogeneous Poisson s-flats in R^d, $\mathcal{P}(s, d)$, underlies most forms of random divisions of space (*cf* Miles, 1972), in particular $\mathcal{P}(0, d)$ where $d = 2$ or 3. Under this notation the standard Poisson process is $\mathcal{P}(0, 1)$. The basic properties of $\mathcal{P}(0, 3)$ are that

$$\mathrm{P}(\text{there are } n \text{ particles in } X \subset V) = e^{-\rho V}(\rho V)^n / n! \qquad (\mathbf{14})_{\mathrm{ii}}$$

where $n = 0, 1, \cdots$, that is the probability is a Poisson (ρV) distribution, and that the numbers of particles in disjoint domains are mutually independent. Miles (1972) gives descriptions of various kinds of random tessellation, for example the box tessellation and particularly the generalised Johnson-Mehl model, described here as Algorithm ℵ, which includes both the standard Johnson-Mehl and the Voronoi tessellation in three dimensions as special cases.

Algorithm 2.1 *Generalised Johnson-Mehl model, Miles (1972)*

for each time step **do**
  while more nuclei to be born **do**
    borns a nucleus;
    if the new nucleus would occupied a site already occupied **then**
      remove the nucleus;
    endif
  endwhile
  for all growing nuclei **do**
    for all its rays still growing **do**
      nucleus **radiates** with speed v;
    endfor
  endfor
  for all those nuclei which has just grown **do**
    for all its rays just grown **do**
      if it has met with a ray of another nucleus **then**
        label both rays as grown;
      endif
    endfor
    if all its rays are grown **then**
      label the nucleus as fully grown;
    endif
  endfor
endfor □

Similar to the Minkowski space, the stochastic nucleus birth process is in (3+1)-dimensional space, $(x, y, z; t)$-space where $t \geq 0$ which can be denoted by R^4_+. This process is homogeneous in (x, y, z) but not necessarily so in t because in the actual development process it is always inhomogeneous with respect to time. Then this birth process is a Poisson point process in R^4_+, which is inhomogeneous in t and with the intensity $\alpha(t)$. For the standard Johnson-Mehl, $\alpha(t) = \alpha$ is a constant, whereas for the Voronoi $\mathcal{V}(3,3)$, $\alpha(t) = \rho\delta(t)$, where $\delta(\cdot)$ is the Dirac δ function. This model is thus a general one which can be fitted to a wide range of data by choosing some appropriate $\alpha(\cdot)$.

Each i-facet of the Voronoi tessellation $\mathcal{V}$, created from $\mathcal{P}(0,3)$, is an i-facet of $4-i$ members of $\mathcal{V}$, with each point on the i-facet being equidistant from the corresponding $4-i$ nuclei where $i = 0, 1, 2$. The exact values of the moments of the 3-d Voronoi tessellation in the notation used by Miles (1972) are: for first order moments, $\mathrm{E}(V) = \rho^{-1}$, $\mathrm{E}(S) = (256\pi/3)^{1/3}\Gamma(5/3)\rho^{-2/3} = 5.821\rho^{-2/3}$, $\mathrm{E}(M_1) = 4^{2/3}\pi^{5/3}\Gamma(1/3)\rho^{-1/3}/(3^{5/3}5) = 1.458\rho^{-1/3}$, $\mathrm{E}(L_1) = 12\,\mathrm{E}(M_1) = 17.50\rho^{-1/3}$, $\mathrm{E}(N_2) = (48\pi^2/35) + 2 = 15.54$, $\mathrm{E}(N_2^*) = 8$, $\mathrm{E}(N_1) = 144\pi^2/35 = 40.61$ and $\mathrm{E}(N_0) = 96\pi^2/35 = 27.07$; for a second moment, $\mathrm{E}(V^2) = 1.180\rho^{-2}$; for the aggregate of edges, $\mathrm{E}(L) = \mathrm{E}(L_1)/\,\mathrm{E}(N_1) = 0.4309\rho^{-1/3}$; for the aggregate of faces, $\mathrm{E}(A) = \mathrm{E}(S)/\,\mathrm{E}(N_2) = 0.3746\rho^{-2/3}$, $\mathrm{E}(B) = 2\,\mathrm{E}(L_1)/\,\mathrm{E}(N_2) = 2.252\rho^{-1/3}$ and $\mathrm{E}(N) = 3\,\mathrm{E}(N_0)/\,\mathrm{E}(N_2) = 5.228$; for the plane section, $\mathrm{E}_2(A) = 1/\rho\,\mathrm{E}(M_1) = 0.6859\rho^{-2/3}$, $\mathrm{E}_2(B) = (6/\pi)^{1/3}5\Gamma(2/3)\rho^{-1/3} = 3.136\rho^{-1/3}$, $\mathrm{E}(N) = 6$ and $\mathrm{E}(A^2) = 0.698\rho^{-4/3}$; and for the line section, $\mathrm{E}_1(L) = 4/\rho\,\mathrm{E}(S) = 0.6872\rho^{-1/3}$, $\mathrm{E}_1(L^2) = 0.682\rho^{-4/3}$, $\mathrm{E}_1(L^3) = 0.668\rho^{-1}$ and $\mathrm{E}_1(L^4) = 0.774\rho^{-4/3}$. In our terminology, ρ, S and L_1 are respectively ρ_c, A and d_e, N_0, N_1, N_2 and B respectively n_c^v, n_c^e, n_c^f and s. The Delaunay tessellation, on the other hand, is better understood since we know that

$$\mathrm{E}(V^k) = \frac{35\pi^{1/2}(k+2)!(2k+4)!}{256\Gamma\left(\frac{1}{2}k+2\right)\Gamma\left(\frac{1}{2}(3k+9)\right)(8\pi\rho)^k}. \qquad (\mathbf{15})_{\mathrm{ii}}$$

Shape is the most fundamental geometrical property. Shape and size are all the geometrical information that remain when location and rotational effects are filtered out from an object (Dryden and Mardia, 2002), and between these two you can take the size away so that only shape remains for further analysis. When we talk about particle sizes in simulation, it is usually the case that we have already assumed some kind of particle shape. This is because the definition of size is only meaningful if you have some idea about the shape. Shape analysis works with landmarks, which are also known as anchor-, control-, design-, key-, model-, profile-, or sampling points, facets, markers, nodes, sites, fiducial markers, *etc.* Dryden and Mardia (*ibid.*) work with three types of landmarks, *viz.* anatomical-, mathematical- and pseudo landmarks. Their work could become very interesting if combined with another problem of object location (*cf* Tiyapan, 1996, KNT4(v) and KNT4(vi)). A landmark can be unlabelled or labelled with a name or number. A particular member of the shape set which is used as a representative of all other members is the icon of that set. For the shape analysis in two dimensions the thin-plate spline is a convenient tool which is bijective and is analogous to the monotone cubic spline.

§ 2.1 Stereographic projection

Stereographic projection (*cf* Phillips, 1949) is used to represent a three-dimensional figure in two dimensions. It is useful in the study of symmetry of crystals. The stereographic projection of a cube is shown in Figure 2.1.

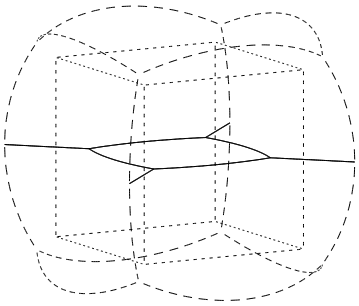

Figure 2.1 *Stereographic projection* of a cube. A stereographic projection is drawn by first projecting each vertex on to the surface of a sphere encircling the polyhedron along the line coming from the origin of the sphere. The projected point on the sphere surface is then projected on to the plane $z = 0$ (ie. $(x, y, 0)$) along the line which originates from it and goes towards the nadir point relative to the half-sphere surrounding it that rests on the $z = 0$ plane.

With this kind of projection, points that are symmetrical to each other with respect to the plane $z = 0$ are projected on to the same point on that plane. Therefore it is a normal practice to

distinguish points of the two hemispheres by drawing those in one of them as dots, while drawing the rest as circles. Continuous lines going from one hemisphere to another will become discontinuous on the projected plane. In Figure 2.1, the top and the bottom squares of the cube is projected on top of each other, while the four edges parallel to the z-axis go to the circumference of the great circle of the projected plane first, then retrace their ways back to their vertices.

Figure 2.1 shows that, in effect, what the stereographical projection does is to bloat a polyhedron out into a spherical balloon, and then project the image obtained on the balloon on to the horizontal plane. What the second projection does is to look at the hemisphere above it with a 90° wide-angled lens from the nadir position. In order to compare the shape of the original polyhedron with the top-view of the balloon as well as the stereographical image, Figure 2.2 draws our cube rotated one radian around the vector $(0.3, 0.4, 0.866)$. Such rotation can be done by using the transformation matrix

$$M = \begin{bmatrix} 1-2(y^2+z^2) & 2(xy-wz) & 2(xz+wy) \\ 2(xy+wz) & 1-2(x^2+z^2) & 2(yz-wx) \\ 2(xz-wy) & 2(yz+wx) & 1-2(x^2+y^2) \end{bmatrix},$$

where $[(x,y,z),w] = q$, a quaternion, $(x,y,z) = u\sin\alpha$ and $w = \cos\alpha$. Here $u = (a,b,c)$ is the direction cosine vector of the axis of rotation and $\theta = 2\alpha$ is the angle of rotation.

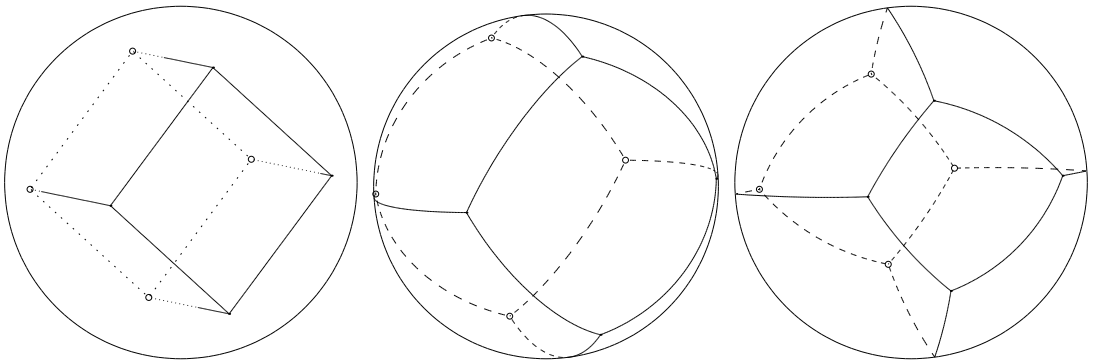

(a) (b) (c)

Figure 2.2 *Rotated cube, (a) top-view, (b) top-view of its bloated sphere and (c) the stereographic projection. While (c) shows the same amount of symmetry information as the other two, it incorporates more information regarding the z-coordinate than the others, (b) being the least informative in this respect.*

The information regarding symmetries of the polyhedron is preserved by the projection. In practice, when it is applicable and possible, the sphere is positioned such that its centre coincides with the centre of symmetry of the polyhedron, the plane $z = 0$ on one of the symmetry planes, and the planes $y = 0$ and $x = 0$ on two others. Thus Figure the projection of 2.2 clearly shows the symmetry around the centre as well as the reflection symmetries with respect to the planes $z = 0$, $y = 0$, $x = 0$, $x = y$ and $x = -y$. Figure 2.2, on the other hand, only shows the symmetry around the centre.

The stereographic projection is an example of a homeomorphism, that is to say, a mapping of one figure onto another that is both continuous and one to one.

A stereographic net is called the Wulff net. It comprises a family of great circles at 2° intervals and a family of small circles. The great circles are equivalent to the meridians of longitude while the small circles the parallel latitudes (*cf* Cox *et al*, 1974).

The stereogram which is made up of two 2-d pictures, one for each eye, can also be used for visualising a crystal structure in three dimensions. It works by tricking or brain to see the virtual 3-d image from the input prepared for both eyes. Unlike the stereoscope which requires a viewing device, an autostereogram requires none and only a little practice. During the 1990's there has been a boom in businesses related to a certain type of stereogram referred to as SIRDS, Single Image Random Dot Stereogram, which was only a new name for the autostereogram. The boom of this business had the origin in Japan and was fueled by consumers in the east-asian countries, including Thailand. In this kind of autostereogram there are no two separate images. The two images appear as dot patterns embedded within a random pattern of dots in the background. This makes one see the 3-d images arising out of the blue amidst a seemingly chaotic random mixing of dots. SIRDS sometimes appears as another variant called Single Image Stereogram, SIS, which uses patterns in

place of dots.

Stereograms and Autostereograms have no depth of field. This gives it a peculiar sharpness because all points from the highest to the deepest appear in focus at once, whereas in viewing the real world our eyes focus on one distance at a time. The reason behind the surge in the popularity of SIRDS's mentioned must be that they help relax the eyes. Because there is no special gadgets required, one needs to look at the image wide-eyed, that is to say, with one eye focusing parallel to the other, and this is very relaxing to the muscles of the eyes. By contrast, cross-eyed viewing can induce headache and eyestrain. One procedure for drawing a stereogram from a crystal or crystal model is shown in Algorithm 2.2.

Algorithm 2.2 *A procedure for drawing stereograms from crystal models.*

make drawings of the crystal;

label all the different faces;

select prominent zones;

for every zone **do**

  measure all the interfacial angles;

endfor

plot the prominent zone in the primitive circle;

mark the centre of the stereogram;

locate a arbitrarily;

mark the remaining face poles;

□

The interfacial angles are measured using a contact goniometre. The sum of the interfacial angles in a complete zone is 360°. Face poles are marks obtained from intersections of small circles with with primitive circles.

The programs on stereographic projection are collectively called `stp.m` and listed in § A.32. Some of the pictures drawn during its developmental stages are given in Figure 2.3 (a) and (b) while those for future developments in Figure 2.3 (c) and (d).

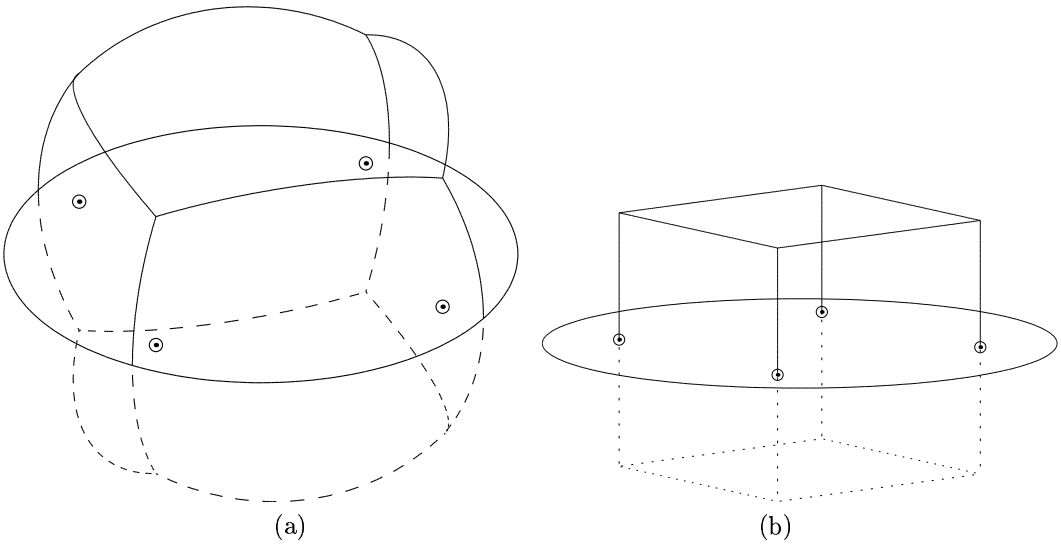

(a) (b)

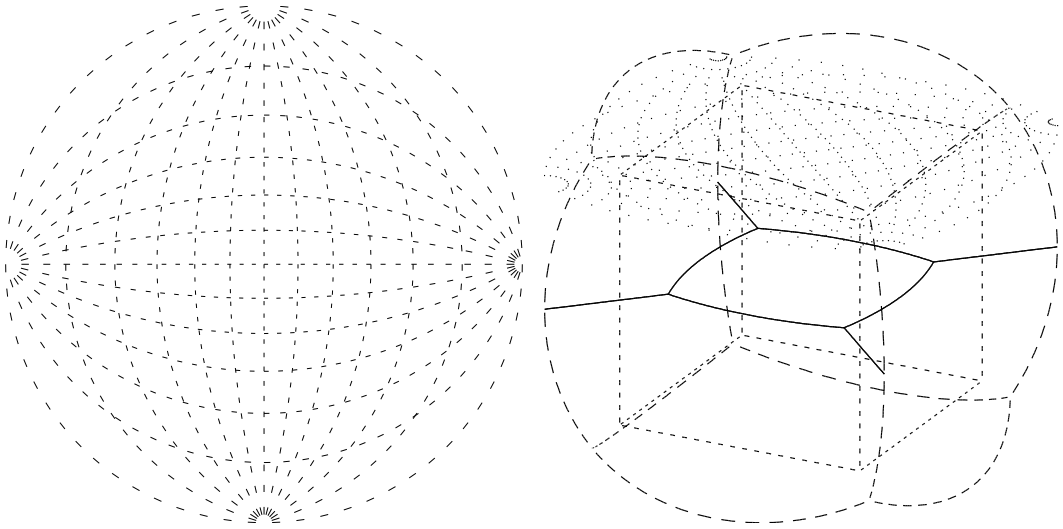

(c) (d)

Figure 2.3 *Developmental stages of programs for the stereographic projection;* (a) *and* (b) *for the cube,* (c) *and* (d) *the great circles.*

The parameters of any two faces of a crystal are always rationally related to each other. One way of uniquely presenting the relationship between angles of the faces and those of the crystallographic axes is by using the Miller indices. These idices are obtained by first finding intersections between a face and a-, b and c axes. Then divide by the b-axis intersection to get parameters of the face, and then divide these by the respective values of the parametral plane chosen. What is obtained after this stage are the ratio of the parameters to those of the parametral plane, the reciprocal of which gives the Miller indices.

§ 2.2 Covering lattices

A covering lattice of any two-dimensional lattice is the lattice obtained by joining midpoints of consecutive edges together. The code in § A.7 finds covering lattices up to the eighth one and computes the total area of the cells for each case.

The square lattice is the only regular covering lattice, that is it is both the dual and the covering lattices of itself. But all polygonal tilings and tessellations can have a covering lattice, or in fact an infinite orders of covering lattices. Coverings of some lattices can be seen in § 3 (*cf* Tiyapan, 2001, KNT8(ii)).

Coverings can be generalised to a general dimension d. In two dimensions they are lines, *i.e.* having two vertices, straight lines each of which join two lines across a corner. For three-dimensional polyhedral tessellations they are planes with three vertices, triangles each of which join three planes across a corner, in other words a coign. Then in four dimensions they may be polyhedra with four vertices, tetrahedra each of which joins four 4-d polytopes across a four-edged corner in four dimensions, and so on. In d dimensions, then, perhaps they are polytopes with d vertices, three-cornered $(d-1)$-polytopes each of which joins d d-dimensional polytopes across a d-edged corner in d-dimensions.

One interesting property of covering lattices is that they leave the voids intact while reducing only their size. Thus the structure and complexity of the original tessellation remain unchanged. This can be useful when we want to exclude some of the volume. In filtering membrane studies, for instance, this is ideal since all the voids still remain in the same position.

The process of covering is similar to that of shrinkage in cell in that there is a retreat away from corners. This could be because corners are hard to maintain. Surface tension is high there, and like a nook, recess, or remote, unstrategic parts of a country the cost of maintaining and governing is high. In the case of a country, conflict in such parts is analogous to the high surface tension in corners of cells.

When an empire or a metropolitan city declines, the process is similar. Such far corners are the first parts to fall into chaos. Law, order and security shrink away from them. The Roman Empire is an excellent example of this. In its heyday it reached out to every corner of Europe, however far. When it came to the decline, it literally *pulled itself together*, though it never could pull itself

together again after that. It drew away first from those far corners, England for instance, and then towards its nucleus and died.

Manchester is another interesting example. After the industrial revolution, and under the governance of the Conservative party, the city declined. And as it did, all the different nuclei became prominent, if only because the distance between them became more so. Thus Bolton, Altrincham and Stockport, for example, shrunk towards their nuclei, leaving behind dangerous districts where mugging, murder and crime are rampant like the Moss Side decades ago until shortly after the IRA bombing of the city centre. When an urban area fades away it does not do so suddenly but like the plant cell subject to a dewatering process or a polygonal tessellation to a covering one.

Random fluctuation can create areas of irregularity within a homogeneous and isotropic universe. These irregularities become nuclei, and from duality of the structure fine partitions start to develop around them which become Voronoi facets. Gradually but steadily the gas shrinks to form the galaxies of our present universe.

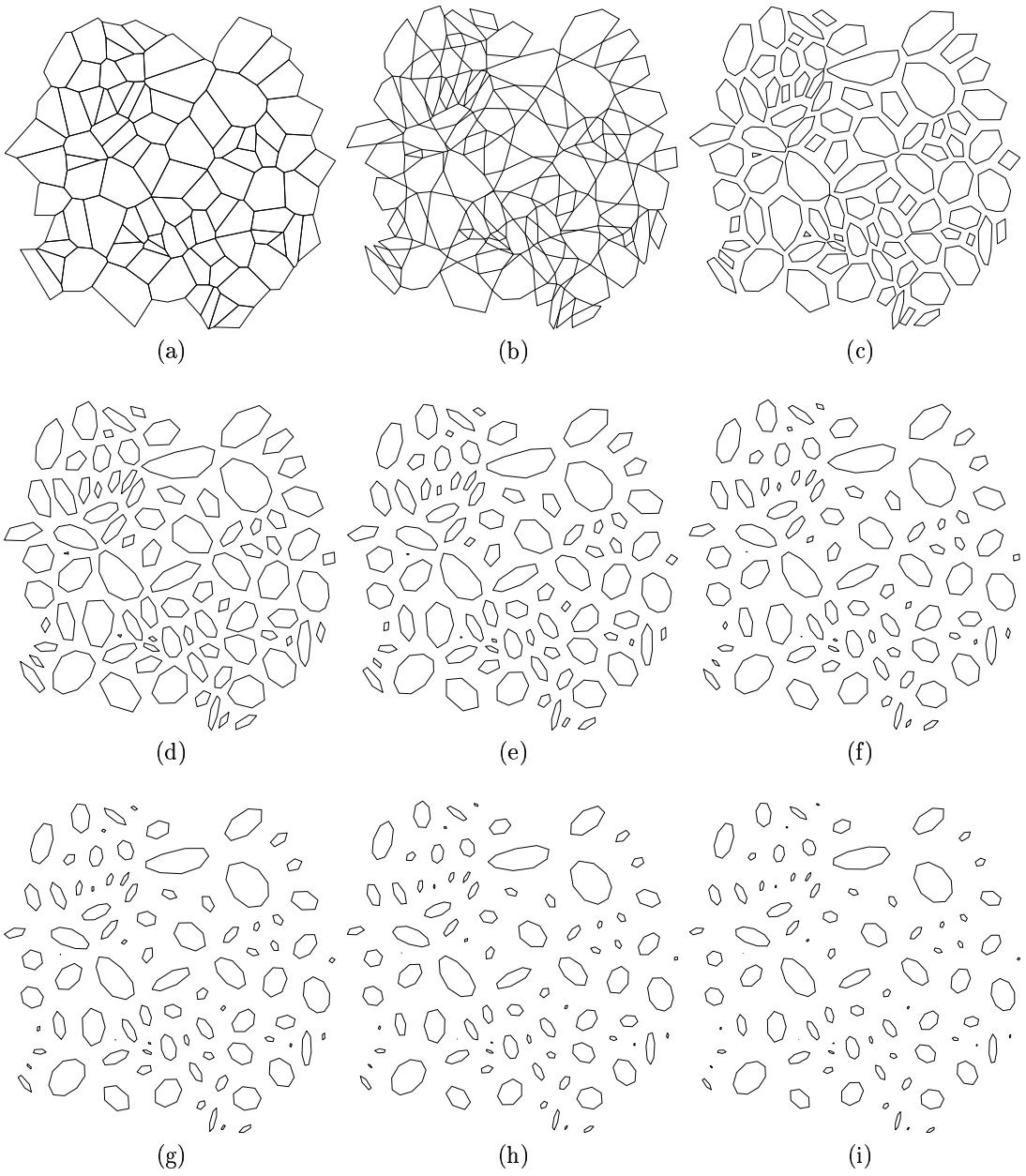

Figure 2.4 *Covering lattices, stone pavements, or galaxies in the forming?* (a) $\mathcal{V}$, (b) $\mathrm{C}^1(\mathcal{V})$, (c) $\mathrm{C}^2(\mathcal{V})$, (d) $\mathrm{C}^3(\mathcal{V})$, (e) $\mathrm{C}^4(\mathcal{V})$, (f) $\mathrm{C}^5(\mathcal{V})$, (g) $\mathrm{C}^6(\mathcal{V})$, (h) $\mathrm{C}^7(\mathcal{V})$, (i) $\mathrm{C}^8(\mathcal{V})$.

Figure 2.5 (a) to (i), which are the results of the covering operator applied to a Voronoi graph eight times in succession, represent this situation. Figure 2.5 shows the area of multiply covered cells $\mathrm{C}^n(\mathcal{V})$, $n = 0$ to 8, where $\mathrm{C}^0(\mathcal{V})$ is the Voronoi graph $\mathcal{V}$. Circles are the per cent total area, and the curve is $y = 10^{-0.8x+2}$. The code `gxy.m` to find the covering contours above is given in § A.8. The area of the cells decreases from the covering operator, not linearly but with deceleration as Figure 2.5 shows.

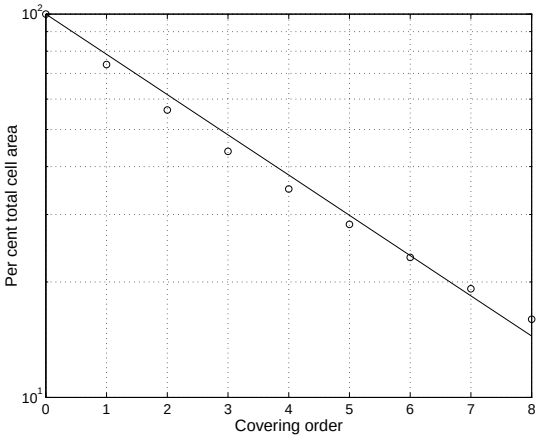

Figure 2.5 The area of multiply covered cells.

On taking a closer look at Figure 2.5, one can interestingly notice that even though all pores shrink from the application of the covering operator, some does so much quicker than others. In particular, round pores shrink but slower. The more corners a pore has the less acute are the angles, which makes it the more stable and thus able to maintain its original size.

Geometrically, one can see that the most unfortunate of all polygons is the triangle. The area of a triangles of any shape reduces by 75 per cent upon being covered. The circle is the most fortunate in this matter since it has no corners and therefore it is impossible for these to be cut. This is in accordance with our argument that corners are unstable region.

§ 2.3 Viscous fingers

Viscous fingering is a happening which occurs when a low viscosity fluid with high pressure penetrates the border of a higher viscosity fluid in a form of thin branching fingers resembling a flash of lightnings in shape. An experimental account as well as descriptive pictures and diagrams are given by Nittmann et al (1985). However, a reference made to one previous work (Hele-Shaw, 1898) was inaccurate in at least three ways, one of which is in the initials of its author, while the rest in the actual contents. The first one can easily be verified with a little research, is that the initials of the author of the paper is H. S., not J. S. S. as given his full name being Henry Selby Hele-Shaw (1854–1941). For the remaining two, firstly the paper by Hele-Shaw is about fluid flow pass free boundary of solid, *not* viscous fingering instability. Secondly, Hele-Shaw was in fact an engineer who has been a professor at University college in Liverpool for 17 years, whose interest was in layer parallel motion (laminar) and sinuous (turbulent) flows pass various bodies of uniform cross section as well as in flows through channels of varying cross section. Born at Billericay, Essex, and a holder of Whitworth scholarships while a student at University college, Bristol, he was elected to the Royal Society in 1899 because of his experiments done on streamline flow. He has successfully introduced the use of air bubbles in experiments to help portray the stream lines of the flow; his cited work mentions neither the physics of nor the application to petroleum science as the context would have us believe. However, his other and subsequent work (Hele-Shaw, 1899) does mention briefly about the importance of viscosity in nature and the difficulty of modelling the motion of viscous fluids mathematically, but nowhere in either one of these two papers did he consider the interaction between fluids of different viscosity.

The simulation for the viscous fingering problem may be related to that for the propagation through rivulets or channels that we study here in § 6.11. It may also be related to the front tracking simulation of dendritic growth. Front tracking has been to solve various problems numerically, for example shocks, flame-, chemical reaction and solidification fronts. In this method a dynamical problem in n dimensions is transformed into a set of partial differential or integro-differential equations which are then solved numerically at a finite set of points on the front or interface (Srolovitz, 1990).

Dendritic growths, on the other hand, are characterised by their rich patterns and share one property that is similar to percolation, which is that it is very difficult, if not impossible, to completely describe the mathematics of their dynamic evolution.

As in other microstructural simulations, the underlying structure where these fingerings occur can be simplified by the mean-field method, which replaces the microstructure by a typical grain, or by making a simple geometrical model to represent it, for example a Voronoi tessellation. The

computer simulation can be done using Monte Carlo methods, which describes the energy of the structure in terms of the location of defects and is based on a kinetic rate, or by numerically integrating the equations of motion that describe the evolution of the defects.

§ 2.4 Crystals, quasicrystals, and polycrystals

Crystals, quasicrystals, and polycrystals

The shape of individual grains in polycrystal and the inter granular surface can be found by stereoscopic microradiography, but using random plane section is more convenient in practice (Aboav and Langdon, 1969). The grains of polycrystals are not arranged at random but in a characteristic way which can be expressed in simple terms and seems to be scale-free (Aboav, 1970). The average number of sides of neighbours of a grain is $n_n^e = 5+8/n_e$ where n_e is the number of sides of the grain. Aboav (1970) studies grains of polycrystalline magnesium oxide and finds $n_e = 5.85$. He also finds that most of the time $n_n^e > n_e$ which seems like a contradiction but is because the probability that a point lies in a grain of a particular shape depends on the size and abundance of such grains. He also finds the average number of n-sided grain $n_c^{n-e} \propto (n-2)$. Grains of a polycrystal are different from cells of a soap foam in that they possess a stable grain diameter, which only depends on the temperature.

This stable diameter of grain, d_e, is the average grain diameter at which the growth ceases, and is $d_e^{1/2} = c(T - T_0)$ (Aboav, 1971). For cadmium $T_0 = -53°\mathrm{C}$, $0°\mathrm{C} < T < 170°\mathrm{C}$. The distribution of grain size is $z = z_m \exp\left\{-\alpha^2\left[(x/x_m)^{1/2} - 1\right]^2\right\}$ where z is the number of grain sections in a plane section, α a constant, x the diameter of grain section and x_m the value of x at z_m.

There are similar patterns of grains in a polycrystalline ceramic, magnesium oxide, cadmium, *etc.* The moments of distribution above $n = 6$ is $\mu_m = \sum_n (n-6)^N f_n$ where f_n is the fraction of cells with n sides. The second moment $\mu_2 > 0$ unless all cells have six sides, and we have a purely topological relation $\sum_n n_n^e n_e f_n = \mu_2 + 36$. If $n_n^e \propto 1/n_e$, then $n_n^e = (6 - a + b\mu^2/6) + (6a + (1-b)\mu_2)/n$. If $a = 1$ and $b = 0$, this equation is reduced to $n_n^e = 5 + (6 + \mu_2)/n$ and furthermore if $\mu_2 = 0$, $n_n^e = 5 + 8n_e$. In a polycrystal the distribution of n_e does not usually vary as the grains grow. Typically $\mu_2 = 2.4$. Soap foams resemble a polycrystal (Aboav, 1980), and $n_n^e = A + B/n_e$, $n_n^e = (6-a) + (6a + \mu_2)/n$, $a = 1.2$.

The growth process of both crystals and quasicrystals are nonlocal in nature, but that of polycrystals is of a multigrain growth. Crystals with a very large unit cell exists. Quasicrystals cannot grow in the same manner as playing a jig-saw puzzle (Penrose, 1989) because no matter how many steps one looks ahead there will come a point where there is a gap that none of the available basic building blocks can fit in. A *legal* tiling contains no gaps or overlaps; if it can be extended to cover the whole plane it is also a *correct* tiling. A *mistake* occurs when a tile added to a correct tiling renders it a legal but incorrect one. By using the basic units to build larger units having the same structure as these basic units and then recursively repeat the process, one can in the end reach a correct tiling. But this is also a nonlocal process since one still requires the ability to look ahead in order to make sure that the units are always structurally the same.

The fact that zeolites are crystalline seems to rule out the randomness assumption that one may otherwise use to model their growths as random continuum percolation. One needs to resort to the methods and tools used by the geologists if one wants to study zeolites, synthetic as well as natural ones.

Krýstallos is the Greek word for ice. Crystallography is nowaday the science of the crystalline state which, apart from the crystals themselves, includes such seemingly unlikely materials as plastics, rubber, silk, wool, liquids and gases (*cf* Phillips, 1949). There are four kinds of symmetry axes in crystal models, corresponding to $n = 2$ to 6 in the formula for the angles $\frac{360°}{n}$ by the rotation of which a crystal will repeat itself. These axes are respectively called *diad*, *triad*, *tetrad*, and *hexad*.

Crystals	*centres of symmetry*	*planes of symmetry*	*diad*	*triad*	*tetrad*	*hexad*
Cube	1	9	6	4	3	
Rhombohedron	1	3	3	1		

Table 2.1 *Symmetries of crystals*

The symmetries of the seven crystal systems, the Triclinic contains no axes of symmetry, Monoclinic one diad axis, Orthorhombic three diad axes, Tetragonal one tetrad ais, Cubic four triad axes, Trigonal one triad axis, and Hexagonal one hexad axis. A *monoclinic* crystal has all three axes unequal and one oblique intersection while an *anorthic*, aka *triclinic*, crystal has all three axes

unequal and intersecting at oblique angles. The relative development of crystals in different forms give rise to the *habit* of crystal. Thus if one gradually truncates the coigns of a cube one will come to an octahedron, and vice versa. All the continuous transformations between the cube and the octahedron are called *cubo-octahedron*. Crystal models of different habits readily yield on inspection the same symmetry group, but real crystals often look irregular and determination of the symmetry is based on the law of consistency of angle and uses goniometers.

The number of faces in crystals are usually even numbers. Take for example the 33 non isometric crystal forms (Klein and Hurlbut, 1993). Here only three have their faces in odd number, *viz.* pedion which has only one face, and trigonal prism and trigonal pyramid which have three faces each. For the rest, those which have two faces are pinacoid, dome and sphenoid; four faces rhombic prism, tetragonal prism, rhombic pyramid, tetragonal pyramid, rhombic disphenoid and tetragonal disphenoid; six faces ditrigonal prism, hexagonal prism, ditrigonal pyramid, hexagonal pyramid, trigonal dipyramid, trigonal trapezohedron and rhombohedron; eight faces ditetragonal prism, ditetragonal pyramid, rhombic dipyramid, tetragonal dipyramid, tetragonal trapezohedron and tetragonal scalenohedron; twelve faces dihexagonal prism, dihexagonal pyramid, ditrigonal dipyramid, hexagonal dipyramid, hexagonal trapezohedron and hexagonal scalenohedron; sixteen faces ditetragonal dipyramid; and twenty-four faces dihexagonal dipyramid. Among these, there is none which has its faces in a number of 5, 7, 9–11, 13–15, 23, or 25 and above. In Figure 2.6 the distribution curve for even numbers of faces is a scaled Chi-square distribution $y = K \cdot (x/3)^{(\nu-2)/2} \exp(-(x/3)/2)/(2^{\nu/2}\Gamma(\nu/2))$, where the degree of freedom ν is four and $K = 35$, while the curve for odd numbers of faces is the contour of a scaled Poisson distribution $y = K \cdot \lambda^{2x} \exp(-\lambda)/(2x)!$, where $K = 12$, $\lambda = 5$, and $2x$ is any positive integer or zero.

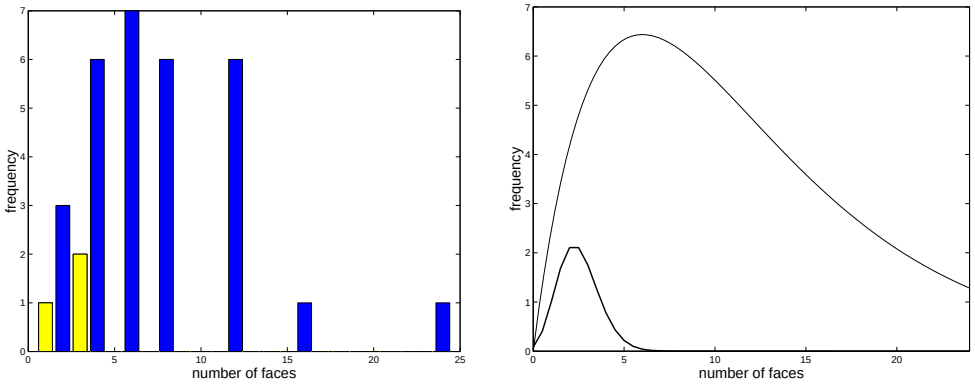

(a) (b)

Figure 2.6 *(a) number of faces of the thirty-three non isometric crystal forms; (b) approximation curves, the heavy line encompasses* $y = 12\exp(-5) \cdot 5^{2x}/(2x!)$ *while the lighter line* $y = (35/12)x\exp(-x/6)$.

Miller indices define the shape of crystals in terms of their faces by numbering their axial intercepts. These indices are $h = a/X$, $k = b/Y$ and $l = c/Z$ where X, Y and Z are respectively the x-, y- and z-intercepts. First, decide the three crystallographic axes. Then choose as the standard or parametral plane a plane that inclines against all these three axes. The shape of crystal, which according to the proportion of each crystal face is called the crystal habit, is governed by the slowest growing face and is affected by the presence of the additive solvent or impurities. Stereoisomerism is the difference in the spatial arrangements of the same atoms and functional groups in a molecule. Enantiomers occur in pairs. They are also known as optical isomers and are mirror images of each other. Polymorphs are substances which can crystallise into different forms the chemical formulae of which are similar to one another. For example, carbon can occur as graphite, diamond, or fullerenes. Isomorphous crystals always appear in one form. In pharmaceutical industries it is important to know the different properties of enantiomorphs of a drug, and to be able to grow each of them separately from the other. Crystalline materials have a tendency to cake or bind together during storage. The dimension of the particles is characterised in one of the following ways: as spheres where $V = \pi d^3/6$ and $A = \pi d^2$; as cubes, $A = 6L^2$, $V = L^3$ and $d = \sqrt{3}L$; as the maximum characteristic chord length of an irregularly shaped particle; as an equivalent diameter or characteristic length. The shape factor for the surface is $f_s = A/L^2$ while for the volume it is $f_v = V/L^3$. Their values are subjected to an inequality constraint, namely $f_s \geq \pi$ and $f_v \geq \pi/6$ where the equality is for the case of a sphere. The ratio $r_f = f_s/f_v$ called the specific surface shape factor, whereas the surface

area ratio between that of the sphere and that of the particle of equal volume is called the sphericity, Ψ. The specific surface is $\alpha = A/V$ and onsequently $r_f = \alpha L$. The specific surface of particles is the surface area of particles per volume of particles, $\alpha_p = r_f/\bar{d}_s$, while the specific surface of bed is the surface area of particles per total volume of bed, $\alpha_b = (1-\varepsilon)\alpha_p$. The particle size distribution is usually described by the cumulative mass fraction which is the fraction of mass of each particle size, the differential mass fraction $x = \mathrm{d}m/\mathrm{d}d$ or $\int_0^\infty x\mathrm{d}d = 1$, or the size increments. The number of particles in mass fraction x_i is $n_i = x_i/(\rho_s f_v d_i^3)$, where x_i is the ratio of the mass in sizes in the i^{th} interval to the total mass of all particles, and n_i is the product between the number, the volume, and the density of particles. The weight- or volume mean size is

$$\bar{d}_w = \frac{\sum_i x_i d_i}{\sum_i x_i} = \sum_i x_i d_i = \frac{\sum_i n_i d_i^4}{\sum_i n_i d_i^3}, \qquad (16)_{\text{ii}}$$

where $\sum_i x_i = 1$. The mean weight- or volume size, $d_{\bar{w}}$, is the size of each particle of a mono-disperse powder such that $f_v d_{\bar{w}}^3 \sum_i n_i = f_v \sum_i (n_i d_i^3)$, which gives

$$d_{\bar{w}} = \left(\frac{\sum_i (n_i d_i^3)}{\sum_i n_i}\right)^{1/3} = \left(\frac{1}{\sum_i (x_i/d_i^3)}\right)^{1/3}. \qquad (17)_{\text{ii}}$$

The surface mean size† is

$$\bar{d}_s = \frac{\sum_i V_i}{\sum_i S_i} = \frac{\sum_i d_i S_i}{\sum_i S_i} = \frac{\sum_i n_i d_i^3}{\sum_i n_i d_i^2} = \frac{\sum_i x_i}{\sum_i (x_i/d_i)} = \frac{1}{\sum_i (x_i/d_i)}. \qquad (18)_{\text{ii}}$$

The mean surface size is the uniform size of mono-disperse particles which makes the surface area of the particles equal to the surface area of actual the powder. In other words, $\sum_i n_i f_s d_s r^2 = \sum_i n_i f_s d_i^2$, which gives $d_s r = [\sum_i n_i d_i^2 / \sum_i n_i]^{1/2} = [\sum_i (x_i/d_i) / \sum_i (x_i/d_i^3)]$. The specific surface is the surface area of a powder per unit mass or volume, $\alpha = f_s \bar{d}_s^2/\rho_s f_v \bar{d}_s^3 = r_f/\rho_s \bar{d}_s$. The coefficient of variation (cv) describes the spread of the distribution about the mean, cv $= \sigma/d$ where d is the mean size and σ standard deviation. The void fraction or voidage, $0 < \varepsilon < 1$, is the ratio of the particulate void volume to the total bed volume which comprises of the volume of voids and solids. Sieve test is used to find the distributions of particles. The mesh number of a sieve is the number of apertures per unit length of sieve, $N = 1/(L+W)$ where L is the aperture size and W the wire width. Crystal defects include point defects, edge- and screw dislocations.

The electrical double layer is $V_d = B' r \exp(-kh)$ where B' is related to the surface charge. The interaction energy from electric field of two charged particles has two minima, $L_1 < L_2$ where L_1 is the primary minimum which occurs at $d_1 < d_2$.

At L_1 the coagulation is rapid whereas at L_2 it is slow. Added polymers may stabilise a colloidal system when the charged adsorbed polymer layers repel each other, or they may destabilise it by making the particles more susceptible to salts or by forming polymer bridges which flocculate the particles.

The superficial velocity, u, is the flowrate per cross-sectional area of bed, $u = Q/A$, and is known as the *velocity flux* or the volumetric flowrate per unit cross-sectional area. The interstitial velocity, v, is the true linear velocity of the fluid. It is the flowrate per unit cross-sectional area of voids, *viz.* $v = Q/(\varepsilon A) = u/\varepsilon$. An ideal particle moves in a fluid with the velocity v as a function of μ, ρ, ρ_s and d. The momentum equation in one dimension for such particle is $\rho_s(\partial/\partial t + v\partial v/\partial z) = B + F - \partial p/\mathrm{d}z$, where B is all the body forces and F all the surface forces acting on the solid phase that is not included in the pressure gradient $-\partial p/\partial z$. The drag force per unit area on a single lone particle is $F/A = c_\infty \rho v^2/2$ where F is force, A the projected area, and c_∞ the single particle drag coefficient at infinite dilution. For sphere, $F = c_\infty \pi d^2 \rho v^2/8$. The force balance equation is $W - B - F = \dot{M}$ or $mg - m'g - F = m\mathrm{d}v/\mathrm{d}t$ where m and m' are the mass of particle and fluid displaced, and thus the second term represents the buoyancy. Balancing the accelerative and the resistive forces leads to $(\pi/6)d^3(\rho_s - \rho)g = c_\infty \pi d^2 \rho v_t^2/8$, where v_t is the terminal velocity, *i.e.* when $\mathrm{d}v/\mathrm{d}t = 0$, which gives $v_t = [4d(\rho_s - \rho)g/3\rho c_\infty]^{1/2}$. The Reynolds number of the particle is $\mathrm{Re} = \rho v d/\mu$. When $\mathrm{Re} < 0.2$ the flow is laminar and Stokes' law applies and the force balance equation becomes $(\pi/6)d^3(\rho_s - \rho)g = 3\pi\mu d v_t = F$, which gives $v_t = d^2 g(\rho_s - \rho)/18\mu$, $c_\infty = 24/\mathrm{Re}$ and the Stokes diameter $d_s t = [18\mu v_t/g(\rho_s - \rho)]^{1/2}$.

The mass flux is defined as the multiplicative product of concentration and velocity. In laminar flow, Darcy's law applies, that is $u = \mathrm{d}V/A\mathrm{d}t = K_1 \Delta P/H$, where K_1 is the bed permeability,

† aka volume mean or Sauter mean.

a measure of the total drag force. The inverse linear relationship between the viscosity and permeability is $u = B\Delta P/\mu H$, where $B = K_1\mu$ is the permeability coefficient in m^2. Let the pore diameter be d_1, its length H_1 and velocity v. Assume that the fluid in pore velocity is $v = u/\varepsilon$, the hydraulic pore diameter is δ is related to $d_1 = v_b\varepsilon/v_b s_b = \varepsilon/s_b$, and the pore length H_1 depends on the bed depth H. For laminar flow through a pipe with viscous drag the Hagen-Poisseuille equation applies, that is $v = d_1^2\Delta P/(32\mu H_1)$. For the capillary model, $v = u/\varepsilon = \varepsilon^2\Delta P/(K_2 s_b^2\mu H)$. The bed specific surface area, s_b, and the particle specific surface area, s_p, are related to each other by $s_b = s_p(1-\varepsilon)$, and thus $u = v\varepsilon = \varepsilon^3\Delta P/(K_2 s_p^2(1-\varepsilon)^2\mu H)$, the Carmen-Kozeny equation, from where $B = \varepsilon^3/(K_2 s_p^2(1-\varepsilon)^2)$, where the Kozeny constant K_2 lies between 3.5 and 5.5 and is normally taken to be 5. In compressible beds voidage is a function of P or ΔP and the Carman-Kozeny equation for dx is $-dp/dx = K_2\mu(1-\varepsilon)^2 s_p^2 u/\varepsilon^3$. For turbulent flow $\Delta P/\Delta H = K'(1-\varepsilon)\rho u^2/(\varepsilon^3 d)$, while a linear sum of the laminar and turbulent flow is $\Delta P/\Delta H = K^3(1-\varepsilon)^2\mu u/(\varepsilon^3 d^2) + K_4(1-\varepsilon)\rho u^2/(\varepsilon^3 d)$ where $K_3 = 150$ and $K_4 = 1.75$ (Jones, 2002). Across a filter cake the modified Darcy equation is $u = dV/Adt = \Delta p_c/(r\mu H)$ where V is the volume of filtrate which passed through the cake. If the specific cake volume, *i.e.* the volume of cake per unit volume of filtrate, is v_c, then the total volume of cake is $Vv_c = HA$ where H is the thickness or height of the cake. Then $dV/dt = A^2\Delta p_c/(r\mu v_c V)$. This, together with the Carman-Kozeny equation for packed beds $u = \varepsilon^3\Delta p_c/[5(1-\varepsilon)^2 s_p^2\mu H]$, gives the specific cake resistance $r = 5(1-\varepsilon)^2 s_p^2/\varepsilon^3$ There are two modes of filtration, the constant rate- and the constant pressure modes. In the former dV/dt is constant and, from $V/t = A^2\Delta p_c/(r\mu v_c V)$ which is also constant, it follows that $\Delta p_c/V$ is also constant. In the latter Δp_c is constant and equals to $\Delta p_{\max}$. It follows that $V^2 = 2A^2\Delta p_c t/(r\mu v_c) = k_1 t$ and $t/V = r\mu v_c V/(2A^2\Delta p_c) = k_2 V$ When the effect of the filter medium is considered Δp will comprise of two components, from the cloth and from the cake. The first one includes also the particles held in the filter. The resistance is $R = r(H+L)$ where L is the equivalent cake thickness of the filter. The filtration equation becomes $dV/Adt = \Delta p/[r\mu(H+L)]$, in other words $dV/dt = A^2\Delta p/[r\mu v_c(V + LA/v_c)]$ For the constant rate filtration $V_1^2 + (LA/v_c)V_1 = (A^2\Delta p/r\mu v_c)t_1$, while for the constant pressure filtration $(t-t_1)/(V-V_1) = [r\mu v_c/(2A^2\Delta p)](V-V_1) + r\mu v_c V_1/(A^2\Delta p) + r\mu L/(A\Delta p)$. Agglomeration of crystals can be on either an individual or collective basis. The first one is sometimes called primary agglomeration examples of which are parallel, dendritic and twin growths. The second one is also known as secondary agglomeration and is essentially those cases where crystals within the solution come together to form clusters. Secondary agglomeration can be perikinetic, from Brownian motion of small particles, or orthokinetic, from velocity gradients in the fluid. Crystals flocculate or coagulate loosely together, then they aggregate by starting to join one another, and then they agglomerate strongly together to become a single poly-crystalline particle. There are four main classes of forces, namely colloidal, stochastic, direct- and indirect systematic forces. Surface adsorbs certain ionic species which in turn attract opposite ions, thus forming electrical double layers which repel each other There are three types of particle interaction, that is van de Waals, electrostatic and steric. These depend on shape and size of the particle, surface charge, solution's pH and ionic strength, temperature and the separation distance between the particles. The van der Waals forces are between molecules having closed shells and do not obey inverse square laws. Three of these are attractive, namely the orientation effect between permanent dipoles, the induction effect between a permanent- and a temporary dipoles, and the dispersion effect or London force between temporary dipoles and induced dipoles. The potential equations is $V_v = -A_{12}\mathrm{f}(h)$ where A_{12} is the Hamaker constant of the material.

§ 2.5 Random lines and percolation

Miles (1964) studies the line system, $p = x\cos\theta + y\sin\theta$, where $-\infty < p < \infty$ and $0 \le \theta < \pi$. Chan (1990) studied numerical properties of such structure of random lines using the same generator and then used it to model the structure of non-woven media. This amounts to the study by simulation of filters the internal structure of which is fibre mat, for example polypropylene. The algorithm he developed deals with mechanical blocking and back-flushing of the fibres. Wilcock's study (1994), on the other hand, deals with woven materials. With them she tried to demistify the myth and mysteries surrounding the rule of thumb techniques in designing wire mesh demisters. Her algorithms first weave the mesh and then apply Monte Carlo to it for the simulation.

The steel and carbon fibres in cement pastes contributes respectively to hole- and electron conductions (Wen and Chung, 2000). This is a problem of percolation of interconnected random lines. On the other hand, we can also study the resistance instead of conductance, which is what Pennetta *et al* (2000) does for a random network of resistors. Interest in researches on random

resistor or conductor networks is strong (for example, Pennetta *et al*, 2001). Cheng *et al*(2001) look at NiMH (nickel metal hydride) batteries' electrodes. In their presentation they wrap all the ends of those fibres that stick out from the prototile. This gives the periodicity which they use in their simulation. The NiMH has high porosity, no less than 97 per cent, and it contains two or more phases.

Some recent developments related to polypropylene are those done by Mironi-Harpaz and Narkis (2001), Narkis *et al* (2000), and Zhang *et al* (2001). Those who study the conductivity and resistivity of materials are, for example, Benoit *et al* (2001), Broderix *et al* (2001), Flandin *et al* (2001), Hindermann-Bischoff and Ehrburger-Dolle (2001), Huang *et al* (2001), Hunt (2001), Jevtic *et al* (2001), Nielson (2000), Petrovsky and Rak (2001), and Stenull *et al* (2001). An example of the application to dentistry is that which is reported by Sharp *et al* (2000). Rong *et al* (2001) look at tensile curves and study the resistance to thermal deformation in nanocomposites.

§ 2.6 Convex hull

The set of extreme points E in some superset S is the smallest subset of S such that the convex hulls of both E and S are identical. Extreme points never lie in a triangle.

The Graham's scan algorithm (*cf* Preparata and Shamos, 1985) positions itself in the midst of the points and then scans around in one direction. It determines three points in turn, and rejects a mid point among the three if the angle made there is reflexive, *i.e.* α such that $\alpha \geq \pi$ in the anti-clockwise direction. In other words, an angle is a right turn if it is reflexive; it is a left turn otherwise. The algorithm is shown in Algorithm 2.3. Here $\{h\}$ is a stack which contains the points on convex hull

Algorithm 2.3 *Graham's scan.*

$i \leftarrow 1$;
$j \leftarrow 2$;
$k \leftarrow 3$;
while there exist unprocessed points **do**
  if $\angle p_i p_j p_k \geq \pi$ **then**
    $j \leftarrow i$;
    $i \leftarrow i - 1$;
  else
    $i \leftarrow j$;
    $j \leftarrow k$;
    $k \leftarrow k + 1$;
  endif
endwhile □

The algorithm starts from a known extreme point. It can also start from two points which are known to be extreme, in which case the space is divide into an upper- and a lower hulls. Similarly to the Graham's scan, Jarvis's march finds one extreme point after another as it wraps a line around the convex hull. The Quickhull algorithm in two dimensions is described in Algorithm 2.4.

Figure 2.4 *Quickhull in two dimensions.*

$l \leftarrow$ the point with the smallest abscissa;
$r \leftarrow$ the point with the largest abscissa;
$\{s\} \leftarrow$ all points above $\overline{lr}$;
$\{s\} \leftarrow$ all points below $\overline{lr}$;
while there remains an unprocessed s_i in $\{s\}$ **do**
  $h \leftarrow$ point in s_i which maximises the area of $\triangle hlr$;
  reject points bound by $\triangle hlr$;
  $\{s\} \leftarrow$ all points outwards from $\overline{lh}$;
  $\{s\} \leftarrow$ all points outwards from $\overline{rh}$;
endfor □

The divide-and-conquer algorithms divides a problem into subproblems, finds the convex hull for each one of them and then merges these together by finding the convex hull of convex hulls. Algorithm 2.5 finds the convex hull of two convex hulls.

Algorithm 2.5 *Convex hull of convex hulls*

$p \leftarrow$ one point in h_1;

if p is also in h_2 **then**
  $h \leftarrow$ **scan** around from p, and **merge** h_1 and h_2;
else
  $(u, v) \leftarrow$ points on h_2 such that $\angle upv$ is maximised;
  $c \leftarrow$ the chain from u to v which is furthest away from p;
  $h \leftarrow$ **merge** c and h_1;
endif □

There are also dynamic algorithms for finding the convex hulls. In this case the input is online and one can not look ahead at the input. This kind of algorithms may be useful for online applications, for example the traffic control in real time. Two things can happen in such dynamic algorithms; points are inserted or points are deleted.

The gift-wrapping methods, which are similar to the Jarvis's march, can be extended to the general d dimensions. Here a point is beneath a facet if it is on the same side of it as the hull, otherwise it is beyond it. Also, with respect to a point p, if p is beneath all facets that contain v then v is concave; if p is beyond the same then v is reflex; otherwise v is supporting.

§ 2.7 From convex hull to the Voronoi tessellation

The earlier studies of the Voronoi structure used the program `qhull` to create the structures. Programs were developed on Matlab to manipulate the data and find the statistics. These programs were tested on small structures first. Contrary to what the literature says, these very small networks turned out to have all the statistics in close agreement with those much larger ones. This confirms an earlier report (Tiyapan, 1995, KNT3(iii)) that the average values of the statistics stays the same over a wide range of network sizes. So a Voronoi is a Voronoi, as one could have said, almost like an Englishman.

Voronoi tessellation is the solution of a proximity problem, namely the division of the space into n partitions around n particles, such that all points within the i^{th} partition is closest to the i^{th} particle than any other particle. There are a host of proximity problems which, in the end, are related to one another and to the Voronoi problem. Some example of these are the problems concerning the nearest neighbour, the closest pair and the Euclidean minimum spanning tree. The minimum spanning tree always contains the shortest edge of the graph.

Given a convex hull containing n points, one can join all the points together by straight line segments such that the whole region inside the convex hull is tessellated by the triangles formed by them. This problem is related to the nearest neighbour problem, since among all straight lines connecting to each point there is one which joins it to its nearest neighbour. Moreover, the problem is related to a problem of spatial proximity the solution of which is the Voronoi tessellation. The solutions of these two problems are dual to each other. The triangular tessellation is called the Delaunay triangulation.

Descartes was the first person to draw a picture of a Voronoi tessellation (Descartes, 1644). In his essay, he imagine vorticities surrounding heavenly bodies. The path of an object through space, he says, passes along edges and vertices of what is now known as the Voronoi tessellation. The idea he introduced was original but the discourse philosophical, which is perhaps why his name was never associated with the tessellation which could easily have borne his name instead of that of Voronoi. Even though we regard Philosophy very highly as the mother of all sciences, as is probably the reason why we call our highest formal education 'Doctor of Philosophy' or Ph.D., but from our experience we could see that philosophy in our dictum generally means only one thing, that is mathematics. Therefore the tessellation is named after Voronoi because he was the first person to have written a *substantial* amount of mathematics on it. In short, Descartes has provided the idea and philosophy, Dirichlet the geometrical description and Voronoi the mathematics. Voronoi could easily have claimed having written the most amount of mathematics on the tessellation which now bears his name, than any other person to date. To see the contest between Voronoi and Dirichlet, for instance, compare their seminal papers (Dirichlet, 1850; Voronoi, 1908, 1909) (*cf* Tiyapan, 2001, KNT8(i)). Ironically it was Descartes' philosophy that all knowledges must be based on mathematics, so he should not have minded.

The pictures of all Voronoi cells in a group of 71 cells are given in Figure 2.7. These are all the inner cells of a larger group of 200, the rest of which are cells on the boundary.

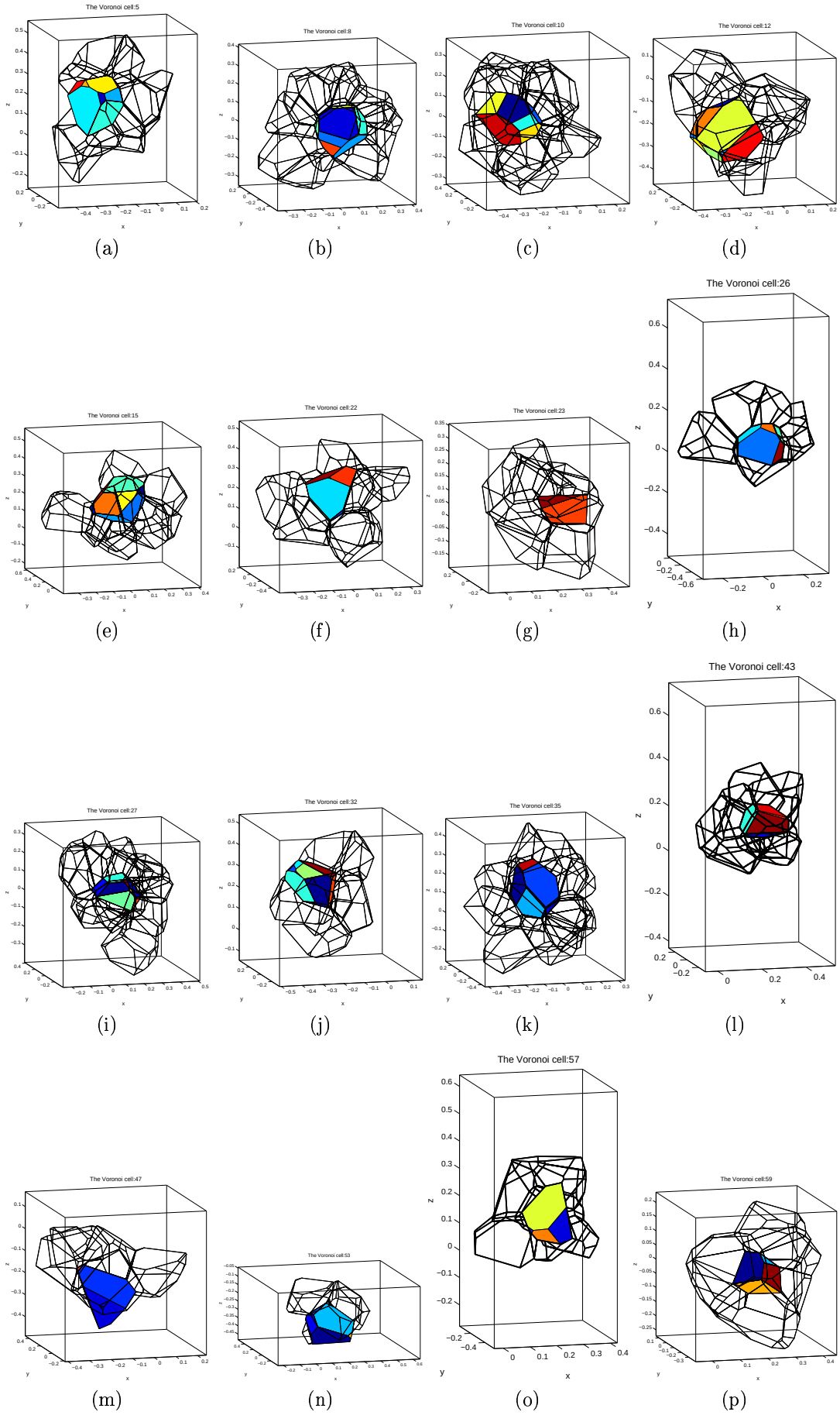
The Voronoi cell:5
The Voronoi cell:8
The Voronoi cell:10
The Voronoi cell:12
(a)
(b)
(c)
(d)
The Voronoi cell:15
The Voronoi cell:22
The Voronoi cell:23
The Voronoi cell:26
(e)
(f)
(g)
(h)
The Voronoi cell:27
The Voronoi cell:32
The Voronoi cell:35
The Voronoi cell:43
(i)
(j)
(k)
(l)
The Voronoi cell:47
The Voronoi cell:53
The Voronoi cell:57
The Voronoi cell:59
(m)
(n)
(o)
(p)

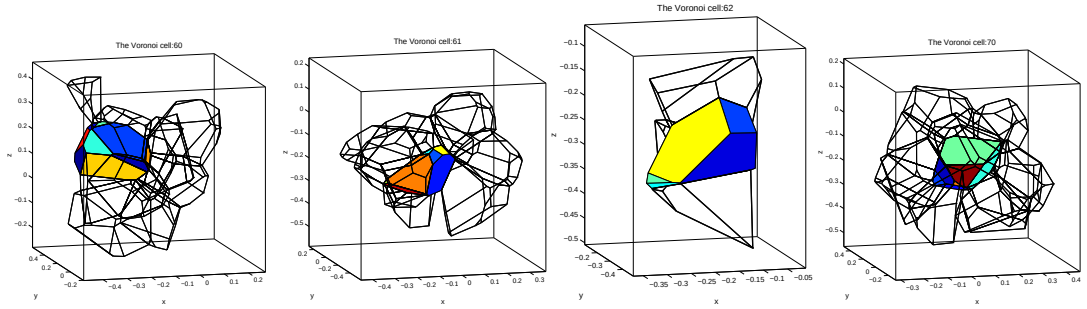

(q) (r) (s) (t)

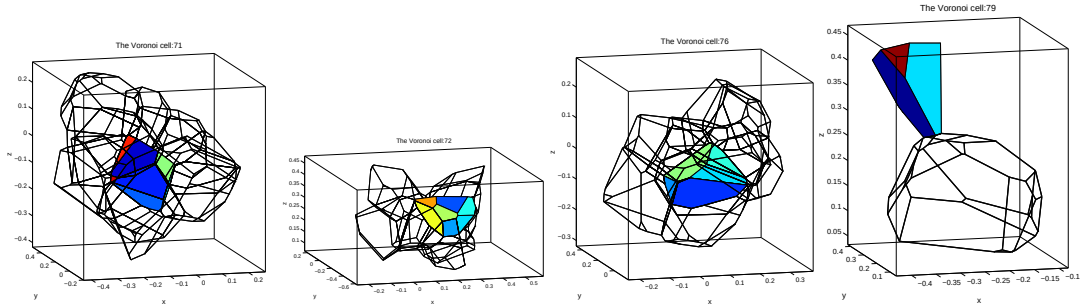

(u) (v) (w) (x)

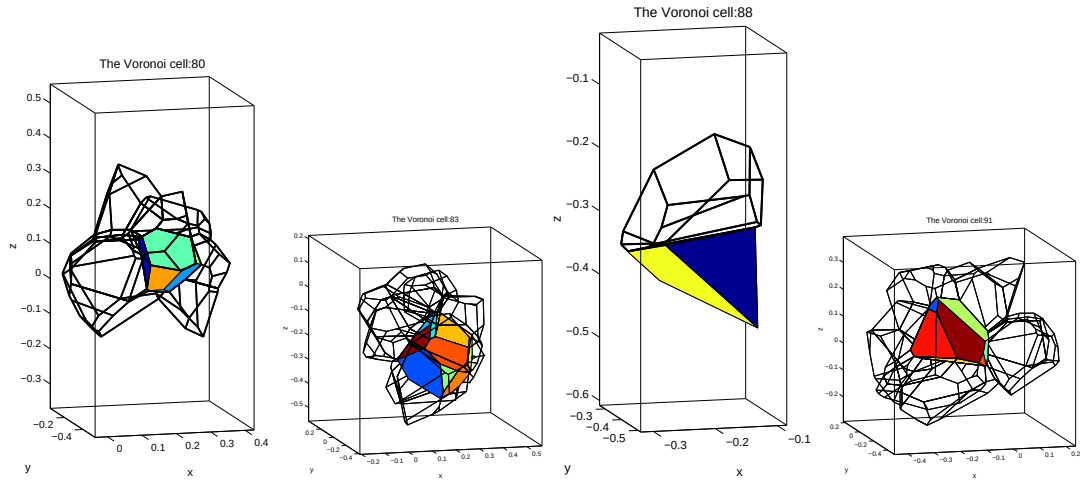

(y) (z) (A) (B)

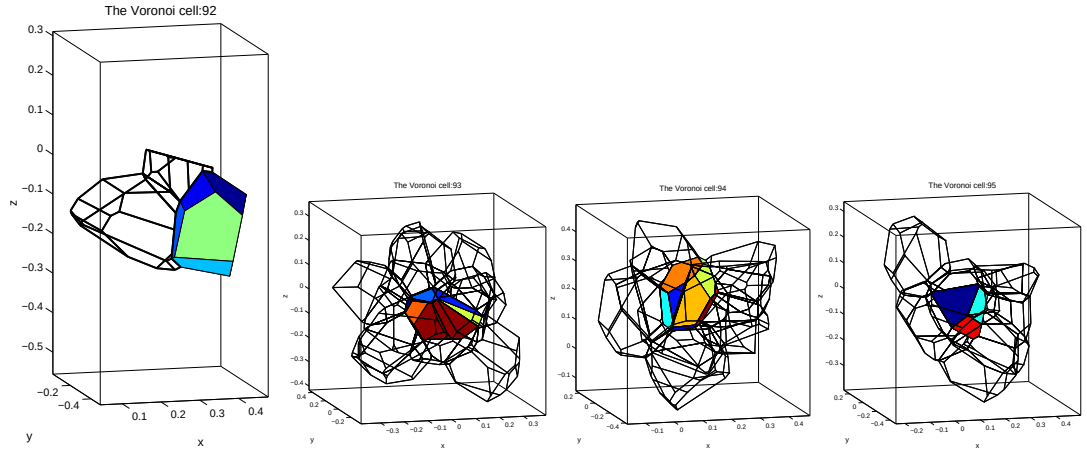

(C) (D) (E) (F)

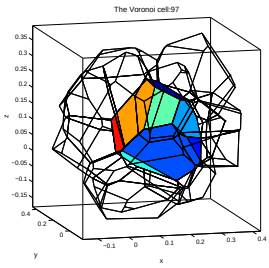

(G)

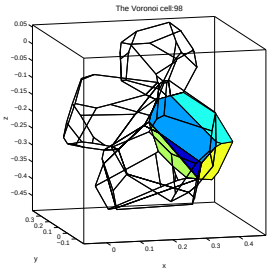

(H)

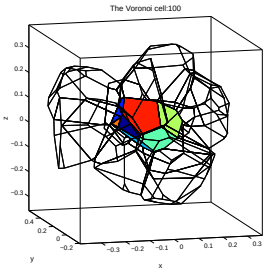

(I)

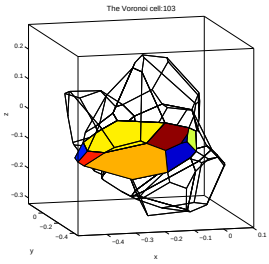

(J)

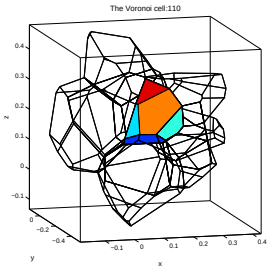

(K)

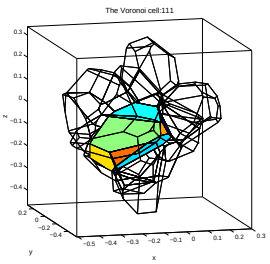

(L)

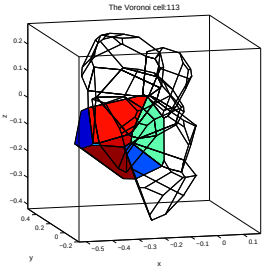

(M)

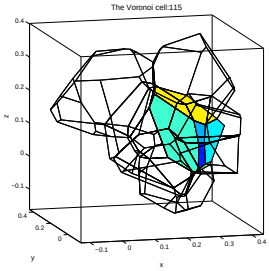

(N)

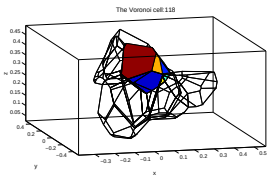

(O)

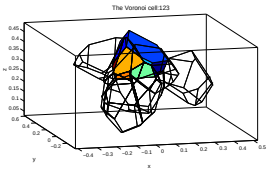

(P)

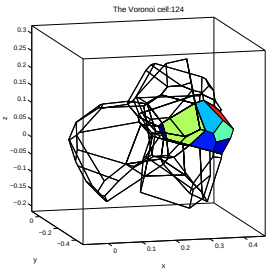

(Q)

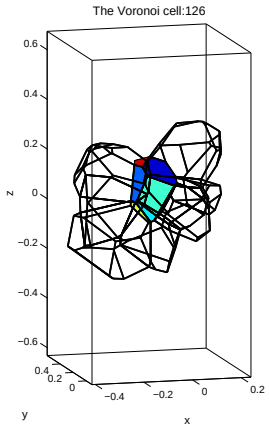

(R)

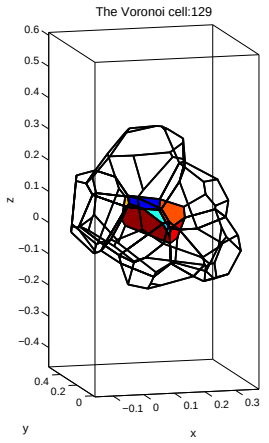

(S)

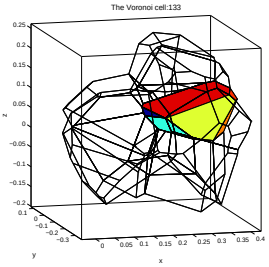

(T)

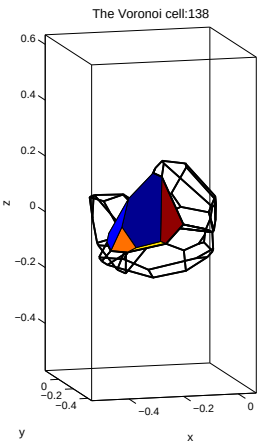

(U)

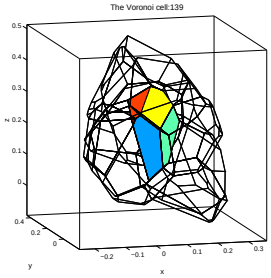

(V)

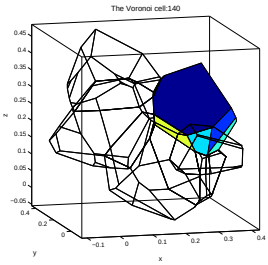

(W)

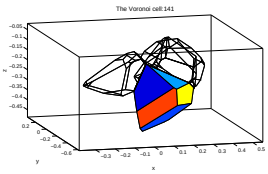

(X)

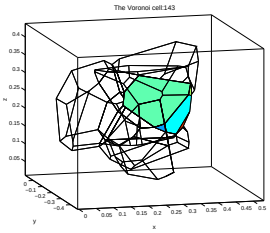

(Y)

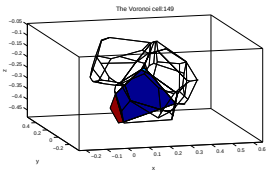

(Z)

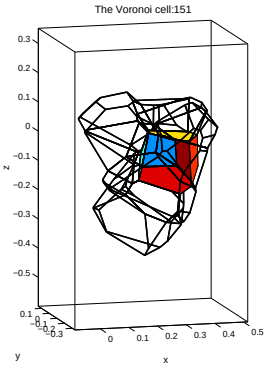

(aa)

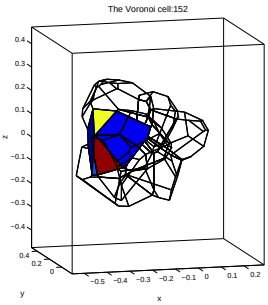

(ab)

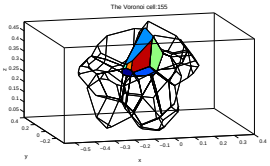

(ac)

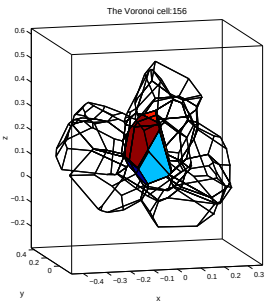

(ad)

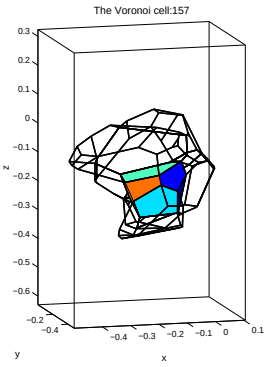

(ae)

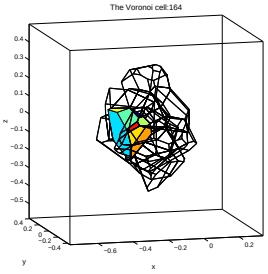

(af)

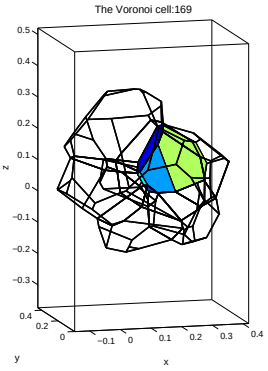

(ag)

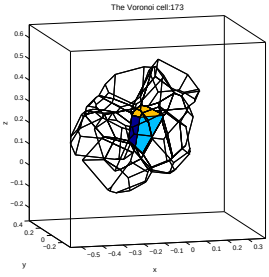

(ah)

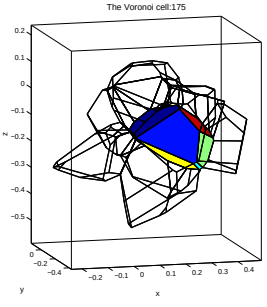

(ai)

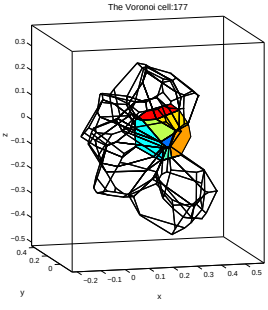

(aj)

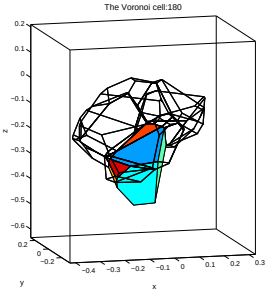

(ak)

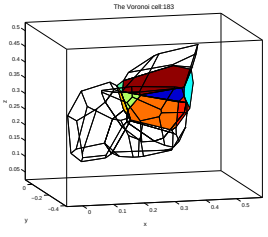

(al)

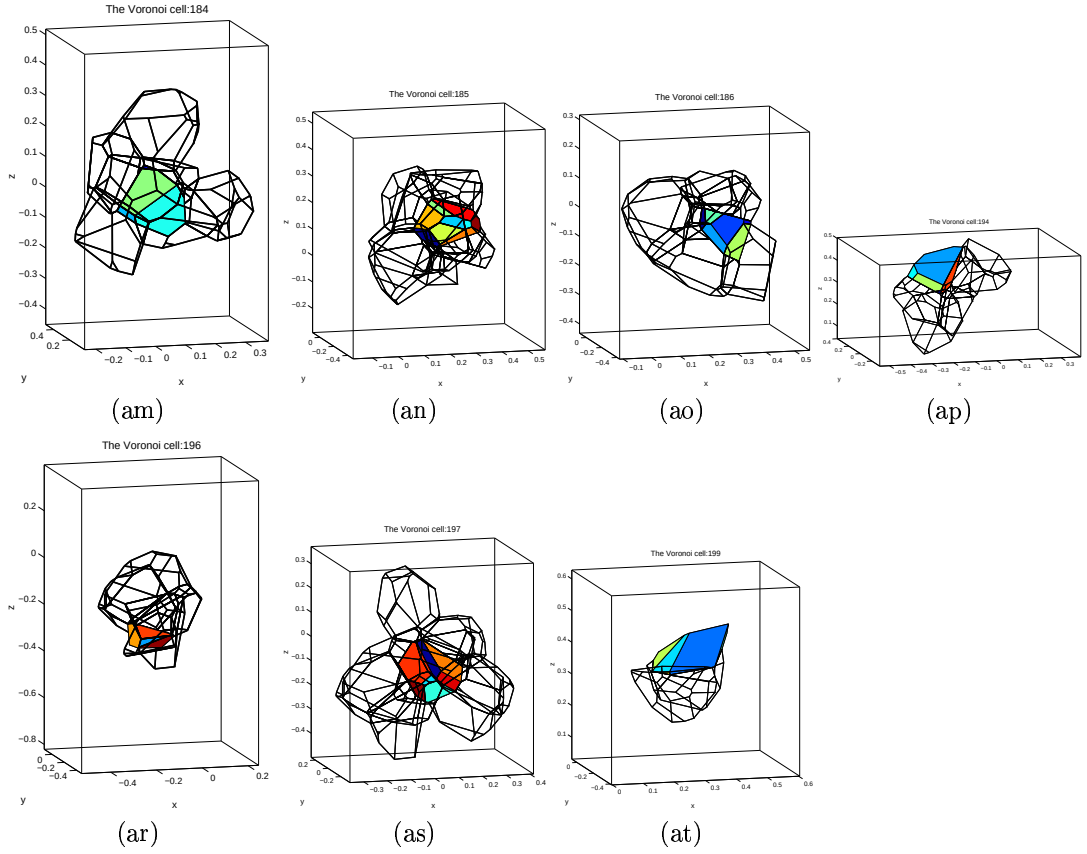

Figure 2.7 *The 71 Voronoi cells in an aggregation.*

The statistics of these 71 cells are the following. There are originally 200 cells, but these statistics represent 71 inner cells among these. The rest, 129 cells, are on the boundary and are not considered. The abbreviation 'mn' stands for the mean-, while 'cb' the cube normal.

Number of faces per inbound cell
Mean: 14.2113
Variance: 11.0262
Minimum: 6
Maximum: 23
Second moment: 10.8709
Third moment: 14.0161
Kurtosis: 3.109624
Geometric mean: 13.8246
Harmonic mean: 13.4227
Median: 13
Mean absolute deviation: 2.7169

Number of vertices per inbound cell
Mean: 24.4225
Variance: 44.1046
Minimum: 8
Maximum: 42
Second moment: 43.4834
Third moment: 112.1287
Kurtosis: 3.109624
Geometric mean: 23.5039
Harmonic mean: 22.5058
Median: 22
Mean absolute deviation: 5.4338

Area of surface of inner cell
Mean: 0.1599
Variance: 0.0024
Minimum: 0.0628
Maximum: 0.2660
Second moment: 0.0023
Third moment: 7×10^{-6}
Kurtosis: 2.3015
Geometric mean: 0.1520
Harmonic mean: 0.1435
Median: 0.1602
Mean absolute deviation: 0.0398

Area of surface of inner cell (mn)
Mean: 1.000000
Variance: 0.0926
Minimum: 0.3928
Maximum: 1.6634
Second moment: 0.0913
Third moment: 0.0017
Kurtosis: 2.3015
Geometric mean: 0.9505
Harmonic mean: 0.8972
Median: 1.0018
Mean absolute deviation: 0.2489

Area of surface of inner cell (cb)
Mean: 0.3031

Variance: 0.0085
Minimum: 0.1191
Maximum: 0.5042
Second moment: 0.0084
Third moment: 4.8×10^{-5}
Kurtosis: 2.3015
Geometric mean: 0.2882
Harmonic mean: 0.2720
Median: 0.3037
Mean absolute deviation: 0.0754

Volume of inbound cell
Mean: 0.0261
Variance: 0.0018
Minimum: 5.5944×10^{-3}
Maximum: 0.3315
Second moment: 0.0017
Third moment: 0.0004
Kurtosis: 42.2383
Geometric mean: 0.0183
Harmonic mean: 0.0153
Median: 0.0167
Mean absolute deviation: 0.0177

Volume of inbound cell (mn)
Mean: 1.0000
Variance: 2.5764
Minimum: 0.2146
Maximum: 12.7188
Second moment: 2.5402
Third moment: 24.1689
Kurtosis: 42.2383
Geometric mean: 0.7012
Harmonic mean: 0.5879
Median: 0.6408
Mean absolute deviation: 0.6795

Volume of inbound cell (cb)
Mean: 1.0000
Variance: 2.5764
Minimum: 0.2146
Maximum: 12.719
Second moment: 2.5402
Third moment: 24.1689
Kurtosis: 42.2383
Geometric mean: 0.7012
Harmonic mean: 0.5879
Median: 0.6408
Mean absolute deviation: 0.6795

Number of vertices per inbound face
Mean: 5.1114
Variance: 2.1650
Minimum: 3
Maximum: 10
Second moment: 2.1619
Third moment: 1.8902
Kurtosis: 3.0234
Geometric mean: 4.9065
Harmonic mean: 4.7086
Median: 5
Mean absolute deviation: 1.1655

Perimeter of inner face
Mean: 0.3899
Variance: 0.0434
Minimum: 0.0017
Maximum: 1.0067
Second moment: 0.0433
Third moment: 9.88×10^{-4}
Kurtosis: 2.3090
Geometric mean: 0.3071
Harmonic mean: 0.1497
Median: 0.3940
Mean absolute deviation: 0.1720

Perimeter of inner face (mn)
Mean: 1.0000
Variance: 0.2854
Minimum: 0.0043
Maximum: 2.5819
Second moment: 0.2850
Third moment: 0.0167
Kurtosis: 2.3090
Geometric mean: 0.7877
Harmonic mean: 0.3839
Median: 1.010419
Mean absolute deviation: 0.4410

Perimeter of inner face (cb)
Mean: 0.3288
Variance: 0.0308
Minimum: 0.0014
Maximum: 0.8488
Second moment: 0.0308
Third moment: 0.0006
Kurtosis: 2.3090
Geometric mean: 0.2590
Harmonic mean: 0.1262
Median: 0.3322
Mean absolute deviation: 0.1450

Area of faces of inner cell
Mean: 0.0110
Variance: 0.0001
Minimum: 4.0594×10^{-8}
Maximum: 7.2892×10^{-2}
Second moment: 1.22×10^{-4}
Third moment: 2×10^{-6}
Kurtosis: 5.2926
Geometric mean: 0.0045
Harmonic mean: 2.2×10^{-5}
Median: 0.0074
Mean absolute deviation: 0.0087

Area of faces of inner cell (mn)
Mean: 1.0000
Variance: 1.0085
Minimum: 3.6840×10^{-6}
Maximum: 6.6151
Second moment: 1.0071
Third moment: 1.4244
Kurtosis: 5.2926

Geometric mean: 0.4086
Harmonic mean: 0.0020
Median: 0.6715
Mean absolute deviation: 0.7933

Area of faces of inner cell (cb)
Mean: 0.1253
Variance: 0.0158
Minimum: 4.6179×10^{-7}
Maximum: 0.8292
Second moment: 0.0158
Third moment: 0.0028
Kurtosis: 5.2926
Geometric mean: 0.0512
Harmonic mean: 0.0003
Median: 0.0842
Mean absolute deviation: 0.0994

§ 2.8 Tilings and patterns

All two dimensional lattices are tilings. The *kagome* latticedeserves some mention here since it is a first-order covering lattice of the honeycomb lattice, which in turn is dual to the triangular lattice. Some physicists conjecture that the name originates from a name of a person. Apart from a few exceptions from the reason that the word is written in the wrong script, those scientists who are japanese should know that the word from their own language which means, according to the dictionary by Nelson (1962), *basket interstices* or *woven bamboo pattern*. A better translation is simply *basket pattern* (*cf* Tiyapan, 2001, KNT8(i)), *kago* (*rad*: *take* and *tatsu*) meaning *basket* and *me* a radical word for *eye* which also means *pattern*.

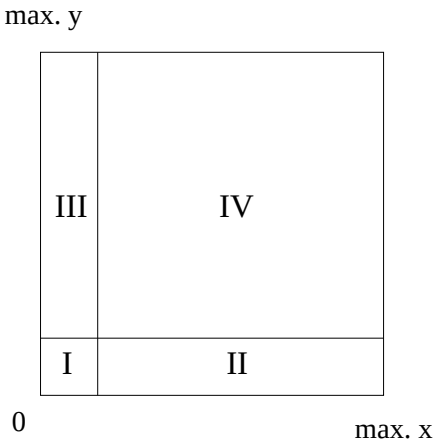

Those who do not know follow the established practice and write it as *kagomé* (*cf*, for example, Tiyapan, 1995, KNT3(iii)) with the *l'accent aigue* (acute accent) as if it were a french word. For the case of two dimensions, Algorithm 2.6 gives the algorithm for producing patterns in general. It is used for producing the 2-homohedral tilings in § 4.9 and is the basis of the program in § A.6. In this algorithm pseudo-prototiles are produced which fill the space. We shall call these our unit tiles. There are four types of these unit tiles corresponding to the four sections or groups as shown in Figure 2.8. The first group contains only one tile, *i.e.* the one at the origin, the second one contains those unit tiles to be put at the bottom row, the third one yet those to be put at the left-most column. The rest and majority of tiles belong to the fourth group.

Figure 2.8 Four groups of tiles.

Vertices in each unit tile are divided into five groups, namely one for the boundary in each direction, *i.e.* north, east, west and south, and the fifth those in the midst of the unit tile. This is essentially in order to avoid creating a vertex twice, which would have resulted in duplicates. Those unit tiles in the fourth group take their left-most vertices from the unit tile to their left and their bottom-most vertices from the unit tile immediately below it. Unit tiles in the third group create their own left-most vertices but still take from the unit tile below them their bottom-most ones. On the other hand, unit tiles in the second group create their bottom-most vertices while taking their left-most ones from their neighbour who lives on their left. Lastly the only unit tile of the first group creates all its vertices, which include the bottom-most and left-most ones.

There are three types of edges, namely internal-, left and bottom edges, the latter two of which link respectively to vertices in their left and bottom neighbours. And then, there are four types of cells, namely middle, south, west and south-west cells, the latter three of which contains the other half of its edges in their neighbour in the corresponding direction. Each unit tile is divided into grids by lines parallel to x and y axes. All vertices lie on some intersection of these grids.

Algorithm 2.6 *Tilings in two dimensions.*

for every unit tile **do**

decide its type;
assign all vertices according to its type;
connect bonds according to the connection rules;
define cells by their vertices;
endfor □

When faced with an unfamiliar tiling, we first decide upon their pseudo-prototile, that is their unit tile. Then list the coordinates of their vertices. And then list the bonds, that is the numbers of the two vertices that define each of them. We also have to divide the bonds into groups as mentioned, and include this information in our input.

The program keeps the two lists of coordinates, one for each axis. Coordinates of vertices are then referred to in grid numbers instead of the actual lengths concerned. This helps reading and using the program and procedure simpler. It marks the division between delight and despair. Also, the group information can then be represented in the program as a mapping of border vertices from a previous unit to the present one.

A cross-border bond normally has one end on the border. However there are those neither ends of which are on the border. These bonds make up a separate group of their own, or rather they make up two groups corresponding to the two groups, II and III.

This program when tried on a few well known regular lattices gives satisfactory results. Because these lattices are small, their coordination numbers x differ from the true values. But since this must be because of the jagged borders of the networks created the discrepancy is systematic and so there is nothing to worry about. Also there is nothing one can do about it unless one makes changes to the program. The problem lessens but never goes away when the size of the network becomes larger. As the four sides that make up the border are in total $4d/d^2$, *i.e.* $4/d$ parts of the area, increasing the network size by one hundred times, *i.e.* $d = 10$, probably would reduce the error by 60 per cent.

It is possible to improve the program as regarding to this problem, and this is the plan for the future work. At present, this shortcoming will have some effect on the values of the six percolation probabilities obtained from each system simulated.

For the first test, the program was run on a square lattice. The six representative networks produced, which subsequently become the ground for the corresponding six values of percolation thresholds, have their statistics as follows:

$n_C = 100$, $x_C = 6.8400$, $n_B = 342$, $x_B = 12.4211$, $n_c = 100$, $x_c = 3.6000$, $n_b = 180$, $x_b = 5.3778$, $n_v = 121$, $x_v = 3.3058$, $n_e = 200$ and $x_e = 5.4100$.

Then from 2×5 runs, *i.e.* two runs for each of the five permuted list of blockages, the values of percolation thresholds are

$p_C = 0.3920 \pm 0.0627$, $p_B = 0.2459 \pm 0.0373$, $p_c = 0.5610 \pm 0.1272$, $p_b = 0.4806 \pm 0.0750$, $p_v = 0.5942 \pm 0.0802$ and $p_e = 0.5040 \pm 0.0740$.

To explain the results, the capital C and B in the subscript mean respectively cells and bonds when neighbours mean that they share at least one vertex. When in lower case letters c and b mean respectively cells and bonds when neighbourhood means sharing at least one edge. Neither the vertices nor the edges, respectively v and e, is ambiguous since the former has zero dimension while the latter has only one. In this case, as it is in general, p_C and p_B are nothing that one normally talks about, while p_c and p_b should be the same as p_v and p_e in that order. Because all connections end at the boundary, it is to be expected that the values of all x's are lower than their exact values for an infinite network. The results above show that, for this case at least, x_c falls short of its exact value by 10 per cent, while similarly x_b by 10.37, x_v by 17.35 and x_e by 9.83 per cent. Because c and b naturally form one pair while v and e another, it is interesting to note that x_c should fare better than x_v while on the other hand x_e is more accurate than x_b. For the probability values, p_c is off the mark by (*cf* § 4) -5.36 per cent and p_b by -3.9 per cent, while p_v does so by 2.5 per cent and p_e by a mere 0.8 per cent. The first one of these pairs seems to be on the lower side while the second one, on the other hand, is on the higher end and more accurate than the first. This first test gives a result in accordance with our expectation that for vertices and edges the results should be more accurate than those from cells and bonds since the first two come from the input, while the last two are secondary values derived up from them by the program. Figure 2.9 shows the networks simulated for this test.

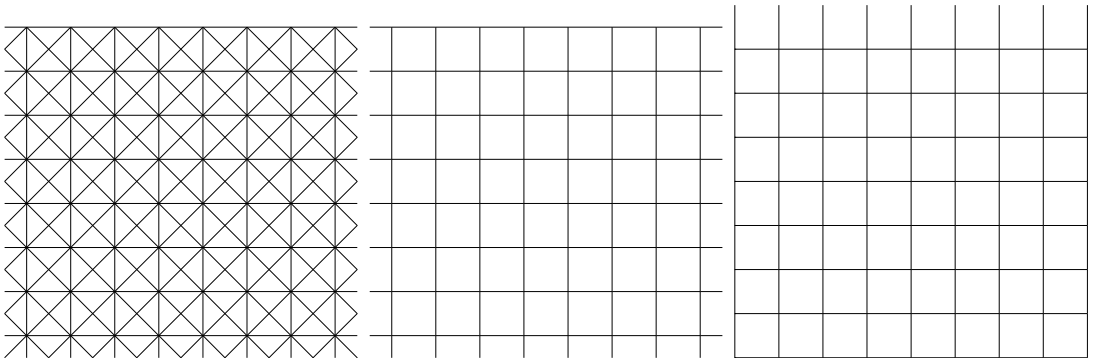

Figure 2.9 *Percolation of networks related to the square lattice. Networks comprising of* (a) *Cells and Bonds,* (b) *cells and bonds, and* (c) *vertices and edges.*

The next test is on the honeycomb lattice. Here the results obtained from the simulation is $n_C = n_c$ 202, $x_C = x_c$ 5.4554, $n_B = n_b$ 551, $x_B = x_b$ 9.2777, $n_v = 479$, $x_v = 2.8058$, $n_e = 672$ and $x_e = 3.8244$. For the probabilities of percolation $p_C = p_c$ 0.4889 ± 0.0704, $p_B = p_b$ 0.3342 ± 0.0385, $p_v = 0.6833 \pm 0.0369$ and $p_e = 0.6382 \pm 0.0410$. These results are obtained from 2×10 simulations in the case of statistics on cells and bonds, whereas in the case of vertices and edges they are obtained from 2×5 runs. Their pictures are shown in Figure 2.10.

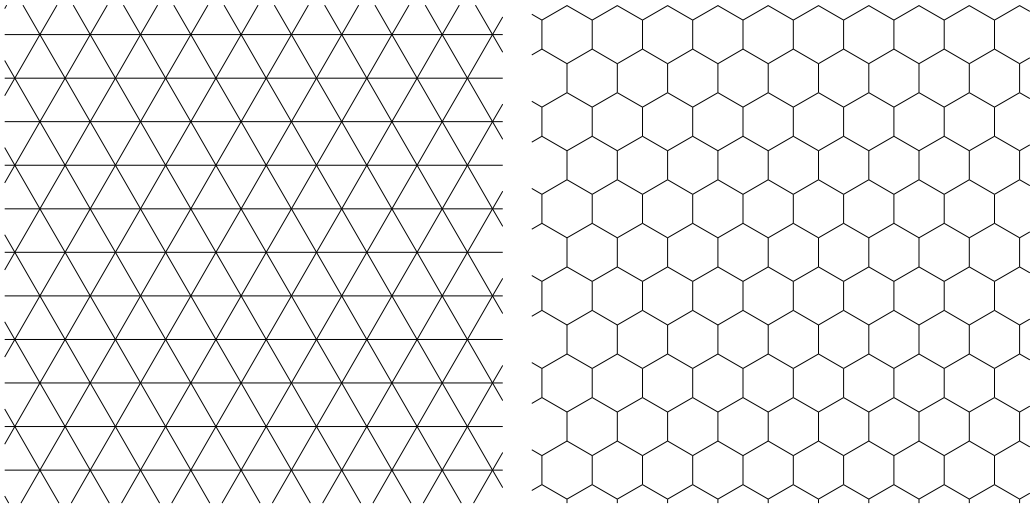

Figure 2.10 *Percolation of networks related to the honeycomb lattice. Networks are made up of* (a) *Cells and Bonds, or cells and bonds,* (b) *vertices and edges.*

For the honeycomb lattice, the errors are for p_c -2.22, for p_b -3.77, for p_v -1.85 and for p_e -2.22 per cent. The errors for the network statistics are for $x_c = -9.08$, $x_b = -7.22$, $x_v = -6.47$ and $x_e = -4.39$ per cent.

The Kagome lattice is the next test. Here the statistics obtained for the networks are

$n_C = 230$, $x_C = 6.4087$, $n_B = 737$, $x_B = 13.1452$, $n_c = 230$, $x_c = 3.2783$, $n_b = 377$, $x_b = 5.2944$, $n_v = 316$, $x_v = 3.7342$, $n_e = 590$ and $x_e = 5.7017$.

The percolation probabilities are

$p_C = 0.4222 \pm 0.0734$, $p_B = 0.2463 \pm 0.0482$, $p_c = 0.6548 \pm 0.0787$, $p_b = 0.5332 \pm 0.0532$, $p_v = 0.6760 \pm 0.0288$ and $p_e = 0.5309 \pm 0.0651$.

Here comparison with literature is already limited as published data begins to be rare. We can compare with exact values and say that x_v obtained contains an error of -6.65 per cent, p_v of 3.68 per cent and p_e of 1.70 per cent. Figure 2.11 shows the networks created and simulated.

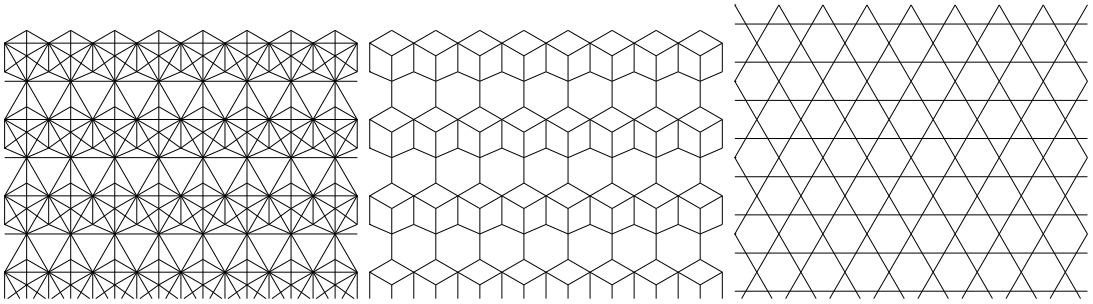

(a) (b) (c)

Figure 2.11 *Percolation of networks related to the basket pattern, kagome lattice. The networks of* (a) *Cells and Bonds,* (b) *cells and bonds, and* (c) *vertices and edges.*

From these tests we can see that, even for a rather small size, our programs for creating the network and finding percolation show approximately five per cent error.

§ 3. Voronoi tessellation

In a puzzle of Figure 3.1 there are five rooms with doors in the position as shown. The problem is whether one can walk through every door only once and the answer according to the graph theory is *no*, because there are more than two rooms which has an odd number of doors. The proof of Theorem 3.1 was from Gomsan Bajàraṇvàṇijẏa around 1989. From this, when one plays a puzzle like that of Figure 3.1 one always starts off from a room with an odd number of doors and ends in another such room.

This is the same thing as saying that one starts and ends outside rooms with an even number of doors. Therefore the number of the latter is of no consequence, but that of the former is crucial for the existence of a solution and must never be any number other than two. Puzzle of five rooms with doors. In Figure 3.1 there are three rooms with five doors, two with four, and one with nine. There are here four rooms with an odd number of doors. Starting off from one of these four one can only end up in one of the other three, which leaves the remaining two rooms unaccounted for. In other words at least two doors will necessarily remain unvisited.

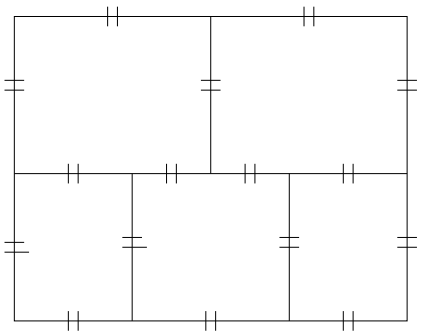

Figure 3.1 Rooms with doors puzzle.

Theorem 3.1. *A travel along a network can only starts and ends at nodes which have an odd coordination number.*

Proof. Looking at Figure 3.2, if one starts from inside a room with an odd number of doors one always ends up outside it. On the other hand one always ends up inside a room with an even number of doors if one starts of from it. In the second picture such a room is all the area outside the circle. □The following Corollaries 3.1[1], 3.1[2] and 3.1[3] assume nondegeneracy of the Voronoi network. Such a path as mentioned in these corollaries is also called *self-avoiding.*

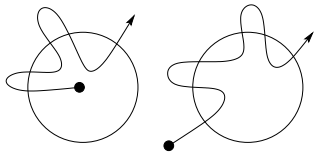

Figure 3.2 Departure and arrival rooms.

Corollary 3.1[1]. *There can be no path which traverses all edges of a Voronoi graph only once.*

Proof. This follows from Theorem 3.1 because a two dimensional Voronoi network has a coordination number three. □

Corollary 3.1[2]. *On a three dimensional Voronoi structure there always exists a path that runs through every edge once and only once.*

Proof. This also readily follows from Theorem 3.1 since a three dimensional Voronoi network has a coordination number of four. □

Corollary 3.1[3]. *Take any Voronoi cell of the three dimensional network, it is impossible to walk through all its edges without repeating some of them.*

Proof. Again from Theorem 3.1 and because the surface of a Voronoi polyhedron is a two dimensional network of polygons which has the coordination number three. □

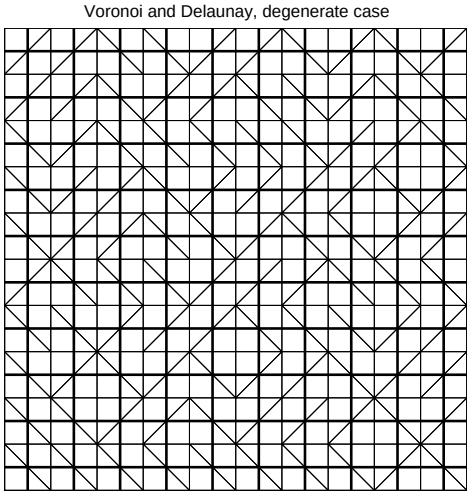

Jerauld *et al* (1984) compared the Voronoi, with the triangular networks and found that the bond percolation probability of the former is 4.3% or 0.015 less than that of the latter, small site clusters more, and small bond clusters less likely. When a square lattice was fed to *voronoi* and *delaunay* in Matlab, by the program `degen.m` in § A.15, there were error messages saying that points were collinear and possibly triangulation is incorrect. This case, Figure 3.3, is degenerative.

Figure 3.3 Voronoi from degenerative data.

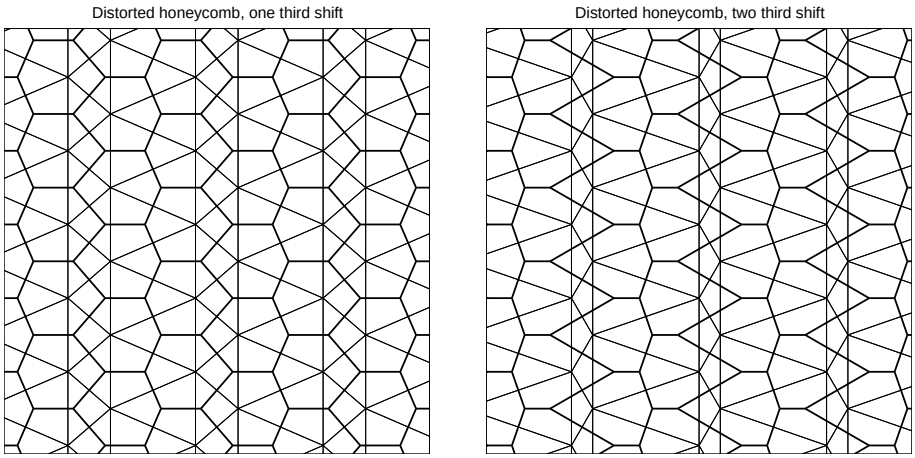

Figure 3.4 *The honeycomb or hexagonal lattice whose alternate y-plane has been shifted (a) one-third, and (b) two-third respectively. Triangulation is shown with thinner lines. The program used is* `honey.m`

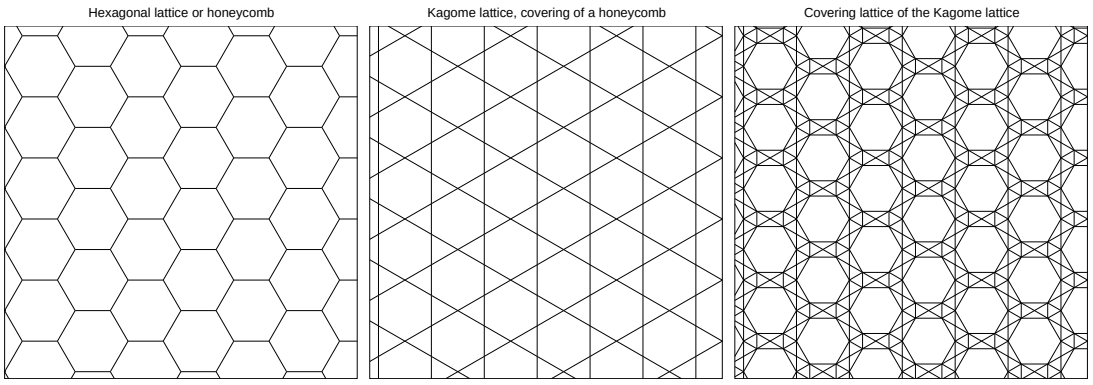

Figure 3.5 (a) *The hexagonal lattice,* (b) *its covering lattice (Kagome), and* (c) *the covering lattice of its covering lattice (i.e. covering of Kagome).* (`cover.m`, `covers.m`, *and* `coverss.m`)

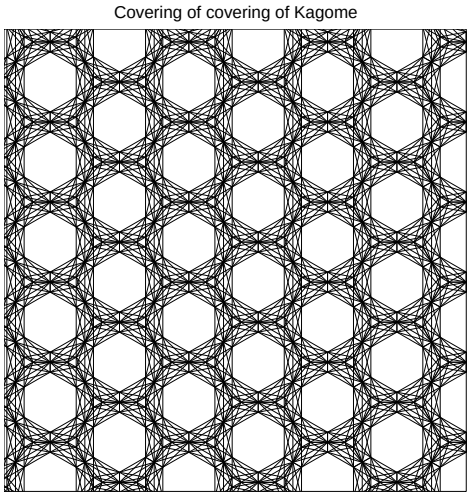

If we indicate by $C_v^n(x)$ the n^{th}-order covering lattice of a lattice x, then the first picture is Hexagonal, the second one Kagome or C_v^1(Hexagonal) and the third one C_v^2(Hexagonal) or in other words C_v^1(Kagome). Figure 3.6 is the next iteration, a C_v^3(Hexagonal) or C_v^2(Kagome). Now let us look at the Voronoi graph and its covering lattices. Pictures in Figure 3.7 are drawn by first creating and cropping a Voronoi graph with the help of the program `crop.m`, then use the recursive procedure described above to find up to the third covering lattice.

Figure 3.6 The next covering lattice.

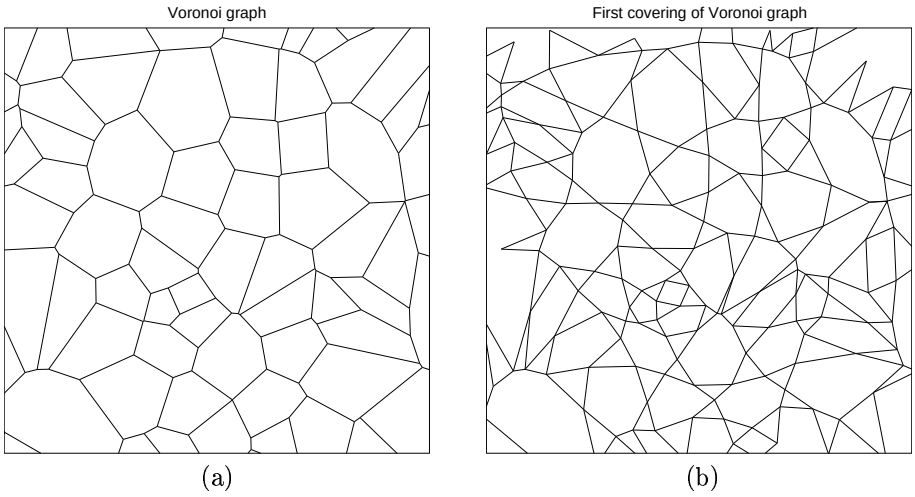

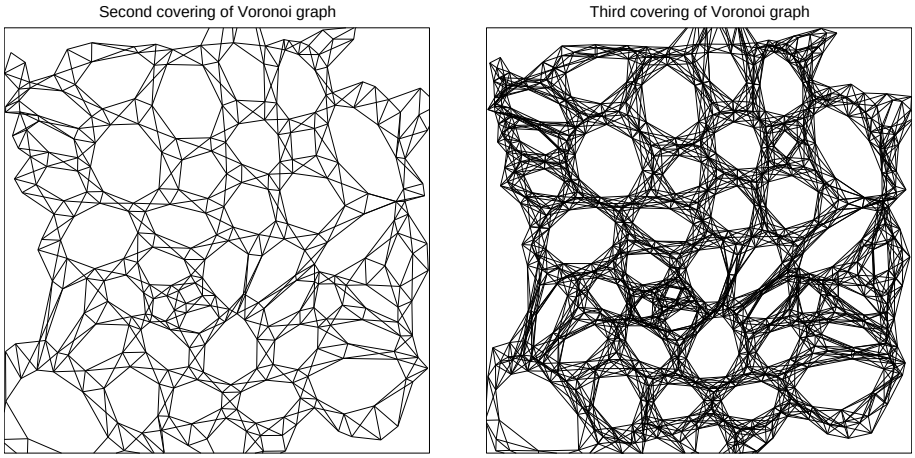

(c) (d)

Figure 3.7 (a) *Voronoi graph (V.g.),* (b) C_v^1(**V.g.**), (c) C_v^2(**V.g.**), (d) C_v^3(**V.g.**).

Notice that the covering lattices retain the skeleton structure of the original Voronoi graph. Those of higher orders represent closer the structures of nature where walls have thickness.

§ 3.1 Quadratic equations

Quadratic equations are equations of binary quadratic forms. Around 400 BC Barbilonia had algorithmic equivalences of quadratic equations which are based on the method of completing the square and where all answers are unsigned, *i.e.* positive, lengths. Because there was no notion for zero, Diophantus considered three types of quadratic equations $ax^2 + bx = c$, $ax^2 = bx + c$, and $ax^2 + c = bx$. Euclid, *circa* 300 BC, used geometric equivalences or quadratic equations whose roots are also lengths. Brahmagupta allowed negative quantities, which he called debts, and used abbreviations for the unknown. Al-Khwarizmi classified quadratics into six types, namely squares equals roots, squares equals numbers, roots equal numbers, squares and roots equal number, squares and numbers equal roots, and roots and numbers equal squares. In his book *Liber embadorum*, published in 1145, Abraham bar Hiyya Ha-Nasi (aka Savasorda) gives the complete solution of quadratic equations. Luca Pacioli published *Summa de arithmetica, geometrica, proportioni et proportionalita* (or Summa) in 1494. He also applied quadratic methods to quartics of the form $x^4 = a + bx^2$. Scipione del Ferro solved the cubic equations of the form $x^3 + mx = n$.

§ 3.2 Quadratic forms

The theory of quadratic forms and the theory of matrix are inseparable though the history of these two subjects are somewhat fragmentary. A bilinear form in the sets x_i and y_i, $i = 1 \ldots n$, is $\sum_{i,j} x_i y_j$, or $\mathbf{x}^{\mathrm{T}}\mathbf{A}\mathbf{y}$. If $x_i = y_i$ for all i, then the form is quadratic in x_i. In other words, a quadratic form is a general expression which contains second order terms.

A quadratic form in the variables x_i is the homogeneous quadratic polynomial $\sum_{i,j=1}^{n} a_{ij} x_i x_j$, where a_{ij} are arbitrary scalars. The set of all quadratic forms in x_i with coefficients in a field $\mathcal{F}$ is a vector space over $\mathcal{F}$. A bilinear form in the variables x_i and y_i is the homogeneous polynomial $\sum_{j=1}^{m} \sum_{i=1}^{n} a_{ij} x_i y_j$, where a_{ij} are arbitrary scalars. The set of all bilinear forms with coefficients in a field $\mathcal{F}$ is a vector space over $\mathcal{F}$ (*cf* Hohn, 1958). A quadratic form can also be represented in a matrix form as $X^{\mathrm{T}}AX$. Distinct $n \times n$ matrices A_1 and A_2 have the same quadratic polynomial if all corresponding $a_{ij} + a_{ji}$ are equal. Given the quadratic form, it is not possible to identify the corresponding matrix A by inspection. This ambiguity is eliminated by replacing each pair of the coefficients a_{ij} and a_{ji} by their mean $(a_{ij} + a_{ji})/2$, which amounts to replacing A by $(A + A^{\mathrm{T}})/2$ which is symmetric. If x_i are independent variables, the rank and the determinant of A are respectively the rank and the discriminant of the form. Two quadratic forms $X^{\mathrm{T}}A_1X$ and $\widetilde{X}^{\mathrm{T}}A_2\widetilde{X}$ are equivalent if and only if there is a nonsingular transformation $X = B\widetilde{X}$ such that $X^{\mathrm{T}}A_1X = \widetilde{X}^{\mathrm{T}}B^{\mathrm{T}}A_1B\widetilde{X} = \widetilde{X}^{\mathrm{T}}A_2\widetilde{X}$, that is if and only if for a suitable nonsingular matrix B, $A_2 = B^{\mathrm{T}}A_1B$. Then A_1 and A_2 have the same rank and are said to be congruent to each other.

Lattice can be represented by quadratic forms and vice versa, therefore the classification of quadratic forms is also the classification of lattices.

§ 3.3 Voronoi algorithms

Green and Sibson (1978) gives the algorithm that produces Voronoi graphs, as summarised in Algorithm 3.1. They call a Voronoi tessellation 'Dirichlet tessellation'. The points outside the window are ignored, and points on the periphery has tile bounded in part by sequences of effective constraints instead of by inter-tile edges. Contiguous tiles have a boundary sequences in common. A degenerate vertex, that is a vertex where four or more tiles meet, causes an incorrect record of diagonal contiguity. From the Euler-Poincaré formula, $f - e + v = 2$, where in the plane the infinite region is counted as a face, gives rise to the total number of contiguities to be recorded $4\times$ `effective constraints` $+6\times$ `accepted points` -6. A square lattice has all its vertices degenerate.

Algorithm 3.1 *Voronoi 2-d algorithm, Green and Sibson (1978)*

define window as a set of linear inequality constraints $ax + by + c < 0$;
do
  add a new point n randomly within the window;
  do
    find the line b_i joining n and its nearest neighbour p_i;
    find l_i the perpendicular bisector of b_i;
    find the intersection between l_i and the edge e_i of its nearest tile,
      going clockwise with respect to n;
    add l_1 to the object- and contiguity lists;
  until 2π radian around n traversed
until no more new points added **enddo** □

Moore and Angell developed a algorithm which can cope with degenerate cases. Because their program could find them, they are no longer considered degenerate and they fittingly called these *vertices of* (> 3)*-hedral valency.*

§ 3.4 Voronoi statistics in literature

Van de Weygaert (1994) studies linear section of three dimensional Voronoi network where the mean length is

$$\langle\lambda\rangle = L = \frac{d\Gamma(d-1/2)\Gamma((d+1)/2)^2}{(d-1)!\rho_c^{1/d}2\Gamma(d/2+1)^{2-(1/d)}\Gamma(2-1/d)}. \qquad (19)_{\text{iii}}$$

For two dimensions $\langle\lambda\rangle = \pi/(4\sqrt{\rho})$, while for three dimensions $\langle\lambda\rangle = [81/(32\pi\rho)]^{1/3}/\Gamma(2/3)$. Consequently for two dimensions $\langle\lambda\rangle = 0.7854\rho^{-1/2}$ while for three dimensions $\langle\lambda\rangle = 0.6872\rho^{-1/3}$, $\langle\lambda^2\rangle = 0.632\rho^{-2/3}$, $0.668\rho^{-1}$ and $\langle\lambda^4\rangle = 0.774\rho^{-4/3}$. For 3-d Poisson-Voronoi tessellation the exact values for the moments are shown in Table 3.1.

ρ_v	$\frac{24}{35}\pi^2\rho_c$	$6.763\rho_c$	number density of vertices	J_0
ρ_e	$\frac{48}{35}\pi^2\rho_c$	$13.535\rho_c$	number density of edges	J_1
ρ_f	$\left(\frac{24}{35}\pi^2+1\right)\rho_c$	$7.768\rho_c$	number density of faces	J_2
ρ_c	ρ_c	ρ_c	number density of cells	J_3
n_c^v	$\frac{96}{35}\pi^2$	27.07	number of vertices per cell	$\mathrm{E}(N_0)$
n_c^e	$\frac{144}{35}\pi^2$	40.61	number of edges per cell	$\mathrm{E}(N_1)$
n_c^f	$\frac{48}{35}\pi^2+2$	15.54	number of faces per cell	$\mathrm{E}(N_2)$
n_f^v or n_f^e	$\frac{144\pi^2}{24\pi^2+35}$	5.228	number of vertices or edges per face	$E_2(N_0)$ or $E_2(N_1)$
V_c	$\frac{1}{\rho_c}$	$\frac{1}{\rho_c}$	volume of cell	$\mathrm{E}(V)$
	$\frac{1.180}{\rho_c^2}$	$\frac{1.180}{\rho_c^2}$		$\mathrm{E}(V^2)$
A_c	$\left[\frac{256\pi}{3\rho_c^2}\right]^{1/3}\Gamma\left(\frac{5}{3}\right)$	$5.821\rho_c^{-2/3}$	surface area of cell	$\mathrm{E}(A_c)$
s_c	$\frac{(4\pi)^{5/3}\Gamma(1/3)}{5(9\rho_c)^{1/3}}$	$17.496\rho_c^{-1/3}$	perimeter of cell	$\mathrm{E}(s_c)$
A_f	$\frac{35(2^{8/3})\pi^{1/3}\Gamma(2/3)}{(9\rho_c)^{2/3}(24\pi^2+35)}$	$0.3747\rho_c^{-2/3}$	area of face	$\mathrm{E}(A_w)$
s_f	$\frac{7(2^{10/3})\pi^{5/3}\Gamma(1/3)}{(9\rho_c)^{1/3}(24\pi^2+35)}$	$2.252\rho_c^{-1/3}$	perimeter of face	$\mathrm{E}(s_w)$
d_e	$\frac{7\Gamma(1/3)}{9(36\pi\rho_c)^{1/3}}$	$0.4309\rho_c^{-1/3}$	length of edge	$\mathrm{E}(L)$

Table 3.1 *Moments of 3-d Poisson-Voronoi tessellation, cf van de Weygaert (1994).*

The moments of 2-d section of 3-d Voronoi tessellation are shown in Table 3.2.

ρ_v	$\frac{2\Gamma\left(\frac{1}{3}\right)\left(\frac{16\pi^5\rho^2}{9}\right)^{1/3}}{15}$	$2.9159\rho_c^{2/3}$	number density of vertices	J_0
ρ_e	$\frac{3}{2}\rho_v$	$4.3739\rho_c^{2/3}$	number density of edges	J_1
ρ_c	$\frac{1}{2}\rho_v$	$1.4530\rho^{2/3}$	number density of cells	J_2
n_c^v or n_c^e	6	6	number of vertices or edges per cell	$\mathrm{E}(N_0)$ or $\mathrm{E}(N_1)$
A_c	$\frac{15}{\Gamma\left(\frac{1}{3}\right)\left(\frac{16\pi^5\rho_c^2}{9}\right)^{1/3}}$	$0.6859\rho^{-2/3}$		$\mathrm{E}(A)$
		$0.698\rho_c^{-4/3}$		$\mathrm{E}(A^2)$
s_c	$\frac{30\Gamma\left(\frac{2}{3}\right)}{(36\pi\rho_c)^{1/3}\Gamma\left(\frac{1}{3}\right)}$	$3.1356\rho_c^{-1/3}$	perimeter of cell	$\mathrm{E}(S)$
d_e	$\frac{5\Gamma\left(\frac{2}{3}\right)}{(36\pi\rho_c)^{1/3}\Gamma\left(\frac{1}{3}\right)}$	$0.5226\rho_c^{-1/3}$	length of edge	$\mathrm{E}(L)$

Table 3.2 *Moments of 2-d section of 3-d Voronoi, cf van de Weygaert (1994).*

The form factor of a cell, $f_c = 36\pi V_c^2/A_c^3$, is a dimensionless parameter which partially describes the shape of the cell. The form factor of a face is $f_f = 4\pi A_f/s_f^2$, which is the unity when the face is a circle. Regularly shaped cells have their shape approaching that of the sphere where $f_f = 1$. Statistics of 3-d VT which van de Weygaert (1994) gives include those listed here in Table 3.3.

	$\mu(\cdot)$	$\sigma(\cdot)$	$\gamma_1(\cdot)$	$\gamma_2(\cdot)$	
ρ_v	6.747 ± 0.014				J_0
ρ_e	13.493 ± 0.028				J_1
ρ_f	7.747 ± 0.014				J_2
ρ_c	1.000 ± 0.000				ρ
n_c^v	26.986 ± 0.055	6.61 ± 0.18	0.346 ± 0.029	-0.029 ± 0.030	N_0
n_c^e	40.479 ± 0.083	9.92 ± 0.27	0.346 ± 0.029	-0.029 ± 0.030	N_1
n_c^f	15.493 ± 0.028	3.305 ± 0.091	0.346 ± 0.029	-0.029 ± 0.030	N_2
V_c	1.000 ± 0.000	0.418 ± 0.009	0.73 ± 0.11	0.70 ± 0.39	V_{cell}
A_c	5.801 ± 0.018	1.461 ± 0.043	0.28 ± 0.11	-0.01 ± 0.17	A_{cell}
s_c	17.443 ± 0.054	3.655 ± 0.094	0.305 ± 0.035	0.00 ± 0.13	S_{cell}
f_c	0.540 ± 0.006	0.082 ± 0.003	-0.565 ± 0.032	0.36 ± 0.11	F_{cell}
n_f^v	5.2255 ± 0.0014	1.564 ± 0.016	0.582 ± 0.016	0.058 ± 0.024	N_0^w
A_f	0.3744 ± 0.0015	0.3722 ± 0.0037	1.266 ± 0.047	1.40 ± 0.19	A_{wall}
s_f	2.2518 ± 0.0092	1.2009 ± 0.0050	0.089 ± 0.022	-0.796 ± 0.029	S_{wall}
f_f	0.6389 ± 0.0005	0.1635 ± 0.0011	-0.855 ± 0.035	0.40 ± 0.13	F_{wall}
d_{cf}	0.6402 ± 0.0017	0.2092 ± 0.0051	-0.024 ± 0.022	-0.333 ± 0.074	D_{nw}
V_{cf}	0.0645 ± 0.0001	0.0579 ± 0.0009	1.177 ± 0.097	1.52 ± 0.47	V_{nw}
d_e	0.4309 ± 0.0018	0.3216 ± 0.0023	0.829 ± 0.020	0.209 ± 0.044	L
α_{ee}	$111°\mathrm{C}107 \pm 0.018$	$35°\mathrm{C}310 \pm 0.078$	-0.499 ± 0.012	-0.276 ± 0.039	α_{ee}
α_{ff}	$120°\mathrm{C}0 \pm 0.0$	$23°\mathrm{C}53 \pm 0.30$	-0.296 ± 0.014	-0.255 ± 0.038	α_{ww}

Table 3.3 *Statistics of 3-d VT, van de Weygaert (1994).*

His statistics on the planar section of the 3-d Voronoi tessellation is shown here as Table 3.4.

	$\mu(\cdot)$	$\sigma(\cdot)$	$\gamma_1(\cdot)$	$\gamma_2(\cdot)$
ρ_s^c	1.4530	0.0592	0.2871	-1.0099
ρ_s^v	2.9060	0.1134	0.2871	-1.0099
ρ_s^e	4.3590	0.1776	0.2871	-1.0099
n_s^v	6.0000	1.6895	0.3311	-0.1142
A_s^c	0.6882	0.4741	0.4573	-0.3902
s_s^c	3.1418	1.2212	-0.5819	-0.2879
f_s^c	0.7050	0.1433	-1.3425	2.0875
d_s^e	0.5221	0.3631	0.6223	-0.2321
α_s^{ee}	120°C0000	31°C6039	-0.6351	0.1321
α_s^{ff}	63°C1812	18°C5232	-0.6351	-0.3520

Table 3.4 *Statistics of the planar section of the 3-d Voronoi tessellation, van de Weygaert (1994).*

Then Table 3.5 lists the statistics he gave for the line section of 3-d VT.

	$\mu(\cdot)$	$\sigma(\cdot)$	$\gamma_1(\cdot)$	$\gamma_2(\cdot)$
λ	0.6703	0.3942	0.2600	-0.6923
$\sigma(\lambda)$	0.6123	0.1159	0.0643	0.0204
α_l^{fl}	44°C69	19°C5325	0.0067	-0.8080
α_l^{ff}	75°C4123	30°C9389	-0.0185	-0.5829

Table 3.5 *Statistics for the line section of the 3-d Voronoi tessellation, van de Weygaert (1994).*

Tables 3.5, 3.5 and 3.5 are all on VT's which are created from $\mathcal{P}(0,3)$. Apart from these, van de Weygaert (*ibid.*) also gives results based on VT's with anticorrelated- and correlated nuclei the statistics of which are not listed here.

Another interesting statistics is the correlation between the number of sides of a grain n_e, and the expected number of sides of its neighbouring grains n_n^e. Aboav (1970), in his investigation of polycrystalline MgO, empirically found it to be $n_n^e = 5+8/n_e$ and Weaire (1974) found a theoretical value of $n_n^e = 5+6/n_e$.

Later Aboav (1983) published another finding in which he studied a thin film of arsenic-selenium glass, As_2Se_3. This time with the initial assumption that $n_n^e = 6-a+(6a+\mu_2)/n$ and $\mu_2 = \sum_n (n-6)^2 f_n = \langle (n-6)^2 \rangle$ he empirically finds $n_n^2 = 4.79+8.98/n$.

§ 3.5 Voronoi statistics

In two dimensions the statistical descriptions are as follows.

The curve in Figure 3.8 is

$$y = 0.62/n^{0.13}.$$

First the edge lengths are normalised by the edge length of the equivalent or characteristic square . A *equivalent square* is defined as the square figure whose area is equal to the area of the polygon in question, here a Voronoi polygon. Then find the average of the edge lenghts in each cell.

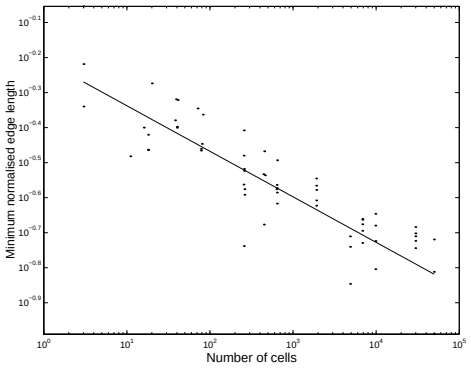

Figure 3.8 The minimum of the average normalised edge length.

In Figure 3.9 the curve is

$$y = \left| (n/15)^{1/2} \right| + 0.7 \ .$$

Of these cell-averaged normalised edge length obtained from simulations on various sizes of networks the minimum values are plotted in Figure 3.8, the maximum in Figure 3.9, and the expected value in Figure 3.10. Note that the last quantity is the average over the whole structure of all the averages obtained one from each cell.

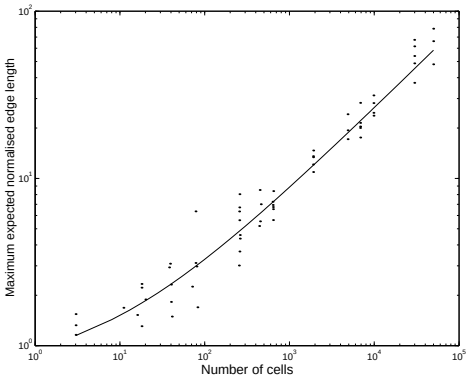

Figure 3.9 The maximum of the average normalised edge length.

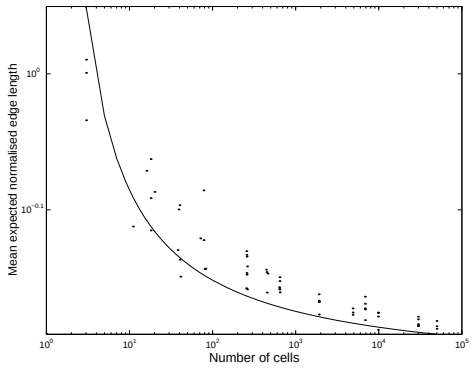

In Figure 3.10 the curve is

$$y = 10^{0.2/\log x} - 0.4$$

To summarise, as the networks gets larger its minimum, maximum, and mean of the edge lenghts when compared with the characteristic length approach constant values. The characteristic length is defined as $l = [\sum_{i=1}^{n} A_i/n]^{1/2}$, where A_i is the area of the i^{th} polygon and n is the number of cells.

Figure 3.10 The mean of the average normalised edge length.

That the three values mentioned become constant may not seem obvious by the look of Figures 3.8 to 3.10 because the scale used there is a logarithmo-logarithmic scale, not a Euclidean one. These figures emphasise the smaller ranges of size. Figure 3.11 below on the other hand is plotted using a normal scale which enables one to see the asymptotic effect more clearly. Here the figures (a), (b), and (c) are respectively Figure 3.8, 3.9, and 3.10. Let the term *representative* stands for 'of the cell-average normalised', and *length* means 'edge length' in this context.

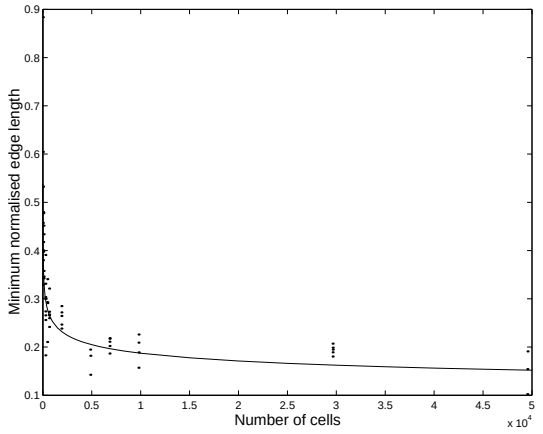

(a)

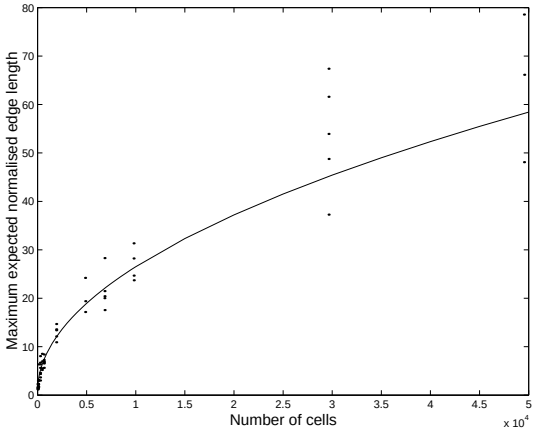

(b)

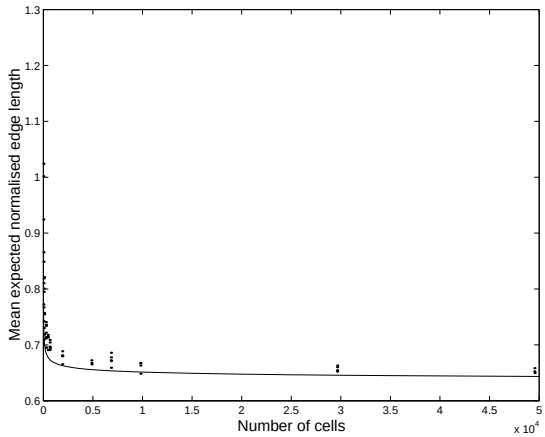

Then the *minimum representative length* approaches 0.15 from Figure 3.11 (a), the *maximum representative length* is ever increasing, seemingly by a power law of approximately 0.5, while *mean representative length* approaches the value of 0.65. Properties of the Voronoi tessellation can be divided into individual and collective properties. With this in mind the term *length* above represents a property, *representative* means individual, and *minimum*, *maximum* and *mean* show the collective attributes.

Figure 3.11 Mean, maximum, and mean of the cell-average normalised edge length..

This $\sigma^2(\mathcal{N}_v^c(E(l_e)))$ increases very slowly with the increasing sizes of the networks. The curve shown has the equation

$$y = \left| \left[\frac{x}{8 \times 10^4} \right]^{1/3} \right| + 0.05 \ .$$

The number of vertices per cell increases dramatically as one goes up the dimension ladder. The program in § A.10 contains the essential part of the code which produces Figure 3.13.

Figure 3.12 The variance of the expected values of the normalised length of edges of a cell.

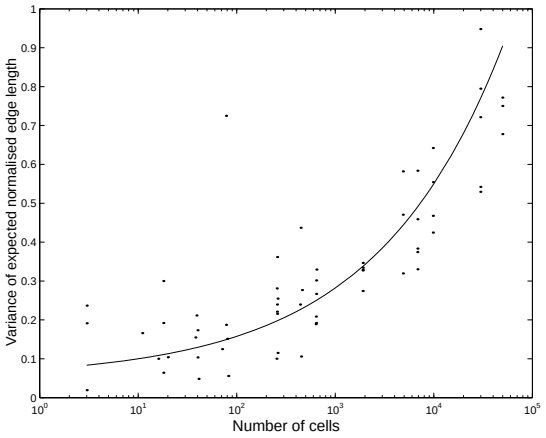

The straight line shown is $0.093(4+e)^n$. Notice the trend towards a greater rate of increase at dimensions higher than the maximum six shown. Only Voronoi cells which lies within the original domain and the vertices of these are considered. The same program also gives Figure 3.14. The expanse and the hypervolume of the Voronoi tessellation increases at an enormous rate, which results in the number of cells totally bounded within the original domain decreasing rapidly in Figure 3.14 as the dimension goes up.

Figure 3.13 Number of vertices per cell.

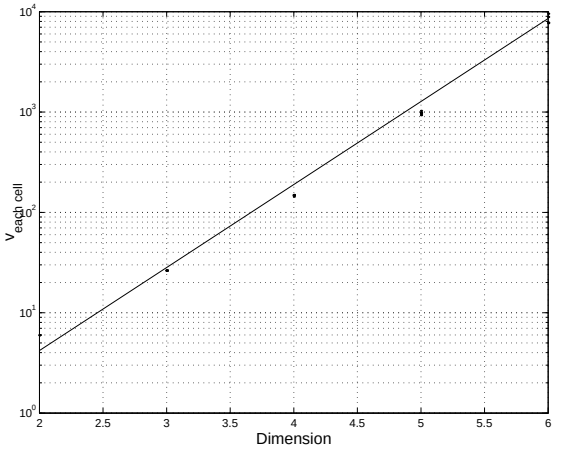

The effect at close to the zero ratio is emphasised by using the log scale for the y-axis. Also with the logarithmic scale the polynomial estimation curves that give negative values of the ratio is automatically excluded. One can fit the polynomial $p(x) = p_1x^n + p_2x^{n-1} + \ldots + p_nx + p_{n+1}$ to the data with a least square algorithm. If $\mathbf{x}$ is the vector containing the data, then the the $(n+1)$ coefficients of the estimated polynomial can be found from $\hat{\mathbf{x}} = (\mathbf{x} - \mathrm{E}(\mathbf{x}))/\sigma(\mathbf{x})$.

Figure 3.14 Ratio of cells in the original domain.

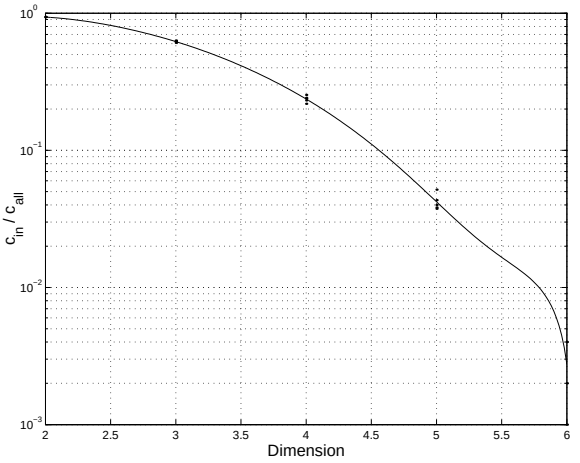

For data containing independent normal errors with a constant variance, the error bounds contain at least half of the predictions. The curve shown in Figure 3.14 is $p(x) = -0.048x^4 + 0.064x^3 - 0.203x^2 - 0.459x + 0.263$, the average value $\mathrm{E}(\mathbf{x})$ is 3.917, and the standard deviation $\sigma(\mathbf{x})$ is 1.412. The structure of the polynomial fit can be described using the Cholesky factor of the Vandermonde matrix

$$R = \begin{bmatrix} -12.19 & -1.56 & -6.08 & -0.47 & -3.17 \\ 0 & 8.46 & -0.45 & 4.47 & -0.44 \\ 0 & 0 & 1.21 & 0.33 & 2.93 \\ 0 & 0 & 0 & -1.63 & 0.30 \\ 0 & 0 & 0 & 0 & 2.25 \end{bmatrix},$$

the degree of freedom which is 19, and the norm of the residuals which is 0.034 in this case.

§ 3.6 Voronoi section

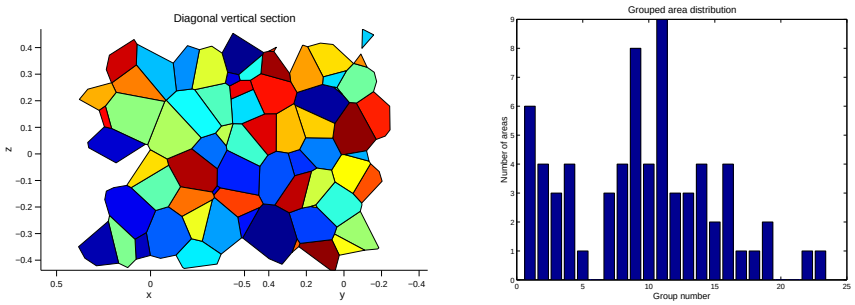

(a) (b)

Figure 3.15 *(a) Section by the plane $x - y + \epsilon z = \epsilon, \epsilon = 10^{-4}$. (b) Grouped distribution of area, the number of groups is approximately one-third the number of regions.*

	$\mathcal{V}_c$	$\aleph_c$	A_c^{fr}	V_c^{fr}	n_c^e	$E(n_{f,c}^e)$	$\sigma(n_{f,c}^e)$
min	8	6	2.2191×10^{-4}	9.9722×10^{-5}	12	4	0.6030
max	46	25	4.7015×10^{-3}	0.14364	69	5.52	2.5690
μ	26.338	15.169	1.8975×10^{-3}	1.8975×10^{-3}	39.507	5.1712	1.5586
σ^2	40.608	10.152	5.2144×10^{-7}	4.2313×10^{-5}	91.368	0.035983	0.1186
σ	6.3725	3.1862	7.2210×10^{-4}	6.5048×10^{-3}	9.5587	0.18969	0.3444
μ_g	25.543	14.829	1.7572×10^{-3}	1.1575×10^{-3}	38.315	5.1676	1.5169
μ_h	24.703	14.478	1.6026×10^{-3}	8.5548×10^{-4}	37.054	5.1638	1.4700
med	26	15	1.8125×10^{-3}	1.1660×10^{-3}	39	5.2	1.5706
mad	5.0068	2.5034	5.6975×10^{-4}	1.4250×10^{-3}	7.5103	0.14465	0.2715
$\mathcal{M}^2$	40.531	10.133	5.2045×10^{-7}	4.2233×10^{-5}	91.195	0.035915	0.1184
$\mathcal{M}^3$	72	9	2.5644×10^{-10}	5.4435×10^{-6}	243	-8.3404×10^{-3}	-0.0060
$\mathcal{M}^4$	5088.9	318.06	1.0467×10^{-12}	7.6653×10^{-7}	25763	7.9566×10^{-3}	0.041906
$\mathcal{K}$	3.0978	3.0978	3.8644	429.77	3.0978	6.1689	2.9916

Table 3.6 *Simulation uses rbox (1000 random points, seed 234985) and qhull (option v and o); $d = 3$, $n^c = 527$, $n^v = 6357$, CPU time 6,466.99 sec for the counting of statistics, 270.56 sec for finding area of the faces, 4.47 sec for calculating cell volume and 2.8 sec for finding the number of edges.*

§ 3.7 Number of vertices and edges

It has been observed from the simulations that in three dimensions cells always have vertices in even numbers and edges odd ones. This can be explained by the following theorems.

Theorem 3.2. *(cf Miles, 1972) In a simple three dimensional Voronoi tessellation, $3n_c^v = 2n_c^e$.*

Proof. Pick any Voronoi cell of the tessellation. Suppose that it has n^v vertices. Add up the number of edges connected to all vertices. Because every cell is a simple polyhedron, there are exactly three edges connected to each vertex. The number of edges thus counted is therefore $3n^v$. But each of the edges is connected to two vertices, so we have counted every one of them twice. Therefore,

$$2n^e = 3n^v.$$

This is the case for any cell, hence the theorem is proved. □

This theorem gives rise the following two theorems.

Theorem 3.3. *The number of vertices of any cell within a simple three dimensional Voronoi tessellation is an even positive integer.*

Proof. Observe that the term $2n_c^e$ in the theorem above is divisible by 2. This term is equal to $3n_c^v$, therefore the latter is also divisible by 2. Since 2 can not divide into 3, the only term left, n_c^v, must be divisible by 2 and hence even number. □

Theorem 3.4. *The number of edges of any cell within a simple three dimensional Voronoi tessellation is a positive integer divisible by three.*

Proof. With the same line of reasoning as above, observe that $3n_c^v$ is divisible by 3. Therefore $2n_c^e$, and hence n_c^e, is also divisible by 3. □

Another proof for both the above theorems is the following.

Proof. For an equality to hold, both sides must have the same factors. By supposing an unknown common factor i and by cross-multiplying the coefficients on both sides, one obtains $2\cdot(3\cdot i) = 3\cdot(2\cdot i)$, where i is a positive integer. Therefore $n_c^e = 3i$ and $n_c^v = 2i$. In other words, n_c^e is divisible by three and n_c^v is even. □

The theorems above assume that every cells are simple. This can not be the case in real situation where edges have dimensions and rather represent tubes than one-dimensional lines. Such case is similar to the so-called *degenerative* case in a computational model of Voronoi tessellation where there exist vertices the number of edges connected to each of which exceeds four. Even in the degenerative case, one would perhaps still expect a tendency for n_c^v to be an even number and for n_c^e to be divisible by three to hold.

In nature there are things which have a tendency towards even numbers. The following graph shows the the abundance in cosmic materials from the compilation by Cameron (1973). The year of publication of this paper is often misquoted as 1970, due to misprints in a footnote on the first page of the paper. Even the legendary Fred Hoyle had consistently made this mistake and never corrected it all through the whold of his career, that is to say, in two of his books and at least one of his papers, spanning the period of approximately forty years in total (*cf* Hoyle, 1977). Out of a sample of 278 of those papers which cite this work, this misprint resulted in 80% of the total number of errors in the year cited, which in turn amounts to 1.8% of the number of samples.

The abundances of the chemical elements in the universe. They are assumed to be the same as those found in the primitive solar nebula, which had been deduced from data on abundances found in chondritic meteorites and those found in the Sun. All abundances are relative to that of Si which is taken to be 10^6. Missing bars appear where the atomic numbers are unstable. Except for the atomic number 1 of Hydrogen, which is the most universal element, all other elements with even atomic numbers are locally more abundant than those with near-by odd atomic numbers.

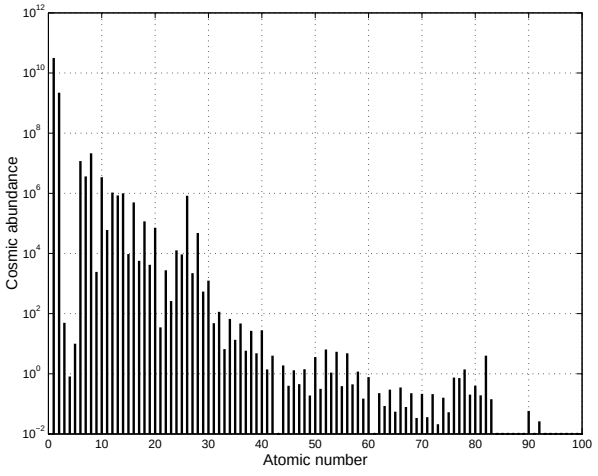

Figure 3.16 Abundance of elements.

Of interest are also the electrical resistivity and conductivity of solid matters.The conductivity σ is by definition the reciprocal of the resistivity ρ. Some of the solids, particularly boron, carbon, silicon, sulphur, germanium, selenium and tellurium, have a distinctively higher resistivity than the majority. Interestingly all of these, with only one exception of boron whose atomic number is five, are of an even atomic number, which respectively from carbon are 6, 14, 16, 32, 34, and 52. This can be seen in Figure 3.17 the data of which are taken from Podesta (2002).

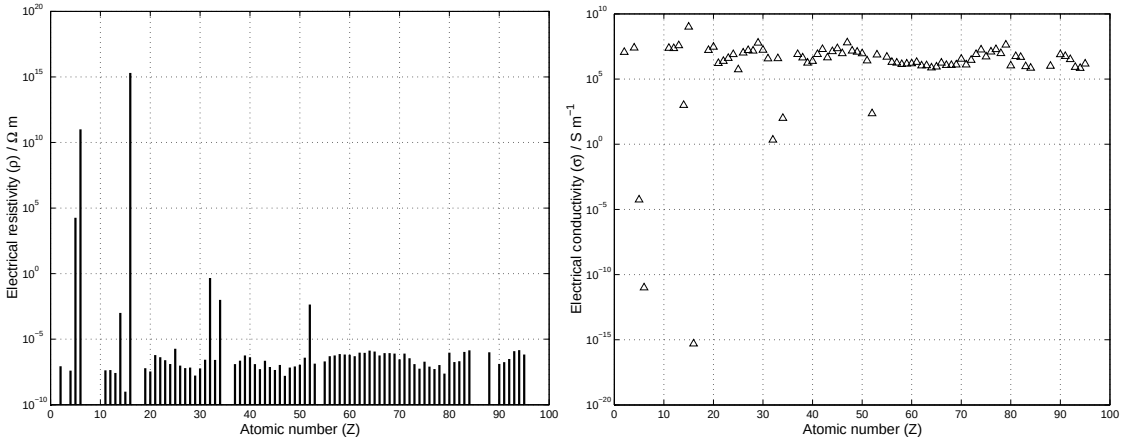

(a) (b)

Figure 3.17 *The electrical resistivity, (a), and conductivity, (b), of elements which are solid at the room temperature.*

	n_c^e	$\mathcal{N}_v^c(E(l_c^e))$	$\mathcal{N}_v^c(\wp_c)$	$\mathcal{N}_v^c(A_c)$
min	3	0.20716	0.2749	0.058428
max	11	8.1072	10.134	22.307
μ	5.8973	0.70626	1.0089	1
σ^2	1.8955	0.18607	0.2942	1.4379
σ	1.3768	0.43136	0.54241	1.1991
μ_g	5.742	0.66036	0.94795	0.79225
μ_h	5.5904	0.62941	0.89999	0.61799
med	6	0.65709	0.96614	0.84267
mad	1.0736	0.17995	0.24357	0.49216
$\mathcal{M}^2$	1.8912	0.18565	0.29355	1.4347
$\mathcal{M}^3$	1.6194	0.96371	1.7931	22.703
$\mathcal{M}^4$	12.438	6.8376	15.785	468.03
$\mathcal{K}$	3.4775	198.38	183.18	227.39

Table 3.7 *Neighbour statistics. Here for the normalisation purpose,* $l^e_{\text{basis}} = 0.046662, \wp_{\text{basis}} = 0.18665, A_{\text{basis}} = 0.0021773$. *Simulation uses* `voronoin` *command in Matlab;* $d = 2$, $n^c = 448$, $n^v = 946$, *CPU time 1.19 seconds.*

Next simulation was done with $d = 2$, $n^c = 3$ to 49551.

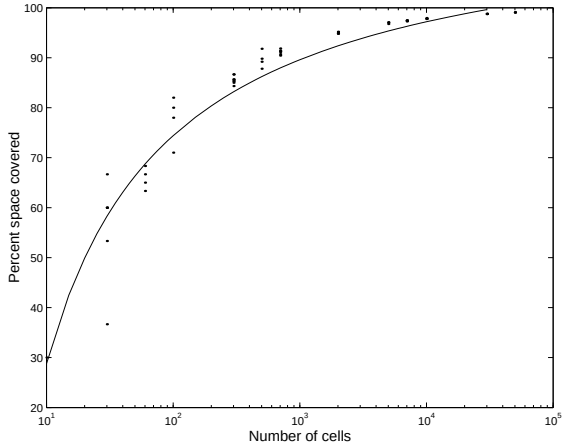

Figure 3.18 shows the percentage of space covered by a Voronoi structure. The number of cells is the total number of cells generated. The percent space covered is the volume of the structure after boundary cells, that is cells which extrude the unit volume boundary, have been excluded. The equation of the reference curve is

$$y = -210/\log x + 120.$$

Figure 3.18 Space covered by Voronoi.

The reference line in Figure 3.19 is the linear equation

$$y = 2x + 10.$$

In other words the relationship between n_c and n_v is linear, which is to be expected in any random tessellation and is a necessity in any regular tessellation. The larger the network the more linear this relationship becomes. Bound ary cells have been excluded.

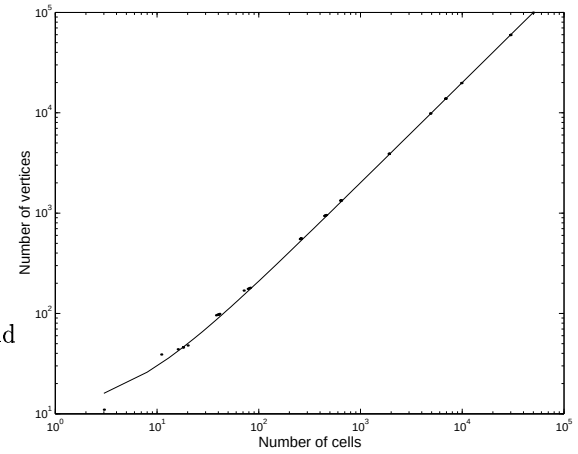

Figure 3.19 Number of vertices versus number of cells.

The curve in Figure 3.20 is the result of curve fitting by cubic spline interpolation which fits a different cubic polynomial between each pair of data points.

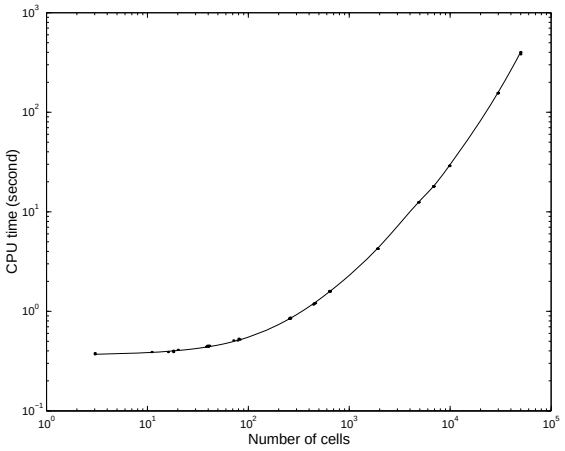

Figure 3.20 The CPU time in seconds.

The characteristic length is the length of the side of the cubic structure having the same number of cells and the same total volume as the Voronoi structure. The characteristic lengths in Figure 3.21 are shown as dots. The reference line is

$$y = 0.7/x^{0.45}.$$

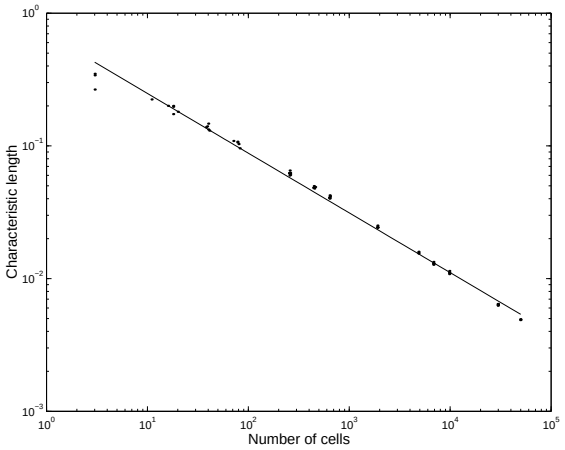

Figure 3.21 Characteristic length versus the number of cells.

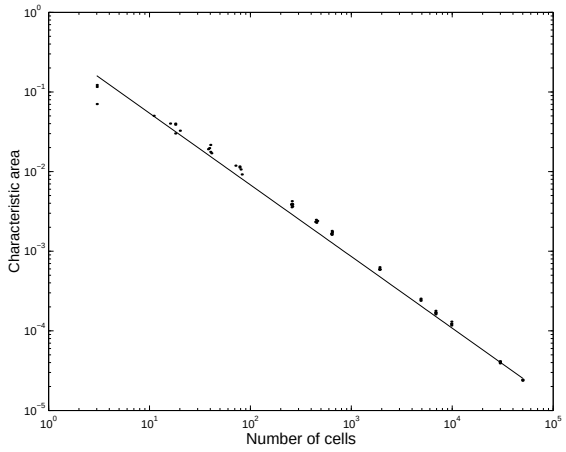

The characteristic area is the area of each square in the assembly the total volume and the number of cells of which are the same as those of the Voronoi graph. The reference curve shown in Figure 3.22 is

$$y = 0.43/x^{0.9}.$$

Both Figure 3.21 and Figure 3.22 are hyperbolic.

Figure 3.22 Characteristic area versus the number of cells.

	n_c^v	n_f^v	$\mathcal{N}_v^c(\mathcal{P}_c^f)$	$\mathcal{N}_v^c(A_f)$	$\mathcal{N}_v^c(A_c)$	$\mathcal{N}_v^c(V_c)$	n_c^f
min	8	3	0.001414	4.6179×10^{-7}	0.11908	0.21464	6
max	42	10	0.84885	0.82919	0.50425	12.719	23
μ	24.423	5.1114	0.32876	0.12535	0.30315	1.0000	14.211
σ^2	44.105	2.1650	0.030844	0.015846	0.008511	2.5764	11.026
μ_g	23.504	4.9065	0.25897	0.051216	0.28815	0.70118	13.825
μ_h	22.506	4.7086	0.12620	2.50×10^{-4}	0.27198	0.58794	13.423
med	22	5	0.33219	0.084165	0.30368	0.64077	13
mad	5.4338	1.1655	0.14499	0.099433	0.075445	0.67950	2.7169
$\mathcal{M}^2$	43.483	2.1619	0.030800	0.015823	0.008391	2.5401	10.871
$\mathcal{M}^3$	112.13	1.8902	5.92×10^{-4}	0.002805	4.8×10^{-5}	24.169	14.016
$\mathcal{K}$	3.1096	3.0234	2.3090	5.2926	2.3015	42.238	3.1096

Table 3.8 *From* `rbox` *(200 random points, seed 34565473) and* `qhull` *(option v and o);* $d = 3$, $n^c = 71$.

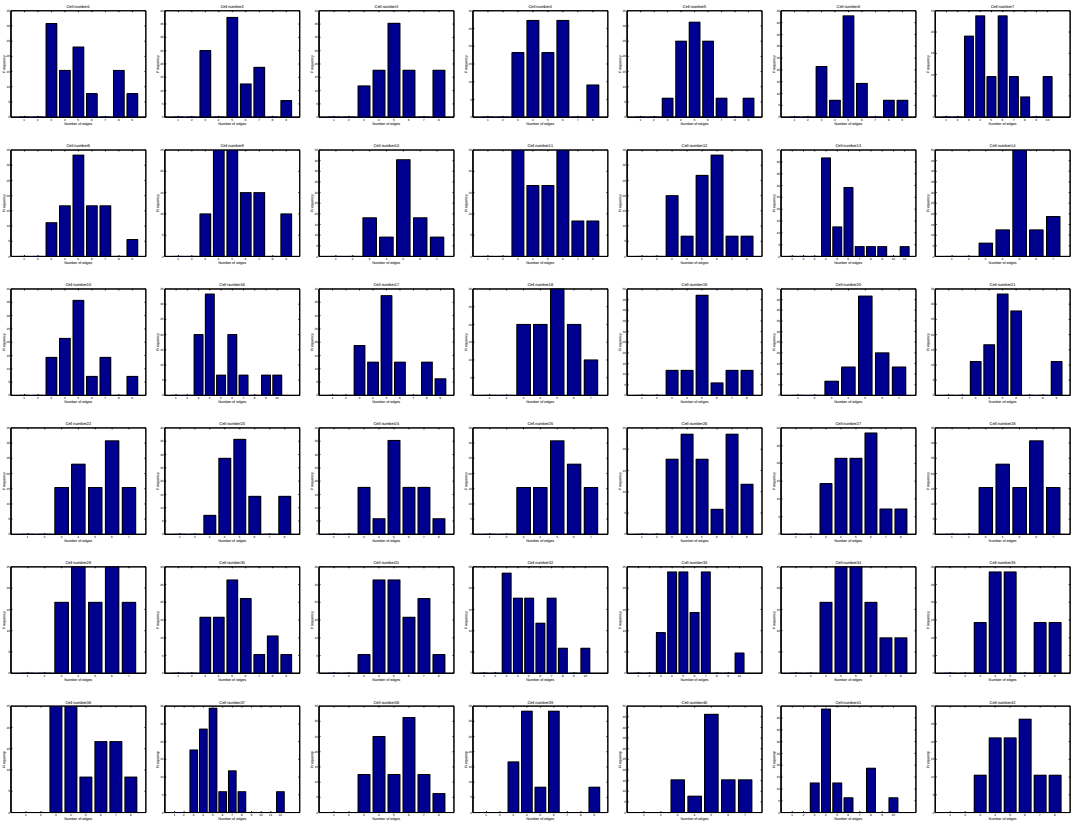

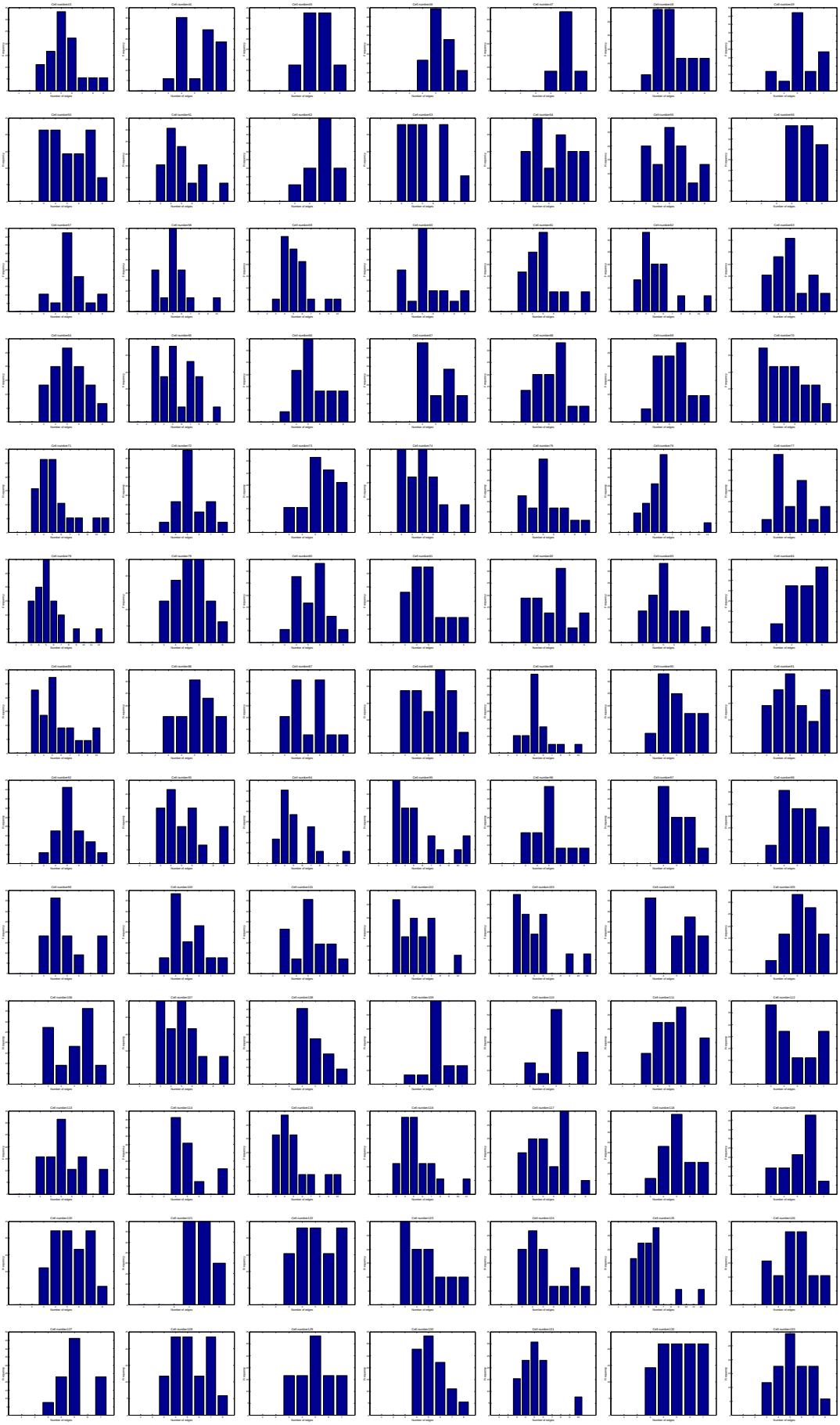

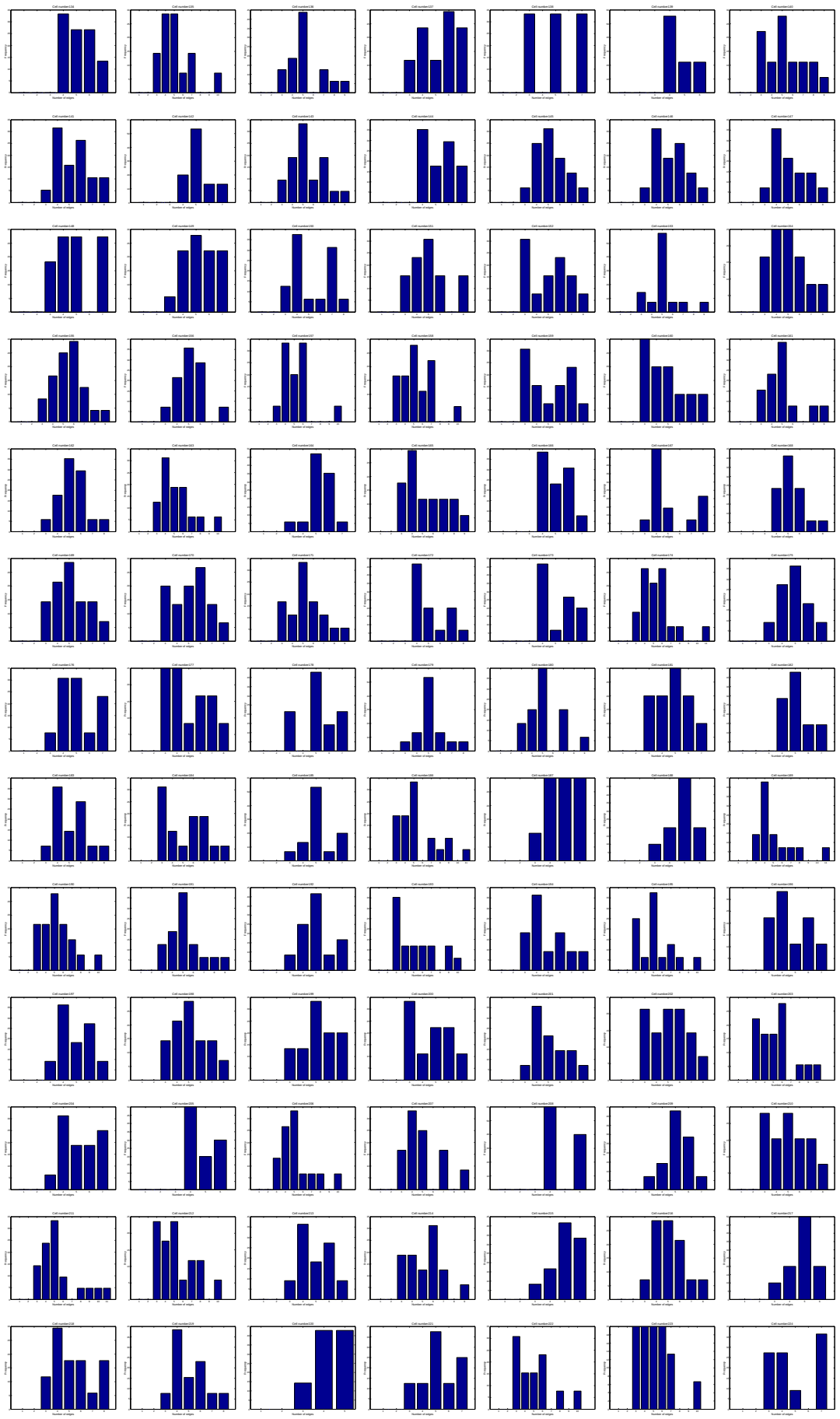

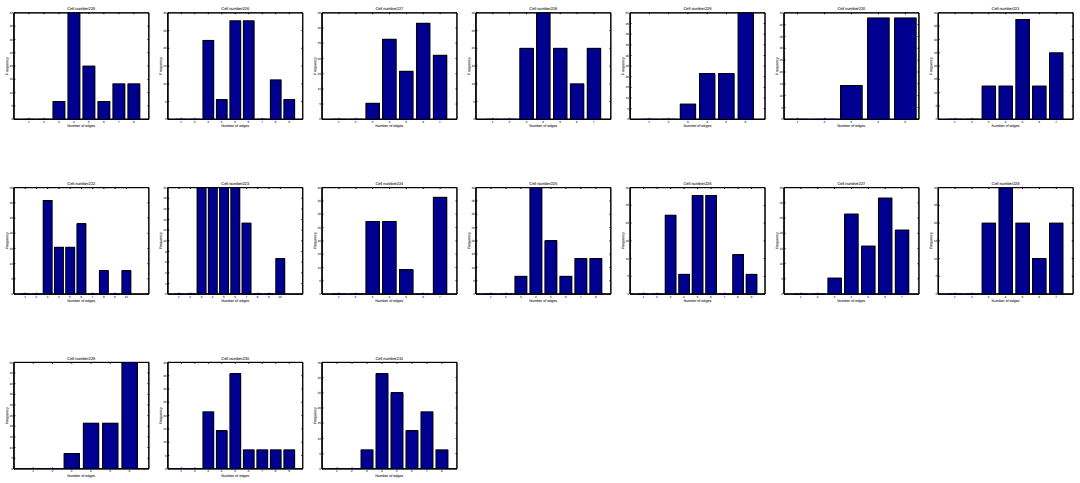

Figure 3.23 *Distribution of the number of edges per face. Each picture is an individual cell. The distribution shows the relative abundance or the number of faces (the vertical axes) having the number of edges as shown by the horizontal axes. The horizontal axis scales are positive integers starting from zero at the origin. Simulation uses* `rbox` *(500 random points, seed 893280) and qhull (option v and o); $d = 3$, $n^c = 231$, $n^v = 3{,}107$, CPU time 81.1 sec for finding face area, 2.22 sec for cell volume, 49.59 sec for counting edges and 0.03 sec for finding the number of edges and faces.*

The minimum number of edges for each face is three. This number is the same as the number of vertices of that face. From these figures most of the cells have at least one face with three edges. There are only 19 cells (8.23 per cent) which does not have any three-edged face, and all of them have some four-edged faces. Therefore there is no cell with five as the minimum number of edges per face. The maximum number of edges per face is less clear-cut. There are twelve cells (5.19 per cent) with 11 as the maximum number of edges per face and two (0.87 per cent) with 12.

	n_c^v	$\aleph_c$	A_c^{fr}	V_c^{fr}	α	n_c^e	$E(n_{f,c}^e)$	$\sigma(n_{f,c}^e)$
min	10	7	1.0989×10^{-3}	2.5790×10^{-4}	0.0406	15	4.2857	0.6030
max	44	24	1.0956×10^{-2}	0.24840	4.2505	66	5.5000	2.7028
μ	25.974	14.987	4.3290×10^{-3}	4.3290×10^{-3}	1.2515	38.961	5.1601	1.5450
σ^2	40.852	10.213	3.3308×10^{-6}	2.9419×10^{-4}	0.3802	91.916	0.0372	0.1243
σ	6.3915	3.1958	1.8250×10^{-3}	1.7152×10^{-2}	0.6166	9.5873	0.1928	0.3526
μ_g	25.166	14.642	3.9633×10^{-3}	1.8465×10^{-3}	1.0816	37.749	5.1564	1.5030
μ_h	24.323	14.288	3.6026×10^{-3}	1.2471×10^{-3}	0.8241	36.484	5.1526	1.4580
med	26	15	4.1467×10^{-3}	1.5715×10^{-3}	1.1915	39	5.2000	1.5315
mad	5.1532	2.5766	1.4064×10^{-3}	4.5864×10^{-3}	0.4720	7.7298	0.1505	0.2794
$\mathcal{M}^2$	40.675	10.169	3.3163×10^{-6}	2.9291×10^{-4}	0.3785	91.518	0.0370	0.1238
$\mathcal{M}^3$	59.377	7.4222	5.7258×10^{-9}	6.3817×10^{-5}	0.2143	2.0040×10^{2}	-0.0071	0.0058
$\mathcal{M}^4$	4.5398×10^{3}	2.8374×10^{2}	4.6684×10^{-11}	1.5395×10^{-5}	0.7390	2.2983×10^{4}	0.0063	0.0463
$\mathcal{K}$	2.7440	2.7440	4.2448	1.7943×10^{2}	5.1578	2.7440	4.5730	3.0230

Figure 3.24 *Statistics of a 231 cells Voronoi structure.*

Because the Voronoi tessellation being studied is simple, $\aleph_c^v = \aleph_c^f = n_c^f$. In other words, any two cells having at least one vertex in common are neighbours to each other, and the number of neighbours around any cell in an infinite network is equal to the number of its faces.

Figure 3.25 shows the distributions of the number of faces and edges per cell.

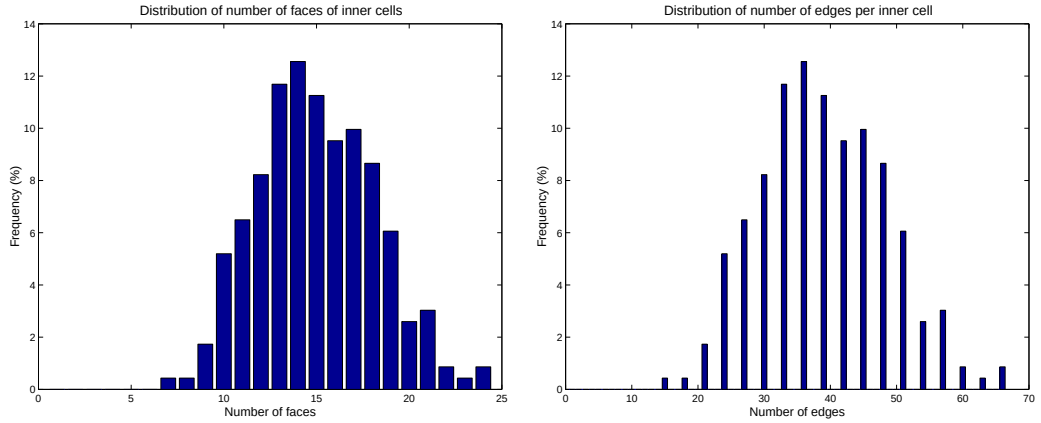

Figure 3.25 *The distributions of the number of* (a) *faces, and* (b) *edges, per cell.*

The results from 527 Voronoi cells are shown next. Table 3.9 is from a 3-d Voronoi structure generated from 1,000 cells. The creation codes started with a random seed of 234985. They spent 6,466.99 seconds for the counting of statistics, 270.56 for finding area of the faces, 4.47 for calculating cell volume and additional 2.8 seconds to find statistics for the number of edges. There are 6,357 vertices generated, plus another added distant vertice. Boundary cells were discarded, which leaves us with 527 inner cells which are taken into account.

	$v_{c_{in}}$	$\aleph_{v,c_{in}}$	$A_{fr,c_{in}}$	$V_{fr,c_{in}}$	$n_{f,c_{in}}$	$n_{e,c_{in}}$	
Min	8	6	2.2191×10^{-4}	9.9722×10^{-5}	6	12	
Max	46	25	4.7015×10^{-3}	0.14364	25	69	
μ	26.338	15.169	1.8975×10^{-3}	1.8975×10^{-3}	15.169	39.507	
σ[2]	40.608	10.152	5.2144×10^{-7}	4.2313×10^{-5}	10.152	91.368	
σ	6.3725	3.1862	7.2210×10^{-4}	6.5048×10^{-3}	3.1862	9.5587	
μ_g	25.543	14.829	1.7572×10^{-3}	1.1575×10^{-3}	14.829	38.315	
μ_h	24.703	14.478	1.6026×10^{-3}	8.5548×10^{-4}	14.478	37.054	
Med	26	15	1.8125×10^{-3}	1.1660×10^{-3}	15	39	
δ_μ	5.0068	2.5034	5.6975×10^{-4}	1.4250×10^{-3}	2.5034	7.5103	
M[2]	40.531	10.133	5.2045×10^{-7}	4.2233×10^{-5}	10.133	91.195	
M[3]	72	9	2.5644×10^{-10}	5.4435×10^{-6}	9	243	
M[4]	5088.9	318.06		1.0467×10^{-12}	7.6653×10^{-7}	318.06	25763
κ	3.0978	3.0978	3.8644	429.77	3.0978	3.0978	

Table 3.9 *Statistics from 527 Voronoi cells.*

The mean value of the mean numbers of edges per face obtained was 5.1712. This can be called $\mathrm{E}(\mathrm{E}(n_{e,f}))$, the expected value over all cells of the mean number of edges in a face averaged over all its faces. The variance was 0.035983, minimum value 4, maximum 5.52, standard deviation 0.18969, geometric mean 5.1676, harmonic mean 5.1638, median 5.2, mean absolute deviation 0.14465, 2^{nd} moment 0.035915, 3^{rd} moment -0.0083404, and kurtosis 6.1689. The mean and standard deviation of all faces are given in Appendix 9.6. The standard deviation of $\mathrm{E}(n_{e,f})$ averaged over all faces of bounded cells is 1.5586. The rest are $\sigma^2 = 0.1186$, $\sigma = 0.3444$, minimum 0.6030, maximum 2.5690, $\mu_g = 1.5169$, $\mu_h = 1.4700$, median 1.5706, $\delta_\mu = 0.2715$, $M^2 = 0.1184$, $M^3 = -0.0060$, and $\kappa = 2.9916$.

Figure 3.26 shows the ratios between the number of vertices and the number of cells in Voronoi networks of various dimensions. The line shown in Figure 3.26 is

$$y = 0.2410e^n,$$

where n is the dimension of the network and is the horizontal axis; the coefficient of the exponential term is obtained by averaging over the averages in each dimension, each of which in turn comes from five batch runs.

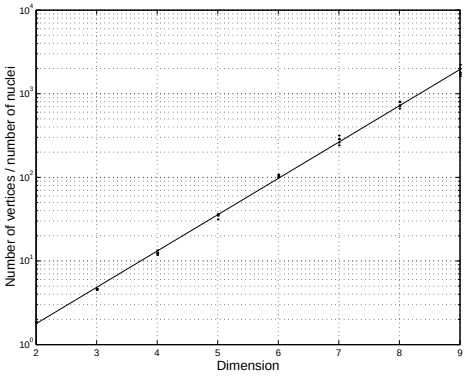

Figure 3.26 v_n/c_n in Voronoi networks of various dimensions.

Figure 3.27 shows the CPU time in creating the Voronoi networks for Figure 3.26. The line shown in Figure 3.27, found manually by trial and error, has the equation

$$y = 4.61 \times 10^{-6}(2 + e)^n.$$

In comparison, substituting the average cpu time for each dimension for y in the equation $y = Ae^n$ to obtain A and then find the average again over all dimensions results in $\overline{A} = 1.612 \times 10^{-4}$. The program which produces both Figure 3.27 and ℵ is given in § A.9.

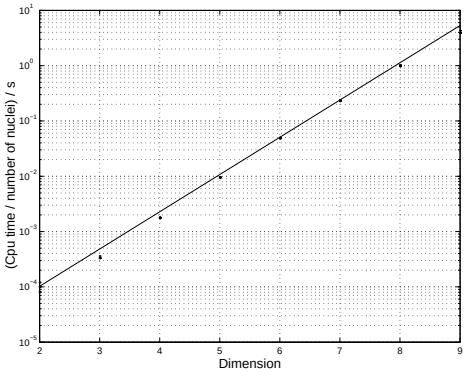

Figure 3.27 CPU time in creating the Voronoi networks.

The number of vertices of higher dimensions is investigated briefly in the following Table 3.10 and Figure 3.28 the simulation of which was carried out by the program in § A.18.

Dimension	4	5	6	8	9	10
N_c	300	300	300	30	30	30
N_v	6,577	27,150	118,534	5,465	10,467	17,442
n_c	132	104	14	2	3	0
$\min(n_c^v)$	26	244.00	1,020.0	952.002	2,353.0	4,287.0
$\max(n_c^v)$	255	1,142.0	5,852.0	2,638.0	5,534.0	9,528.0
$\bar{n}_c^v$	109.90	543.51	2,766.5	1,640.2	3,489.7	6,396.0
$(\sigma^2_{n_v})_c$	1,155.9	22,974	6.0898×10^5	1.7964×10^5	7.0328×10^5	2.3635×10^6
$\sigma_c^{n_v}$	33.999	151.57	780.37	423.84	838.62	1.5374×10^3
$\mu_g(n_c^v)$	104.41	523.06	2,666.1	1,589.9	3,398.4	6,225.6
$\mu_h(n_c^v)$	98.389	502.94	2,571.4	1,542.3	3,313.9	6,065.2
$\mathrm{med}(n_c^v)$	107.50	527.00	2,651.0	1,568.5	3,272.5	5,816.5
$\mathrm{mad}(n_c^v)$	27.366	119.39	588.19	331.96	687.47	1,296.6
$m^2(n_c^v)$	1,152.1	22,897	6.0695×10^5	1.7365×10^5	6.7984×10^5	2.2847×10^6
$m^3(n_c^v)$	15,555	2.2871×10^6	5.1556×10^8	4.7965×10^7	3.9108×10^8	1.8988×10^9
$m^4(n_c^v)$	4.5760×10^6	1.8905×10^9	1.7964×10^{12}	8.5043×10^{10}	1.1967×10^{12}	1.1638×10^{13}
$\kappa(n_c^v)$	3.4476	3.6059	4.8764	2.8202	2.5892	2.2296

Table 3.10 *Statistics of the number of vertices in 4, 5, 6, 8, 9, and 10 dimensions.*

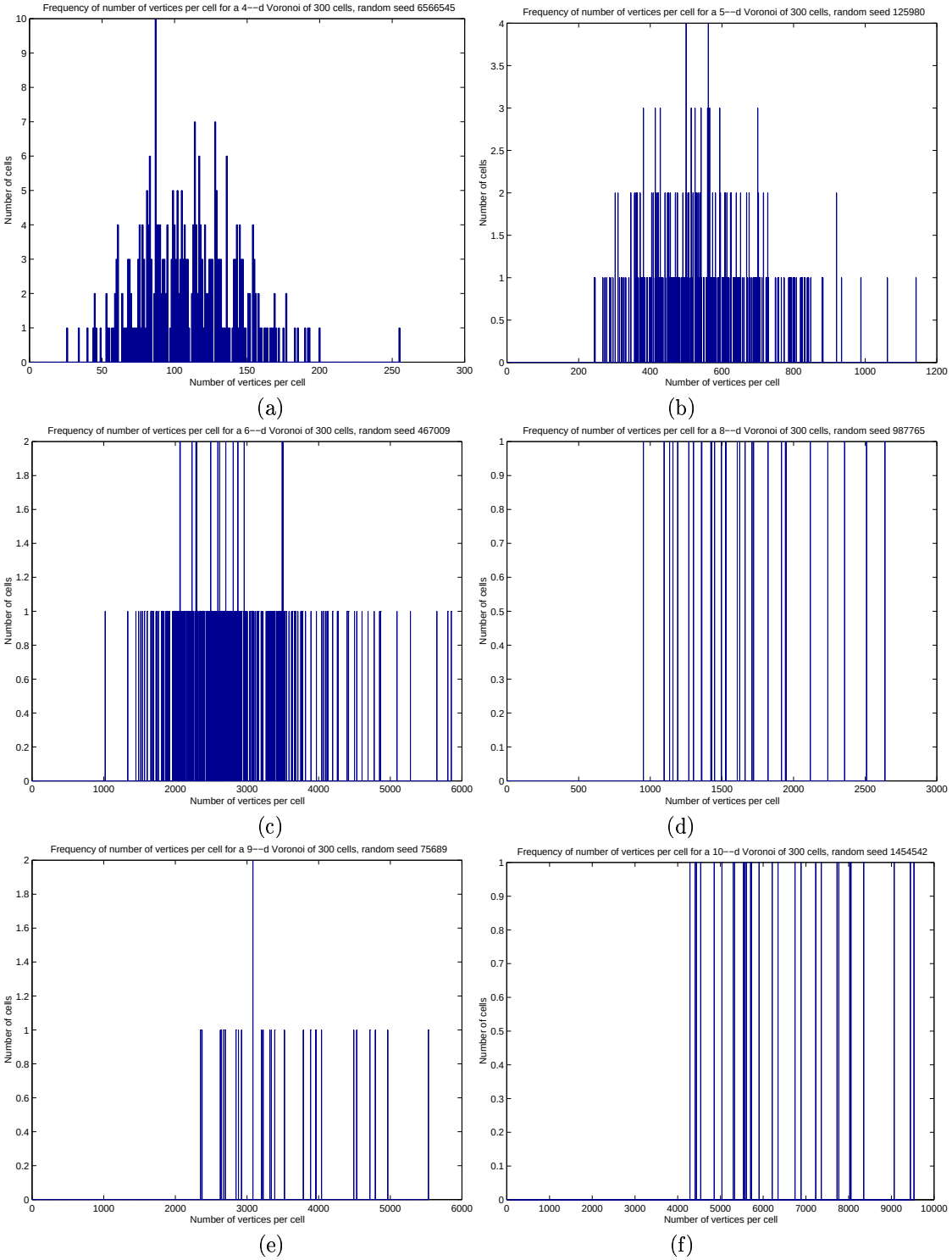
Frequency of number of vertices per cell for a 4−−d Voronoi of 300 cells, random seed 6566545
Number of cells
Number of vertices per cell
(a)
Frequency of number of vertices per cell for a 5−−d Voronoi of 300 cells, random seed 125980
Number of cells
Number of vertices per cell
(b)
Frequency of number of vertices per cell for a 6−−d Voronoi of 300 cells, random seed 467009
Number of cells
Number of vertices per cell
(c)
Frequency of number of vertices per cell for a 8−−d Voronoi of 300 cells, random seed 987765
Number of cells
Number of vertices per cell
(d)
Frequency of number of vertices per cell for a 9−−d Voronoi of 300 cells, random seed 75689
Number of cells
Number of vertices per cell
(e)
Frequency of number of vertices per cell for a 10−−d Voronoi of 300 cells, random seed 1454542
Number of cells
Number of vertices per cell
(f)

Figure 3.28 *Distribution of vertices in* (a) *4,* (b) *5,* (c) *6, and* (d) *8,* (e) *9,* (f) *10 dimensions.*

To obtain the number of vertices per cell, n_c^v, of a six-dimensional Voronoi structure of 1,000 cells a batch program was used, for instance the one listed in § A.19. The Matlab macro that this program refers to opens and reads from a file the number of vertices and then finds the statistical values, *viz.* $\min(n_c^v) = 1{,}198$; $\max(n_c^v) = 9{,}923$; $\bar{n}_c^v = 4{,}201.1$; $(\sigma^2_{n_v})_c = 1.4069 \times 10^6$; $\sigma_c^{n_v} = 1186.1$; $(\bar{n}_g)_c^v = 4035.4$; $(\bar{n}_h)_c^v = 3866.8$; $\mathrm{med}(n_c^v) = 4122.5$; $\mathrm{mad}(n_c^v) = 931.81$; $m^2(n_c^v) = 1.4055 \times 10^6$; $m^3(n_c^v) = 1.0462 \times 10^9$; $m^4(n_c^v) = 7.7148 \times 10^{12}$; and $\kappa(n_c^v) = 3.9053$.

The following figure shows the frequency of the number of vertices. Interested readers may find the data in § 9.6 which give rise to Figure 3.29 interesting. These results are not the most useful ones because of the presence of border cells.

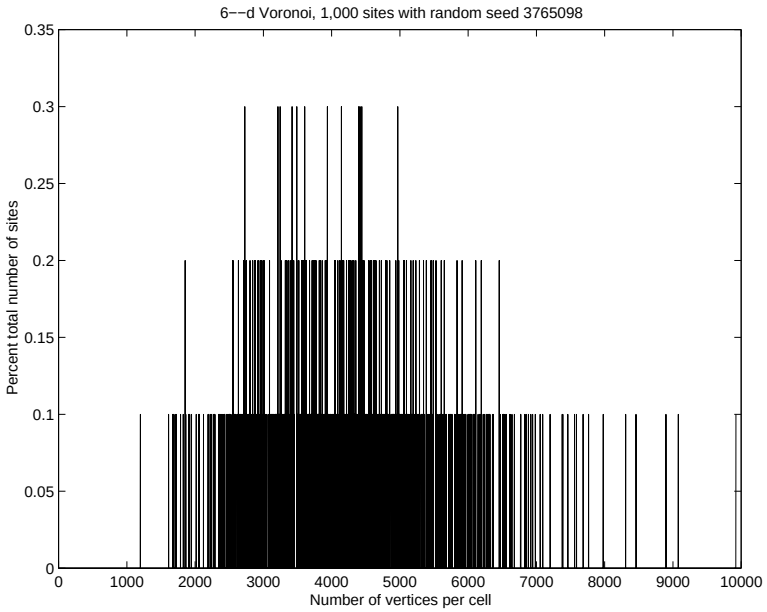

Figure 3.29 *Distribution of vertices in a 6-d Voronoi structure*

AVS

The first picture I created on AVS was a Trigonal Dipyramidal. The program was the following .inp file.

```
5 2 0 0 0
1 0 0 1.2910
2 2 0 1.2910
3 1 1.7321 1.2910
4 1 0.5774 0
5 1 0.5774 2.5820
1 1 tet 1 2 3 4
2 1 tet 1 2 3 5
1 2
```

The connection of modules was ReadUCD to ExternalEdges to UViewer3D.

The following simulation was done on a 3–d systems with a joggled-input option in `qhull`. The number of vertices, however, also takes into account those belonging to the boundary cells. The minimum $n_{v,c}$ was 6, maximum $n_{v,c}$ 52, $\bar{n}_{v,c}$ 25.269, 2^{nd}–Moment 49.363, 3^{rd}–Moment 228.87, 4^{th}–Moment 8,704.9, $\sigma^2_{n_{v,c}}$ 49.412, $\sigma_{n_{v,c}}$ 7.0294, $\mu_{g,n_{v,c}}$ 24.317, $\mu_{h,n_{v,c}}$ 23.365, $\widetilde{n}_{v,c}$ 24, $\delta_\mu(n_{v,c})$ 5.5428, $\kappa(n_{v,c})$ 3.5725 .

Following figure is a distribution graph.

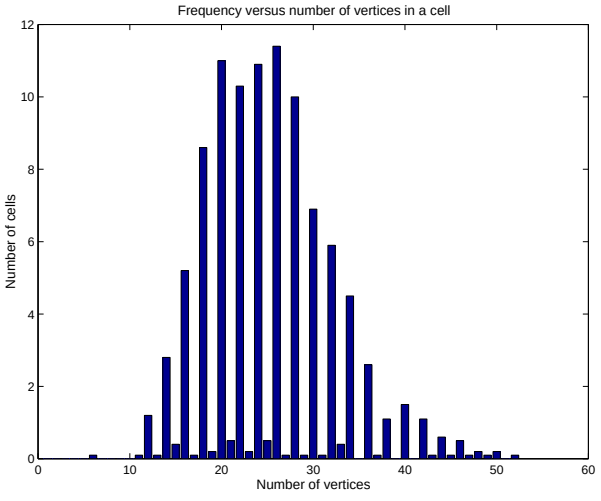

In Figure 3.30 boundary cells have not been excluded. So there are still some cells which have an odd number of vertices. But even these are few and far between, and only because of them that the lacks of odd vertice-numbered cells has been noticed. Had there been nothing there it is difficult to see how this uniform characteristic, or invariance, of the Voronoi tessellation could have come to light.

Figure 3.30 Number of cells having a particular number of vertices.

Theorem's 3.4 and 3.4 above are observations which are not only useful but essential when you try to understand the valence relations. Assuming that the Euler's theorem is true, then these two theorems give rise to Algorithm 3.2 which I have devised for counting all the components in these relations. Here n_e and n_v are all the edges, and respectively vertices, of the original structure originally counted, n_b^e all the additional edges, going to infinity, which are drawn to complete the valences of some of the boundary vertices, c_n cells with n edges and f_n the frequency occurences of c_n.

Algorithm 3.2 *Valence relations for planes in two dimensions.*

draw an addition bond for all boundary vertices which have valence 2;
$e \leftarrow \lfloor \mathbf{n_e} + \mathbf{n_b^e}/3 \rfloor$;
draw an additional $(n_e + n_b^e - e)$ on boundary vertices;
if $\lfloor n_v/2 \rfloor \bmod 2 \neq 0$ **then**
  draw an additional vertex at infinity;
  $v \leftarrow n_v + 1$;
else
  $v \leftarrow n_v$;
endif
$f \leftarrow 1 + e - v$;
label all the f_n bound faces;
if $(n_f + n_b^f) = f$ **then**
  label all the f_b^n unbound faces;
else
  label $(f - n_f)$ unbound faces;
  label all the remaining $(n_f + n_b^f - f)$ unbound faces together as a single face;
endif

□

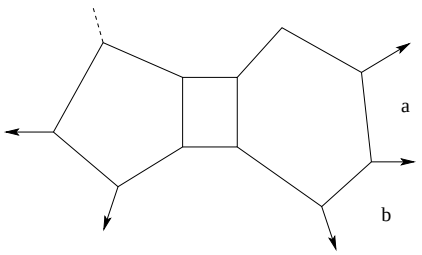

In Algorithm 3.2 the vertex at infinity mentioned does not necessarily have to be literally at the infinity. Although Algorithm 3.2 is for planes in two dimensions, it should be possible to extend it to other topolgical objects and to higher dimensions by simply changing the Euler's equation to the appropriate one. When labelling f, if $(n_f + n_b^f) \neq f$, we know that $(n_f + n_b^f) > f$ with probability one.
Paradoxically this relation holds only for infinite networks, but its derivation, as well as its verification, can only be done on a tessellation of finite size. Counting the components of the valence relation one sees in a graph involves both the Euler's theorem and Theorem's 3.4 and 3.4.

Figure 3.31 Counting the valences.

§ 3.8 Faces in different dimensions

Considering only those cells bound within the unit box, vertices and all, the following, namely Tables 3.11, 3.12 and 3.13, are the results from five simulations in two, three and four dimensions respectively, using the program listed in § A.16.

	Random seed				
	829247	134315	67453	432243	231215
N_v	187	187	186	189	183
n_v	170	167	168	163	170
n_c	72	69	70	65	72
n_c^v	169	165	166	159	170
μ_c^v	5.875	5.8116	5.8429	5.9077	5.8194
$(\sigma_v^2)_c$	2.0264	1.8022	1.6706	1.7726	1.5022
$m^2(n_c^v)$	1.9983	1.7761	1.6467	1.7453	1.4813
$m^3(n_c^v)$	1.1263	1.6917	0.96591	0.57642	0.96103
n_{1f}	241	235	237	227	241
n_c^{1f}	240	233	235	223	241
t_{CPU}(second)	20.36	20.39	20.09	20.6	19.76

Table 3.11 *Faces of Voronoi in two dimensions.* $N_c = 100$.

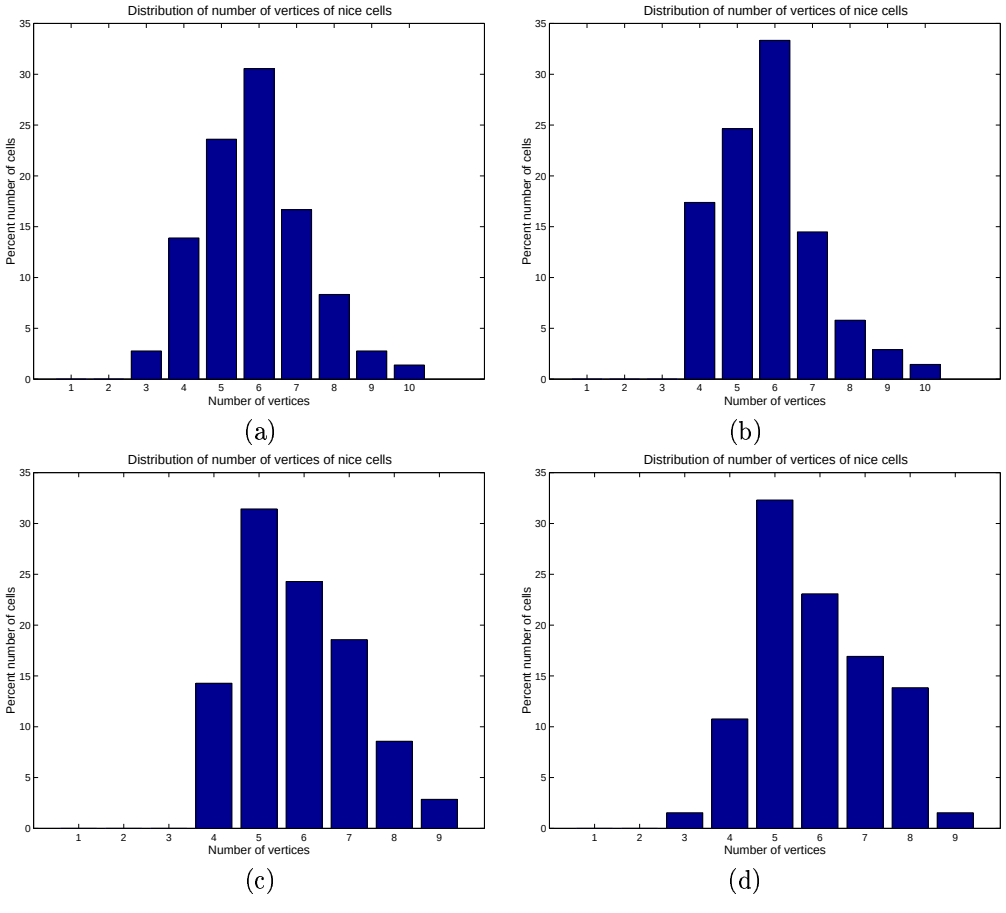

Figure 3.32 shows the distribution of v_c in each simulation on 2-d Voronoi. The size of the network is very small, which explains why the shape of the distribution varies greatly from one simulation to another. This is also the reason why all the bars in the graph have only limited number of possible heights.

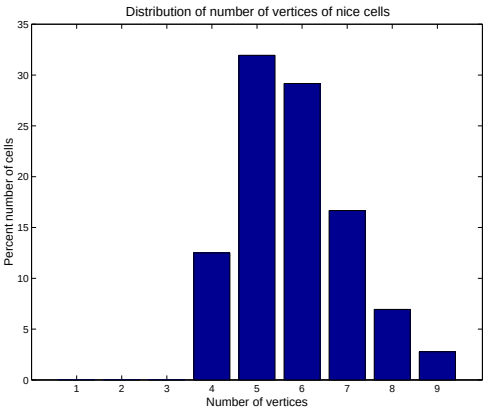

Figure 3.32 Distribution of v_c in two dimensions.

	Random seed				
	42398198	83250	34959	743690	1321
N_v	204	221	224	225	214
n_v	148	147	143	155	146
n_c	7	5	7	8	7
n_c^v	99	79	85	109	97
μ_c^v	21.714	23.6	20.286	21	21.714
$(\sigma_v^2)_c$	4.5714	14.8	31.238	34.286	21.905
$m^2(n_c^v)$	3.9184	11.84	26.776	30	18.776
$m^3(n_c^v)$	-4.6181	-16.128	-42.402	171	69.831
n_{2f}	114	110	111	123	113
μ_{2f}^v	4.9211	4.7727	4.7928	4.8293	4.7788
$(\sigma_v^2)_{2f}$	1.2592	1.6268	1.5476	2.0772	1.656
$m^2(n_{2f}^v)$	1.2482	1.612	1.5336	2.0603	1.6413
$m^3(n_{2f}^v)$	0.16453	0.99264	1.1334	1.7676	1.1444
n_c^{2f}	76	60	69	88	75
$(\mu_{2f}^v)_c$	5.0526	5.05	4.9855	4.9545	5.0533
$(\sigma_v^2)_c^{2f}$	1.1439	1.811	1.3674	2.0209	1.7268
$m^2((n_{2f}^v)_c)$	1.1288	1.7808	1.3476	1.9979	1.7038
$m^3((n_{2f}^v)_c)$	0.19004	0.28275	1.5224	1.4544	0.98057
n_c^{1f}	167	133	146	187	163
t_{CPU}(second)	24.28	25.67	28.49	34.23	26.46

Table 3.12 *Various faces of Voronoi in three dimensions.* $N_c = 50$.

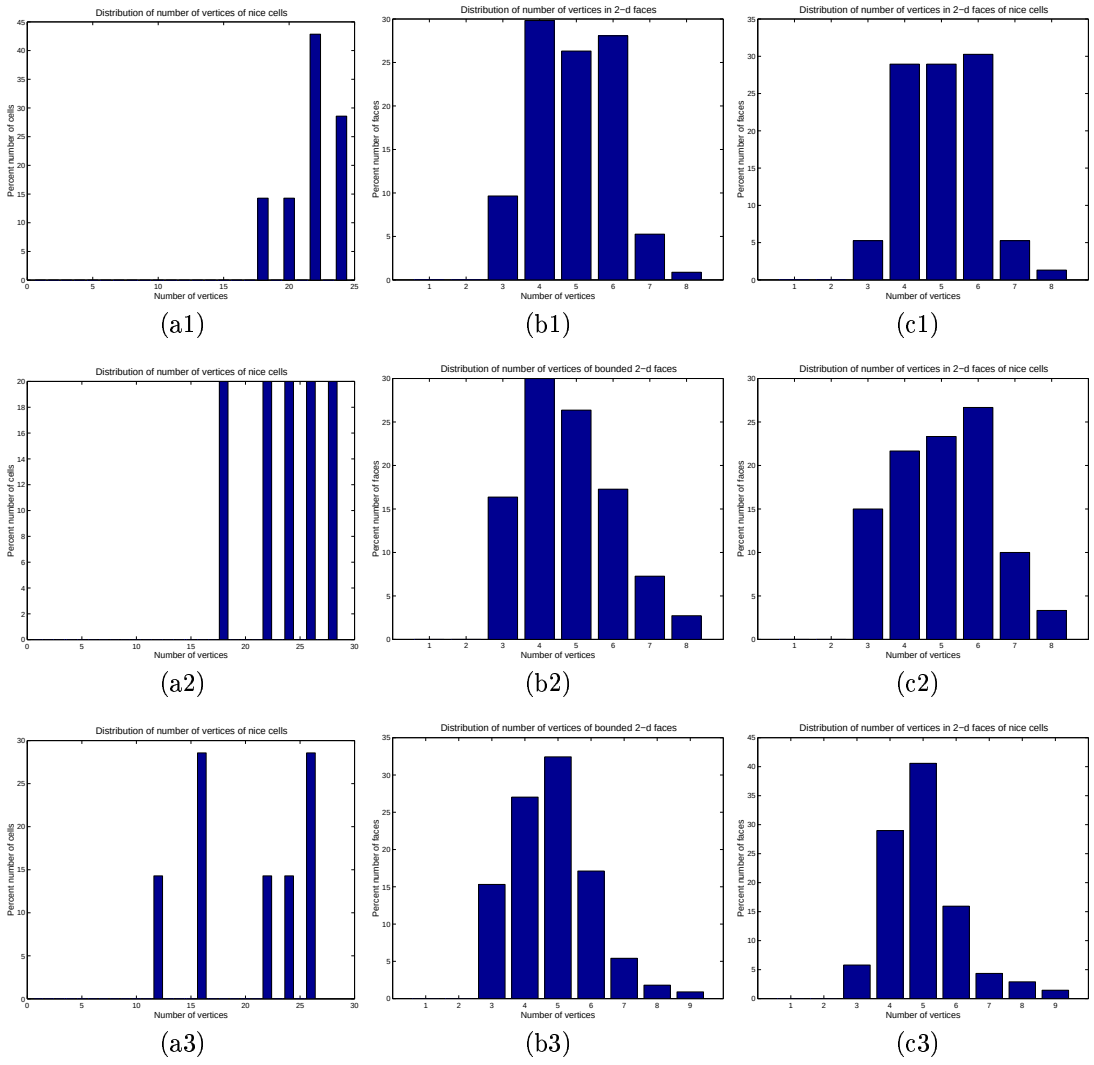

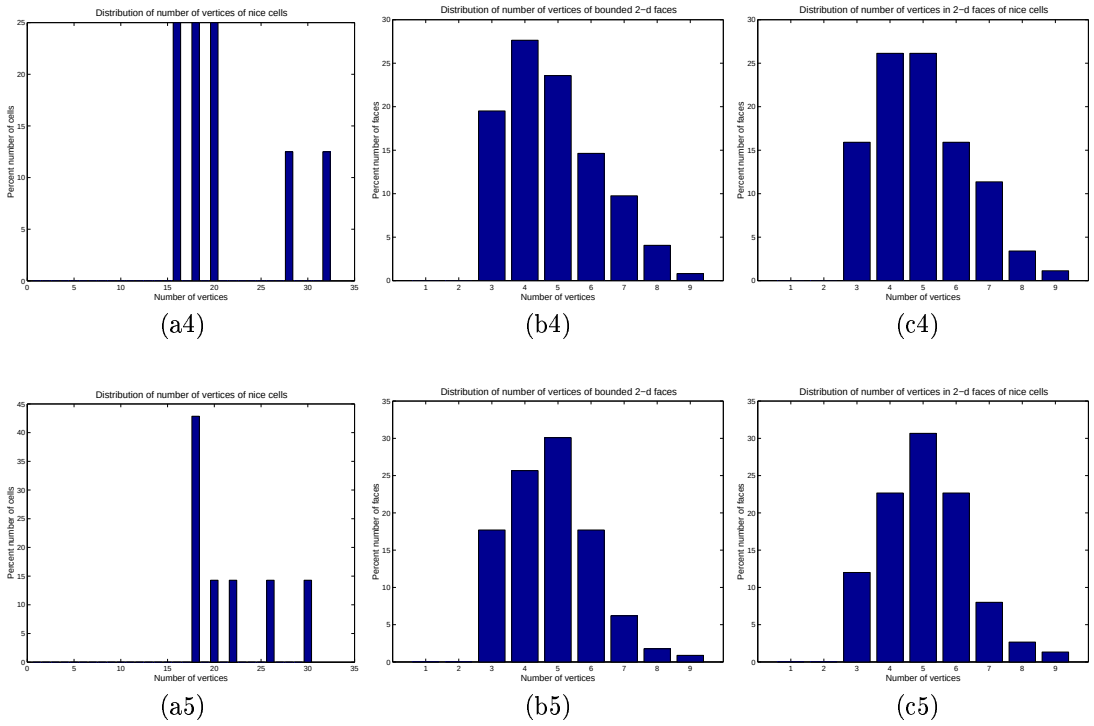
Distribution of number of vertices of nice cells
Percent number of cells
Number of vertices
(a4)
Distribution of number of vertices of bounded 2−d faces
Percent number of faces
Number of vertices
(b4)
Distribution of number of vertices in 2−d faces of nice cells
Percent number of faces
Number of vertices
(c4)
Distribution of number of vertices of nice cells
Percent number of cells
Number of vertices
(a5)
Distribution of number of vertices of bounded 2−d faces
Percent number of faces
Number of vertices
(b5)
Distribution of number of vertices in 2−d faces of nice cells
Percent number of faces
Number of vertices
(c5)

Figure 3.33 *Distribution of* (ai) v_c, (bi) $v_{2\mathrm{f}}$, *and* (ci) $v_c^{2\mathrm{f}}$ *of the* i^{th} *simulation on 3-d Voronoi.*

	Random seed				
	24098	802723	1453	732849	20480
N_v	1684	1719	1674	1586	1600
n_v	938	921	860	889	904
n_c	5	1	1	1	2
n_c^v	442	172	149	117	200
μ_c^v	114	172	149	117	110
$(\sigma_v^2)_c$	174.5	0	0	0	72
$m^2(n_c^v)$	139.6	0	0	0	36
$m^3(n_c^v)$	-547.2	0	0	0	0
$n_{3\mathrm{f}}$	83	102	84	83	95
$\mu_{3\mathrm{f}}^v$	8.8675	8.3137	8.5952	8.9398	8.7789
$(\sigma_v^2)_{3\mathrm{f}}$	18.848	18.198	19.449	17.496	19.77
$m^2(n_{3\mathrm{f}}^v)$	18.621	18.019	19.217	17.286	19.562
$m^3(n_{3\mathrm{f}}^v)$	75.225	102.38	95.854	62.919	118.61
$n_c^{3\mathrm{f}}$	32	8	10	7	19
$(\mu_{3\mathrm{f}}^v)_c$	8.8675	9.25	10.8	11.143	9.8947
$(\sigma_v^2)_c^{3\mathrm{f}}$	18.848	13.643	21.511	14.476	28.655
$m^2((n_{3\mathrm{f}}^v)_c)$	18.621	11.938	19.36	12.408	27.147
$m^3((n_{3\mathrm{f}}^v)_c)$	75.225	18.281	66.624	8.5364	195.1
$n_c^{2\mathrm{f}}$	11	0	5	2	7
$n_c^{1\mathrm{f}}$	2	0	0	0	1
$\mathrm{t_{CPU}}$(second)	315.07	358.94	324.56	281.85	283.82

Table 3.13 *Faces of Voronoi in four dimensions.* $\mathrm{N}_c = 100$.

The number of vertices in each 2-d face is a constant equals to three while that of a 1-d face is two. In the first run the number of vertices in each of the cells is 95, 108, 117, 120 and 130; in the last run, this number is 104 and 116.

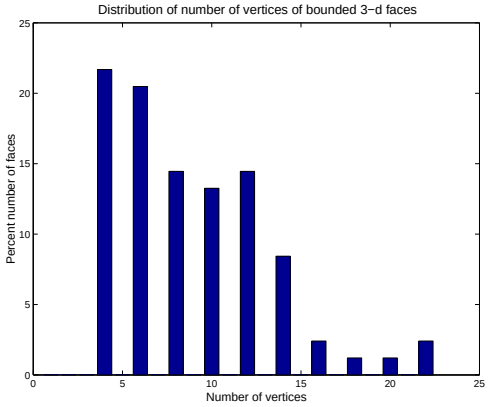

(a1)

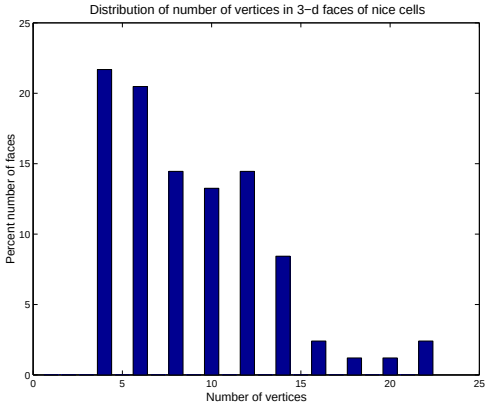

(b1)

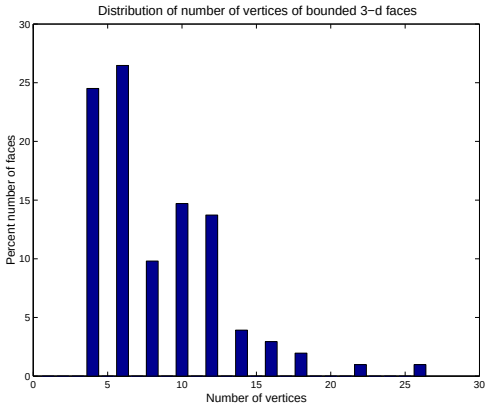

(a2)

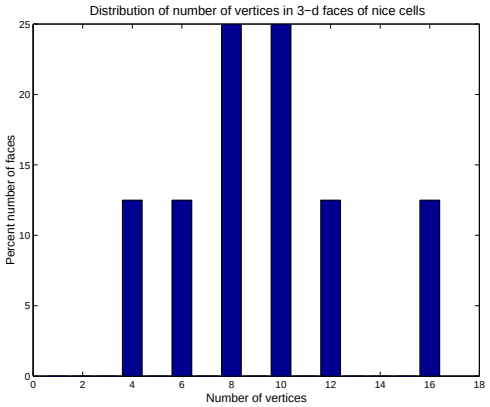

(b2)

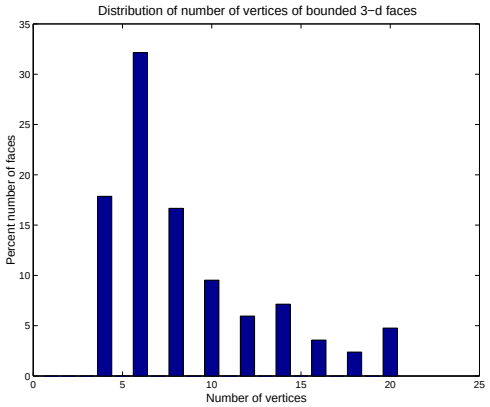

(a3)

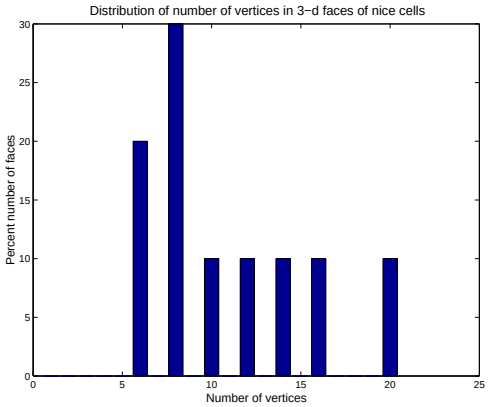

(b3)

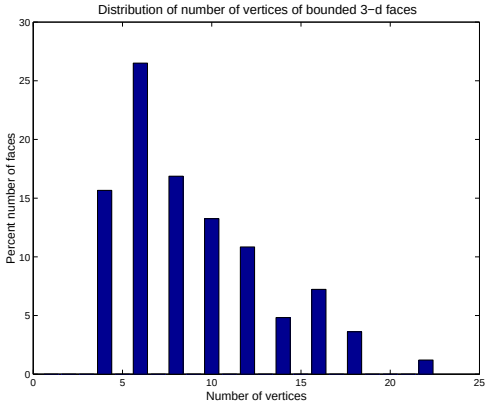

(a4)

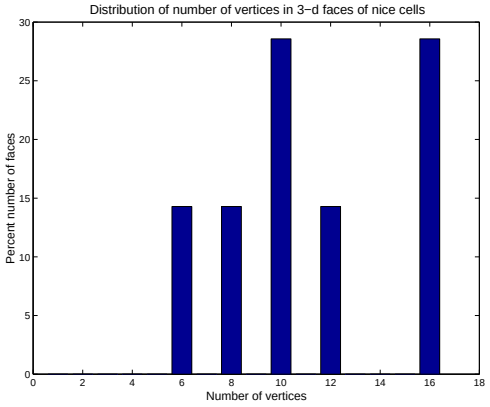

(b4)

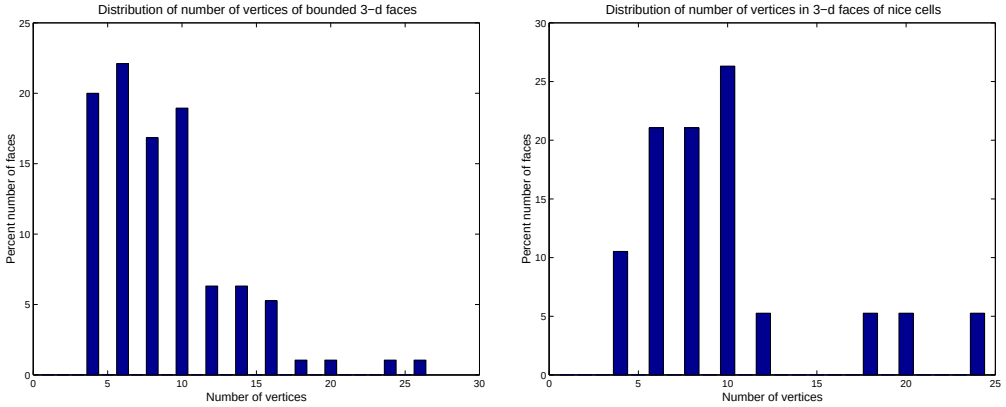
Distribution of number of vertices of bounded 3−d faces
Percent number of faces
Number of vertices
Distribution of number of vertices in 3−d faces of nice cells
Percent number of faces
Number of vertices

(a5) (b5)

Figure 3.34 *Distribution of* (ai) $v_{3\mathrm{f}}$ *and* (bi) $v_c^{3\mathrm{f}}$ *of the* i^{th} *simulation on 4-d Voronoi.*

Table 3.14 contains the results obtained from a 4-d Voronoi network of 300 original nuclei. The numbers of vertices of the sixteen cells are 97, 99, 112, 141, 145, 160, 170, 171, 176, 176, 184, 186, 188, 192, 216 and 235.

Random seed	91876				
N_v	6776	$m^3(n_c^v)$	-1.7507×10^4	$(\mu_{3\mathrm{f}}^v)_c$	9.9875
n_v	3848	$n_{3\mathrm{f}}$	444	$(\sigma_v^2)_c^{3\mathrm{f}}$	31.1697
n_c	16	$\mu_{3\mathrm{f}}^v$	9.1486	$m^2((n_{3\mathrm{f}}^v)_c)$	30.9748
n_c^v	1687	$(\sigma_v^2)_{3\mathrm{f}}$	24.0411	$m^3((n_{3\mathrm{f}}^v)_c)$	203.3116
μ_c^v	165.5000	$m^2(n_{3\mathrm{f}}^v)$	23.9869	$n_c^{2\mathrm{f}}$	60
$(\sigma_v^2)_c$	1.5100×10^3	$m^3(n_{3\mathrm{f}}^v)$	170.4755	$n_c^{1\mathrm{f}}$	3
$m^2(n_c^v)$	1.4156×10^3	$n_c^{3\mathrm{f}}$	160	$\mathrm{t_{CPU}}$(second)	1.6013×10^4

Table 3.14 *Face statistics of 300 nuclei Voronoi in four dimensions.*

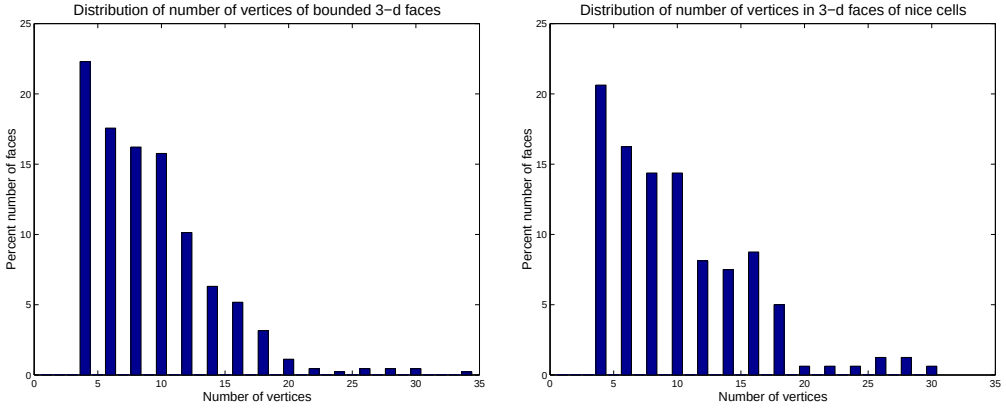
Distribution of number of vertices of bounded 3−d faces
Percent number of faces
Number of vertices
Distribution of number of vertices in 3−d faces of nice cells
Percent number of faces
Number of vertices

(a) (b)

Figure 3.35 *Distribution of* (a) $v_{3\mathrm{f}}$ *and* (bi) $v_c^{3\mathrm{f}}$ *of 4-d Voronoi, 300 nuclei.*

Table 3.15 is obtained from Voronoi in five dimensions.

Random seed	39378			N_v	16212
n_v	6449	$n_{4\mathrm{f}}$	175	$(\sigma_v^2)_c^{4\mathrm{f}}$	352.2909
n_c	1	$\mu_{4\mathrm{f}}^v$	15.9200	$m^2((n_{4\mathrm{f}}^v)_c)$	320.2645
n_c^v	864	$(\sigma_v^2)_{4\mathrm{f}}$	163.7752	$m^3((n_{4\mathrm{f}}^v)_c)$	351.8362
μ_c^v	864	$m^2(n_{4\mathrm{f}}^v)$	162.8393	$n_c^{3\mathrm{f}}$	1
$(\sigma_v^2)_c$	0	$m^3(n_{4\mathrm{f}}^v)$	4.8764×10^3	$(\mu_{3\mathrm{f}}^v)_c$	4
$m^2(n_c^v)$	0	$n_c^{4\mathrm{f}}$	11	$n_c^{2\mathrm{f}}$	1
$m^3(n_c^v)$	0	$(\mu_{4\mathrm{f}}^v)_c$	29.0909	$\mathrm{t_{CPU}}$(second)	1.8908×10^4

Table 3.15 *Face statistics of 200 nuclei Voronoi in five dimensions.*

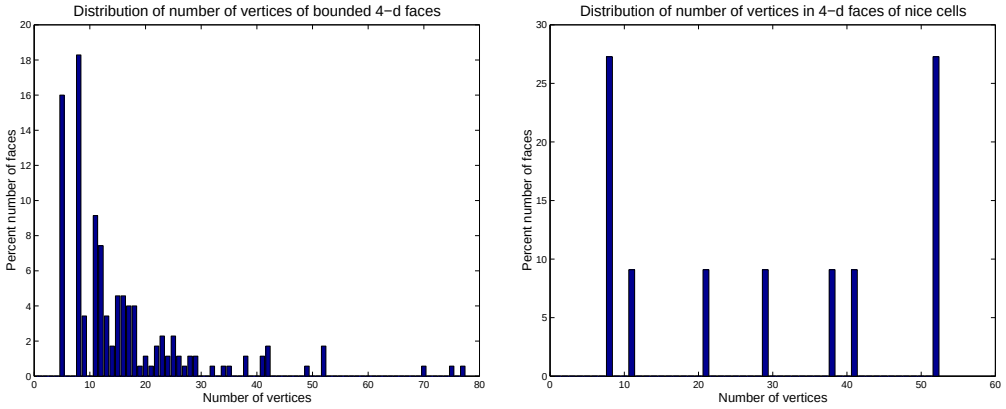
Distribution of number of vertices of bounded 4−d faces
Percent number of faces
Number of vertices
Distribution of number of vertices in 4−d faces of nice cells
Percent number of faces
Number of vertices

(a) (b)

Figure 3.36 *Distribution of* (a) $v_{4\mathrm{f}}$ *and* (bi) $v_c^{4\mathrm{f}}$ *of 5-d Voronoi, 200 nuclei.*

§ 3.9 Beam intersection study

For this study of sectioning by a line the Voronoi in two dimensions, first generate on Matlab 500 points within a square box from -0.25 to 1.25 in both axes. The beam is simply a straight line $y = mx + c$ where m is the slope and c a constant. The term *pencil beam* is used in Astronomy to describe the probing into the depth of the universe with a window of very narrow width. The data collected thus therefore in effect represent data along a Euclidean straight line at various distances. It is largely a very limited technique, but there are no other choices in Astronomy as regard the vast space that separates us from anywhere.

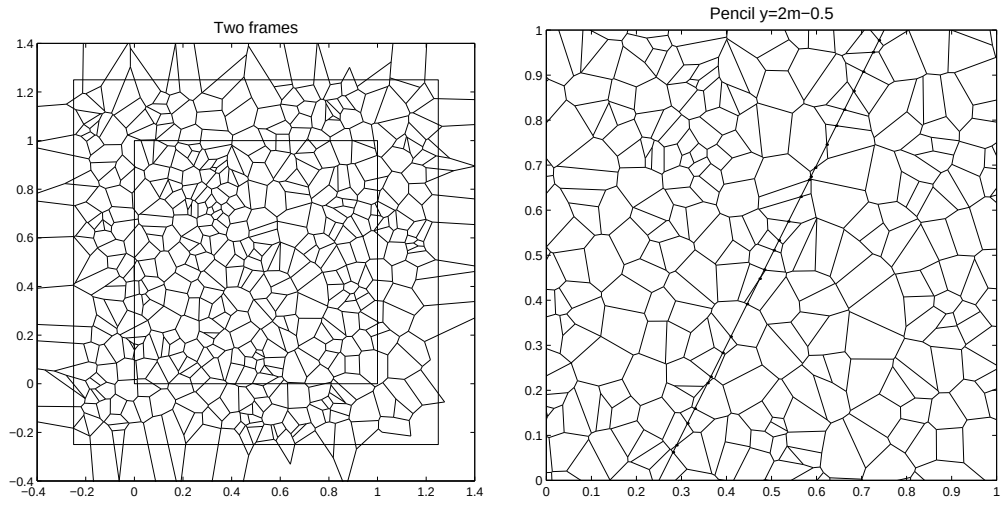

(a) (b)

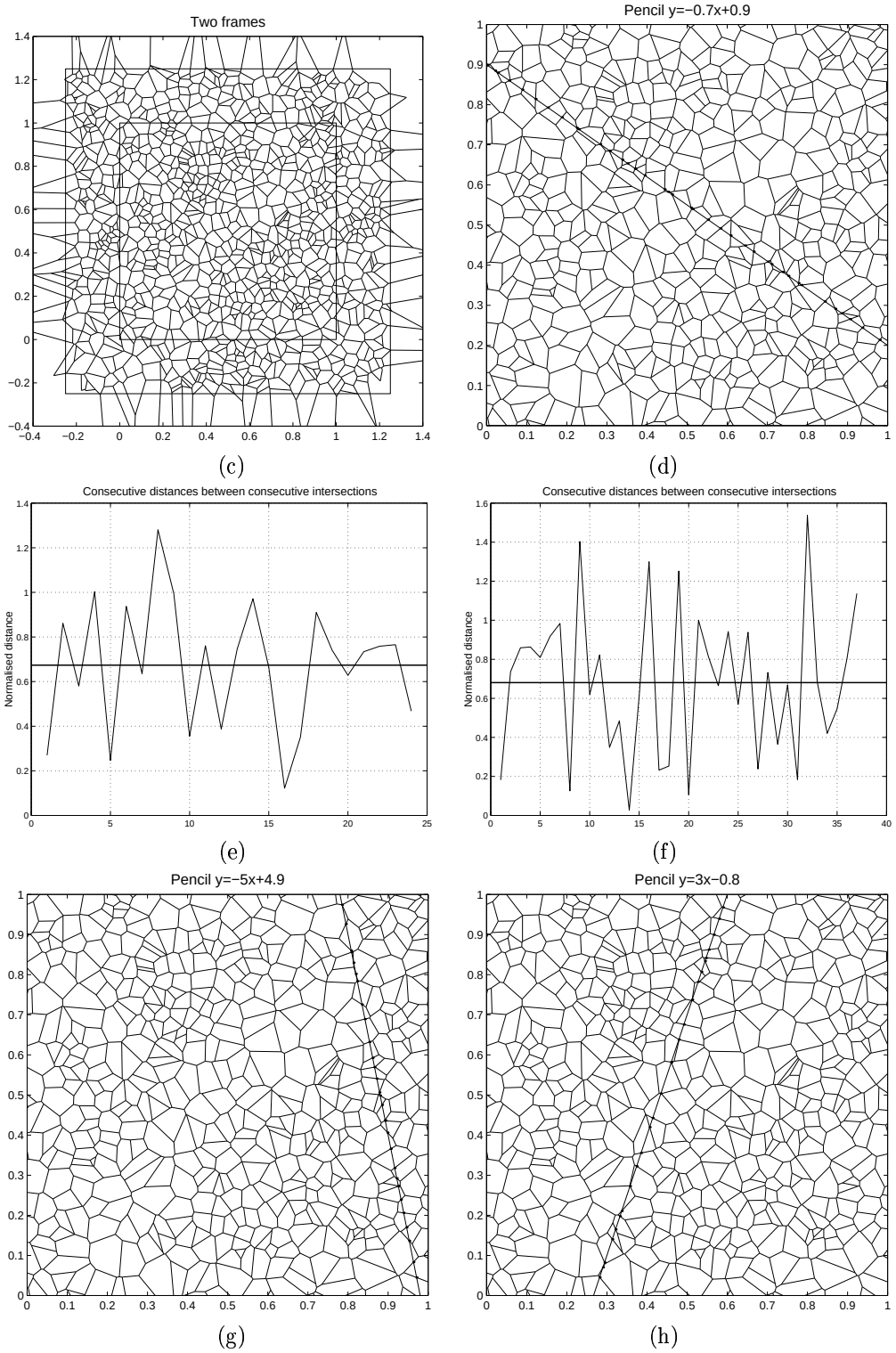

Figure 3.37 *Intersection by a line.* (a) *is intersected by* (b) $y = 2x - 0.5$*;* (c) *is intersected by* (d) $y = -0.7x + 0.9$*;* (e) *and* (f) *are corresponding distances of respectively* (b) *and* (d)*;* (c) *is intersected by* (g) $y = -5x + 4.9$ *and* (h) $y = 3x - 0.8$.

A natural basis for the normalisation is the expected distance. Another possible basis is $(1/\sqrt{239}) = 0.064685$. I call *mean normalisation* the normalisation using the first-, and *homogeneity normalisation* the second basis. Graphs of the closest pair distances look the same for both types of normalisation.

Simulation	1	2	3	4
N_c	500	1,000		
N_e	1,463	2,955		
n_c	239	463		
n_e	789	1,455		
Line equation	$y = 2x - 0.5$	$y = -0.7x + 0.9$	$y = -5x + 4.9$	$y = 3x - 0.8$
$\bar{d}$	4.6867×10^{-2}	3.163×10^{-2}	3.2448×10^{-2}	3.7843×10^{-2}
σ_d^2	3.9422×10^{-4}	3.1174×10^{-4}	2.9005×10^{-4}	4.9535×10^{-4}
Normalisation				
by mean	1 ± 0.4237 0.1713 -8.1332×10^{-3}	1 ± 0.5582 0.3032 3.5783×10^{-2}	1 ± 0.5249 0.2656 -3.7762×10^{-3}	1 ± 0.5881 0.3321 2.2989×10^{-2}
by homogeneity	0.7245 ± 0.3070 8.9936×10^{-2} -3.0936×10^{-3}	0.68059 ± 0.3799 0.1404 1.128×10^{-2}	0.6982 ± 0.3665 0.1295 -1.2853×10^{-3}	0.81428 ± 0.4789 0.2202 1.2412×10^{-2}

The program used is listed in § A.17. The space position vector of the intersection between the two vectors AB and CD is $P = A + r(B - A)$, where $AB = B - A$ and $CD = D - C$ are vectors or directed lines and A, B, C, D are space vectors, $r = \begin{vmatrix} CD' \\ CA' \end{vmatrix} \Big/ \begin{vmatrix} AB' \\ CD' \end{vmatrix}$ and $s = \begin{vmatrix} AB' \\ CA' \end{vmatrix} \Big/ \begin{vmatrix} AB' \\ CD' \end{vmatrix}$ Here $AB = A + r(B - A)$, and $CD = C + s(D - C), 0 \leq r, s \leq 1$ are directed lines. P exists if $0 \leq r \leq 1$ and $0 \leq s \leq 1$.

If the denominator $\begin{vmatrix} AB' \\ CD' \end{vmatrix}$ is zero, then the two lines are parallel. Also, if the nominator of r is zero, that is $\begin{vmatrix} CD' \\ CA' \end{vmatrix} = 0$, then both lines are collinear.

Consider the line section of Rayleigh distributed Voronoi where both the coordinates x and y are random numbers with Rayleigh distribution. The probability density function of the Rayleigh distribution is $y = f(x/b) = (x/b^2)\exp(-x^2/2b^2)$. The mean of this distribution is $b\sqrt{\pi/2}$ and the variance is $((4 - \pi)/2)b^2$. With $b = 1, 2, \ldots, 1000$ choose the random numbers from the Rayleigh distribution, then scale and use them as the coordinates.

In Figure 3.38 the structure in (a) is intersected by (b) $y = 3x - 0.8$, (c) $y = x$, (d) $y = 2x$, (e) $y = 0.2x$, (f) $y = -x + 1$, (g) $y = -x + 0.3$.

The following codes generate and scale the points of Rayleigh distribution.

```
X=raylrnd([1:NumCell])';Y=raylrnd([1:NumCell])';Max=0.8*max([X;Y]);X=X/Max;Y=Y/Max;
```

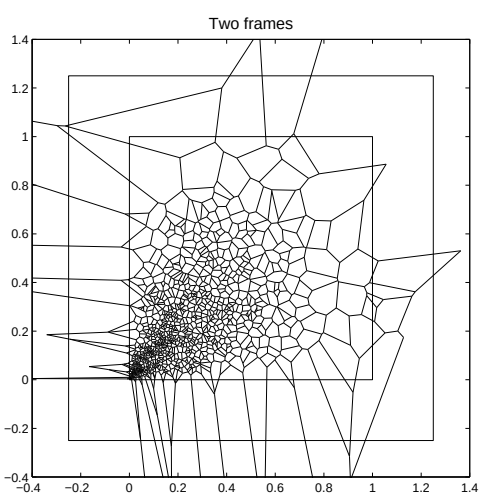

(a)

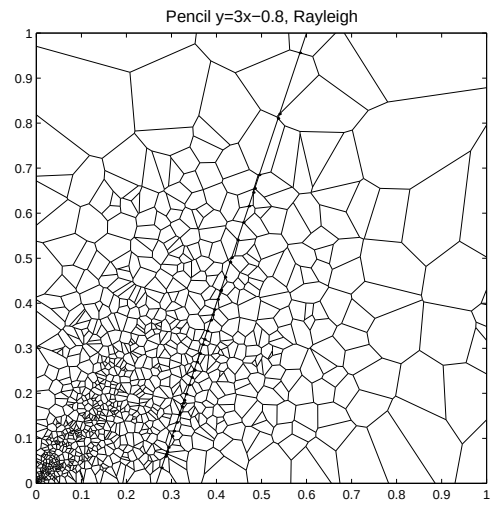

(b)

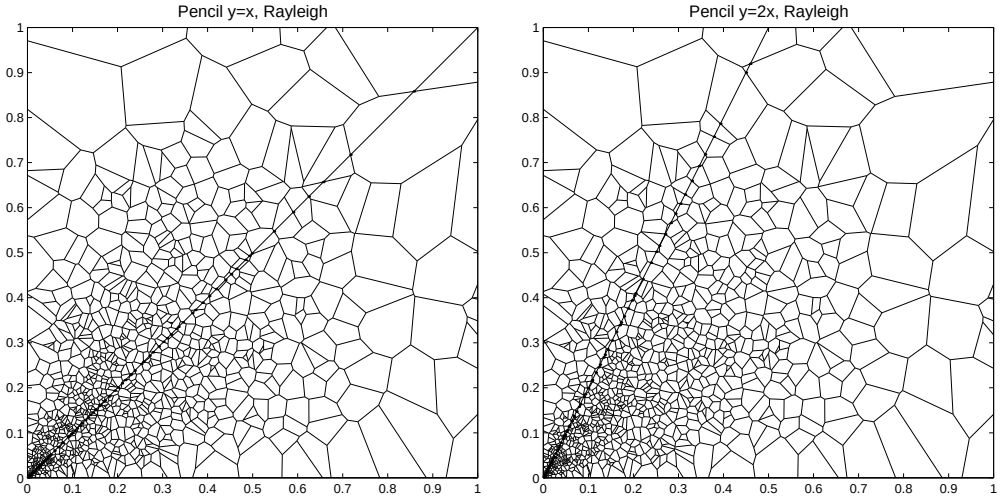

(c) (d)

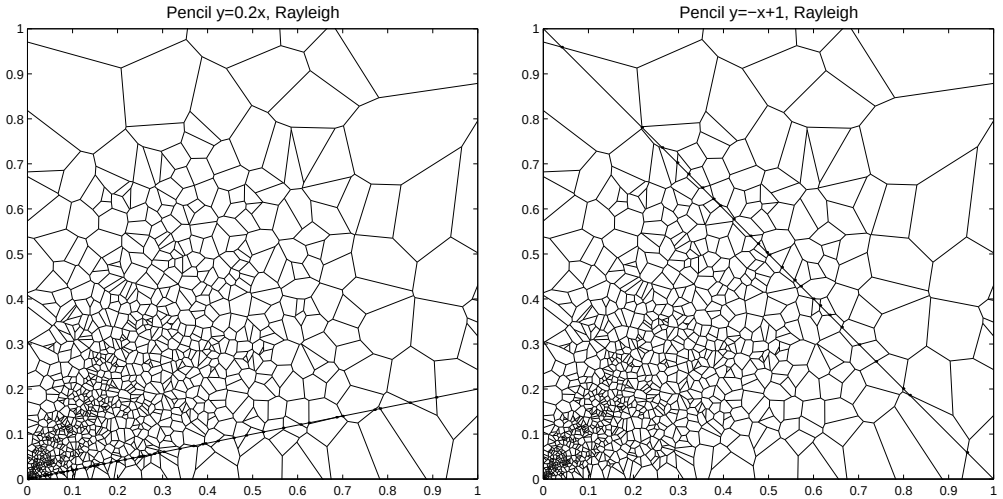

(e) (f)

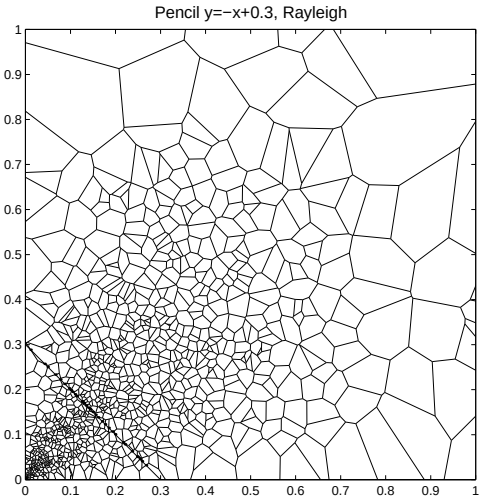

(g)

The values of Cx and Dx will need to be adjusted manually from the pencil beam equation. It is the value of x at both points of intersection between the beam and the $[0, 1]$ square box. A random Voronoi network can either be both homogeneous and isotropic or, nonhomogeneous and nonisotropic depending on whether the probability distribution function is a constant.

Figure 3.38 Line intersection in a Voronoi with Rayleigh distribution.

Simulation	1	2	3	4	5	
N_c	1,000					
N_e	2,975					
n_c	988					
n_e	2,912					
Line eq.	$y = 3x - 0.8$	$y = x$	$y = 2x$	$y = 0.2x$	$y = -x + 1$	$y = -x + 0.3$
$\bar{d}$	2.3621×10^{-2}	1.4253×10^{-2}	1.3853×10^{-2}	1.7434×10^{-2}	4.4401×10^{-2}	1.027×10^{-2}
σ_d^2	8.1582×10^{-4}	6.2922×10^{-4}	2.9647×10^{-4}	3.0991×10^{-4}	1.1584×10^{-3}	3.5365×10^{-5}
Normalised						
by mean	1±1.2092 1.4256 5.5516	1±1.7599 3.0609 28.351	1±1.2429 1.5239 7.6499	1±1.0098 1.0004 1.6643	1±0.7665 0.56204 1.2114	1±0.5791 0.3245 0.1755
by homog.	0.7425±0.8978 0.7859 2.2721	0.4480±0.7885 0.6144 2.5493	0.4354±0.5412 0.2890 0.6316	0.548±0.5533 0.3004 0.2739	1.3956±1.0698 1.0947 3.293	0.3228±0.1869 3.3813×10^{-2} 5.9021×10^{-3}

Table 3.17 *Line intersection statistics of Rayleigh distributed Voronoi.*

§ 3.10 Voronoi of a Voronoi

A Voronoi of a Voronoi is still a Voronoi, provided that by 'Voronoi' one means Voronoi Tessellation. But what are the effects of applying the Voronoi tessellating operator on a set of points? And what are the effects of applying this operator twice?

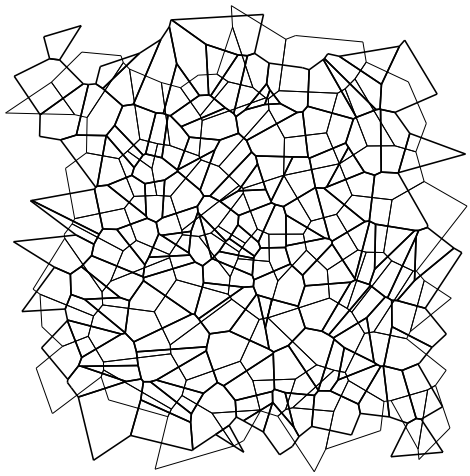

It is an interesting question to consider whether Voronoi tessellation as an operator alters, for instance, the nature of the distribution of the original set of points. Figure 3.39 shows the first Voronoi operator applied to the original points and then the second Voronoi operator applied to the vertices obtained. Here the Voronoi operator is applied twice in succession. In Figure the Voronoi operator is twiced in succession, *i.e.* $\mathcal{V}^2(\cdot)$, starting from a set of 100 points.

Figure 3.39 Two Voronoi operators applied in succession.

Let $\mathcal{V}^n(\cdot)$ be the n^{th}-order Voronoi operator. Figure 3.39 shows as an example $\mathcal{V}^2(x)$ where x is the original generator points. In Figure 3.40 this operator is applied six times in succession. The Voronoi operator is a mapping which maps a set of points into a set of Voronoi vertices having the former points as the Voronoi nuclei. The program used for Figures 3.39 to 3.41 is listed in § A.20.:

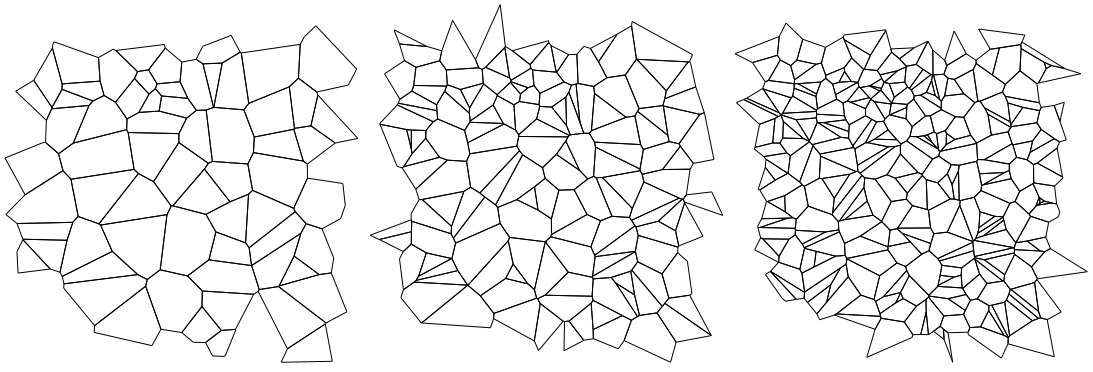

(a) (b) (c)

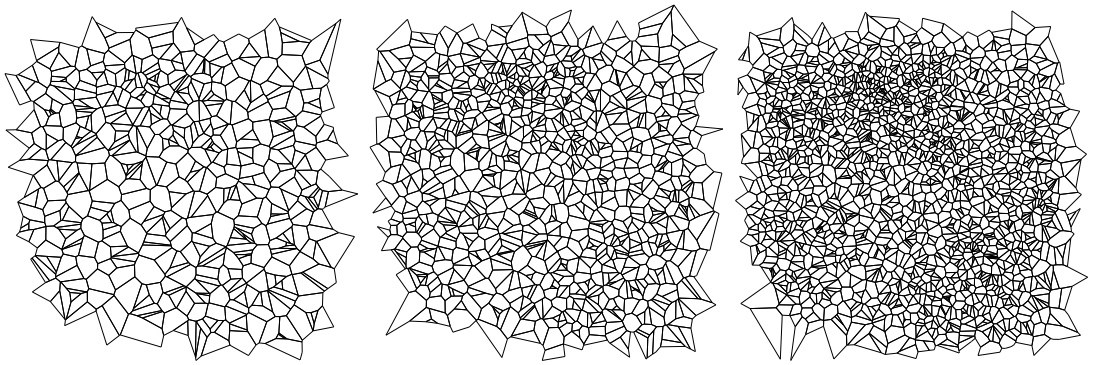

(d) (e) (f)

Figure 3.40 *The Voronoi operations,* (a) $\mathcal{V}(x)$, (b) $\mathcal{V}^2(x)$, (c) $\mathcal{V}^3(x)$, (d) $\mathcal{V}^4(x)$, (e) $\mathcal{V}^5(x)$, (f) $\mathcal{V}^6(x)$, *where* x *is the original set of 100 points.*

Figure 3.41 shows the effect produced by the Voronoi operators of various degrees on the number of cells, n_c, and vertices, n_v of the network.

Figure 3.41 recursively apply the Voronoi operators of various orders. The number of cells and vertices when recursively applying the Voronoi operators of various orders on the set of point x is shown in Figure 3.41, that is to say, $\mathcal{V}(x)$, $\mathcal{V}^2(x)$, $\cdots$, $\mathcal{V}^6(x)$. From Figure 3.41, the increase of n_c and n_v with the order n of $\mathcal{V}^n(\cdot)$ is exponential. And from Figure 3.41 (a) to (f), apart from the unevenness affected at the boundary, the grephs shows the degree of lumpiness in the original distribution retained by the Voronoi operator. This is analogous to the increase in the entropy in physical processes.

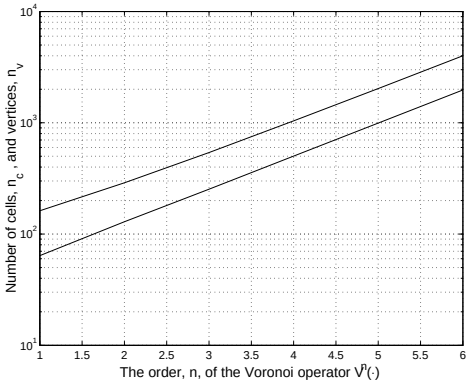

Figure 3.41 The number of cells and vertices when recursively applying the Voronoi operator.

§ 3.11 Transformations of a Voronoi

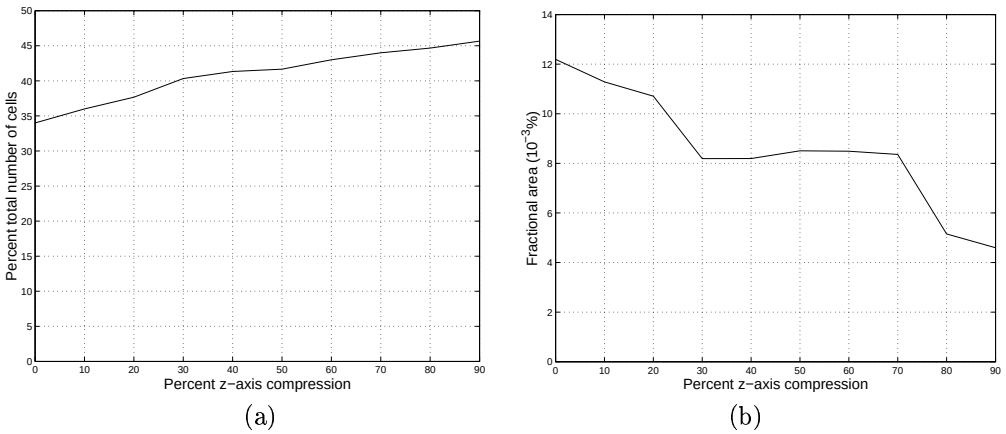

(a) (b)

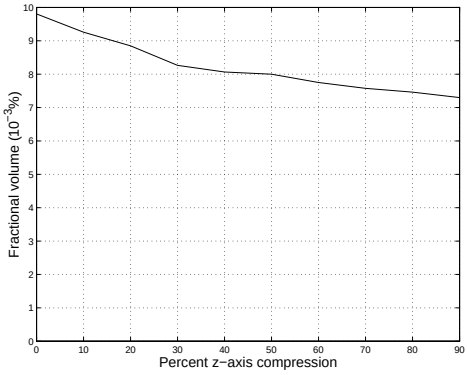

The simplest of transformations is compression where the coordinates of each vertex in multiplied by a factor less than one. Figure 3.42 shows, within a fixed box, the effect the compression along the z-axis has on the number of cells, surface area and volume of cells within the box. It shows the effects of a z-axis compression on (a) the number of cells in the box, (b) the surface area of a cell and (c) the volume of a cell.

(c)

Figure 3.42 The effects of axis compression.

§ 3.12 Compressed Voronoi

The following study looks at compression of the Voronoi tessellation in three dimensions. With the compression simultaneously in the x- and y axes, the mean and standard deviation of cell's surface area are shown as contours in Figure 3.43. The numerical values are shown in Figure's 3.18 and 3.19. Here x_i and y_i are respectively transformed to $r_x x_i$ and $r_y y_i$. All the values here are normalised by their corresponding values in the case without compression. In this case, the network was created from 100 generators within one unit cube, only 21 inner cells are considered, the mean and the standard deviation of the cell surface area are respectively 0.2330 and 0.0544.

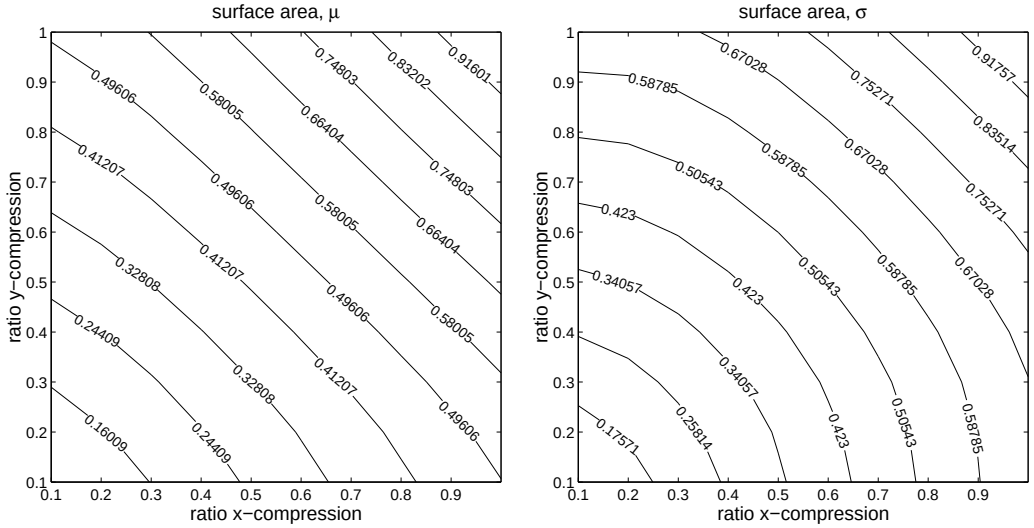

(a) (b)

Figure 3.43 (a) *Mean, and* (b) *standard deviation of surface area of cells under compression, normalised against the corresponding values of the uncompressed case. In other words,* (a) $\mu(a_{ij})/\mu(a_{11})$, *and* (b) $\sigma(a_{ij})/\sigma(a_{11})$.

$\boxed{\mu(a_{ij})}$

		r_x									
		1.0	*0.9*	*0.8*	*0.7*	*0.6*	*0.5*	*0.4*	*0.3*	*0.2*	*0.1*
r_y	*1.0*	1.0000	0.9337	0.8688	0.8058	0.7450	0.6870	0.6326	0.5828	0.5396	0.5060
	0.9	0.9318	0.8683	0.8061	0.7457	0.6873	0.6315	0.5790	0.5310	0.4892	0.4566
	0.8	0.8650	0.8042	0.7447	0.6866	0.6305	0.5768	0.5261	0.4797	0.4391	0.4073
	0.7	0.8001	0.7419	0.6847	0.6290	0.5749	0.5230	0.4740	0.4289	0.3893	0.3581
	0.6	0.7375	0.6816	0.6267	0.5730	0.5208	0.4706	0.4230	0.3789	0.3400	0.3092
	0.5	0.6777	0.6240	0.5711	0.5193	0.4687	0.4199	0.3734	0.3300	0.2914	0.2605
	0.4	0.6217	0.5699	0.5188	0.4685	0.4193	0.3715	0.3257	0.2826	0.2439	0.2123
	0.3	0.5707	0.5205	0.4708	0.4217	0.3735	0.3264	0.2808	0.2375	0.1979	0.1648
	0.2	0.5269	0.4779	0.4293	0.3810	0.3333	0.2863	0.2404	0.1962	0.1547	0.1188
	0.1	0.4939	0.4457	0.3976	0.3497	0.3020	0.2546	0.2078	0.1617	0.1171	0.0761

Table 3.18 *Mean of the cell surface area of compressed Voronoi*

$\sigma(a_{ij})$		r_x									
		1.0	*0.9*	*0.8*	*0.7*	*0.6*	*0.5*	*0.4*	*0.3*	*0.2*	*0.1*
	1.0	1.0000	0.9381	0.8789	0.8231	0.7715	0.7255	0.6868	0.6577	0.6407	0.6382
	0.9	0.9360	0.8761	0.8186	0.7641	0.7135	0.6678	0.6288	0.5986	0.5799	0.5751
	0.8	0.8756	0.8173	0.7611	0.7075	0.6573	0.6116	0.5720	0.5403	0.5195	0.5122
	0.7	0.8199	0.7626	0.7071	0.6539	0.6037	0.5574	0.5165	0.4830	0.4596	0.4495
	0.6	0.7699	0.7130	0.6576	0.6041	0.5532	0.5058	0.4631	0.4271	0.4005	0.3870
r_y	*0.5*	0.7269	0.6696	0.6136	0.5592	0.5069	0.4576	0.4123	0.3731	0.3426	0.3249
	0.4	0.6924	0.6340	0.5766	0.5205	0.4661	0.4141	0.3654	0.3219	0.2864	0.2634
	0.3	0.6676	0.6076	0.5482	0.4897	0.4324	0.3769	0.3240	0.2751	0.2331	0.2030
	0.2	0.6536	0.5914	0.5296	0.4682	0.4076	0.3481	0.2902	0.2350	0.1848	0.1451
	0.1	0.6495	0.5853	0.5212	0.4573	0.3936	0.3302	0.2675	0.2059	0.1466	0.0933

Table 3.19 *Standard deviation of the cell surface area of compressed Voronoi*

Mistakes reveal some interesting characteristics worth investigating further, namely those shown in Figure 3.44.

Let a_{ij} be the surface area of cells when subjected to compressions i and j respectively along the x- and y axes, that is to say, $r_x = i$ and $r_y = j$. And let $a_{ij}(k)$ be that surface area of the k^{th} cell among those undergoing these compressions ij. Then Figure 3.44 (b) and (c) are possible when we pick one cell as the basis for our normalisation, while Figure 3.44 (a) is when we normalise each compressed case by its own mean.

For cell volume of the same network the results are shown in Figure 3.45. The mean value and the standard deviation of cell volumes are respectively 0.0075 and 0.0032.

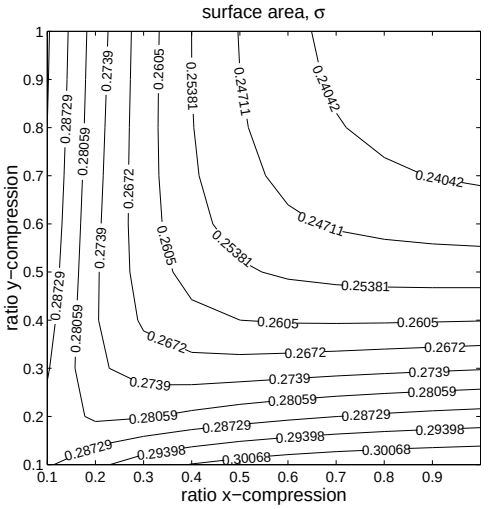

(a)

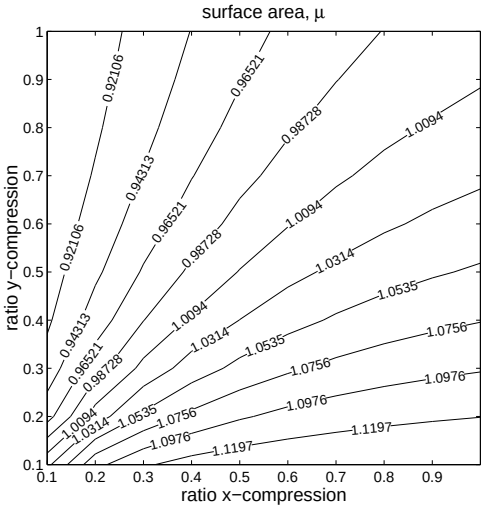

(b)

In Figure 3.44 ome hidden characteristics are revealed from out choice of the normalisation basis; respectively for (a), (b) and (c) the following,

$$\sigma\left(\frac{a_{ij}}{\mu(a_{ij})}\right), \quad \frac{\mu(a_{ij}/a_{ij}(1))}{\mu(a_{11}/a_{11}(1))}, \quad \frac{\sigma(a_{ij}/a_{ij}(1))}{\sigma(a_{11}/a_{11}(1))}.$$

(c)

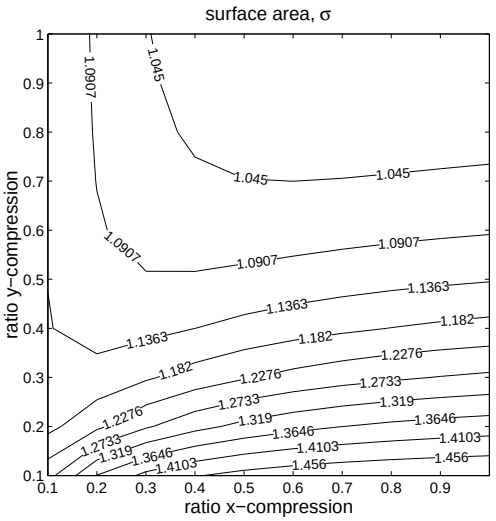

Figure 3.44 Some hidden characteristics revealed.

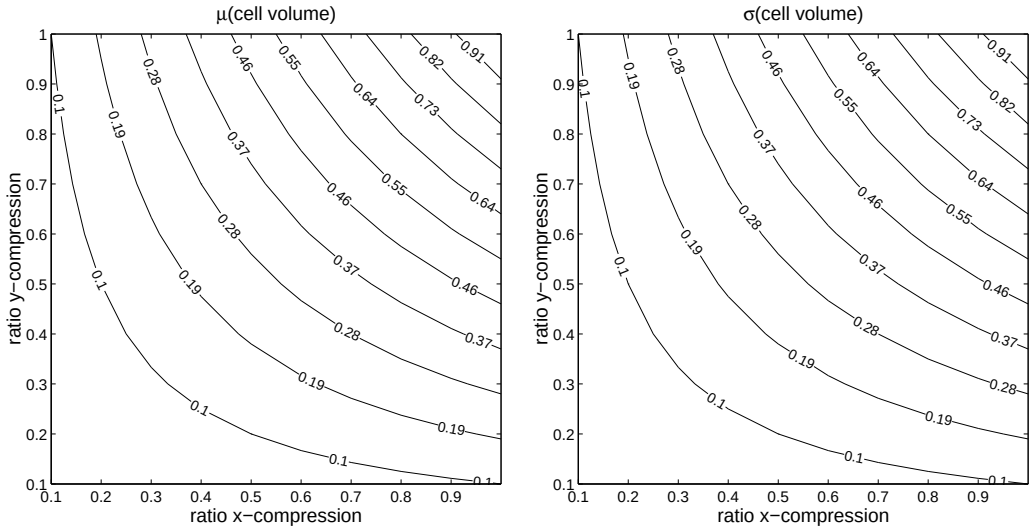

Figure 3.45 *Volume of compressed Voronoi cells;* (a) $\mu(V_{ij}))and$(b) $\sigma(V_{ij})$.

Table 3.20 gives the numerical values of the mean, while Table 3.21 those of the standard deviation plotted in Figure 3.45.

$\boxed{\mu(V_{ij})}$

		r_x									
		1.0	*0.9*	*0.8*	*0.7*	*0.6*	*0.5*	*0.4*	*0.3*	*0.2*	*0.1*
	1.0	1.0000	0.9000	0.8000	0.7000	0.6000	0.5000	0.4000	0.3000	0.2000	0.1000
	0.9	0.9000	0.8100	0.7200	0.6300	0.5400	0.4500	0.3600	0.2700	0.1800	0.0900
	0.8	0.8000	0.7200	0.6400	0.5600	0.4800	0.4000	0.3200	0.2400	0.1600	0.0800
	0.7	0.7000	0.6300	0.5600	0.4900	0.4200	0.3500	0.2800	0.2100	0.1400	0.0700
	0.6	0.6000	0.5400	0.4800	0.4200	0.3600	0.3000	0.2400	0.1800	0.1200	0.0600
r_y	*0.5*	0.5000	0.4500	0.4000	0.3500	0.3000	0.2500	0.2000	0.1500	0.1000	0.0500
	0.4	0.4000	0.3600	0.3200	0.2800	0.2400	0.2000	0.1600	0.1200	0.0800	0.0400
	0.3	0.3000	0.2700	0.2400	0.2100	0.1800	0.1500	0.1200	0.0900	0.0600	0.0300
	0.2	0.2000	0.1800	0.1600	0.1400	0.1200	0.1000	0.0800	0.0600	0.0400	0.0200
	0.1	0.1000	0.0900	0.0800	0.0700	0.0600	0.0500	0.0400	0.0300	0.0200	0.0100

Table 3.20 *Numerical values of the mean and standard deviation of compressed cell volume.*

$\boxed{\sigma(V_{ij})}$

		r_x									
		1.0	*0.9*	*0.8*	*0.7*	*0.6*	*0.5*	*0.4*	*0.3*	*0.2*	*0.1*
	1.0	1.0000	0.9000	0.8000	0.7000	0.6000	0.5000	0.4000	0.3000	0.2000	0.1000
	0.9	0.9000	0.8100	0.7200	0.6300	0.5400	0.4500	0.3600	0.2700	0.1800	0.0900
	0.8	0.8000	0.7200	0.6400	0.5600	0.4800	0.4000	0.3200	0.2400	0.1600	0.0800
	0.7	0.7000	0.6300	0.5600	0.4900	0.4200	0.3500	0.2800	0.2100	0.1400	0.0700
	0.6	0.6000	0.5400	0.4800	0.4200	0.3600	0.3000	0.2400	0.1800	0.1200	0.0600
r_y	*0.5*	0.5000	0.4500	0.4000	0.3500	0.3000	0.2500	0.2000	0.1500	0.1000	0.0500
	0.4	0.4000	0.3600	0.3200	0.2800	0.2400	0.2000	0.1600	0.1200	0.0800	0.0400
	0.3	0.3000	0.2700	0.2400	0.2100	0.1800	0.1500	0.1200	0.0900	0.0600	0.0300
	0.2	0.2000	0.1800	0.1600	0.1400	0.1200	0.1000	0.0800	0.0600	0.0400	0.0200
	0.1	0.1000	0.0900	0.0800	0.0700	0.0600	0.0500	0.0400	0.0300	0.0200	0.0100

Table 3.21 *Numerical values of the mean and standard deviation of compressed cell volume.*

Perimeters prove to be the most difficult to find. Figure 3.46 (a) and (b) show the mean and standard deviation of the cell perimeter while Table 3.22 lists the $\mu(s_c)$ matrix that makes up one of these graphs. The values before normalisation are $\mu(s_{ij}) = 3.0158$ and $\sigma(s_{ij}) = 0.4291$.